University of Kent at Canterbury

Frequency Stabilised Laser Diodes and their use in Length Metrology

by

Geoffrey P Barwood

A thesis submitted for the degree of Doctor of Philosophy

Department of Physics

University of Kent at Canterbury

1992

University of Kent at Canterbury

A Thesis submitted for the degree of Doctor of Philosophy

Frequency Stabilised Laser Diodes and their use in Length Metrology

G P Barwood

Abstract

This thesis is concerned with the use of index-guided GaAlAs laser diodes in length metrology. Since these lasers have important differences from more commonly used HeNe lasers in interferometry, the thesis begins with a review and investigation of these differences. A key problem is the relatively large linewidth (typically 30 MHz). This is reduced, by using the optical feedback from a resonant confocal etalon, to less than ≈10 kHz.

Potential spectroscopic frequency references are discussed and the choice made of the rubidium (Rb) D lines at 780 nm and 795 nm, using either Doppler-free features or the linear absorptions. The optically narrowed laser is then stabilised to the various hyperfine components. By measuring the reproducibility of the difference frequency between two systems, a relative frequency reproducibility of $\approx 1 \times 10^{-10}$ is demonstrated. Laser frequency stabilities are measured for a number of different cases, for example with the lasers free-running and offset locked. For two optically narrowed Rb-stabilised lasers at $\tau = 10$ s, the relative frequency stability is $\approx 4 \times 10^{-12}$. The hyperfine intervals of the two Rb lines are also measured for both isotopes (^{85}Rb and ^{87}Rb), representing the most complete study of Rb-stabilised diode lasers to date. From these results, values for the hyperfine constants and isotope shifts are obtained. Finally, the absolute frequencies of both Rb-stabilised laser diodes are measured by interferometric comparison with an iodine stabilised HeNe laser at 633 nm with a relative accuracy of $\pm 1 \times 10^{-9}$.

To demonstrate the use of a frequency tunable laser diode in distance measurement, a swept wavelength measurement system was developed with a demonstrated accuracy of a few parts per million. The thesis ends with a discussion of longitudinal mode control in laser diodes and some potential future uses in length and optical frequency metrology.

Acknowledgements

I should like to thank my colleagues in the wavelength standards group at the National Physical Laboratory for their help and encouragement during the preparation of this thesis. In particular, I should like to thank Dr WRC Rowley for measurements made on the NPL 1-m Fabry-Perot wavelength comparator which provided the results for the two absolute frequency measurements to $\pm 1 \times 10^{-9}$ (section 5.5.2). Dr Rowley was also very helpful in providing other scientific advice, in particular with regard to the electronics required for this thesis. Thanks are also due to Dr P Gill for useful technical discussions regarding the direction of research and encouragement during the course of this work. At the University of Kent, I should like to thank my supervisor, Prof DA Jackson, and also Dr D Webb for various useful comments on the text of this thesis.

Contents of Thesis

CHAPTER 1

INTRODUCTION TO FREQUENCY STABILISED LASER DIODES

1.1 Introduction; Interferometry and Applications in Metrology

This thesis is concerned with the increasing use of semiconductor (diode) lasers in optical frequency metrology, especially length or displacement measuring interferometers. The two subjects of interferometers and lasers have considerably different histories. Interferometers date back to the experiments by Young in 1807, but, in contrast, lasers were first demonstrated much more recently, in 1960.

Lasers were first demonstrated in the microwave part of the electromagnetic spectrum, and termed masers. The first laser (optical maser) was the ruby laser, operating at 694 nm [1]. This device was unable to operate continuously, but instead emitted short pulses of light. Continuous wave lasers were first demonstrated with the He-Ne system. This was first demonstrated on the Ne line in the infra-red at 1.15 μm [2], which can yield a few mW power. The strong red line at 633 nm was also soon made to lase [3], and it is this line which has played such an important part in length metrology to date. It is interesting to note that although the first laser was a solid-state laser, much of the subsequent development was with gas discharge or liquid-state lasers. Early solid state laser development suffered from the general problem that laser action in solids requires the crystal or material to be highly homogeneous to ensure that laser oscillation is not quenched. Dislocations, for example, or other imperfections will cause scattering in the material seriously reducing the optical gain.

Semiconductor lasers (GaAs devices) were first demonstrated in 1962 [4,5,6], in the near infra-red part of the spectrum. However, early difficulties prevented their widespread use in laser spectroscopy [7,8]. The situation is now reversing, with a greatly renewed interest in solid-state lasers. This is primarily owing to the advent of mass-produced low-cost diodes operating at room temperature. Of all solid state lasers, only diodes achieve their lasing action directly by passing an electrical current through the material. However, there is a further family of solid-state devices, eg doped glass [9], or fibre lasers, which are optically pumped. Optical pumping is achieved either by a high-power argon laser or high power (> 100 mW) diode lasers.

Interferometry is one of a number of subjects which easily pre-dates the advent of the laser, but where the laser has been essential to realise the full potential of the subject. Interferometry is used in a number of forms in a wide field of measurement. It was first used in various applications in earnest in the late nineteenth century by Michelson and Lord Rayleigh. Various forms of interferometer are used today for length or displacement measurement, such as Michelson or Fabry-Perot interferometers [10]. Michelson used his interferometer to measure atomic wavelengths to high accuracy, for example he measured the Cd line at 644 nm [11]. An accuracy of around one part per million was claimed and Michelson clearly recognised the potential for interferometry in high accuracy length measurement [12]. A typical Michelson system is shown in figure 1.1.1. Here, a laser is shown as the light source, although the original work used a spectral lamp as source.

Lasers are naturally suited to nearly all interferometric work. They produce a narrow beam of light which can be expanded and collimated to propagate over many tens of metres. Further, there is a very large

fundamental limit to the distance over which they may be used, as determined by the spectral linewidth of the source. Spectral lamps are limited to ≈0.3 m (the "coherence length"), but for most single frequency cw lasers, this distance is a hundred metres or more. The practical limitation is often that of air turbulence, making the return beam wander spatially by a beam diameter or more. In figure 1.1.1, the light is split at the beamsplitter, with part of the beam travelling a fixed distance and part being reflected by a moveable mirror. Although plane mirrors are simpler, the mirror arrangement shown of mirrors at 90° (a cube corner) is used in practical systems. It has the advantage of retaining optical alignment even if the mount holding the moveable mirror rocks or turns during the movement. Lasers in general do not operate stably with direct optical feedback, and this arrangement prevents that. Such optical feedback causes intensity instability and changes the emitted frequency of the laser.

The basic theory of a Michelson interferometer is readily understood as follows. If the time taken for light to travel to the fixed and moving arms is τ_F and τ_M respectively, then the resulting intensity when the light is recombined is given by

$$I = \tfrac{1}{2} I_o \left| \exp(j\omega\tau_F) + \exp(j\omega\tau_M) \right|^2 \qquad (1.1.1)$$

assuming that both cube corners have identical reflectances and that the beam is well collimated (usually an idealised situation). This equation becomes

$$I = 2I_o \cos^2(\tfrac{1}{2}\omega\tau) \qquad (1.1.2)$$

where $\tau = |\tau_m - \tau_F|$. As τ is changed, by moving the moveable corner cube,

light and dark fringes are observed where the beams re-combine. A detector placed here, linked to an electronic counter, records a measure of the distance moved. If the length difference between the two arms is l, then $\tau = nl/c$. A light fringe is observed when

$$\nu\tau = \nu nl/c = \tfrac{1}{2}N \qquad (1.1.3)$$

if N is an integer. In this formula, n is the refractive index of the air. Therefore,

$$l = Nc/2n\nu \qquad (1.1.4)$$

By zeroing the counter at one point (eg at one end of a scale to be measured), one may then measure the displacement of the cube corner in travelling to the second measurement point. Clearly, however, we need to know the laser frequency, the refractive index of air, and the speed of light. The refractive index of air may be calculated from Edlen's equations [13], together with some recent corrections to this equation [14]. In the case of a diode laser source, the production and measurement of a suitably stable laser frequency is a principal subject of this thesis. The speed of light, c, is fixed in the definition of the metre.

The definition of the metre has a long history [15], but for many years prior to 1960 was defined in terms of the physical length of a platinum-iridium bar. Several countries, including the UK, kept authorised copies. Measurements of the vacuum wavelength of spectroscopic transitions therefore needed to be made relative to the length of this bar. In 1960, however, the definition was changed to reference length to a particularly stable spectral line in krypton at

605 nm. It was ironic that 1960 was also the year of the demonstration of the first laser. Although apparently doomed to change from its inception, therefore, this definition actually survived until 1983. The new definition [16] carefully omits reference to any particular optical source, but instead effectively defines c = 299 792 458 m/s. In thinking about length, we are forced to think about the laser frequency and relating that to the Cs time standard.

In the final part of this section, some of the applications of interferometry to length measurement are considered. Length interferometry is such a ubiquitous tool [17,18] allowing measurements from the nm range to around 100 m, beyond which we might consider using electromagnetic distance measurement (EDM) and time of flight pulse measurements instead. One of the problems of a physical length standard has always been how to divide it down to measure small distances or multiply it up for larger ones. Interferometry is today used in thermal expansion measurements, measurements of the refractive index of gases, and the measurement of gauge blocks for industry. It can be used to compare visible laser frequencies to a few parts in 10^{11} and some of these measurements, particularly of hydrogen, allow determination of fundamental constants to high accuracy. The NPL long-range primary barometer uses interferometry to measure the height of a mercury column of known density and hence measures pressure. Industry routinely uses commercially available laser interferometers for the verification of co-ordinate measuring machines (CMMs) and computer numerically controlled devices (CNCs). Sometimes they are used for convenience, even if the full accuracy available is not required. Such commercially available devices offer direct and easy traceabliity to the UK unit of length. In the more recent moves to achieve nanometric precision in manufacturing ("nanotechnology"), interferometry has been used to

evaluate the roughness of super-smooth mirrors or measure the Si lattice spacing for X-ray work. Clearly, the available accuracy in using optical interferometry in nanometrology is lower, simply because one is relying entirely on fringe subdivision. For example, 0.3 nm corresponds to a thousandth of a fringe and represents roughly the limit of present optical interferometry [19].

Laser interferometry therefore offers and will continue to be a vital tool in length metrology. In the recent past, the source has nearly always been a red (633 nm) He-Ne laser [20]. This thesis partly examines whether diode lasers can offer an alternative; perhaps a more flexible alternative. It also seeks to discover what new interferometric length measurement techniques might be developed using the unique combination of properties of a diode laser.

1.2 Brief Survey of available visible laser sources and advantages of diodes

Lasers are ideally suited for interferometry. Most lasers, other than diodes, produce a diffraction limited spectrally coherent output beam. When expanded to ≈10 mm diameter, the diffraction limited beam can be collimated so that the beam expands by less than a factor of two over distances of ≈100 m. These lasers should, by the very nature of the measurement required, be cw lasers. Generally around 1 mW power is sufficient for interferometry. Such lasers can nearly always be made to operate in a single longitudinal mode. For most lasers, other than diodes, this implies a coherence length of over a hundred metres, corresponding to a linewidth of less than 1 MHz. We restrict ourselves to considering lasers emitting in the visible part of the spectrum (400 nm to 800 nm), excluding infra-red sources. This is necessary both

for general ease of beam alignment and to reduce diffraction problems to an acceptable level.

Lasers generally can be termed either "fixed-frequency" or "frequency tunable". The gain medium in a fixed-frequency laser is typically a gas discharge. Such a laser can, in fact, be made to tune over a short frequency range around each lasing transition, but typically this range is only ≈1 GHz. This width arises from the Doppler width of the transition. Of all such lasers, the He-Ne device, operating at 633 nm is the most popular for interferometry. This is because of the many ways in which the output frequency may be stabilised, and general ease of operation of the He-Ne laser. The most stable lasers are frequency-locked to iodine [21] and form the working optical frequency standard for the unit of length from the definition of the metre [16]. The international agreement on the frequency of this laser is at a 3σ level of $\pm 1 \times 10^{-9}$ of the optical frequency. The laser may also be locked to the Lamb dip, by monitoring the Zeeman beat [22] or by intensity balancing the modes of a two-mode laser [20]. This latter system is especially useful as a source for some displacement measuring interferometers where an accuracy of around $\pm 1 \times 10^{-7}$ needs to be realised [23]. In the measurement of gauge-blocks, for example, other frequency stabilised lasers are required and, for some years at NPL, an Ar/Kr laser was used [24]. This needed computer control to ensure that the laser locked to the correct iodine component [25]. More recently, manufacturers have produced He-Ne lasers operating at 543 nm, 593 nm, and 612 nm and these have been frequency stabilised for use in multi-wavelength interferometry [26]. He-Ne lasers are to be preferred to Ar/Kr lasers because the latter require high electrical power and water cooling, and are generally more costly and complicated to operate.

It has been possible to frequency-stabilise the gas discharge lasers mentioned in the previous paragraph, because of the fortuitous overlap of the emitted frequency with iodine absorptions. However, in many cases, the only way in which some other spectroscopic transitions may be used for this purpose is if the laser is frequency tunable over a wide range. Absorptions other than in iodine may be useful perhaps because the reference frequency needed is outside the absorption band of iodine (≈500 nm to 650 nm) or else because other species produce a narrower, more reproducible feature, such as in an ion trap [27]. The principal types of frequency tunable lasers are either based upon a liquid dye [28] or are solid state. Dye lasers have principally been used to date, because no other tunable laser was available over much of the visible part of the spectrum. However, they require an Ar^+ or Kr^+ pump laser, are very costly to purchase, difficult to operate, and the dyes themselves are generally toxic.

The number of different types of solid-state lasers available rapidly increased during the late 1980s. Some, such as the Ti-sapphire laser [29] require an Ar^+ laser to pump them, but others are pumped by a high power diode laser array. Such a device, for example the Nd:YAG laser at 1.06 μm, is therefore truly an all solid-state laser. Of all the solid-state lasers available, the most important group is probably diode lasers. These have the advantage that they are not optically pumped, but are directly electrically pumped, by passing a current through the semiconductor junction. Diode lasers are available in a number of forms, but the important type for this thesis, are low power index-guided single frequency devices. It is probably only with the advent of room-temperature single mode lasers that diode lasers have found real usefulness in atomic physics [7]. Interest has escalated since about 1981 with the introduction of low-cost devices, chiefly marketed for CD

players or laser printers. Such lasers are GaAlAs devices with a typical design wavelength of 780 nm, although 750 nm and 820 nm diodes are also available. The wavelength coverage may be extended into the blue, by frequency doubling. Although, initially, available powers were small [30,31], strong advances to produce mW levels of blue light have been made [32,33]. During this similar period, interest rapidly grew in optical fibre communications, and for this purpose GaInAsP devices at 1.3 μm and 1.55 μm are marketed. Further, with the wish for diode manufacturers to compete more easily with the He-Ne laser market, for example in bar code readers, advancing technology enabled 670 nm (AlGaAsP) diodes to be marketed from about 1988. Initially, though, devices were not normally single mode, but in late 1989 the first index-guided single mode device at 670 nm was marketed (Toshiba TOLD 9211). Diode lasers are much easier to use than dye lasers, are of much lower cost, yet also have the property of frequency tunability. They also require no high voltage supplies and have low electrical power consumption. A dye laser system with an ion pump laser typically requires 40 kW electrical power to produce 1 W output. In contrast, a diode laser needs typically only 50 mA at 2 V (100 mW) to produce 5 mW laser light output. A diode laser also offers the potential of a more compact system than a He-Ne laser. However, diodes have some operational problems which are outlined in the next section. Many of these are easily corrected and are far outweighed by the overall advantages. However, it usually leaves the operator in the situation where the cost of the external optics and drive electronics is much greater than that of the diode, especially if it emits at a commercially popular wavelength.

This thesis therefore enquires whether and how diodes can be used in interferometry as well as spectroscopy. The operational problems need to

be itemised and solved. Perhaps solid state devices will eventually replace the dye and even the He-Ne laser in such applications.

1.3 General Optical and Spectral Properties of Laser Diodes

The optical properties of the beam emitted from a laser diode have a number of notable differences from other types of laser, as indicated in the previous section. It is important to understand and attend to the resulting problems these differences may provide, before using diodes in either interferometry or spectroscopy.

Although it is not the intention to provide a detailed description of the underlying semiconductor physics of a laser diode, some details will help to explain the laser optical properties. In the previous section, various types of laser diode were briefly mentioned, and it should be re-emphasised that the diodes used here are mainly single-mode index-guided GaAlAs devices. A more detailed description of the spectral and spatial properties of the beam will be given later, but these lasers emit in a fundamental spatial mode and single longitudinal mode. Such devices are therefore the most useful either for spectroscopy or interferometry. Such a laser, sometimes termed a double heterostructure device, is shown schematically in figure 1.3.1. The term "double heterostructure" arises because the active layer ($Ga_{1-y}Al_yAs$) is sandwiched between two layers of $Ga_{1-x}Al_xAs$. The mole fraction of Al in the two outer layers (x) is greater than that in the active layer (y). The bandgap of the active layer, and hence the emitted optical frequency, increases with the mole fraction of Al. Manufacturers are therefore able to use this fact to provide, for example, AlGaAs lasers with nominal wavelengths of 750 nm, 780 nm or 820 nm. When a current flows, as indicated in figure 1.3.1, a population inversion occurs

between the ground and excited states (the valence and conduction bands of the semiconductor respectively) of the active layer. Within this region, electrons (the minority carriers) re-combine with holes to produce photons with a frequency approximately equivalent to the bandgap energy. In addition to assisting the population inversion mechanism, the double heterostructure also aids in providing an effective waveguide for these emitted photons. This is because the active region has a higher refractive index than the adjacent layers. The width of this active region is typically less than one micron. To achieve single-mode operation, the light also needs to be confined in the lateral direction. This is achieved by building into the active region a spatial variation of the real part of the refractive index. If this not done, then the lateral width of the active layer is determined only by the current distribution through the semiconductor. Such lasers are termed "index-guided" and "gain-guided" respectively. Generally, only index-guided devices lase in a single longitudinal mode, and gain-guided devices may emit in up to around ten modes with a total bandwidth of around 1 THz.

In summary, then, this laser consists of a waveguide cavity of length ≈300 μm and cross-section perhaps typically 1 μm by 2 μm. For an index-guided laser the photons are confined by a similar mechanism both parallel and perpendicular to the active stripe, reducing astigmatism in the output beam. We now turn to the effects that these laser parameter values have on the laser beam itself.

The most obvious features of a diode laser output beam are that it is both rapidly divergent and elliptical in shape. This may be readily understood from the small active cross-section of the diode. In the case of Gaussian beams, the 1/e radius, the waist (w_o) and the angular

divergence (θ) are related by

$$\theta = \lambda/\pi w_o \qquad (1.3.1)$$

yielding $\theta \approx 14°$ for $w_o = 1$ μm, for example, at a wavelength (λ) of 780 nm. The elliptical nature can be understood by considering the rectangular cross-section, which will provide a more rapidly divergent beam along an axis perpendicular to the lasing stripe. Although equation (1.3.1) is derived from Gaussian optics [34], the unconventional nature of the cavity suggests that we should not necessarily expect a Gaussian output from a diode laser [35]. In contrast, for interferometry, a collimated, nominally Gaussian circular beam is preferred. To overcome these problems, the first task is to collimate the beam. There are a number of suitable diode laser collimators available commercially and a choice can be made depending upon the size of the beam required. It is likely that some of the output beam will be apertured, although this will depend upon the lens numerical aperture (NA). For example, for an 0.276 NA lens the collection efficiency for a Mitsubishi ML-4102 laser was measured to be 50%. For the same laser and an 0.46 NA lens, this efficiency was increased to 70%. Microscope objectives typically produce a beam of a few mm in diameter. In some experiments described here, a small beam is required and can be generated as needed using a further pair of lenses. A small beam ($w_o \approx 1$ mm) can be produced directly using a graded-index (GRIN) lens [36]. Such a lens is typically 2 mm in diameter and 4 mm long and a radial refractive index gradient is produced by an ion diffusion process. In deciding which lens to use, and hence the required beam diameter, consideration needs to be given to the non-Gaussian nature of the beam and the way in which it propagates in free space. Whereas a true Gaussian beam will simply diverge as it propagates and retain a Gaussian shape, a diode laser beam is prone to both diverge and

distort. The beam will propagate without too much distortion over distances $\approx kw_o^2$ ($k = 2\pi/\lambda$), which in Gaussian optics, is the confocal parameter. In the case of one lens which provided an 8 mm diameter beam, this corresponds to a distance of around 10 m. Once the beam is collimated, it may be made circular using either anamorphic prism pairs or a pair of cylindrical lenses [37]. The former method was used exclusively here, because it has the advantage of compactness. In figure 1.3.2, the beam profiles of a Mitsubishi ML-4102 laser are shown just after collimation and transmission through a 3:1 anamorphic prism pair and at $z \approx 8$ m from the diode. The profile was measured using a 200 μm pinhole on a micrometer slide both parallel and perpendicular to the active stripe of the laser. The beam is apertured partly by the collimating lens and partly by the anamorphic prism giving a typical overall transmission of 50%, so that around 1.5 mW is available from a 3 mW diode.

It has already been stated that the manufacturers can vary the design wavelength by varying the Al content in the active layer. Given a particular diode, the frequency is further determined by the operating temperature and current. Typical tuning curves have been published before [7,38] and similar features were found for our diodes (figure 1.3.3), but with no examples of anomalous tuning [39]. Since the effective cavity length is so short (≈300 μm), the cavity mode spacings are large - typically 120 GHz for Mitsubishi or Hitachi 780 nm lasers. A tuning curve for a 670 nm diode (Toshiba TOLD 9211) is also presented (figure 1.3.4), which has a similar cavity mode spacing (180 GHz). The optical frequency measurements for figures 1.3.3 and 1.3.4 were performed using an NPL-designed wavemeter [40] referenced to a Zeeman-beat stabilised He-Ne laser [22]. The diode is mounted on a copper heatsink which may be heated or cooled with a Peltier device, and

it is the temperature of this block which controls the laser frequency over a large range. At a typical laboratory temperature of 19°C, the copper heatsink could be controlled over the range -17°C to +55°C. This changes the emitted frequency by ≈8 THz (17 nm). The slope of the continuous lines in figure 1.3.3 is about 30 GHz/°C. The continuous tuning with temperature results from a changing effective cavity length. Temperature also tunes the band gap, but with a larger coefficient, so that after some continuous tuning, the laser mode-hops. These mode-hop frequencies are quite reproducible in the short-term, but it is observed that the mode-hop positions shift with time. The mode-hop frequencies are a function of output power, as demonstrated in figure 1.3.3. This figure also demonstrates the existence of tuning hysterisis to a small extent, and that mode-hops are not necessarily to the adjacent mode. For spectroscopic applications, these tuning properties will need to be considered when buying a diode.

A further problem to consider when dealing with diode lasers is the spectral linewidth, which is considerably greater than for other cw single frequency lasers [41,42,43]. This is a very important topic because of the consequences in interferometry and spectroscopy and chapter 3 concentrates on its analysis and techniques for its reduction. In interferometry, the laser linewidth determines the available fringe visibility and in spectroscopy, a large laser linewidth limits the spectral resolution available. Furthermore, although these lasers are described as "single frequency", no diode is truly single mode. Perhaps around 95% of the power will be in one mode. Relaxation oscillation sidebands a few GHz away will exist, as well as weak adjacent longitudinal modes ≈120 GHz away. At some temperatures and currents a "single mode" diode may lase simultaneously in two or more modes of comparable power or not lase stably in one mode. A laser operating in

such a way is clearly unusable in spectroscopy or interferometry. However, in general it is possible to ignore the ~5% power or less emitted from a diode laser not in the main lasing mode.

The presence of weak optical feedback is also observed to be a problem when operating laser diodes, even at feedback levels of around 1×10^{-5} (50 dB). Higher feedback levels affect the linewidth and single mode operation of the laser. This suggests that special care is required and that all optical components such as lenses, detectors, silica cell windows or even optical choppers need to be thought of as potential feedback sources. In general, tilting at a small angle away from normal incidence may be sufficient.

The final two properties worth noting are that the output is polarised, and that the output may be slightly astigmatic. The polarisation properties arise from the waveguide nature of the cavity [7] and, although this was not independently checked, the polarisation ratio is claimed to be over 100 by manufacturer's data sheets. The emitted beam is polarised parallel to the direction of the lasing stripe. Such information is useful when specifying dielectric reflecting or partly-reflecting optical coatings or when designing length-measuring interferometers which use the polarisation of the laser source to achieve bi-directional counting [23]. In practice, astigmatism in index-guided lasers turns out to be small and of little importance. No steps were necessary to correct for this.

In conclusion, the diode laser beam needs to be collimated and made circular. Care needs to be taken to avoid optical feedback. The diode laser linewidth is sufficiently narrow for much initial useful work to be done, as described in chapter 2.

1.4 Overview of Spectral Lines coincident with Commercially-available laser diode wavelengths

In this section, the spectral lines that might be investigated with a laser diode are reviewed. These spectroscopic transitions will be used to provide a frequency-stabilised diode laser. It is therefore useful firstly to consider the requirements of such a frequency reference.

The primary requirements for a high quality standard are that the atomic or molecular transition should provide a narrow feature, reproducible in frequency. The atoms or molecules used for the reference should ideally be usable at room temperature in an evacuated glass or silica cell, for general ease of use. It should not readily be susceptible to the effects of electric or magnetic fields. A typical order of magnitude estimate for the magnetic field (Zeeman) shift is $\approx e/2\pi m$ = 28 GHz/T, where e/m is the electron charge to mass ratio. For the earth's field of ≈0.1 mT, this will produce shifts of about 1×10^{-8} of the optical frequency. Ideally, therefore, the first-order Zeeman shift should be zero, which will be the case for selected transitions. It has been stated that the transition should be narrow, and, generally we shall consider transitions "allowed" by the normal selection rules of quantum mechanics, which typically have a width of a few MHz and interrogate using a Doppler-free technique. So-called "forbidden" transitions involving states with a very long lifetime (typically > 1 ms) cannot be used, since their full potential could only be realised with a very narrow linewidth laser (< 1 kHz). As already mentioned in the previous section, diode lasers have broad linewidths, and even "allowed" transitions will be further broadened by the laser width.

Diode lasers are available at the infra-red wavelengths of 1.3 μm, 1.55 μm

(InGaAsP diodes), and from 3 μm to 30 μm for the lead salt family of diodes. The stabilisation of infra-red diodes, especially at 1.3 μm and 1.55 μm is of great importance in optical fibre coherent communications systems. Efforts to produce a narrow linewidth system [44] and frequency stabilisation of the output [45] are directed towards this market. However, for interferometry, a shorter wavelength output is desirable. This is partly because optical alignment is much easier if the beam is easily visible to the human eye, but also diffraction errors are much reduced at the shorter wavelength. Such visible or near-visible wavelengths available with diodes are 670 nm and 740 nm to 840 nm (GaAlAs lasers).

Before discussing potential absorbers, methods for containing such vapours or gases need to be reviewed briefly. For many gaseous atoms or molecules, containment in a silica or Pyrex cell is most appropriate. If a vapour is considered, where the cell also contains the element as a solid, the pressure and temperature can be separately controlled. This is achieved by providing a delibrate cold point in the cell (T_c) which is controlled by one temperature controller, and heating the cell wall to another temperature (T_w, where $T_w > T_c$). The temperature T_w then determines the vapour temperature, and hence the occupancy of the lower states, and T_c determines the vapour pressure. The use of a cold point well away from the windows prevents the solid material depositing on the windows. Atomic or molecular species which cannot be satisfactorily heated in a cell can often be heated in a heatpipe oven [46,47]. This straightforward method provides a vapour with a homogeneous temperature distribution, and also keeps the vapour away from the windows.

For fixed-frequency lasers, such as He-Ne or Ar^+ lasers, operating in the 500 nm to 650 nm region, iodine has been the obvious choice to date

[48]. Not only does iodine fulfill all the advantages listed above, but it provides a vast comb of thousands of lines from the dissociation limit at 500 nm to the red part of the spectrum. These lines arise from the molecular rotational-vibrational quantum levels and give a high probability that any laser which can tune a few hundred MHz can be tuned to a hyperfine transition of a particular rotational-vibrational sub-level. The limit at 650 nm is not exact, but arises because the absorptions become weaker as the transitions have to involve lower states with a high vibrational quantum number. The lower state, however, can be populated by heating the cell, perhaps to 100°C, and using longer cells to enhance the absorption. This should provide many suitable references at 670 nm. By heating the cell to 100°C, use of iodine has been reported at 830 nm [49]. Two other possible molecular absorbers at 670 nm are Na_2 and K_2, which may both be used in a heatpipe oven. Flourescence of Na_2 at the He-Ne line at 640 nm has been observed [50], for example. An alternative would be the Li D resonance lines and Li can be used in a heatpipe oven, but needs to be heated to 1000°C [51]. However, clearly iodine is the favoured canditate for the 660 nm to 670 nm wavelength region.

In the 750 nm to 850 nm region, the choice appears rather more limited [7]. Apart from some weak absorption lines in water vapour [52] or NO_2 [53], only atomic transitions appear to be available. Lines in Ar, Ne and Kr are accessible, but since the states involved are not ground states, these lines can only conveniently be accessed by optogalvanic spectroscopy (section 2.2). Another group of atoms which may be used are the alkali metals K, Rb and Cs. The principal resonance lines which may be accessed are 767 nm or 770 nm in K [54], 780 nm or 795 nm in Rb [55,56,57,58], and finally 852 nm in Cs [59,60]. Lines in Bi and Na have also been investigated in this part of the spectrum. Heatpipe ovens are

necessary for Bi, Na and K, but the absorptions in Rb and Cs are so strong that room temperature silica cells may be used. These lines can also be investigated using the optogalvanic effect.

Finally, we may briefly observe that the second harmonic of the diode output may also be used. This may be generated either with a non-linear crystal such as $KNbO_3$ [31], but a small proportion of the natural laser output, typically 10 pW, is actually at the second harmonic. The line in K, for example, at 405 nm ($5p^2P_{1/2} \rightarrow 4s^2S_{1/2}$) has been observed in this way [61]. An IR laser at 1.59 μm has also been similarly been used to investigate the Rb D_2 line at 795 nm [45].

The majority of this thesis is concerned with the lasers in the 780 nm region, although some results on the newly-available 670 nm or 660 nm diodes are also presented. The Rb D lines were therefore selected as the most convenient reference at ≈ 780 nm. These nominally 780 nm lasers have been found to emit between 775 nm and 794 nm and all of these could be temperature tuned to the region of one of the two D lines at 780 nm or 795 nm. Rb can be used in a room temperature Pyrex cell, typically only 75 mm long. Since only two lines are present in Rb, there is no ambiguity in tuning to these lines. If an absorption is observed, it will be obvious which D line is being accessed and no routine use of a wavemeter is necessary as it would be, for example, if iodine were used, with its vast comb of transitions [48]. The principal disadvantage, as will be seen is that the lines are all broadened by an applied magnetic field. The general ease of use of Rb, however, appeared to outweigh this disadvantage and so the choice was made to concentrate on Rb.

1.5 Brief survey of recent related work

This section sets the thesis in the context of similar work reported in the literature. Although this thesis contains much original work, nevertheless it draws upon published ideas in the areas of diode laser frequency stabilisation, Rb spectroscopy and length measurement. The area of atomic beam cooling is also mentioned because it is such an interesting future application of laser diodes in the area of optical frequency metrology.

All the work referred to on diode lasers has been published since the early 1980s when room temperature single frequency diode became readily available commercially [7]. Although frequency stabilisation of laser diodes was reported quite quickly [62,63], such a system was not actually applied in metrology. However, the authors mention optical metrology as a possible application [63], although such an application requires the measurement of particular frequencies by various national standards laboratories. It would also require a study of causes of frequency shifts and reproducibility to the required accuracy. For such an application, a standard based upon a simple absorption cell is likely to be much more satisfactory because of shifts which may be associated with the nature of the lamp in optogalvanic spectroscopy. Rubidium spectra obtained with diodes using cells or Rb beams have been published [55-57,64,65,66]. FM spectroscopy, of a type similar to that demonstrated on Rb in section 4.4, has also already been demonstrated in Rb at 780 nm [67]. However, these authors were primarily interested in obtaining spectra *per se*, rather than necessarily obtaining them in a form suitable for frequency stabilisation. In general, the spectra obtained here, particularly with the optically narrowed diode of chapter 3, are of noticeably better quality than previously published.

The Rb D lines are also useful to demonstrate spectroscopic techniques not only with diode lasers, but also with a single frequency $Ti:Al_2O_3$ laser [68]. The higher power available from this laser, as opposed to diodes, enables these authors to probe two-photon transitions in Rb also. Of the other alkali metals, K [54] and Cs [59,60] D lines can be accessed by diode lasers, or the $Ti:Al_2O_3$ laser.

The alkali metal transitions have been fairly well catagorised [69] in terms of their state lifetimes, hyperfine constants and $^{87}Rb:^{85}Rb$ isotope shift. However, the Rb hyperfine constants, isotope shift and absolute optical frequencies have not previously been determined to the precision demonstrated in this thesis. Work has also been published on the theoretical linear absorption line strengths in Rb [70] and how these relate to the saturated absorption line strengths in Rb [71].

There is considerable interest in Rb and Cs in particular, because of the importance of the ground state splitting in time and frequency standards work [72]. Diode lasers could provide the new basis for observing the transition used in Cs in the definition and realisation of the second. Such a method of realisation would not be practicable without the use of a relatively simple diode laser as the source. Also, an atomic clock must run continuously, clearly ruling out a dye laser as such a source. A similar motivation lies behind work on cooling a beam of Cs atoms [73] or Rb [74]. Also, Cs or Rb are useful to investigate atomic cooling just because diode lasers can be used instead of the more costly dye laser. It is clearly an exciting possibility that a future microwave standard might utilise a laser cooled Cs atom in an atomic trap. Ion trap optical frequency standards, too, are bound only to receive widespread use when these, too, can use only diode or all-solid state laser sources.

Finally, we turn to work already published on diode lasers in length measurement applications. To date, no one has simply used diodes in precision length interferometry with a stabilised reproducible diode laser frequency to replace a stabilised He-Ne laser. The advantages of diode lasers are not fully realised by such a direct replacement. For example, the low cost of diodes might increase the widespread use of interferometry in low accuracy work. Some diode laser interferometer systems are already on the commercial market. Some applications, for example in surface roughness measurement, require high resolution, but not great accuracy. An unstabilised diode laser might be sufficient. One might also devise new methods of length measurement [75,76,77,78], based upon diode frequency or amplitude modulation, or multi-wavelength interferometry.

There is clearly a growing interest in the use of laser diodes in many areas of optical frequency metrology, and this thesis sets out to explore some of these, with special emphasis on length interferometry.

1.6 Outline and Scope of Thesis

The general aim of this thesis is to explore the potential for laser diodes in the area of interferometry, specifically aimed towards length or displacement mesurement. Some of the results, for example in chapter 3 on linewidth reduction, will be relevant for optical frequency metrology generally, for example in the area of ion trapping [79], or Cs beam atom cooling and atom traps [73]. Wider applications for such techniques might be found in the areas of coherent optical communications or optical fibre sensors. The emphasis of this thesis is experimental rather than theoretical, and furthermore concentrates on results achieved on the quantum optical and spectroscopic aspects of the

work. Electronic circuit diagrams are generally available elsewhere [80,81]. Also, spectroscopic techniques such as saturation spectroscopy are described in detail if used extensively in this thesis. However, other techniques are available in spectroscopy, and these are described in detail in review articles [82,83]. The remaining chapters of this thesis are described, in broad outline, below.

The following chapter contains work on spectroscopy achieved using a basic laser, with no external modifications, for example to reduce the emitted linewidth. It will become clear, however, that a special effort is needed to reduce the linewidth, and that considerable advantages will be afforded if this is done. A complete chapter is devoted to the laser linewidth, together with efforts to reduce it. This third chapter concludes with a section on a spectroscopic application of the linewidth-reduced system.

In order to use diode lasers in absolute interferometric length measurements, the laser frequency needs to be stabilised. This is achieved using the Rb D line absorptions as frequency references. It is also necessary to understand some of the theory behind the energy level structure of Rb. Measurements of the stabilised laser frequency and frequency interval measurements between closely spaced (hyperfine) transitions will also be necessary. Chapter 4 is therefore concerned with discussions of the means to stabilise the laser frequency and assessment of how stable the frequency actually is. Chapter 5 details measurements on the frequency reproducibility, hyperfine interval measurements and determination of the optical frequency. This chapter also contains analysis of the Rb spectral lines.

The main part of the thesis concludes, in chapter 6, with an application

in distance measurement, using the technique of swept wavelength interferometry. This application draws upon the results and technology developed in the previous chapters. The accuracy of such a system is discussed, together with efforts to automate such a measurement process. The main achievements of the whole thesis are finally summarised in chapter 7, together with ideas for further areas of progress, suggested by work in this thesis.

References

[1] TM Maiman, Nature, 187, 493-4, (1960)

[2] A Javan, WR Bennett Jr, DR Herriot, Phys Rev Lett, 6, No 3, 106-10, (1961)

[3] AD White, EI Gordon, JD Rigden, Appl Phys Lett, 2, No 5, 91-3, (1963)

[4] RN Hall, GE Fenner, JD Kingsley, TJ Soltys, RO Carlson, Phys Rev Lett, 9, No 9, 366-8 (1962)

[5] MI Nathan, WP Dumke, G Burns, FH Dills, G Lasher, Appl Phys Lett, 1, 62-4, (1962)

[6] TM Quist, RJ Keyes, WE Krag, B Lax, AJ McWhorter, RH Rediker, HJ Zeiger, Appl Phys Lett, 1, 91-2 (1962)

[7] JC Camparo, Contemp Phys, 26, No. 5, 443-77 (1985)

[8] CE Wieman, L Hollberg, Rev Sci Instrum, 62, No 1, 1-20, (1991)

[9] TJ Kane, RL Byer, Opt Lett 10, No 2, 65-7 (1985)

[10] J Dyson, "Interferometry as a measuring Tool", Machinery Publishing Co Ltd, Brighton (1970)

[11] AA Michelson, J Phys 3, 5-22 (1894)

[12] AA Michelson, "Metre in terms of Wave-lengths of light", Travaux et Mém. Bur. Intern. des Poids et Mesures, 11, 1-237 (1895)

[13] B Edlen, Metrologia, 2, 71-80 (1966)

[14] MJ Downs, KP Birch, Appl Opt, 28, No 5, 825, (1989)

[15] WRC Rowley, Phys Bull, 35, 282-4 (1984)

[16] Metrologia, 19, 163-77 (1984)

[17] DR Herriot, "Some application of lasers to Interferometry", Progress in Optics, 6, 171-209 (1967) ed by E Wolf

[18] AL Bloom, "Gas lasers and their applications to precise length measurements", Progress in Optics, 9, 1-30, (1971), ed by E Wolf

[19] O Kafri, Opt Lett, 14, No 13, 657-8, (1989)

[20] SJ Bennett, RE Ward, DC Wilson, Appl Opt, 12, No 7, 1406, (1973)

[21] AJ Wallard, J Phys E, 5, 926-30, (1972)

[22] WRC Rowley, Meas Sci Technol, 1, 348-51, (1990)

[23] KW Raine, MJ Downs, Prec Eng, 85-88 (1979)

[24] P Gill, SJ Bennett, Metrologia, 15, 117-23 (1979)

[25] P Gill, JA Clancy, J Phys E;Sci Instrum, 21, 213-8 (1988)

[26] WRC Rowley, P Gill, Appl Phys, B51, No 6, 421-6, (1990)

[27] RC Thompson, GP Barwood, P Gill, Optica Acta, 33, No 4, 535-43, (1986)

[28] TF Johnston Jr, RH Brady, W Profitt, Appl Opt, 21, 2307-16, (1982)

[29] PA Schulz, IEEE J Qu El, 24, 1039-44 (1988)

[30] EJ Lim, MM Fejer, RL Byer, WL Kozlovsky, Electron Lett, 25, No 11, 731-2, (1989)

[31] JC Baumert, P Günter, H Melchior, Opt Comm, 48, No 3, 215-20 (1983)

[32] WJ Kozlovsky, W Lenth, EE Latta, A Moser, GL Bona, Appl Phys Lett, 56, No 23, 2291-2 (1990)

[33] L Goldberg, MK Chun, Appl Phys Lett, 55, No 3, 218-20 (1989)

[34] H Kogelnik, T Li, Proc IEEE, 54, No 10, 1312-29 (1966)

[35] W Striefer, RD Burnham, DR Scrifres, IEEE J Qu El, QE-15, No 3, 136-41 (1979)

[36] EW Marchand, "Graded Index Lenses", Progress in Optics, 11, 305-337, (1973), ed by E Wolf

[37] D Kuntz, Laser Focus/Electro-Optics, 44-55, March 1984

[38] M Nakamura, K Aiki, N Chinone, R Ito, J Umeda, J Appl Phys, 49, No 9, 4644-8 (1978)

[39] JC Camparo, CH Volk, IEEE J Qu El, QE-18, No 12, 1990-1, (1982)

[40] SJ Bennett, P Gill, J Phys E;Sci Instrum, 13, 174-7,(1982)

[41] D Welford, A Mooradian, Appl Phys Lett, 40, No 10, 865-7, (1982)

[42] CH Henry, IEEE J Qu El, QE-18, No 2, 259-64 (1982)

[43] J Arnaud, Electron Lett, 22, No 10, 538-40 (1986)

[44] R Wyatt, WJ Devlin, Electron Lett, 19, No 3, 110-2 (1983)

[45] M Ohstu, E Ikegami, Electron Lett, 25, No 1, 22-3 (1989)

[46] CR Vidal, FB Haller, Rev Sci Inst, 42, No 12, 1779-84, (1971)

[47] MM Hessel, P Jankowski, J Appl Phys, 43, No 1, 209-11, (1972)

[48] P Luc, J Mol Spect, 80, 41-55 (1980)

[49] H Ludvigsen, E Ikonen, Annual Meeting of the Finnish Society, 30 March to 1 April 1989

[50] SE Johnson, K Sakurai, HP Broida, J Chem Phys, 52, No 12, 6441-2, (1970)

[51] H Welling, B Wellegehausen, Springer Series in Optical Sciences, 7, Laser Spectroscopy III, New York, Springer-Verlag, 365-9, (1977)

[52] H Tsuchida, M Ohstu, T Tako, Japan J Appl Phys 21, No 1, L1-L3 (1982)

[53] W Lenth, M Gehrtz, Appl Phys Lett, 47, No 12, 1263-5, (1985)

[54] VL Velichanskii, AS Zibrov, VS Kargopol'tsev, OR Kachurin, VV Nikitin, VA Sautenkov, GG Kharisov, DA Tyurikov, Sov J Qu El, 10, No 10, 1244-7, (1980)

[55] JC Camparo, CM Klimcak, Am J Phys, 51, No 12, 1077-81, (1983)

[56] T Sato, S Yashima, M Shimba, Electron Lett, 22, No 19, 979-81, (1986)

[57] H Tsuchida, M Ohstu, T Tako, N Kuramochi, N Oura, Japan J Appl Phys, 21, No 9, L561-3, (1982)

[58] DC Webb, JDC Jones, DA Jackson, Electron Lett, 24, No 16, 1002-4 (1988)

[59] B Bölger, JC Diels, Phys Lett A, 28, No 6, 401-2 (1968)

[60] VA Sautenkov, VL Velichanskii, AS Zibrov, VN Luk'yanov, VV Nikitin, DA Tyurikov, Sov J Qu El, 11, No 9, 1131-4, (1981)

[61] K Sakurai, N Yamada, Opt Lett, 14, No 4, 233-5, (1989)

[62] S Yamaguchi, M Suzuki, Appl Phys Lett, 41, No 7, 597-8, (1982)

[63] S Yamaguchi, M Suzuki, IEEE J Qu El, QE-19, No 10, 1514-9, (1983)

[64] AM Akulshin, VA Sautenkov, VL Velichansky, AS Zibrov, MV Zverkov, Opt Comm, 77, No 4, 295-8 (1990)

[65] M Suzuki, S Yamaguchi, IEEE J Qu El, 24, No 12, 2392-9, (1988)

[66] M Têtu, B Villeneuve, N Cyr, P Tremblay, S Thériault, M Breton, IEEE J Lightwave Tech, 7, No 10, 1540-8, (1989)

[67] S Nakanishi, H Ariki, H Itoh, K Kondo, Opt Lett, 12, No 11, 864-6, (1987)

[68] CS Adams, AI Ferguson, Opt Comm, 75, No 5,6, 419-24, (1990)

[69] E Arimondo, M Inguscio, P Violino, Rev Mod Phys, 49, No 1, 31-75, (1977)

[70] A Gallagher, EL Lewis, J Opt Soc Am, 63, No 7, 64-9, (1973)

[71] S Nakayama, Japan J Appl Phys, 23, 879-83, (1984)

[72] PB Coates, J Phys E;Sci Instrum, 21, 812-6, (1988)

[73] RN Watts, CE Wieman, Opt Lett, 11, No 5, 291-3 (1986)

[74] A Hemmerich, DH McIntyre, D Schropp Jr, D Meschede, TW Hänsch, Opt Comm, 75, No 2, 118-22 (1990)

[75] T Kubota, M Nara, T Yoshino, Opt Lett, 12, No 5, 310-2, (1987)

[76] G Beheim, K Fritsch, Electron Lett, 21, No 3, 93-4, (1985)

[77] H Kikuta, K Iwata, R Nagata, Appl Opt, 25, No 17, 2976-80, (1986)

[78] CC Williams, HK Wickramasinghe, Opt Lett, 14, No 11, 542-4, (1989)

[79] DJ Wineland, WM Itano, RS Van Dyck Jr, Adv At Mol Phys, 19, 135-86, (1983)

[80] GP Barwood, P Gill, WRC Rowley, NPL Report MOM 85, (1987)

[81] KC Shotton, WRC Rowley, NPL Report Qu 28, (1978)

[82] AI Ferguson, J Mod Optics, 35, No 3, 283-95, (1988)

[83] RC Thompson, Rep Prog Phys, 48, 531-78, (1985)

between the ground and excited states (the valence and conduction bands of the semiconductor respectively) of the active layer. Within this region, electrons (the minority carriers) re-combine with holes to produce photons with a frequency approximately equivalent to the bandgap energy. In addition to assisting the population inversion mechanism, the double heterostructure also aids in providing an effective waveguide for these emitted photons. This is because the active region has a higher refractive index than the adjacent layers. The width of this active region is typically less than one micron. To achieve single-mode operation, the light also needs to be confined in the lateral direction. This is achieved by building into the active region a spatial variation of the real part of the refractive index. If this not done, then the lateral width of the active layer is determined only by the current distribution through the semiconductor. Such lasers are termed "index-guided" and "gain-guided" respectively. Generally, only index-guided devices lase in a single longitudinal mode, and gain-guided devices may emit in up to around ten modes with a total bandwidth of around 1 THz.

In summary, then, this laser consists of a waveguide cavity of length ≈300 μm and cross-section perhaps typically 1 μm by 2 μm. For an index-guided laser the photons are confined by a similar mechanism both parallel and perpendicular to the active stripe, reducing astigmatism in the output beam. We now turn to the effects that these laser parameter values have on the laser beam itself.

The most obvious features of a diode laser output beam are that it is both rapidly divergent and elliptical in shape. This may be readily understood from the small active cross-section of the diode. In the case of Gaussian beams, the 1/e radius, the waist (w_o) and the angular

(i) z = 0.3 m

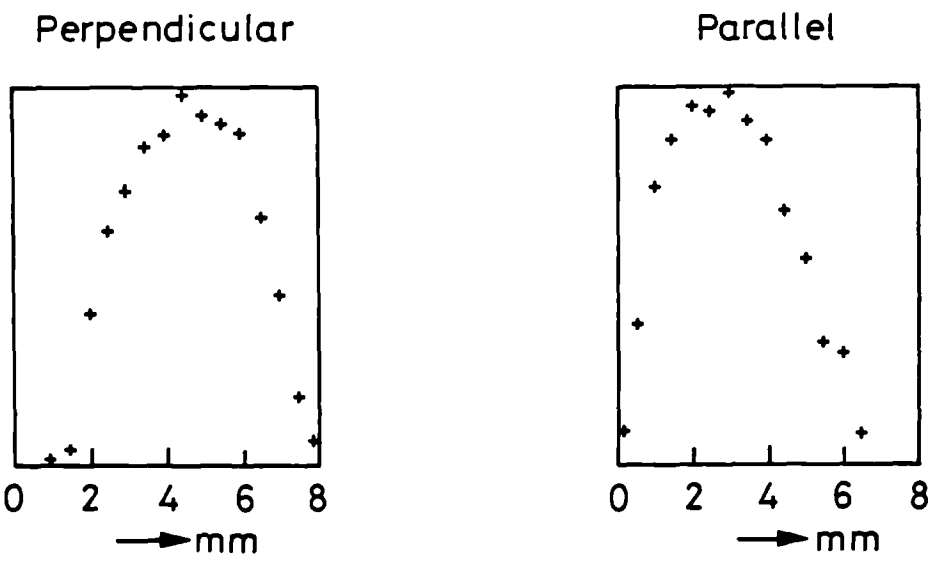

(ii) z = 8 m

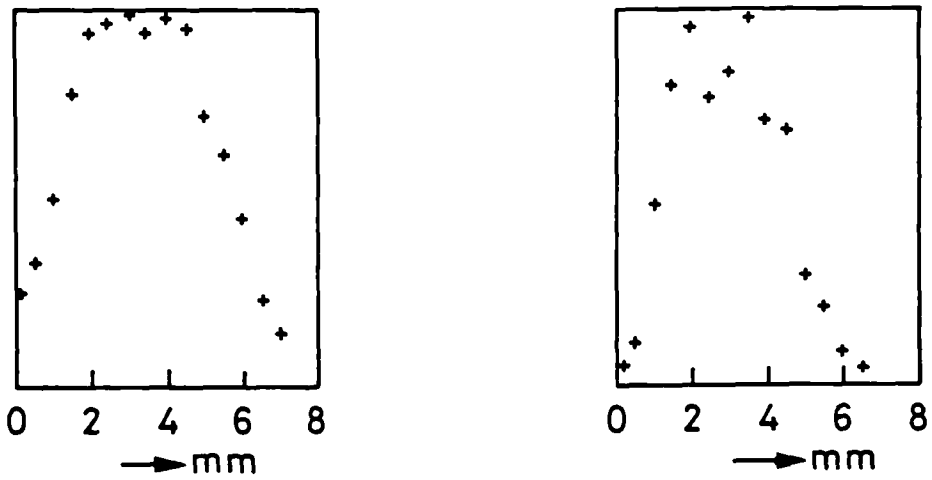

1.3.2 Measured beam profile of a 780 nm laser diode (Mitsubishi ML-4102), parallel and perpendicular to the lasing stripe at z = 0.3 m and z = 8 m

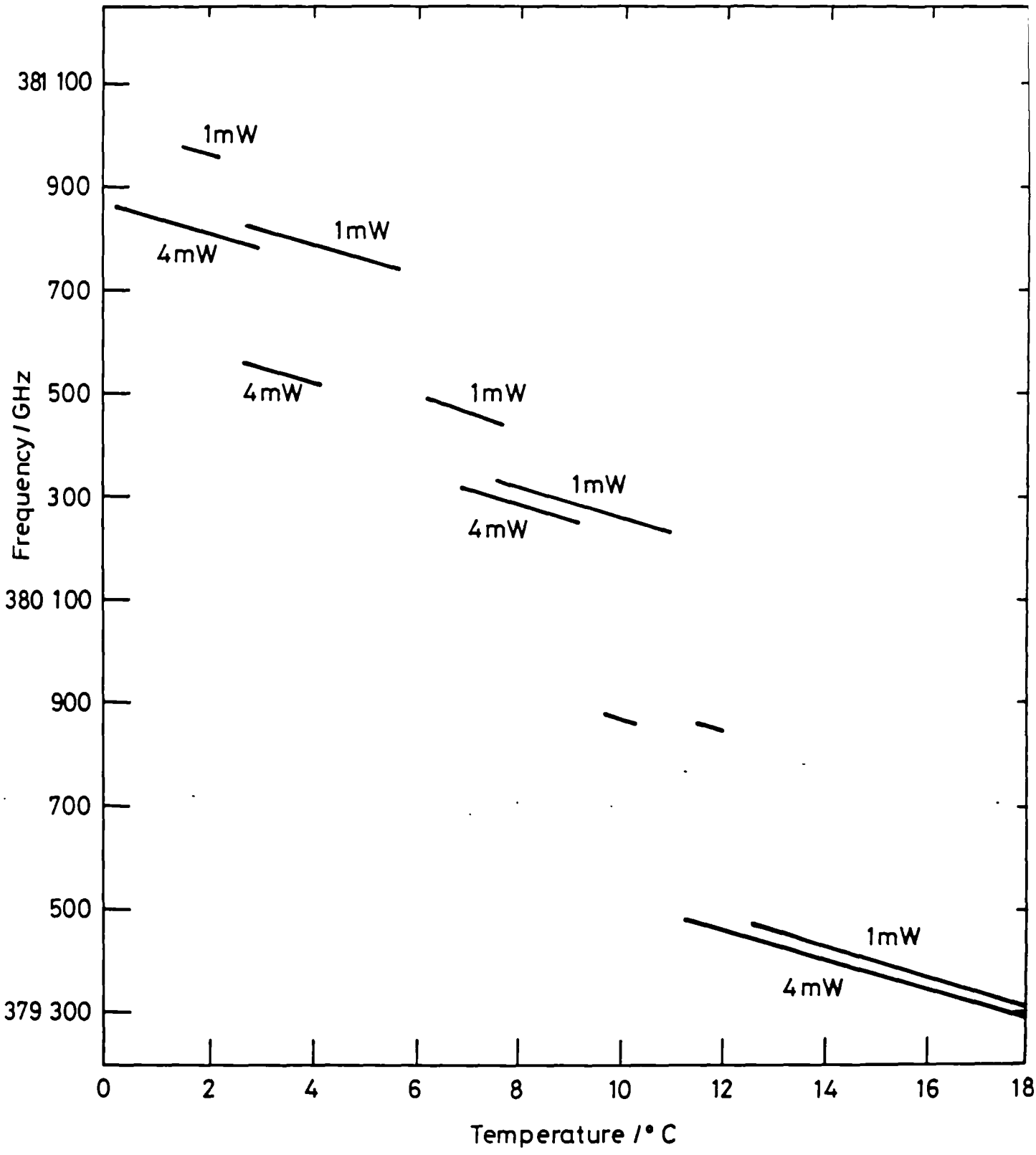

1.3.3 Typical frequency tuning curve for GaAlAs laser from 0°C to 18°C

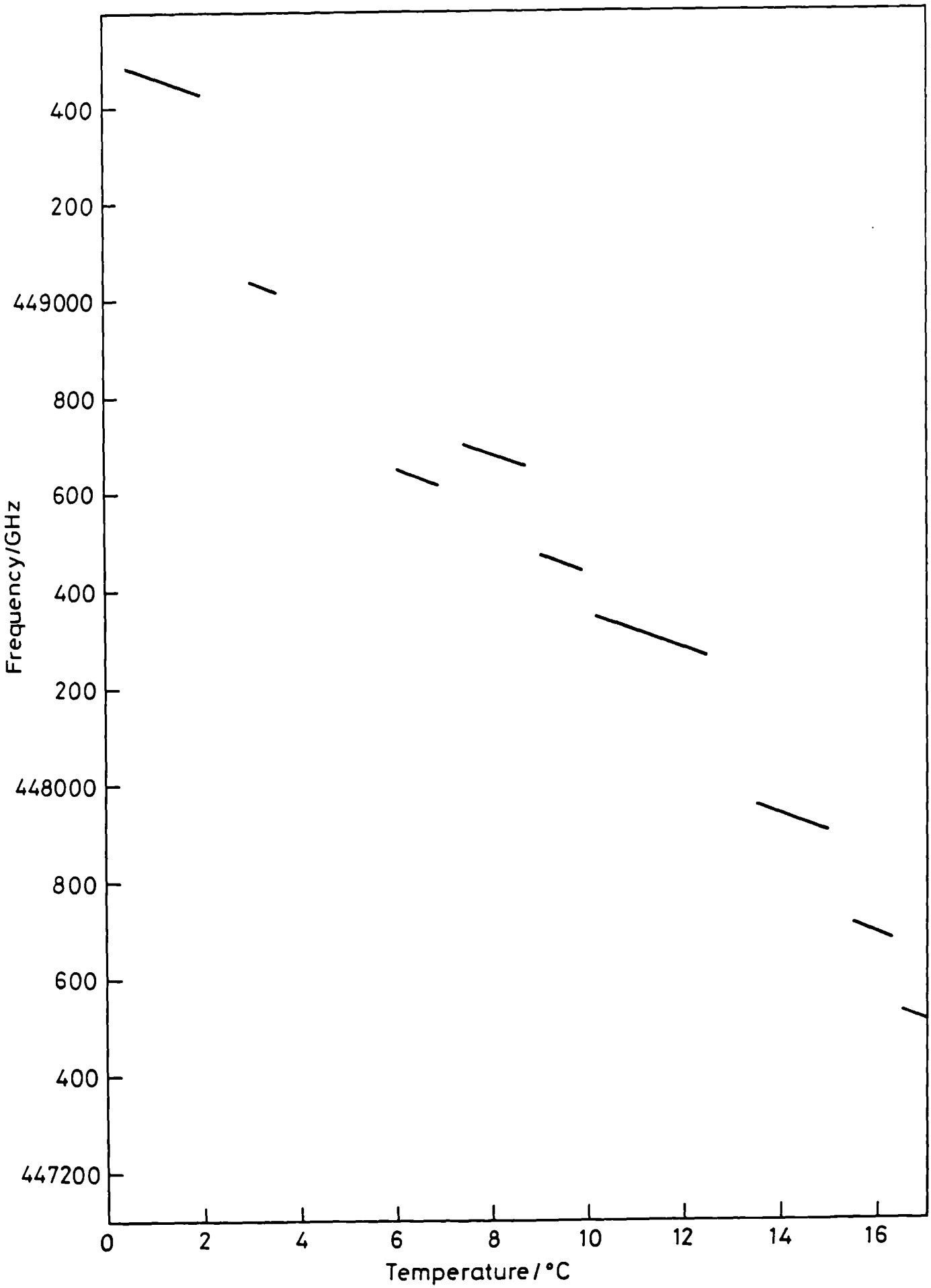

1.3.4 Typical frequency tuning curve for an index guided 670 nm diode (Toshiba TOLD 9211) for 4 mW output power.

CHAPTER 2

SPECTROSCOPIC STUDIES WITH A LASER DIODE

2.1 Introduction and description of apparatus for Doppler-limited work

This chapter describes the spectroscopic results obtained with basic, unmodified diodes with no linewidth reduction. Results are obtained using either the optogalvanic effect (section 2.2), and linear or saturated absorption (sections 2.3 and 2.5) as appropriate. This section describes the apparatus used in both this and following chapters.

In order to use diode lasers in most applications, the light has to be collimated, as described in section 1.3. It is also convenient to make the beam profile circular. The result of the investigation of the laser tuning characteristics (figure 1.3.3) shows also that careful design of the laser driver and heatsink temperature controller will be required. Typical laser tuning coefficients for current and temperature are 3 GHz/mA and 30 GHz/°C respectively. In order to achieve control at the level of 1×10^{-7} of the optical frequency (30 MHz), the laser drive current noise level needs to be better than 10 μA. This is readily achieved by the Lightwave model LDX 3620, used for most of the work in this thesis. This also provides the slow "turn-on" and "turn-off" needed since any transients would destroy the diode. Temperature control needs to be better than 1 mK, and the diode should be sufficiently well-insulated to protect against room-temperature fluctuations. This was achieved through the use of an NPL-designed heatsink and a temperature control circuit. The diode could be heated or cooled using a Peltier heat pump, and a thermistor mounted near the diode provided feedback sensing for the temperature control circuit. A temperature of

35°C below room temperature could be achieved. The temperature control circuit provided an estimated 13 mK temperature stability during the course of a working day. This would cause a frequency drift of 400 MHz.

Temperature is generally a slow parameter to control, owing to the thermal capacity of the heatsink, and provides only course control over the laser frequency. In order to scan over a spectroscopic feature of width 1 GHz, say, current control is better suited. This may be very rapid, usually limited by the response of the drive electronics rather than the diode, which may be modulated at a rate of more than 10 GHz [1,2]. This method has the slight potential disadvantage that one is also scanning the power. However, in order to scan 1 GHz, a typical power change is only 3%, which is generally not significant.

Two main systems of mechanical mounting were used. In work involving the basic, unmodified diode, as described in this chapter, the diode was mounted on a "minibench" system from Ealing Electro-Optics, with a specially designed mount for the laser diode itself. This provided great flexibility, but at the expense of mechanical rigidity. For later work, in chapters 3 to 6, a Photon Control breadboard mounted on vibration isolators was used. The Ealing components were then mounted on the breadboard using specially designed aluminium mountings. Beam-steering was then achieved using Melles-Griot adjustable mini-mirrors, similarly mounted on the breadboard. This was essential for the applications described in chapter 3, for example, where mechanical rigidity and stability are critically important.

Given that there are a limited number of spectroscopic transitions, the next step is to obtain a diode that will tune to any of these. This is not a straightforward matter, since a nominally "780 nm" diode could

actually lase anywhere between about 775 nm and 794 nm at 25°C. For the most popular laser chips, UK agents generally carry a good stock, and are usually co-operative in sending only those within say ± 3 nm of the desired wavelength. Most of the results of this thesis at ≈780 nm were obtained using either Mitsubishi ML-4102 or Hitachi HL 7801G lasers. Given that the band gap of a particular laser can be temperature tuned within the region of interest, there remains the problem of whether the laser will simply mode-hop over the transition and therefore be useless. Typically, an average success rate here appears to be 20%, suggesting that at least half a dozen lasers should be purchased of nominally the right wavelength. Particular care therefore needs to be taken of any lasers found to be of use. However, it is observed here and elsewhere [3] that even useful lasers may eventually fail to lase at the right frequency. The time to failure probably depends on how close the desired frequency is to a mode-hop position to begin with. Lasers which only tune to a transition at a current where the emitted frequency is bi-stable (ie may be one of two frequencies depending upon the direction of the current ramp) are most vulnerable to this problem.

Figure 2.1.1 shows a typical experimental arrangement for observation of Doppler-limited features by absorption. A similar arrangement is used for optogalvanic work (section 2.2), except that the photo-detector becomes unneccesary. If the beam is optically chopped and a signal fed into a phase sensitive detector (PSD), then a simple Doppler profile is obtained. Often it will be found more convenient to frequency modulate the laser and observe the signal with a PSD. The laser is frequency modulated by modulating the current. Unfortunately, using this method, the laser power is also slightly modulated. When a photo-electric signal is used, the PSD signal therefore has a slight offset. Where this is important, it is small enough just to be offset slightly using an

electronic offset adjustment in the psd. A first derivative of the profile is obtained by frequency modulating the diode and synchronous detection of the photo-electric signal. This is readily understood by considering the effect of a small modulation dither ($\nu_m \sin\Omega_m t$) on the profile, which in general may be written as $f(\nu - \nu_o + \nu_m \sin \Omega_m t)$. Here, ν is the optical frequency. As $\nu_m \ll \nu$, then the component at Ω_m is simply $\nu_m \sin\Omega_m t . f'(\nu - \nu_o)$ using a Taylor series expansion, where the dash (') denotes a derivative. The PSD signal is therefore proportional to the derivative.

The experiments which are to be described in this chapter use hollow cathode lamps with a few torr pressure of either Ar or Ne and Ti electrodes. These were supplied either by Cathodeon or, for the "see-through" version, by Hamamatsu. A mixed isotope Rb lamp and Rb cell were also used to investigate the Rb D lines.

2.2 The Optogalvanic effect - Results with Ar and Ne

The optogalvanic effect [4] is a change in the impedance of a discharge when it is illuminated by light at a wavelength corresponding to an atomic transition in the discharge. The effect was first reported by Penning in 1928 [4] and the technique has been revived in more recent times as laser optogalvanic spectroscopy in 1976 [5]. One of the principal attractions of this method is its simplicity, since the discharge itself acts as a detector. When the laser is tuned to a resonance, the impedance change in the discharge is readily converted into a voltage change (figure 2.2.1) and this is fed into a PSD. A coupling capacitor, which in this system was 0.15 μF, protects the PSD from the dc voltage across the discharge. The discharge itself is operated from a high voltage supply through a ballast resistor. A second

important feature of the method is that it allows investigation of transitions between excited energy levels.

The actual size of the optogalvanic signal for a given transition is not easily predicted. Furthermore, the impedance change can be positive or negative, depending upon the processes involved. For example, if the laser excites atoms from a state where the ionisation probability is small to one where the ionisation probability is greater, then the discharge current will increase and the voltage fall. If the two probabilities involved are of opposite relative size, then the voltage will rise [4]. Transitions in the part of the spectrum under consideration here ($\approx$ 800 nm) are likely to be between high-lying atomic energy levels, and so signals will be smaller than observed in the visible part of the spectrum. This is partly because the levels involved will not be so well-populated, and partly because the levels will also probably also have similar ionisation probabilities.

The optogalvanic effect may best be observed in hollow-cathode discharges where the electron temperature is sufficiently high to create significant upper-state populations. Commercially-available hollow-cathode lamps were used for this study. They were purchased either from Cathodeon or Hamamatsu. This has the advantage of simplicity, but does not enable design optimisation of the lamp to get the best signal to noise ratio. This is strictly necessary to the get the best results, and a well-designed lamp may actually have a noise level less than the shot-noise limit [4]. It may also be desirable to design the lamp to operate at low gas pressures, for example. This is especially important if it is required to observe narrow Doppler-free signals, minimising pressure broadening. With the commercially-available lamps used here, discharge noise was dominant in the detection

electronics, and Doppler-free signals could not be observed. Discharge noise, and even oscillation, was a particular problem with a lamp filled with Ar, rather than Ne. One solution to this problem with Ar and Kr is to fill the lamp with a mixture containing Ne (eg Ar/Ne) to provide a quieter discharge. The lamps were filled with typically a few torr pressure of gas. They generally needed ≈ 150 V to strike and required ≈ 10 mA current. A ballast of typically 40 kΩ was used, but this was frequently varied to suite the lamp and current being used. The ballast was generally chosen so that the operating voltage was high enough for the lamp to strike, but low enough to avoid excessive heat generation in the ballast. As an example, 10 W is generated by 10 mA through 100 kΩ, which requires a good heatsink. Varying the ballast by ≈ 10 kΩ had little effect on the discharge noise.

Optogalvanic signals were observed initially with the apparatus shown in figure 2.2.1 in Ar and Ne [6,7]. The laser light was chopped at 400 Hz and the signal detected synchronously with a PSD. Once a signal was observed, it could be optimised by varying the laser beam size in the lamp, the position of the beam, and the lamp current. Some of the stronger signals could also be observed by removing the chopper wheel and frequency modulating the laser at 500 Hz instead. Again, a PSD was used to recover the signal, but this technique provided a discriminant with a zero crossing at line-centre, suitable for frequency locking the laser. Several lines in Ar and one in Ne were observed in the region of 794 nm. The Ne line, measured at 794.52 nm (figure 2.2.2) was observed [8] in a lamp operating at 3.5 mA. The linewidth (FWHM) was measured to be ≈ 1 GHz with a signal to noise ratio of 25, using a PSD time constant of 100 ms. This line was also observed by frequency modulating the laser (figure 2.2.2b). However, the primary disadvantage here is that a modulation depth of several hundred MHz is necessary to obtain a good

signal to noise ratio. Such a large modulation depth is highly undesirable for interferometric applications. Although some interferometric techniques require modulated light, it is desirable to be able to vary the modulation parameters for interferometry independently of the requirements for Rb spectroscopy. Transitions in Ar were also observed in a lamp operating at 22.6 mA, which was several times above the recommended operating current. However, the strongest line observed, at 794.74 nm, had a signal-to-noise ratio of 90 when observed with the laser beam chopped. The peak voltage change on this line across the lamp was only 0.6 mV. Two other fairly strong Ar lines were observed in this wavelength region, at 794.50 nm and 794.01 nm, as well as around half a dozen much weaker lines. Although clearly a very useful instructive first step in providing spectroscopic references for diode laser frequency stabilisation, this does not appear to provide a satisfactory solution to the problem.

2.3 Observations with a see-through Rb hollow-cathode lamp and a cell

Since noble gas optogalvanic transitions do not provide a feature with a sufficiently good signal-to-noise ratio, consideration must be given to other potential reference transitions. From section 1.4, rubidium clearly also provides potentially convenient standards at 780 nm and 795 nm. The D lines, the principal resonance lines in Rb, should provide strong signals, observed optogalvanically. The principal disadvantage is probably that only two groups of hyperfine features are available, rather than three or four optogalvanic signals in Ar which may be expected within the tuning range of a given diode near 790 nm.

Initially, the Rb transitions were observed optogalvanically, using commercially available hollow-cathode Ne-filled lamps. Unfortunately,

the signal-to-noise ratio obtained was not significantly better for Rb than for that observed with the noble gas transitions. To achieve a reproducibility of ±1 part in 10^7 with the lamp, we would need to achieve a signal to noise ratio of ~20, for a Rb feature linewidth (FWHM) of 700 MHz. This should also be achieved with only a modest (~50 MHz peak to peak) modulation depth. However, one of the two lamps used was of a "see-through" design, enabling a beam to pass right through the hollow cathode. It was observed that, with the discharge switched on, the rubidium transitions could be observed photo-electrically, by absorption through the discharge. The absorption could be conveniently altered by varying the current through the discharge. The Rb absorption spectra at 780 nm and 795 nm are plotted in figure 2.3.1. These spectra were obtained by frequency modulating the laser and observing the absorption in the discharge synchronously with a PSD. The absorption at the central peak at 780 nm and 795 nm is plotted versus lamp current in figure 2.3.2.

Although a hollow-cathode lamp is convenient for preliminary investigations, calculations on the absorption together with results from other workers [9] suggested it should be possible to use the absorption in a room-temperature Pyrex cell. Therefore, a 75-mm long cell was purchased from Opthos Instruments [10], and at room temperature (~ 19°C), the maximum linear absorption was measured to be ~ 34% at 780 nm and ~ 15% at 795 nm. The features were observed to be rather narrower than in the lamp, due to the increased effective temperature in the lamp. The FWHM linewidth in the cell is ~ 500 MHz, whereas in the lamp it is ~ 720 MHz. This is some 40% larger than for the cell, corresponding to a gas temperature of ~ 600 K. The features observed in the cell are shown in figure 2.3.3 for both 780 nm and 795 nm. The absorption was so strong that a sufficiently good signal-to-noise ratio was obtained even if the

laser was only modulated at 50 MHz peak-to-peak. The typical power levels in the cell used to record these data were ≤ 10 μW in order to avoid saturation effects, discussed more fully in the next section. At room temperature, the Rb self-pressure is calculated to be only 20 μPa (1.5×10^{-7} torr) [11], implying that the self-pressure broadening may be entirely neglected. However, there remains the possibility of contamination by foreign gases, as discussed more fully in section 3.7. Although diode lasers have previously been used to obtain Doppler-limited derivative spectra, suitable for frequency stabilisation at 780 nm [9], this is the first time that the line at 795 nm has been observed in this way.

A rubidium cell, therefore, appears to be especially straightforward and convenient for use as a frequency reference for diode lasers. There is now the considerable problem of analysing the spectra, obtaining Doppler-free spectra and understanding the limitations of Rb as a frequency reference at 780 nm and 795 nm.

2.4 Analysis of Rb absorption profiles and potential causes of frequency shift

This section analyses the Doppler-limited spectra observed in the previous section, beginning with the designation of the hyperfine transitions contributing to the overall features. Secondly, calculations are presented of the expected absorption profiles for the case of the hollow-cathode lamp. Finally, various shifts in the line-centre of the absorptions are measured and examined.

The alkali metal transitions are well-documented [12] as regard their designations. The lines in Rb at 780 nm and 795 nm are due to the

$5S_{1/2} \rightarrow 5P_{3/2}$ and $5P_{1/2}$ transitions respectively. The cell and lamp both contain a natural mixture of the two isotopes, ^{85}Rb and ^{87}Rb. These isotopes have a nuclear spin of I = 5/2 and 3/2 respectively, giving rise to the observed hyperfine structure. The energy level structure for the two isotopes is shown schematically in figure 2.4.1. The transitions have a natural width of 6 MHz [13], although the observed profile is broadened in a cell or lamp by the Doppler effect. In the lamp, owing to the presence of the Ne buffer gas, pressure broadening must also be considered. In the lamps, a typical pressure of a few torr is generally used, and a broadening of 13 MHz/torr may be calculated [14]. For 5 torr pressure, for example, this corresponds to 65 MHz FWHM. In the case of the cell, the vapour pressure is given by

$$\log_{10}N = A - B/T + CT + (D + 1)\log_{10}T + 24.985 \qquad (2.4.1)$$

where the temperature, T, is in K and N, the number of atoms per unit volume, is in m^{-3}. The constants, when the Rb is a solid, (Rb melts at 39°C) are A = -94.04826, B = 1961.258, C = -0.03771687 and D = 40.57526 [15]. At a cell temperature of 19°C, this yields $N = 5.1 \times 10^{15}$ m^{-3}. The broadening due to self-pressure is negligible, estimated to be of the order of 1 Hz.

In the case of the cell, the Rb profile will be of the form $\exp(-x^2)$ or $x.\exp(-x^2)$ in derivative form, with a Doppler width (FWHM) of 500 MHz. The profile in the case of the lamp will depend upon the extent of the pressure broadening. If there is a significant Lorentz component, then a Voigt profile [16] may be expected. This is the real part of a complex function, usually denoted by w(z), where z is the complex variable defined by

$$z = (\nu - \nu_o + \tfrac{1}{2}j\gamma)/\nu_D \qquad (2.4.2)$$

and ν_D is the 1/e Doppler half-width. The transition centre frequency and Lorentzian FWHM are given by ν_o and γ respectively. Tables of w(z) are available [17]. The derivative of the Voigt profile may also be established through the relation

$$\frac{d[Re\{w(z)\}]}{d\nu} = -2[(\nu - \nu_o)Re\{w(z)\} - \tfrac{1}{2}\gamma Im\{w(z)\}]/\nu_D^2 \qquad (2.4.3)$$

From these tables, it can be established that if the FWHM of the profile is 720 MHz, and the Doppler FWHM ($= 2\nu_D\sqrt{ln2}$) is 500 MHz (as measured for the cell), then the Lorentz FWHM is 360 MHz. Allowing for the natural linewidths of the laser and the transition, then this yields 320 MHz for the pressure broadening. It is interesting to compare the derivative of the Voigt and Gaussian profiles, which both give the same FWHM (720 MHz), as in figure 2.4.2. The differences are always less than 10 % of the peak signal size and so, given that there is underlying hyperfine structure, it would be difficult experimentally to distingiush between the two profiles.

The analysis of the hyperfine structure will be discussed further in chapter 5, but the hyperfine component separations are given by [12]

$$H_{hfs} = \tfrac{1}{2}hAK + hB\frac{\{3K(K + 1)/2 - 2I(I + 1)J(J + 1)\}}{2I(2I - 1)2J(2J - 1)} \qquad (2.4.4)$$

where $K = F(F + 1) - I(I + 1) - J(J + 1)$.

Here, A and B are constants with B = 0 unless $I,J > \frac{1}{2}$. I and J are the spin and electronic quantum numbers respectively and $\underline{F} = \underline{I} + \underline{J}$. The isotope shifts are reported to be 77 MHz and 80 MHz on the D_1 and D_2

lines respectively [18,19]. The values for A and B for the states involved are published, but these are re-evaluated in chapter 5. However, the existing values are sufficiently accurate for analysis of the Doppler-limited profiles. The expected profile used is a set of weighted delta functions convolved with a function of the form $x.\exp(-x^2)$. The weightings used are given in table 2.4.1 [18], correcting for the relative adundances (72.7% for ^{85}Rb and 27.3% for ^{87}Rb).

TABLE 2.4.1

Table of theoretical linear linestrengths, for both Rb D lines, reproduced from [18], and used to calculate the profile of figure 2.3.1

780 nm		795 nm	
Component	Theoretical Intensity	Component	Theoretical Intensity
b	0.026	a	0.374
d	0.133	c	0.374
f	0.374	a'	1.000
b'	0.123	c'	0.800
d'	0.432	b'	0.286
f'	1.000	d'	1.000
a'	0.333	b	0.075
c'	0.432	d	0.374
e'	0.346		
a	0.053		
c	0.133		
e	0.133		

These calculations, in the case of the results with the lamp, are given

in figure 2.4.3 and may be compared with the experimental profiles (figure 2.3.1). Only the Doppler width and vertical scale have been adjusted to yield the best fit. The designation of each hyperfine component is noted underneath in the form $F_{ground} \rightarrow F_{upper}$.

It is possible, in the case of the cell, to provide a calculation of the expected linear absorption, which agrees well with the observed figure in the preceeding section, measured at 19°C. The transmitted signal obeys a Beer-law formula, being proportional to $\exp(-k_o N l)$. Here, N is the number of atoms per unit volume, and l is the path length in the cell. The constant k_o is given by [11]

$$k_o = \frac{(2F + 1)e^2 f}{8(2I + 1)\varepsilon_o mcv_D\sqrt{\pi}} \qquad (2.4.5)$$

For the two Rb peaks measured, I = 5/2 (for ^{85}Rb), and F = 2, and f, the oscillator strength, = 0.673 at 780 nm and 0.317 at 795 nm. Using $N = 5.1 \times 10^{15}$ m^{-3} at 19°C and correcting for the isotopic abundance (78%) of ^{85}Rb yields an absorption of 34% at 780 nm and 18% at 795 nm for a cell length l = 75 mm. These compare well with observed absorptions of 34% and 15% (±4%) respectively.

Finally, in this section, the possible causes of shift in the centre frequency of the Doppler-limited features are considered. This is especially important if these absorptions are to be used as frequency references. Following precision measurements on iodine stabilised lasers [20,21], it is expected that shifts may occur with changes in gas or vapour pressure, laser power, and gas temperature. This latter parameter is equivalent to lamp current for the purposes of this study. The depth of modulation is also likely to affect the signal zero crossing point. At this stage, and for the precision required here, these offsets were

measured by splitting the light from a laser, directing the beams either into a cell and the lamp or into the the two cells. The laser was then frequency modulated and tuned to the Rb lines, and the discriminant from the two PSDs measured simultaneously. A frequency offset was determined from the failure of both PSD signals to cross through zero at the same frequency. Laser power, and lamp/cell shifts could be determined in this way. Lamp/cell shifts were clearly caused by both increased temperature and pressure in the lamp.

Laser power will begin to affect the absorption profile when the light intensity approaches the saturation intensity. Laser light at the right frequency for absorption is also at the right frequency to produce stimulated emission. At the saturation intensity, the incident light begins to reduce appreciably the Rb excited upper state lifetime. Each Doppler-broadened profile masks a number of features, each with a width of 6 MHz, corresponding to the natural lifetime. If this width is broadened, then we might expect the Doppler-broadened profile to change, if the saturation parameter of each hyperfine transition is different. The effective centre of the various peaks can then be expected to shift. This begins to occur at ≈ 0.4 Wm^{-2} (10 μW power, for a 8 mm diameter beam) for the cells. Power shifts of up to 40 MHz for the central components ("c") were measured at 100 μW power, for the two D lines. For the lamp, however, the shift was less than 3 MHz at this higher power. This smaller effect is presumably because the lines were already broadened by the few torr pressure of Ne gas in the lamp.

A shift was also observed between the lamp and the cell, because of the combined effect of pressure shifts and increased Doppler broadening in the lamp. The result for the offset at 780 nm, where a positive shift indicates that $f_{lamp} > f_{cell}$, is -20 MHz for both peaks "b" and "c". At

795 nm, the shifts for the peaks "b" and "c" were -28 MHz and +6 MHz respectively. The shifts of these components between two nominally identical cells were also measured and found to be less than 2 MHz, with a 3σ uncertainty on these results of ±3 MHz. For the lamp, the magnitude of published Rb/Ne pressure shifts [14] suggests shifts ≈10 MHz assuming a Ne pressure of several torr. For the D_2 line, for example, the shift is calculated to be -0.19×10^{-9} rad s^{-1} cm^3 $molecule^{-1}$ (-1.0 MHz/torr). In the case of the cell, the self-pressure is calculated to be only 20 μPa [15] at 19°C, and the self-pressure shift should thus be negligible. The measured shift between identical cells should set an upper limit on the pressure of the background gas, depending upon the contaminant. For example, data are available [22] on the ^{87}Rb D_2 line shift in the presence of xenon, nitrogen and methane.

Finally, an estimate may be made of the modulation shift, from the asymmetry of the lineshapes, for the central component ("c") of both D lines. In an asymmetric line, the frequency difference between the peak and half-intensity points on the high and low frequency sides are not equal. Suppose that these frequency intervals are designated by f_a and f_b respectively. As the modulation depth is increased, the detail of the asymmetry in the line is lost. As the modulation is increased to around $(f_b + f_a)$, the line centre shifts by $\approx\frac{1}{2}(f_b - f_a)$. The shift is therefore approximately expected to equal the asymmetry, namely

$$\text{Modulation shift} \approx (f_b - f_a)/2(f_b + f_a) \qquad (2.4.6)$$

For the D_2 and D_1 lines, the estimated shifts are less than ≈10 MHz/GHz in magnitude and ≈-90 MHz/GHz respectively.

In conclusion, therefore, the centre frequencies of these

Doppler-limited lines in the cell are estimated to be reproducible to ±10 MHz. This sets a limit on the reproducibility of the frequency of a laser locked to the centre of such a component. This section has given the first reported results on the frequency shifts of Doppler-limited line-centres and their offsets from the line-centre observed with the hollow cathode lamp. To improve upon the results in this section, Doppler-free features are required, as described in the next section.

2.5 Doppler-free Rb Spectroscopy

Although Doppler-limited spectroscopy has the advantage of simplicity, there are clear advantages in being able to observe each hyperfine component Doppler-free. Observation on the hyperfine components, for example, will enable measurements to be made pertaining to the Rb hyperfine constants (equation 2.4.4). Since the features are much narrower than the Doppler-limited profiles, we may also expect the centre frequency to be a better frequency reference. A problem which may be expected is that the laser linewidth of 30 MHz (section 1.3) will limit the potential resolution, since the natural linewidths of the Rb lines is 6 MHz.

The Doppler-free technique used, of saturation spectroscopy, is one of a number of techniques which may used to obtain sub-Doppler resolution [23]. The experimental apparatus used for these results is shown in figure 2.5.1. The concept of a saturating laser power was briefly introduced in the last section to explain power broadening. In this system, shown in figure 2.5.1, the stronger beam is delibrately saturating and has a power of 30 μW. In this case, a significant number of Rb atoms are in the upper state and the transmitted power is no longer as much as $P_o.\exp(-k_oNl)$, for an incident power P_o. The

absorption is saturated. The counter-propagating beam, typically 10% of the saturating beam, therefore is absorbed less at line centre. This is because, away from line centre, the two beams interact with different velocity groups of atoms. At line centre, both beams interact with the same, zero, velocity group. The laser is modulated at ≈810 Hz to a depth of 50 MHz peak to peak. A second probe beam is used to subtract off the signal due to the linear absorption alone, before being fed to the PSD. In this case, a frequency tripling unit, which produces oscillatory outputs at f and 3f is used to enable the PSD to observe the signal at three times the modulation frequency (3f). This technique also helps to remove the signal due to the linear absorption [24]. This method produces a signal proportional to the third derivative of the profile. This may readily be understood, as in section 2.1, by considering the effect of modulation on the general profile shape. This becomes $f(\nu - \nu_o + \nu_m \sin\Omega_m t)$, and we require, to good approximation, the lowest term in the Taylor expansion containing $3\Omega_m$. The third derivative term is $\Omega_m^3 \sin^3\Omega_m t . f'''(\nu - \nu_o)$, and using the identity $\sin^3\theta \equiv (3\sin\theta - \sin 3\theta)/4$, the lowest term involving $3\Omega_m$ is therefore proportional to the third derivative of $f(\nu - \nu_o)$. In general, detection at nf, for n integral, results in an n^{th} derivative signal from the PSD. However, n needs to be an odd number for the line centre to be at a zero crossing. The Lorentzian components are much narrower compared with the Doppler-limited background, and therefore are much more pronounced in third derivative form. The enhancement of the Lorentzian signal to background slope varies as the cube of the Doppler to Lorentz linewidth ratio. The FWHM of the Doppler-free features is observed to be ≈50 MHz, mainly limited by the laser linewidth. This third derivative technique does not work so well as it would for a narrow-linewidth laser, where the Lorentz linewidth is only the natural linewidth of the transition. Therefore, as shown in figure 2.5.1, it is necessary to subtract off the

linear absorption signal first, to achieve a completely flat background.

The observed spectra at 780 nm and 795 nm are shown in figure 2.5.2, obtained by current tuning of the diode. The observed FWHM of 50 MHz comprises 30 MHz laser width, 6 MHz Rb natural transition width, broadening of ≈2 MHz due to the Earth's magnetic field, and modulation depth broadening. This represents the first report of third harmonic Rb spectra using a laser diode at either 780 nm or 795 nm.

The labelled components in figure 2.5.2 are due to hyperfine transitions in ^{85}Rb or ^{87}Rb. A dash (') indicates transitions due to ^{85}Rb. Unlabelled features half-way between labelled transitions are called level-crossings and are often observed in saturation spectroscopy. They arise between components with a common ground state, where the laser interacts with a non-zero velocity group of atoms. Atoms with some non-zero velocity can interact simultaneously with two counterpropagating laser beams, when the frequency lies half-way between the two transitions. If the absorption is saturated, this will give rise to a Doppler-free feature, sometimes of a size comparable with genuine transitions.

These results suggest strongly that a narrow-linewidth laser diode would provide two important advantages in the observation of these spectra. Firstly, the spectra at 780 nm should be better, if not completely resolved. At present, the 780 nm line is virtually useless for laser frequency reference work, because the lines are unresolved. Secondly, a narrow-linewidth laser would produce narrower lines at 795 nm, enabling a flat background to be obtained by the third derivative technique alone. A second probe beam, to remove the Doppler-limited background, would become unnecessary.

Therefore, before further work on Rb spectroscopy or laser frequency stabilisation is considered, work on laser linewidth reduction is described.

References

[1] S Kobayastu, Y Yamamoto, M Ito, T Kimura, IEEE J Qu El, QE-18, 582-95, (1982)

[2] KY Lau, A Yariv, IEEE J Qu El, QE-21, 121-38, (1985)

[3] JC Camparo, Contemp. Phys., 26, No. 5, 443-77 (1985)

[4] JEM Goldsmith, Contemp. Phys., 22, No. 2, 235-48 (1981)

[5] RB Green, RA Keller, GG Luther, PK Schenck, JC Travis, Appl Phys Lett, 29, No 11, 727-9 (1976)

[6] S Yamaguchi, M Suzuki, Appl. Phys. Lett., 41, No. 7, 597-8 (1983)

[7] S Yamaguchi, M Suzuki, IEEE J Qu El, QE-19, No. 10, 1514-9, (1983)

[8] CRC Handbook of Physics and Chemistry 70th edition, 1989/1990, p E214-5 (for Ar lines) and E271-3 (for Ne lines)

[9] H Tsuchida, M Ohtsu, T Tako, N Kuramochi, N Oura, Japan. J Appl. Phys., 21, No. 9, L561-3 (1982)

[10] Opthos Instruments Inc., Maryland, MD20855, USA.

[11] A Gallagher, EL Lewis, J Opt. Soc. Am., 63, No 7, 864-9 (1973)

[12] E Arimondo, M Inguscio, P Violino, Rev Mod Phys, 49, No. 1, 31-75 (1977)

[13] OS Heavens, J Opt Soc Am, 51, No. 10, 1058-61 (1961)

[14] Y Shimoni, AD Wilson, Chem Phys, 11, 289-95 (1975)

[15] An N Nesmeyanov, "Vapour pressure of the elements", Infosearch Ltd., London (1963)

[16] Advances in Laser Spectroscopy, ed. by FT Arecchi, F Strumia, HW Walther NATO ASI Series; Series B:Physics, Vol 95, Lecture by CJ Bordé, p40, Plenum Press (1983)

[17] Handbook of Mathematical Functions, edited by M Abramowitz and IA Stegun, National Bureau of Standards (1964)

[18] JR Beacham, KL Andrew, J Opt Soc Am, 61, No. 2, 231-5, (1971)

[19] HM Gibbs, GC Churchill, J Opt. Soc Am, 62, No. 10, 1130-3, (1972)

[20] WRC Rowley, NPL Report MOM 54 (1981)

[21] WRC Rowley, NPL Report MOM 56 (1981)

[22] VN Belov, Opt Spectros, 51, No. 1, 22-4 (1981)

[23] RC Thompson, Rep Prog Phys, 48, 531-78, (1985)

[24] AJ Wallard, J Phys E, 5, 926-30 (1972)

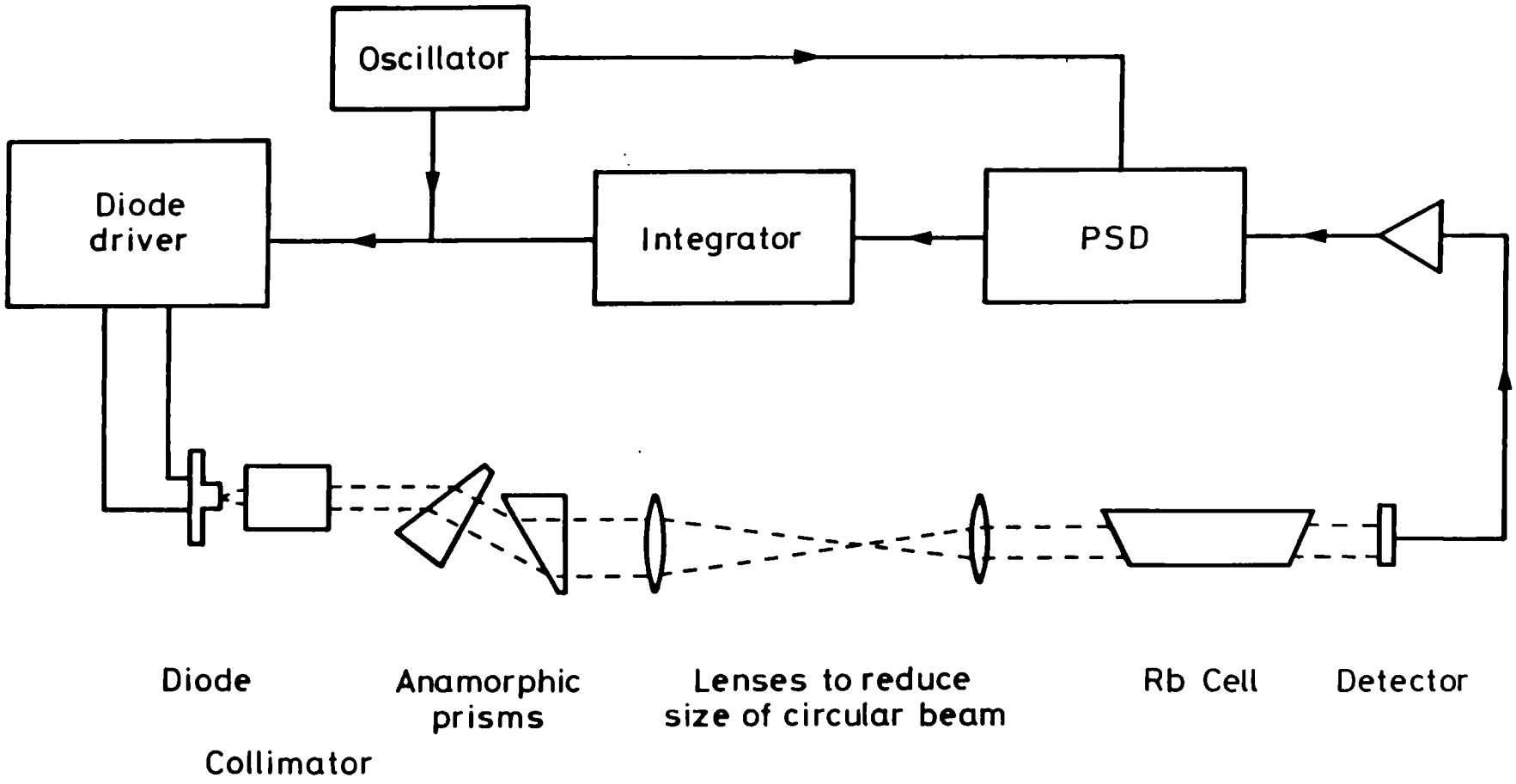

2.1.1 Schematic of laser diode optics and absorption stabilisation

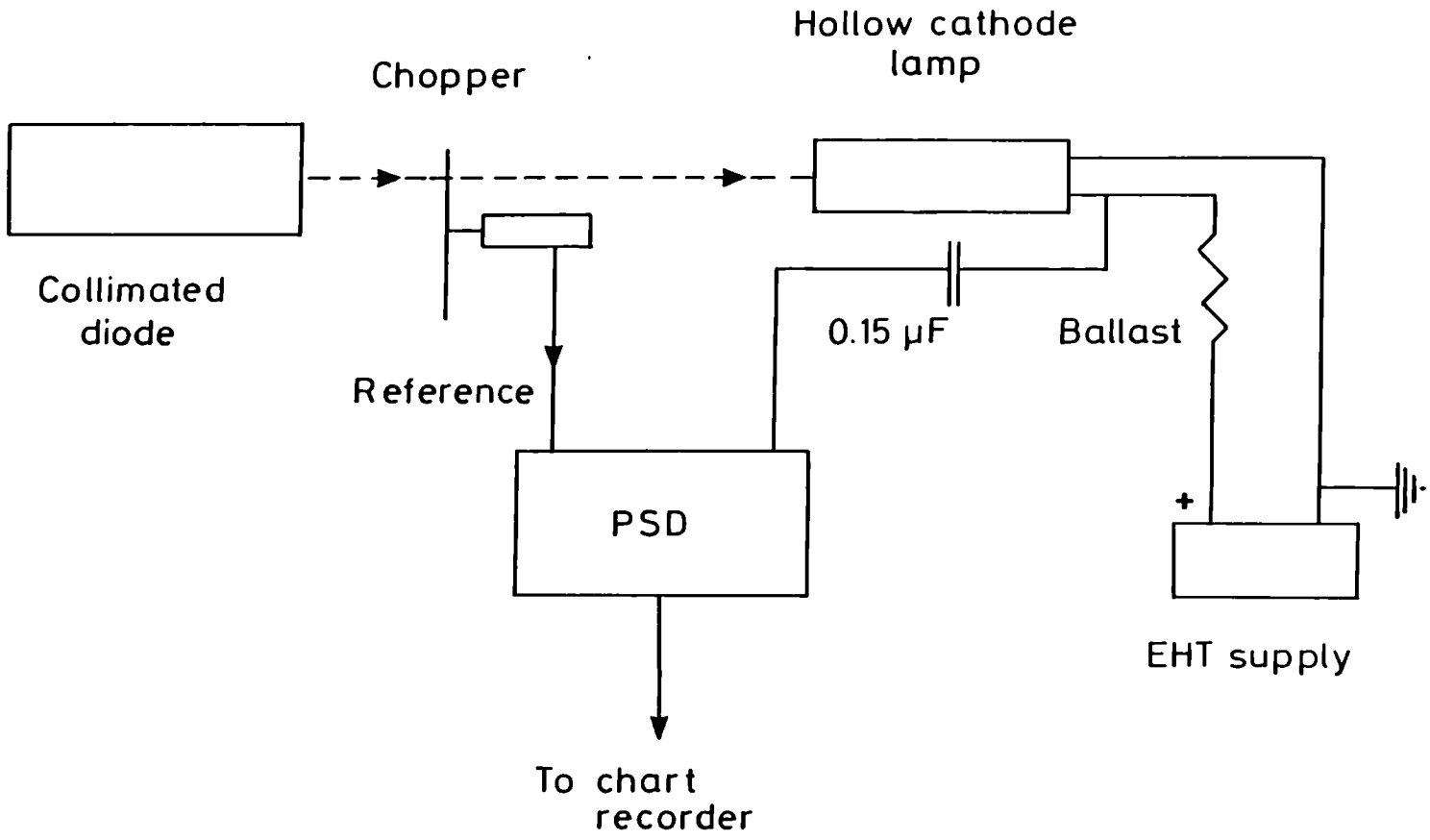

2.2.1 Schematic of apparatus to observe the optogalvanic effect

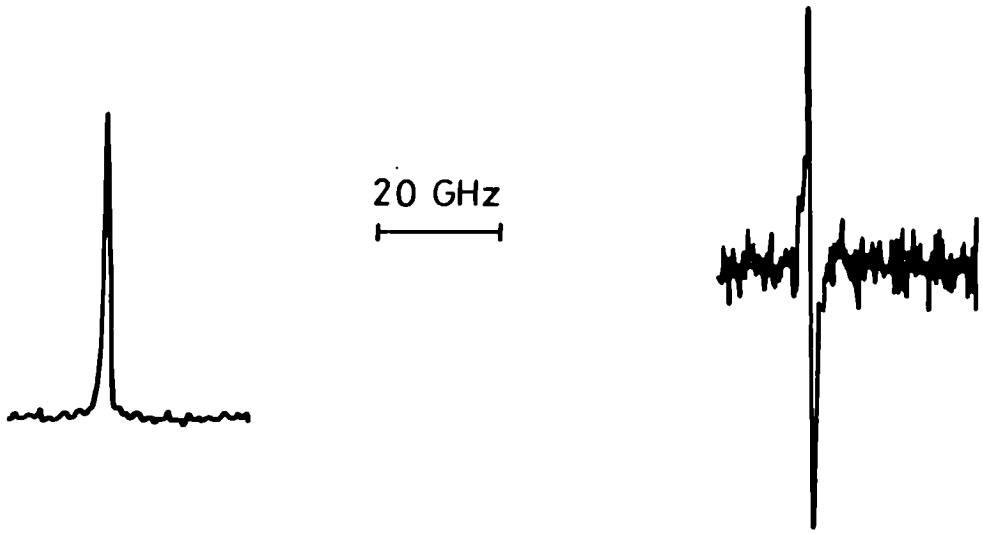

2.2.2 Optogalvanic spectrum of Ne at 794.5 nm observed (a) by amplitude modulation and (b) in derivative form by modulating the frequency. The FWHM is 1 GHz, and in (b), the signal noise corresponds to a frequency uncertainty in the lock point of 100 MHz. The frequency modulation amplitude was 200 MHz peak to peak at 500 Hz. The lamp current is 3.5 mA and a laser power of ≈2 mW was incident on the lamp.

a) 780nm

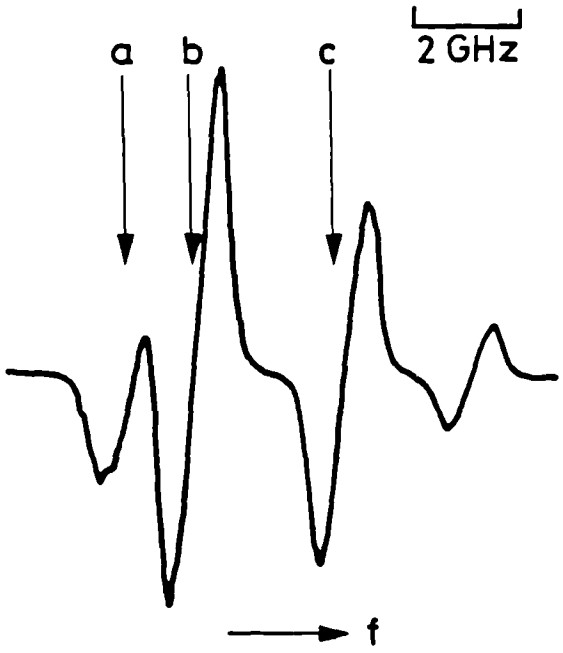

b) 795nm

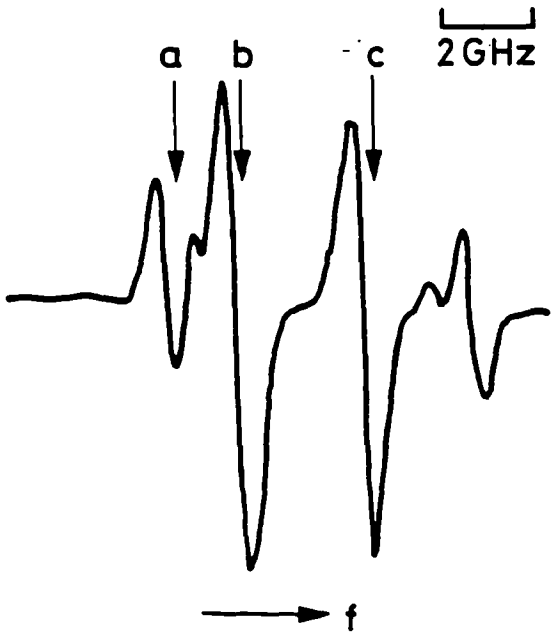

2.3.1 Rb D lines at 780 nm and 795 nm, measured by absorption in the hollow cathode lamp

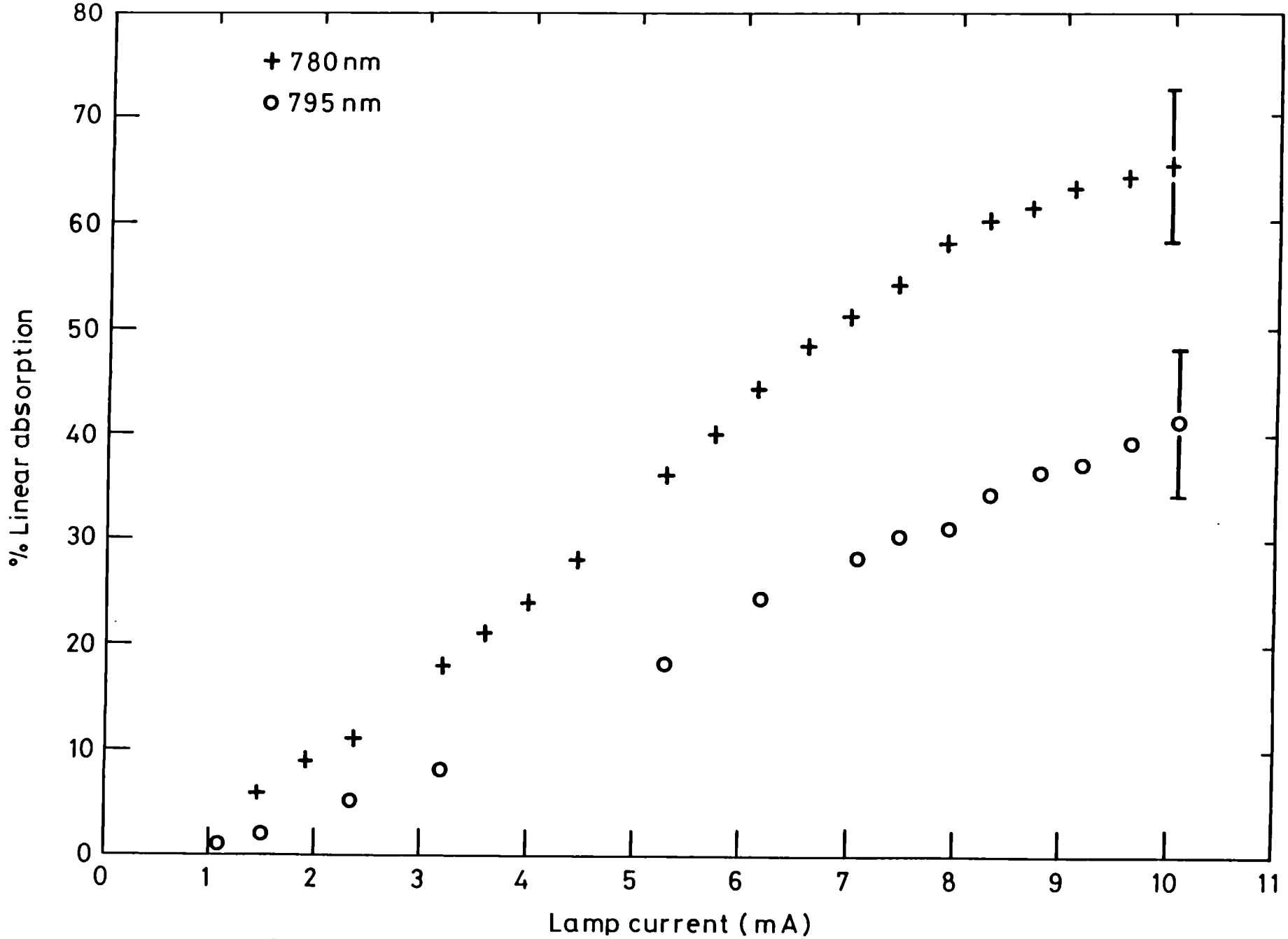

2.3.2 Absorption at the central peak at 780 nm and 795 nm versus lamp current, in a 2 cm length of discharge

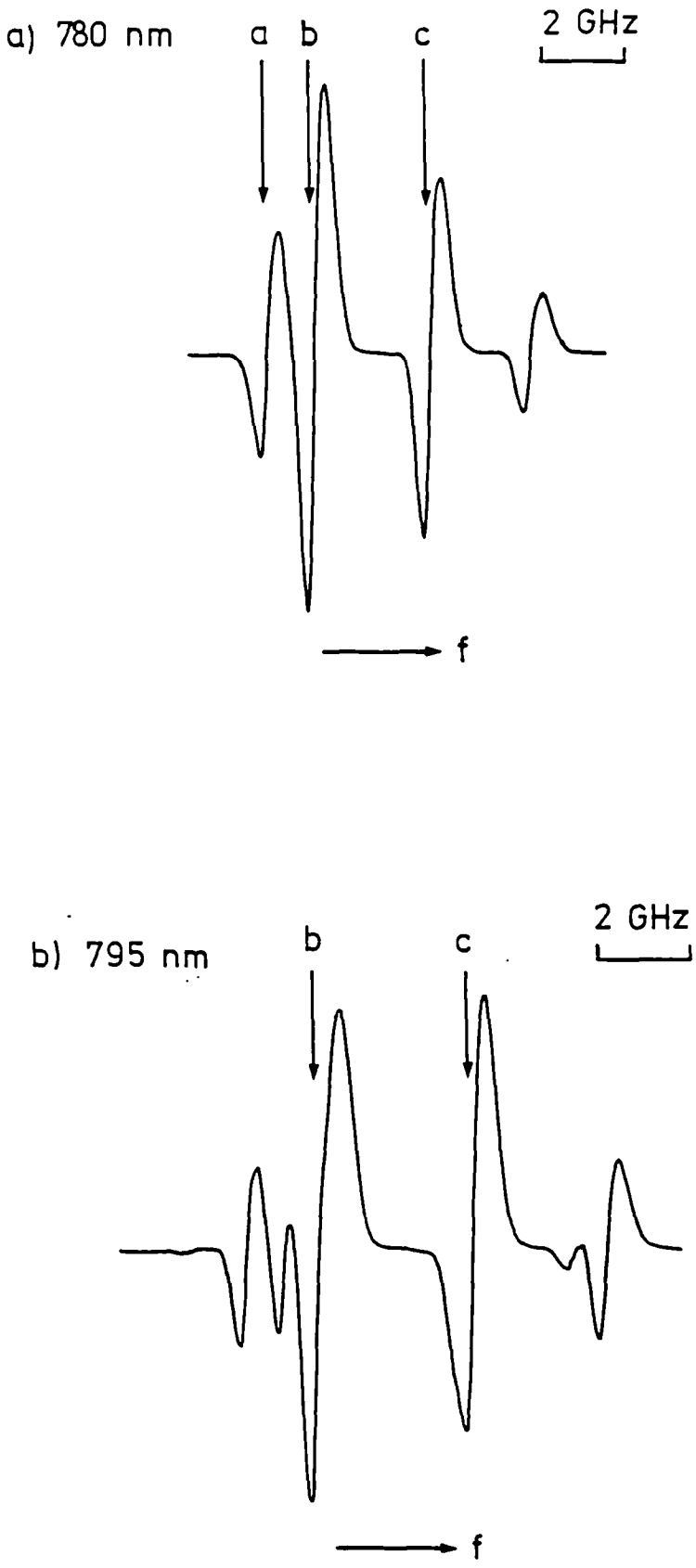

2.3.3 Rb Doppler-limited derivative spectra at 780 nm and 795 nm, measured in a cell

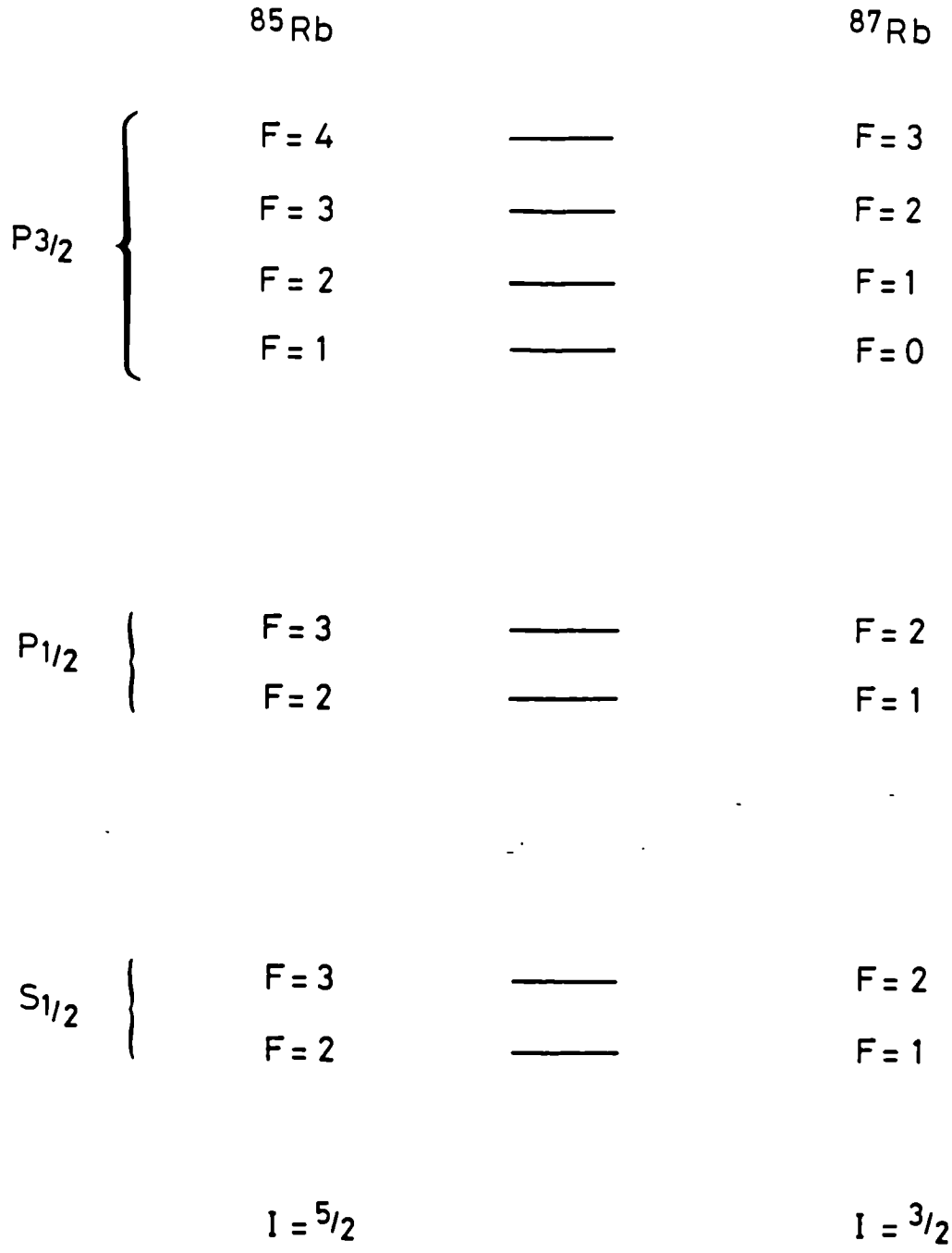

2.4.1 Atomic energy level structure of ^{85}Rb and ^{87}Rb

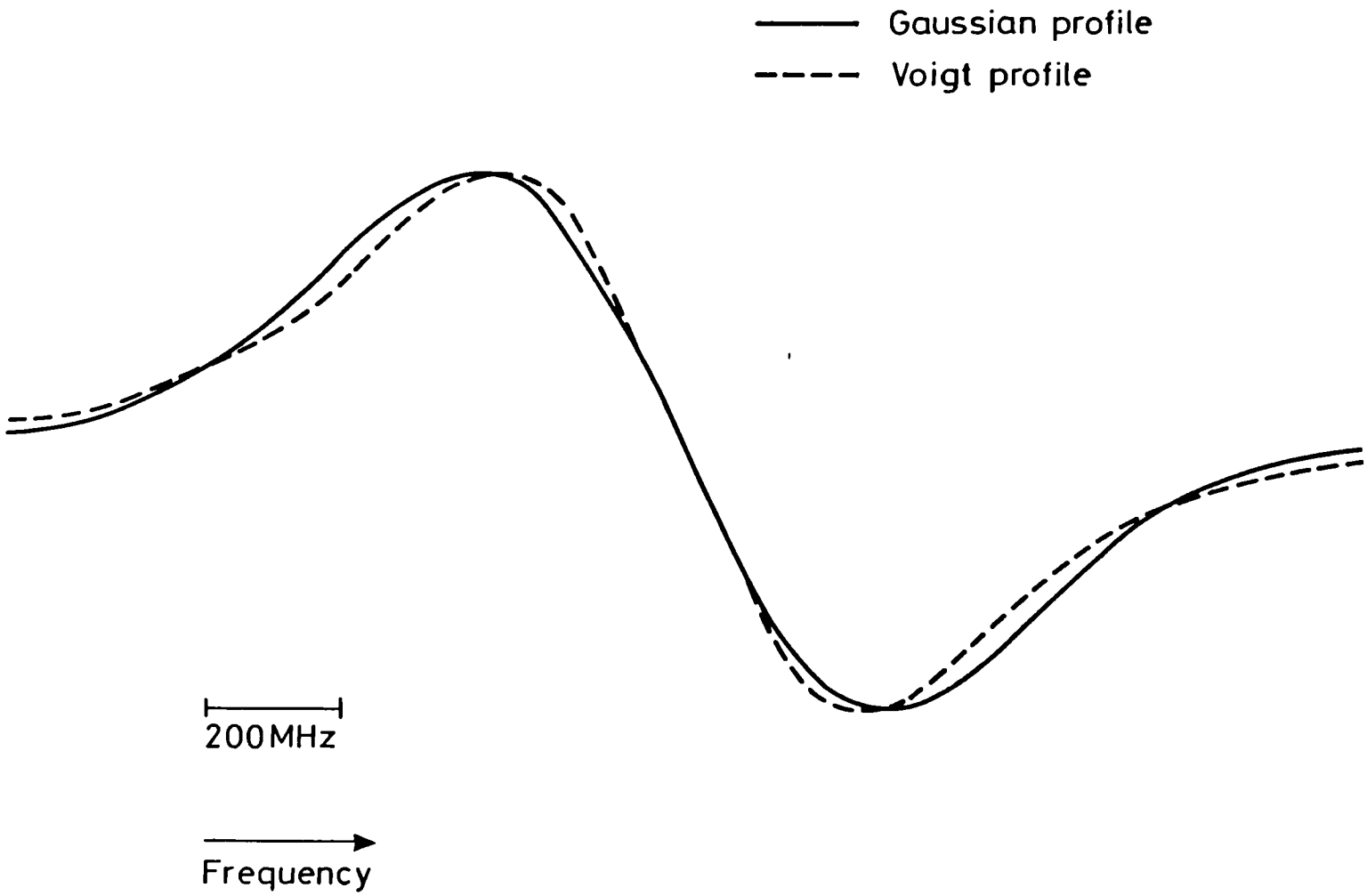

2.4.2 Comparison between Voigt and Gaussian profiles in derivative form, with the same width (700 MHz FWHM). The Voigt profile contains a Gaussian component of 500 MHz and Lorentz component of 360 MHz.

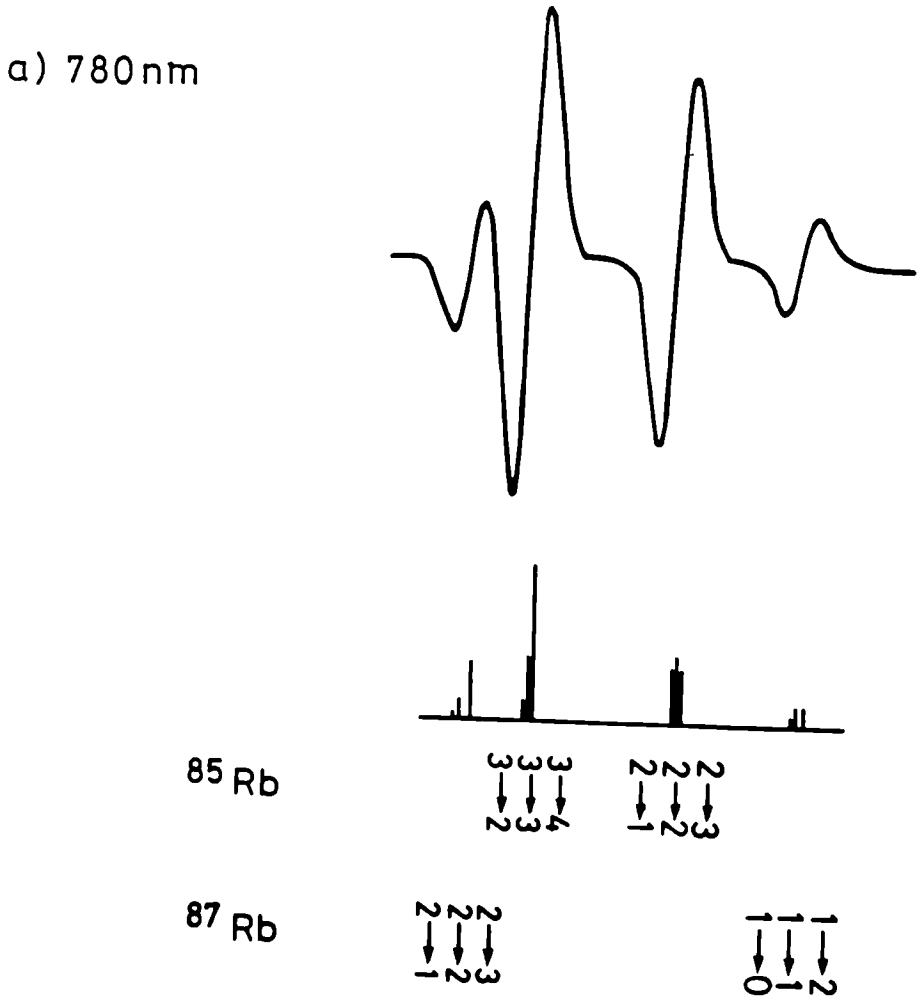

2.4.3 Calculated Rb absorption profiles for the hollow cathode lamp

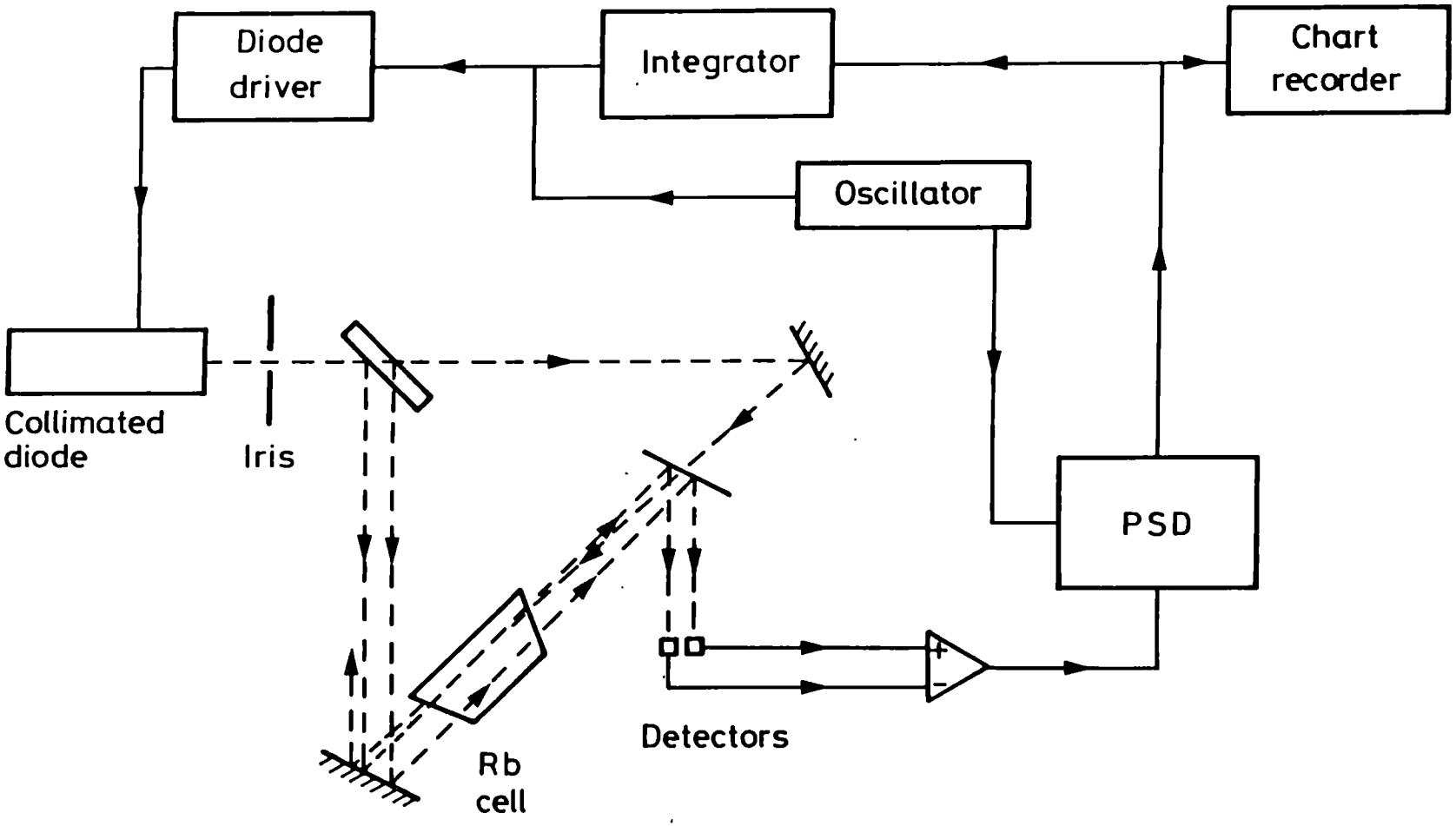

2.5.1 Experimental arrangement used to record hyperfine spectra of Rb

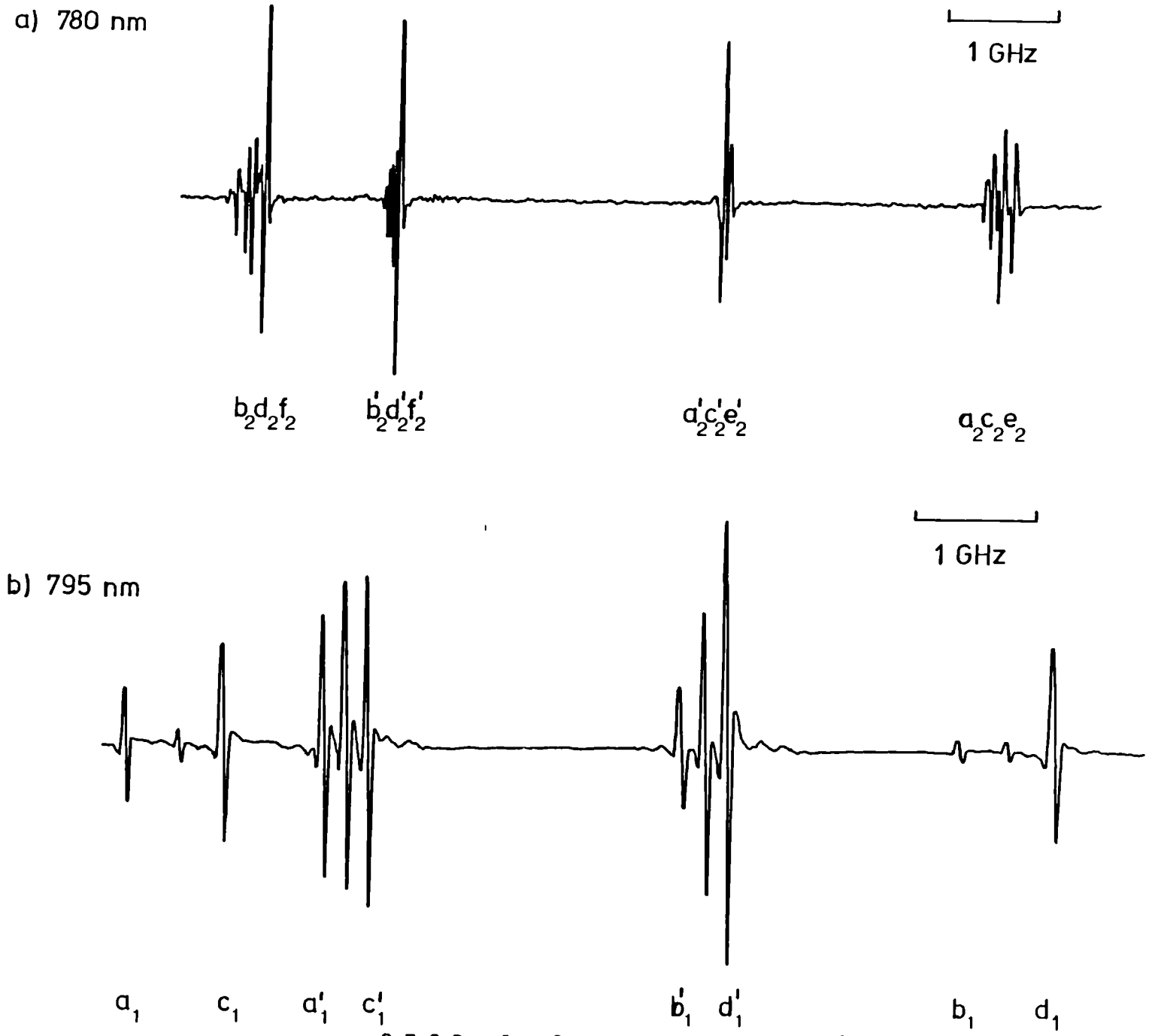

2.5.2 Doppler-free spectra of Rb at 780 nm and 795 nm for a mixture of ^{85}Rb and ^{87}Rb.

CHAPTER 3

ANALYSIS OF THE LASER LINEWIDTH AND TECHNIQUES FOR ITS REDUCTION

3.1 Introduction and Review of the theory of Laser Linewidth

The relatively large linewidth of the emitted frequency of laser diodes gives rise to problems in a number of key areas. Two such areas are the available resolution in laser spectroscopy and the fringe visibility in interferometry. In many common cw single frequency lasers, such as He-Ne devices, the linewidth is determined often by the level of air or ground bourne vibrations in the laboratory, perturbing the cavity length and hence the emitted frequency. If these vibration levels are reduced, then there remains the problem of noise due to the discharge (plasma oscillations). However, with laser diodes, the dominant problem is with the quantum limit, which arises from the very short, low-finesse cavity of a diode. Most texts on the subject of laser linewidths usually begin with a discussion of this fundamental quantum mechanical limit. It is caused by noise due to spontaneous emission in the cavity, and an equation describing this limit is rigorously derived in a number of textbooks [1,2] - the so-called Schawlow-Townes formula. The laser output may be represented by

$$E = E_o \exp\{j(\Omega t + \phi(t))\} \qquad (3.1.1)$$

with the phase $\phi(t)$ a randomly varying function of time. A particular spontaneous emission event in the laser cavity will change the field intensity from I to I + ΔI and the phase from ϕ to $\phi + \Delta\phi$ in a random fashion. In this analysis, however, field intensity fluctuations are

ignored. The probability distribution for the phase changes is assumed to be Gaussian because they are due to the many independant spontaneous emission events. If this distribution has variance ϕ_o^2, then the electric field autocorrelation function may be written

$$\langle E(t+\tau)E^*(t)\rangle = E_o^2 \exp(j\Omega\tau)\int_{-\infty}^{\infty} \exp(j\phi)P(\phi,\tau)d\phi \qquad (3.1.2)$$

where $\langle\rangle$ denotes an average over time t and $P(\phi,\tau)d\phi$ is the probability that the phase will change by an amount in the range ϕ to $\phi + d\phi$ in time τ. For a normal distribution of $P(\phi,\tau)$, this becomes

$$\langle E(t+\tau)E^*(t)\rangle = E_o^2 \exp(j\Omega\tau).\exp(-\tfrac{1}{2}\phi_o^2) \qquad (3.1.3)$$

Now it may be shown that [1]

$$\phi_o^2 = h\eta\Omega|\tau|/2\pi P\tau_c^2 \qquad (3.1.4)$$

where η is the inversion factor $N_2/(N_2-N_1)$, P the emitted laser power and τ_c the cavity lifetime. If the laser cavity half width is $\Delta\nu_{\frac{1}{2}}$, then $\tau_c = 1/2\pi\Delta\nu_{\frac{1}{2}}$. From the Wiener-Kintchine theorum, the Fourier transform of the electric field autocorrelation function yields the power spectrum. In this case, this gives rise to a Lorentz spectral broadening. The FWHM of this follows from equation 3.1.3, namely

$$\gamma = h\eta\Omega/2\pi P\tau_c^2 = 2\pi h\eta\nu(\Delta\nu_{\frac{1}{2}})^2/P \qquad (3.1.5)$$

For a typical cw laser system, we may make an order-of-magnitude calculation of γ. For P = 1 mW, ν = 500 THz, and $\Delta\nu_{\frac{1}{2}}$ = 1 MHz, $\gamma \approx 2$ mHz. It is therefore clear why, in the case of a He-Ne laser for example, other noise sources nearly always predominate. Such narrow linewidths are

gradually being realised only through the use of fast servo-control electronics, with linewidths of as little as 50 mHz being reported [3]. In the case of a diode laser, however, the quantum limit represents the most predominant limitation [2]. The very considerable difference in the quantum limit is due to the much greater value of $\Delta\nu_{\frac{1}{2}}$ for a diode laser. This, in turn, arises from the short cavity length and low Q of the cavity. The cavity half width is given by

$$\Delta\nu_{\frac{1}{2}} = (1 - R)c/2\pi nl\sqrt{R} \qquad (3.1.6)$$

for a cavity length l, refractive index n and facet reflectivity R. For a diode laser, nl = 1.3 mm, and R = 0.3 so that $\Delta\nu_{\frac{1}{2}}$ = 47 GHz. Hence, for P = 3 mW, γ = 1.5 MHz. Although this does indeed yield a much larger value for the linewidth, this is actually not sufficiently large to account for the observations of the value of the linewidth. The difference can be explained by considering the phase-intensity correlation that occurs inside the diode laser cavity [2]. Following each spontaneous emission event in a diode laser, there is a small change, $\Delta n''$, in the imaginary part of the refractive index from the steady state value. The change $\Delta n''$ is caused by a carrier density change, which in turn, alters the real part of the refractive index by $\Delta n'$. This produces a delayed phase shift of the laser radiation, causing further line broadening. This effect is in addition to the instantaneous phase change caused by the spontaneous emission. If α is defined by

$$\alpha = \Delta n'/\Delta n'' \qquad (3.1.7)$$

then equation 3.1.5 becomes [2]

$$\gamma = 2\pi h\nu\eta(\Delta\nu_{\frac{1}{2}})^2(1 + \alpha^2)/P \qquad (3.1.8)$$

Then, taking $\eta = 2.6$ and $\alpha = 5.4$ [2], this increases the linewidth by a factor of ≈ 30, yielding a width, as observed, of ≈ 45 MHz.

The ratio of the Schawlow-Townes limit for a diode laser to a He-Ne laser, both operating at 3 mW is therefore $\approx 7 \times 10^{10}$. It will prove to be of a considerable advantage to reduce this ratio, as described in the remaining sections of this chapter.

3.2 Measurements of the Natural Laser Linewidth

In this section, some of the methods used to measure laser linewidth are described. Use is then made of some of these methods to measure the linewidths of laser diodes, before any linewidth reduction techniques are applied. Two requirements of the chosen method are that it must not affect the linewidth of the laser it is supposed to measure and that it must have sufficient resolution for measuring the laser linewidth or jitter.

Perhaps the easiest method for many lasers is to use a scanning confocal cavity as an optical spectrum analyser. Confocal cavities are especially useful, since all the cavity spatial modes are degenerate, making it an easy to use cavity [4]. However, when one is used with a diode laser, it rapidly becomes clear that these analysers are quite unsuitable, except perhaps for low-accuracy monitoring of the laser mode, owing to optical feedback from the analyser. For weak levels of feedback, the linewidth of the laser is perturbed, and for high feedback levels ($>10^{-3}$), the laser can no longer operate in a single frequency. It was observed that an analyser was usable for monitoring the laser output only if the laser input was strongly attenuated, severely reducing the signal to noise ratio, and the analyser was not optimally aligned. However, this latter

measure certainly reduces the cavity finesse, making the linewidth appear broader than it really is. The non-Gaussian nature of the beam will also make the observed fringe width greater than that expected from the laser linewidth alone, unless the cavity is truly confocal. Finally, an acousto-optic modulator with a 40 MHz drive frequency was inserted between the laser and analyser. For a narrow-linewidth laser, this procedure alone usually provides near-perfect isolation, but in this case it was insufficient. This is presumeably because the drive frequency needs to be much greater than the linewidth. Commercially-available Faraday isolators, with a 30 dB reverse transmission, also did not provide sufficient isolation. Once the analyser feedback level is increased, for example by better alignment, then the observed transmitted signal becomes very complicated. It is therefore clear that a scanning confocal cavity cannot easily be used for linewidth measurements.

Two further methods often encountered are the use of a non-scanning confocal cavity and the optical delay homodyne method [5]. These are discussed here, but were not used owing to potential problems in interpreting the results. In the first method, the laser frequency is tuned so that it is halfway up to the maximum transmission fringe of a confocal cavity, similar to that used in the preceeding paragraph. This is then at a maximum sensitivity in terms of signal change to laser frequency excursion. However, it is subject to all the problems associated with optical feedback, as previously discussed. The method is most commonly used when this signal is also used to frequency lock, for example, a dye laser [6]. However, potentially serious problems arise if the detector/amplifier bandwidth is less than that of the frequency noise bandwidth, leading to an anomalously low observed width. This appears to be the problem with at least one anomalous published

result [7]. It may also be possible to overestimate the linewidth due to acoustic or other noise in the reference cavity. Intensity noise might also wrongly be interpreted as frequency noise. Essentially, the problem becomes one of ensuring that the observed signal truly reflects only laser frequency noise. In the second, delayed optical homodyne, method, frequency noise is measured by feeding part of the light into a fibre. The light is split, with one arm shifted in frequency by an acousto-optic modulator and the light sent down a long fibre. Essentially, this is a fibre version of a Mach-Zehnder interferometer. The light is recombined and focussed onto a detector, with the rf spectrum observed on a spectrum analyser. If the delay time τ_c is much greater than the reciprocal of the linewidth, a Lorentzian rf spectrum results. If the laser power is P, the acousto-optic drive frequency is $\Omega_a/2\pi$, then the spectrum is given by [5]

$$S = \tfrac{1}{2}P^2\tau_c/\{1 + (\Omega + \Omega_a)^2\tau_c^2\} \qquad (3.2.1)$$

The FWHM of this distribution is $2/\tau_c$ and the laser FWHM is therefore $1/\pi\tau_c$. However, this analysis assumes a white noise spectrum of the frequency. Such a measurement can give erroneous results in cases where 1/f noise predominates, for example [8]. However, this method has been used to measure the linewidth of Nd:YAG diode laser pumped lasers [5].

The two methods used here are measurements of interferometric fringe visibility and the rf spectrum of the difference (beat) frequency between two similar lasers. Either method may provide analysis of both the spectral lineshape and linewidth. The interferometric fringe visibility measurements were made only on lasers before linewidth reduction methods were implemented. A simple single-pass interferometer was used. Visibility loss can be caused both by the non-Gaussian nature

of the beam, and the large laser linewidth. The beam does not propagate well in free space, but begins to distort over distances of more than a few metres. An 8 mm beam size was used and an aperture was used to sample only the central 2 mm diameter of the beam. Even over path differences of a few metres, the fringes were well-formed across the 2 mm aperture. The observed loss of fringe visibility with optical path difference should therefore all be due to the laser linewidth. The detector used had a relatively slow response of ≈ 5 kHz. The detector bandwidth will determine the timescale on which laser frequency jitter is perceived to be an increased linewidth, giving rise to reduced fringe visibility. A fast detector, for example, would detect fast frequency jitter, and produce a slightly smaller value for the "instantaneous" linewidth. The relation between the timescale of the detection process and the observed linewidth and frequency jitter is extremely important and is discussed further in section 3.5. In this case, however, a fast measurement on a timescale comparable with the reciprocal of the linewidth is not attempted. It may also be noted that the fringe visibility method does not involve any risk of optical feedback to the laser, which would affect the laser linewidth. In order to discuss the results, we firstly define interferometric fringe visibility by

$$V = (I_{max} - I_{min})/(I_{max} + I_{min}) \qquad (3.2.2)$$

where I_{max} and I_{min} are the maximum and minimum transmitted intensities respectively. The fringe visibility results may be analysed to yield information on the linewidth and spectral profile [9]. In this reference, for example, which deals with InGaAsP (1.3 μm) lasers the lineshape is not Lorentzian, and some interesting fringe visibility curves result. The fringe visibility is the modulus of the electric field autocorrelation function. Therefore, from equations 3.1.3 and

3.1.4 an expression is obtained for V of the form $V = V_o \exp(-x/x_o) = V_o \exp(-\tau/\tau_o)$. Here, the interferometer time and path length delays are written as τ and x respectively. Taking the Fourier transform, we get the power spectrum, showing that the FWHM is $\gamma = 1/\pi\tau_o$. Since $\tau_o = x_o/c$, then

$$\gamma = c/\pi x_o \qquad (3.2.3)$$

In figure 3.2.1, V is plotted versus optical path difference. The results are fitted to a curve, as shown, of the form $V = V_o \exp(-x/x_o)$. A least squares fit yields x_o = 3.5 m (30 MHz FWHM) at 5 mW power for the Mitsubishi or Hitachi lasers. Linewidth varies inversely with power, according to the theory described in the previous section. It might therefore be expected that the higher power 780 nm diodes available (up to 30 mW) might have a narrower linewidth. However, this will depend upon how the higher power is achieved. In a Sharp LT024MD laser, increased power is achieved [10] by anti-reflection coating the front laser facet and coating the back facet with a highly reflecting film. For this laser, operating at 20 mW, x_o is measured to be only 1.2 m (80 MHz FWHM). For a higher power Mitsubishi laser (model 6101A) operating at 20 mW, x_o was determined to be 3.3 m, similar to the 5 mW devices. In figure 3.2.2, results for an index-guided, single frequency laser, operating at 670 nm and 3 mW are shown (Toshiba model TOLD 9211). This device has x_o = 2.06 m (46 MHz FWHM). This is the first detailed report of the variation of interferometric fringe visibility with optical path difference for these commercially available diodes.

Secondly a measurement of the laser linewidth at 780 nm was made by analysing the spectral width of the rf difference (beat) frequency between two lasers. If the beams from two lasers emitting at two similar frequencies Ω_1 and Ω_2 are overlapped on a partly-transmitting mirror and

imaged onto a fast detector, the detector photocurrent I is proportional to

$$I \propto |A_1 \exp(j\Omega_1 t) + A_2 \exp(j\Omega_2 t)|^2 = A_1^2 + A_2^2 + 2A_1 A_2 \cos\{(\Omega_2 - \Omega_1)t\} \quad (3.2.4)$$

assuming A_1 and A_2 are real. If this is not the case, then the cosine term must contain an extra phase factor. If this signal is fed into an rf spectrum analyser, a peak is observed at $|\Omega_2 - \Omega_1|$. In this case a BPW 28 Telefunken avalanche photodiode was used, which had a frequency response to about 3 GHz, together with an rf frequency low-noise amplifier (eg from Avantek). Both lasers have a Lorentzian spectral profile of the form

$$L(\gamma,\nu) = \tfrac{1}{2}\gamma(\gamma^2/4 + (\nu - \nu_o)^2)^{-1} \quad (3.2.5)$$

where ν is the optical frequency, ν_o the carrier frequency and γ the laser FWHM. The beat frequency is then a convolution of $L(\gamma_1, -\nu_1)$ and $L(\gamma_2, \nu_2)$ if $\nu_2 > \nu_1$. This may readily be evaluated as $\sqrt{(\tfrac{1}{2}\pi)}L(\gamma_1+\gamma_2, \nu_2-\nu_1)$. This may be proved either through the Fourier properties of a convolution or directly using the complex residue theorum. For two diodes, each with a FWHM of 30 MHz the expected beat width is therefore 60 MHz. This method has one principal disadvantage, namely that only a combined linewidth of two lasers can be measured. If the lineshape is Lorentzian and both lasers are similar, then this analysis shows some justification for halving the result for the linewidth of one laser. This method yields an accurate and reliable result especially when narrow linewidth lasers are investigated. The resolution is limited only by the rf spectrum analyser bandwidth, typically < 1 kHz. This method is therefore that used in the following sections when measuring the spectral width of linewidth-reduced diode lasers.

3.3 Advantages and Applications of a Linewidth-reduced Laser

Before describing work on the linewidth reduction of diode lasers, the disadvantages are summarised of the relatively large linewidth of diodes as well as the corresponding advantages of linewidth reduction. It has already been observed, for example, that GaAlAs index-guided diodes are limited in interferometry to path differences of ≈3 m. Further, the resolution in spectroscopy is limited to ≈30 MHz, normally greater than the natural width of the transition being investigated. Transitions forbidden by the normal selection rules of quantum mechanics, which generally have linewidths of less than a few kHz, certainly cannot readily be investigated. Further, one of the less expensive and more convenient means of optical isolation, using an acousto-optic modulator, fails to work successfully. This is because the drive frequency needs to be considerably greater than the linewidth. The large laser linewidth is also observed as a large beat frequency spectral width. This proves to be a problem for accurate measurements of the difference frequency between two laser diodes. Use is often made in such measurements of an rf tunable bandpass filter to cut down on wideband rf noise not at the beat frequency. This improves the reliability of a counter used to measure the beat. Commercially available filters typically have a FWHM passband of 5% of the frequency; eg 50 MHz at 1 GHz. Since the beat width of the natural diode is ≈60 MHz, this filter bandwidth is far too narrow. If such a signal is then fed into a counter, it is observed that the displayed frequency tunes with the filter centre frequency. In these various straightforward ways, therefore, a diode laser with a linewidth reduced at least to 1 MHz would then behave in many ways like any other cw single frequency laser.

A 30-fold improvement in linewidth would put diode lasers on equal terms

with commercially available dye lasers as far as linewidth is concerned. Dye lasers might still be necessary if more than 100 mW were required or if the wavelength needed was outside the diode laser availability range. Commercially-available single mode diode laser powers are increasing all the time, and 150 mW is at present available at ≈820 nm from Spectra Diode Labs. If a diode laser could easily be made to oscillate with a narrower linewidth than commercially available dye lasers, then this has excellent potential metrological importance. Considerable effort is being put into producing dye lasers with ultra narrow linewidths in order to provide the next generation of optical frequency standards. These are likely to be based on transitions in ions which have been trapped and cooled in an electromagnetic trap [11]. Spectroscopic transitions are known which have very narrow linewidths, corresponding to an excited state lifetime of as long as several days. For an optical transition of 5 days, this corresponds to a resonance Q of a staggering 2×10^{20}. This particular application is discussed a little further in section 7.2. For dye lasers, linewidths of less than 1 Hz have already been realised, but diode lasers are potentially so much simpler. However, even a laser linewidth of 1 Hz will broaden the observed linewidth by many orders of magnitude, if the Q is 2×10^{20}. The problem, ultimately, appears to centre on the design of the cavity and cavity mounting to minimise external noise sources. Further, such a laser ideally needs a stability comparable with the linewidth, at least on a timescale of a few seconds.

Diode lasers, therefore, need investigation to see whether they can also fulfill a role as part of a new optical frequency standard. Linewidth reduction can greatly enhance the usefulness of diodes in high resolution spectroscopy, optical frequency metrology and laser interferometry. It should also improve their usefulness in other areas

such as coherent fibre communications and as a source in fibre sensor applications. The next two sections therefore survey possible methods and the results obtained.

3.4 Survey of Techniques and choice of Preferred Method

Given the need for linewidth reduction of a diode laser, this section focusses upon the methods which are available to achieve this. In general, methods divide into electrical and optical feedback techniques. Several of the techniques, including that studied in detail in the next section, are capable of producing linewidths of ≈10 kHz or better. It should be said that this section is concerned with the reduction of diode laser linewidths *per se*. Diodes may, for example, be used to pump other solid state lasers such as Nd:YAG which also achieves a 10 kHz linewidth. Such lasers may be further reduced in linewidth by servocontrol methods to achieve ≈10 mHz linewidths [12,13].

The first possibility for diodes is to extend the electronic servocontrol methods developed for commercial dye lasers [6]. This references a dye laser frequency to the transmission peak (or reflection minimum) of a confocal cavity. In the simplest method, the laser is frequency locked to the side of a transmission fringe. Such a system requires the development of faster servocontrol techniques than those used for dye lasers. This is principally because of the different causes of spectral broadening in dye and diode lasers. Commercial dye laser electronics operate at up to a few kHz to achieve a linewidth reduction from 20 MHz rms to 0.5 MHz rms. The frequency jitter arises from instability in the dye jet. Diode lasers, however, are limited by quantum effects and so the servocontrol bandwidth needs to be comparable with the linewidth. A 560 Hz linewidth has been reported with fast

servocontrol [14]. For best results, the cavity reflected signal is used, since this can give a faster error signal, not limited by the cavity response time. The laser is locked to a reflection minimum by rapidly phase modulating the laser using an electro-optic modulator and recovering the signal synchronously with a double balanced mixer. This can provide an error signal suitable for locking the laser. Such electronic techniques may appear straightforward, giving good linewidths, but the electronics are not easy to develop and, at least for a 10 kHz linewidth, optical techniques have the advantage of simplicity.

All optical techniques rely upon overcoming the fundamental reason for the large diode laser linewidth. This is the very short low-Q cavity, and so the optical techniques involve extending it or coupling it to another one. The methods involve either strong or weak optical feedback. In the case of strong feedback, the laser facets are AR coated and an external mirror and grating are used. Lasing action then occurs between the external mirror and grating, which provides the frequency tuning. This method has been reported to achieve a 10 kHz linewidth for an infra-red laser [15]. The method, although requiring the laser chip to be anti-reflection (AR) coated on one facet, allows the laser to be tuned anywhere within the emission band gap. The laser loses the "staircase tuning" characteristic of the basic unmodified diode. Using weak optical feedback techniques retains this tuning characteristic, although the laser does not need modification. The simplest example of this [16] is to reflect a small proportion of the collimated laser light ($\approx 1 \times 10^{-5}$) back to the laser from an external plane mirror. In figure 3.4.1, the effect of using a plane mirror $\approx$1 m from the laser with a feedback level of $\approx 3 \times 10^{-5}$ is shown. The spectrum analyser FSR is 2 GHz and the upper and lower traces correspond to no feedback and with

feedback respectively. There is a critical optimum feedback level for a given laser to mirror separation to achieve the best linewidth. Up to a 100-fold reduction in linewidth has been reported [16]. If the feedback level exceeds the critical value, then many external cavity modes begin to appear, increasing rather than reducing the linewidth. In figure 3.4.1, the feedback level is just at the critical value, and two extra external cavity modes are observed in the wings of the main mode, in the lower trace, consistent with theory. This is the type of instability expected for a three-mirror cavity. Further, the position of the feedback mirror needs to be piezoelectrically adjusted in order to obtain continuous laser tuning. An attempt to obtain an error signal which could be used to control the position of the feedback mirror was unsuccessful. It was thus not possible to prevent modes hops between external cavity modes. If the feedback mirror is not sufficiently rigidly mounted, then vibration of this mirror will cause laser frequency jitter.

Two further techniques involving weak optical feedback may briefly be noted. The first is that applicable to lasers pig-tailed to optical fibres, which have been linewidth-reduced using the frequency dependent optical feedback from a fibre interferometer system. Such a technique has been developed to achieve good short-term frequency stability for fibre sensor work [17]. Secondly, there is a weak optical feedback technique suitable for diode arrays, which can produce several watts output, a much higher power than the index-guided devices used in this work. However, diode arrays normally produce a broad spectrum of light, typically a few nm in linewidth in many modes. This technique, termed injection locking, promises to provide high power in a narrow linewidth from an array. A small portion of light from a single frequency narrow linewidth source is fed into a segment of the array. A power of 90 mW in

a linewidth of 300 kHz has been reported using this method [18]. The output frequency of the array becomes single mode and the emitted frequency locks optically to that of the low power injected laser. The spatial mode of the array changes, becoming diffraction limited. This technique may soon give diode lasers all the advantages of a dye laser in this part of the spectrum, but without the problems of dye degradation and difficulties associated with the ion pump laser.

In recent years, however, the most highly successful weak optical feedback technique involves feedback from an off-axis resonant confocal cavity [8,19,20] or some comparable arrangement [21]. This technique works extremely well, although this system still tunes discontinuously. A linewidth reduction of at least 1000 is readily achieved. This produces linewidths comparable with external cavity systems. This method can only be used where the laser mode is completely stable and has no tendency to mode-hop to another mode. Such a situation often occurs near a mode-hop position, and the perturbation caused by the optical feedback can then induce a mode-hop away from the desired frequency. The method relies upon the feedback being at a minimum of typically around $\approx 1 \times 10^{-3}$ to $\approx 1 \times 10^{-4}$ at the resonant frequency of an interferometer. A simple means of achieving this is shown in figure 3.4.2. When used off-axis, the confocal cavity emits four beams (labelled "a" to "d"). Beams "a", "b" and "c" are at a maximum on resonance whereas beam "d" has a minimum on resonance. Beam "d" is prevented from returning to the laser by means of an aperture, and only beam "c" with a maximum on resonance, feeds back into the laser. This arrangement not only reduces the spectral linewidth, but the laser frequency also locks optically to the cavity resonance. The initial laser frequency must be close enough to a cavity resonance for both these effects to occur. It is essential to control the length (ie the phase) between the laser and cavity so that it equals

an integral number of half-wavelengths. If this is not done, then changes in this length will firstly pull the laser frequency and secondly broaden the spectral linewidth. In our system this length is controlled by a Brewster-angled tipping plate similar to that used to tune dye lasers. This has the advantage of a greater tuning range than a piezoelectrically mounted mirror. The properties of such a tuning plate may be derived from geometrical optics. If the plate is of thickness y, refractive index n and the beam is incident at an angle θ, then the path length varies as

$$p = p_o + y\{(n^2 - \sin^2\theta)^{\frac{1}{2}} - \cos\theta\} \qquad (3.4.1)$$

In this case, a 10 mm square 2 mm thick silica plate was fixed to a General Scanning G108 galvo unit. Differentiating equation 3.4.1 for $\theta = 56°$ and $n = 1.5$, yields $dp/d\theta = 0.46y$. For $y = 2$ mm and $\Delta\theta = 1°$, $\Delta p = 16$ μm. The next section describes in detail the results obtained on linewidth reduction using this method of resonant optical feedback.

3.5. Predicted and Observed Laser Linewidths

Various linewidth-reduced laser diode systems were assembled using the basic experimental arrangement of figure 3.4.2. The feedback parameter, β, was varied and one of two pairs of cavities with free spectral ranges 0.3 GHz and 2 GHz were used, obtained from Technical Optics. The feedback parameter was estimated from the transmission and reflection of the various feedback optical components. The collimation optics used transmitted 50%, the loss being due to aperturing. The collimator used for the experiments described in most of this thesis was a compound lens producing an 8 mm diameter beam. The beamsplitter had a 20% reflectance and the cavity reflectance on resonance was measured to be between 2%

and 5%. A maximum reflectivity of 25% on resonance from an off-axis confocal cavity may be expected. The loss here is probably due to the non-Gaussian nature of the beam. Indeed, the reflectivity for the 0.3 GHz cavity was somewhat less than for the 2 GHz cavity at 2% and 5% respectively. This might be as one would expect if the losses were due to poor beam quality, and the increasing distortion of the diode beam with distance.

In figure 3.5.1, the transmitted signals are shown for the case $\beta = 2 \times 10^{-4}$, a cavity FSR of 2 GHz and a cavity to laser separation of 1 m. The two results are for scanning the cavity (a) and laser current (b). The signals may be explained by recalling that resonant feedback causes the laser frequency to lock to the cavity resonance. This locking only occurs if the laser frequency is sufficiently close to a cavity resonance. From figure 3.5.1. we observe that in this case, the capture range is 300 MHz. In figure 3.5.1a, the cavity to laser distance is not controlled, and the optical lock is optimum only when this distance is also an integral number of half-wavelengths. The separation of the modes within the optical capture range therefore corresponds to the laser to cavity distance. In figure 3.5.1b, once the laser current is used to tune the frequency within the optical capture range, a servo-system controls the laser to cavity distance to be an integral number of half-wavelengths until the laser abruptly falls out of lock. This yields an unusual flat-topped Fabry-Perot fringe with a 300 MHz width. This capture range is a function of the feedback coupling (β) and may be predicted from published theory. This gives a double check for the measured value of β, and it also turns out that the capture range is very similar for the two cavities used, provided that β is the same. For example, for $\beta = 2 \times 10^{-4}$ and 5×10^{-4} the predicted capture ranges are 270 MHz and 420 MHz respectively.

The servo-system which controls the laser to cavity distance comprises a PSD and integrator [22], acting upon the signal transmitted through the cavity. Path length modulation at 500 Hz and feedback are provided via the Brewster angled tuning plate. Once the laser frequency was optically locked to the cavity, the servo-system then holds the transmitted signal to a maximum. It is important to minimise the Brewster plate modulation amplitude for this servo-system, since this will pull the laser frequency. In the case where the narrowest linewidths were observed using the 0.3 GHz FSR cavity, this amounted to no more than 5 kHz on the linewidth.

The sharp reduction in linewidth may best be understood from published theory [8] by considering the increase in the total stimulated energy (E_{tot}) in the laser mode as a result of coupling to the cavity. If the confocal cavity and laser cavity storage times are given by τ_s and τ_d respectively, then the stimulated energy increases by a factor $(1 + \beta\tau_s/\tau_d) \approx \beta\tau_s/\tau_d$. The linewidth is given by the modified Schawlow-Townes expression

$$\Delta\nu = E_{sp}/4\tau E_{tot} \qquad (3.5.1)$$

Here, E_{sp} is the steady-state spontaneous energy and τ the storage time. This time corresponds to either τ_s or τ_d, depending upon whether the feedback cavity is present or not. The confocal cavity length and finesse are denoted by L and F respectively. The subscript d denotes the corresponding diode laser cavity parameters, and ηL_d is the laser cavity optical length. The linewidth is then reduced by a factor $\beta(\tau_s/\tau_d)^2 = \beta(LF/\eta L_d F_d)^2$ from the Schawlow-Townes width. In order to obtain the narrowest linewidths, it is therefore essential to use a long, high-finesse cavity and optimise β. Although increasing β reduces the

linewidth, the laser will no longer emit in a single mode if this is increased too much. Theory also suggests that there is a threshold value for β ($\approx 2 \times 10^{-6}$) below which optical locking will not take place, though this was not tested.

The measurement of the laser linewidth was made by assembling two identical systems and observing the beat frequency on an rf spectrum analyser. A Faraday isolator was used to prevent unwanted feedback from the fast detector monitoring the beat. Various feedback levels from the 0.3 GHz and 2 GHz cavities were tried. In order to ascertain the general effect on the beats spectrum, a log plot of signal size at low resolution (300 kHz bandwidth) and large scan range was made on a Hewlett-Packard 8554B analyser. The chart recorder response was rather longer than the 100 Hz video filter bandwidth selected on the analyser, and care was taken to ensure that the true narrowed signal height was obtained. If the analyser bandwidth is b, and the FWHM of the natural diode beat linewidth is γ_o ($\gamma_o \gg b$), then the difference between the peak heights in the two cases is given by

$$S = 10\log_{10}(\gamma_o/b) + 1.7 \text{ dB} \qquad (3.5.2)$$

where the result is in dB. The extra factor of 1.7 dB arises [23] because the analyser and chart recorder filter the signal <u>after</u> the signal log spectrum is determined. In contrast to figure 3.5.2b, where $\gamma_o \gg b$, in figure 3.5.2a the signal width is $\ll$ b. The 1.7 dB may be seen as a correction for the analyser bandwidth. Since b = 300 kHz and γ_o is observed to be 80 MHz here, S = 26 dB. This compares quite well with the 28 dB observed directly.

There now remains the problem of determining the laser linewidth. This

is not as straightforward as it might appear, because of the observed associated frequency jitter. It should firstly be ensured that this jitter is not simply due to poor cavity stability or design of the overall system. Some initial problems with this system needed to be overcome to optimise the performance. These included insufficiently rigid mountings for some of the optics, optical feedback from unwanted sources, air-bourne vibration or draughts through the laser to cavity airspace and, finally, noise on the high-voltage supply to the cavity piezoelectric. Particular frequency components in laser frequency noise could be monitored by feeding the beat signal into a frequency to voltage converter. The output from this was then monitored on a rf spectrum analyser. A component at ≈500 Hz could be observed in this way, for example, due to the dither on the Brewster plate.

In order to measure the beat linewidth, several scans across the beat signal were made at a scan rate of 100 kHz/s, at a spectrum analyser bandwidth of 3 kHz (figure 3.5.3). A weak offset-lock prevented excessive frequency drift between measurements. The mean of 13 measurements was 21 ± 10 kHz (FWHM), compared to the 80 MHz beat width with no feedback. There is a particular measurement problem here, namely that of measuring the laser linewidth in the presence of significant frequency noise and Brewster plate modulation. If a more rapid measurement could be made, the linewidth contribution from certain types of frequency noise would be reduced, and the effect of Brewster plate modulation eliminated. Naturally, one is eventually limited by the uncertainty principle in the time available to measure the linewidth. An alternative method to measure the linewidth was therefore employed, which corresponds to a more rapid measurement. The spectrum analyser voltage output is a measure of power in a given bandwidth. For a given laser linewidth, a decreasing analyser bandwidth eventually will result

in a decreasing output signal. Detailed considerations show that the peak signal size (S) should decrease according to the relation.

$$S = -10\log_{10}(1 + \gamma/b) \qquad (3.5.3)$$

where γ is the FWHM narrowed linewidth and b is the spectrum analyser bandwidth. Figure 3.5.4 shows a logarithmic plot of the signal size versus bandwidth, together with the expected roll-off from equation (3.5.3) for a linewidth of 4 kHz. The timescale of this measurement, limited by the spectrum analyser response, is ≈1 ms. This represents a 20 000-fold improvement in the linewidth, which is all achieved optically. This is the first reported use of rf spectrum analyser bandwidth to measure optically narrowed diode laser linewidths. Our result is the best reported enhancement using resonant optical feedback, although the measured linewidth is a function of the timescale of the measurement method. The actual linewidth of either laser will be less than this beat width but the exact relationship will depend upon the lineshape. For example, the laser linewidth would be half this value (2 kHz) if both lineshapes were Lorentzian and of equal width. For longer measurement times of several seconds, however, we confirm that the spectral profile is no longer Lorentzian. Indeed a dependence of

$$S \propto \{\gamma^2/(\gamma^2 + 4(\nu - \nu_o)^2)\}^{3/2} \qquad (3.5.4)$$

has been reported elsewhere [8]. When plotted logarithmically, our experimental results can be fitted to such a formula to within ±1.5 dB.

The calculated linewidth reduction factor, however, for F = 170 and F_d = 2.6 is ≈34 000 [8]. However, this is the reduction from the Schawlow-Townes width, which differs from the observed width by a factor

$(1 + \alpha^2) \approx 30$. This yields a calculated width of 40 Hz, well below that observed. The degradation is due to the 1/f noise source which is in addition to the assumed white noise source.

Having obtained a definitive value for the linewidth, the remaining task is to demonstrate an application of such a system. The final two sections of this chapter describe the use of this optically narrowed laser in Rb spectroscopy.

3.6 Development of a Scannable Narrow-linewidth Laser

With the technique for producing a diode laser with a linewidth in the region of 10 to 100 kHz established, it is necessary to constuct a fully tunable system for use in spectroscopy. The laser frequency in this system, is essentially controlled by the cavity which is piezoelectrically tunable. Long range scans appear desirable, but this requirement is at variance with that of stability or linewidth. The piezoelectric can tune four cavity mode spacings, or 1.2 GHz and 8 GHz for the 0.3 GHz and 2 GHz FSR cavities respectively. However, the longer cavity produces the best linewidths. Furthermore, for a short cavity, frequency stability is more dependent upon the stability of the piezoelectric voltage supply. Any mains-locked noise, for example (typically 2 mV peak to peak) will be more noticeable as frequency noise on the shorter cavity. For interrogating allowed transitions in Rb, stability and linewidth can easily be traded for increased scan range. Furthermore, the long cavity was found to be more difficult to operate, since the transmitted signals became very complicated once the capture range became comparable with or greater than the FSR. Such a system can be bi- or even multi-stable, increasing operational problems. The linewidth of the beat frequency between two systems optically locked to

two different 2 GHz FSR cavities is 200 kHz. This is in contrast to the 20 kHz width of figure 3.5.3, and is more than sufficient for laser spectroscopy of Rb.

It may also be noted that these cavities are air-spaced and so the drift of either laser is probably predominantly related to air refractive index changes and much larger than the beat frequency drift rate. The actual frequency drift of either laser may readily be calculated to be [24] +365 MHz/°C and -100 MHz/mbar respectively at 780 nm. In addition to the effect upon the frequency drift, this will also affect the duration of the optical lock. For example, if in figure 3.5.1 the laser is set in the middle of the captive range, an air pressure change of ±1.5 mbar will cause the lock to be lost. For this reason, and to remove the frequency noise discussed in the previous section, it may be desirable in some situations to pre-stabilise the system to a second more stable cavity by electronic servocontrol. If such a cavity were evacuated and made from an ultra-low expansion material it would produce a highly stable system with a linewidth probably less than 2 kHz. This could easily be suitable for optical frequency metrology based on ion traps [11].

Figure 3.6.1 shows the scannable narrow linewidth system, generally used with a 2 GHz FSR cavity. The laser frequency is controlled by tuning the cavity. A small proportion of the voltage required is also fed to the laser diode driver. This controls the laser current sufficiently well to keep the laser frequency within the optical lock range. The Brewster plate servo follows the laser tuning. If required, the laser frequency may be modulated by modulating the cavity piezoelectric voltage. Such a system is well suited to the Rb spectroscopy described in the final section.

3.7 Doppler-free Spectroscopy with a Narrow-linewidth Laser

The apparatus shown in figure 3.6.1 was used to observe the Doppler-free components of the Rb D_2 line. A simple two-pass saturation arrangement through the Rb cell is shown and a third-harmonic technique used to remove the Doppler-limited background [25]. The saturating power was typically 30 μW in a 8 mm diameter beam. The result of an overall scan over the Rb D_1 and D_2 lines at at 795 nm and 780 nm is shown in figure 3.7.1. A maximum signal to noise ratio of about 300 is observed on the strongest lines. The picture is quite complex, partly because a mixed-isotope cell was used. The groups of lines labelled (i) and (iv) are associated with ^{87}Rb. The centre two groups, (ii) and (iii), have their components labelled with a dash (') and are due to ^{85}Rb. Since such a wide scan makes it hard to appreciate fully the resolution achieved, four shorter-range scans were made at 780 nm, and the results shown in figure 3.7.2. The structure here is due to the hyperfine interaction. Figure 3.7.2 shows the first reported complete resolution of the closely spaced hyperfine structure at 780 nm using a laser diode. A full analysis is not attempted here, but some understanding of the structure may be made by reference to figure 2.4.1. Each group contains six third-derivative signals, not all clearly resolved, of which three are due to spurious signals called level crossings. These arise in saturation spectroscopy and have previously been explained in section 2.5. Group (i) is the most clearly resolved and the six components in order of increasing frequency may readily be designated.

(i) $F = 2 \rightarrow F = 1$

(ii) Level crossing between signal (i) and signal (iii)

(iii) $F = 2 \rightarrow F = 2$

(iv) Level crossing between signal (i) and signal (vi)

(v) Level crossing between signal (iii) and signal (vi)

(vi) $F = 2 \rightarrow F = 3$

The remaining three groups may similarly be designated. Group (ii) is basically due to $F = 3 \rightarrow F = 2,3,4$ and (iii) due to $F = 2 \rightarrow F = 1,2,3$ transitions both in ^{85}Rb. Group (iv), like group (i) is due to ^{87}Rb and is due to $F = 1 \rightarrow F = 0,1,2$ transitions. Further analysis is left until section 5.3.

The linewidth expected on these transitions is 6 MHz [26], together with a little additional broadening of < 1 MHz due to the earth's magnetic field and the Zeeman splitting of the lines. A further measured broadening of 1.2 MHz was due to laser power broadening and there was also a 0.7 MHz modulation broadening. This yields an expected linewidth of 9 MHz. The linewidth (FWHM) was measured by measuring the change in beat interval between closely spaced components firstly with the two lasers locked to line centre on both components involved and then with one laser was locked to a subsidiary zero crossing. A third derivative signal has a electronic zero crossing at line centre, and two further zero crossings, separated by the FWHM, of opposite slope to the main zero crossing. This may readily be proved by examining the third derivative of a Lorentzian, which is

$$L''' \propto \frac{(\Omega - \Omega_o)(\beta^2 - (\Omega - \Omega_o)^2)}{(\beta^2 + (\Omega - \Omega_o)^2)^4} \qquad (3.7.1)$$

This equation also shows that the subsidiary zero crossings lie at $\pm\beta$ (ie at $\pm$ the half width at half maximum) from line centre. By changing the PSD phase by 180°, the laser may be locked to these zero crossings. In this way, a determination of the linewidth to $\pm$ 2 MHz (3σ) may be made. On level crossings "b/f" and "d/f" (figure 3.7.2), linewidths of 11 MHz and 12 MHz (FWHM) with an asymmetry of only 1% were measured. These

linwidths suggest some contamination of the cells by foreign gases and requires further investigation. This foreign gas broadening presumably amounts to around 1 MHz from these measurements. Such contamination is almost certain to produce frequency shifts, as it does in iodine cells [27].

However, these Rb features can now be observed with no significant broadening of the feature being due to the laser itself. Using these spectra, optically narrowed diode lasers can now be locked to at least some of the Rb D_2 components, as well as those of the Rb D_1 line at 795 nm. These latter components do not necessarily need linewidth reduction to resolve the components. These results may be compared with other Rb spectra obtained using optically narrowed diodes [28] published at a similar time to the data reported here [29]. The spectra reported in this section represent the first Doppler-free thired harmonic spectra obtained with an optically narrowed laser diode. These results will be used in the following two chapters to demonstrate the most comprehensive study to date of Rb-stabilised laser diodes.

References

[1] A Yariv, "Quantum Electronics" (3rd edition), John Wiley & Sons (1989)

[2] C H Henry, IEEE J Qu. El., QE-18, No 2, 259-64 (1982)

[3] D Hils, J L Hall, Proceedings of 4th Symposium on Frequency Standards and Metrology, Ancona, Italy, Sept 5-9 1988, p 162-73.

[4] M Hercher, Appl Opt, 7, No 5, 951-66 (1968)

[5] S P Bush, A Güngör, C C Davis, Appl Phys Lett, 53, No 8, 646-7 (1988)

[6] T F Johnston Jr, R H Brady, W Profitt, Appl Opt, 21, 2307-16 (1982)

[7] Y C Chung, T M Shay, Electron Lett, 23, No 20, 1044-5 (1987)

[8] P H Laurent, A Clairon, C H Bréant, IEEE J Qu El, 25 No 6, 1131-42 (1989)

[9] E Eichen, P Melman, Electron Lett, 20, No 20, 826-8 (1984)

[10] Sharp Laser Diode User's Manual, p16.

[11] D J Wineland, W M Itano, R S Van Dyck Jr. Adv. Atom. Molec. Phys, 19, 135-86 (1983)

[12] D Shoemaker, A Brillet, C N Man, O Cregut, G Kerr, Opt Lett, 14, No 12, 609-11 (1989)

[13] T Day, A C Nilsson, M M Fejer, A D Fainas, E K Gustafson, C D Nabors, R L Byer, Electron Lett, 25, No 13, 810-2 (1989)

[14] M Ohtsu, M Murata, M Kourogi,IEEE J Qu El, 26, No 2, 231-41 (1990)

[15] R Wyatt, W J Devlin, Electron Lett, 19, No 3, 110-2 (1983)

[16] L Goldberg, H F Taylor, A Dandridge, J F Weller, R O Miles, IEEE J Qu El, QE-18, No 4, 555-64 (1982)

[17] JP Dakin, PB Withers, Optica Acta, 33, No 4, 489-99 (1986)

[18] S-Q Shang, H J Metcalf, Appl. Opt. 28, No 9, 1618-23 (1989)

[19] B Dahmani, L Hollberg, R Drullinger, Opt Lett, 12, No 11 876-8 (1987)

[20] C H Shin, M Teshima, M Ohtsu, Electron Lett, 25, No 1, 27-8 (1989)

[21] H Li, H R Telle, IEEE J Qu El, 25, No 3, 257-64 (1989)

[22] K C Shotton, W R C Rowley, NPL Report Qu28 (2nd revision 1978)

[23] Hewlett-Packard Application Note 150-9 (1976)

[24] B Edlen, Metrologia, 2, 71-80 (1966)

[25] A J Wallard, J Phys E, 5, 926-30 (1972)

[26] O S Heavens, J Opt. Soc. Am, 51, No 10, 1058-61 (1961)

[27] W R C Rowley, B R Marx, Metrologia, 17, 65-6 (1981)

[28] A Hemmerich, DH McIntyre, D Schropp Jr, D Meschede, TW Hänsch, Opt Comm, 75, No 2, 118-22 (1990)

[29] GP Barwood, P Gill, WRC Rowley, J Mod Optics, 37, No 4, 749-58 (1990)

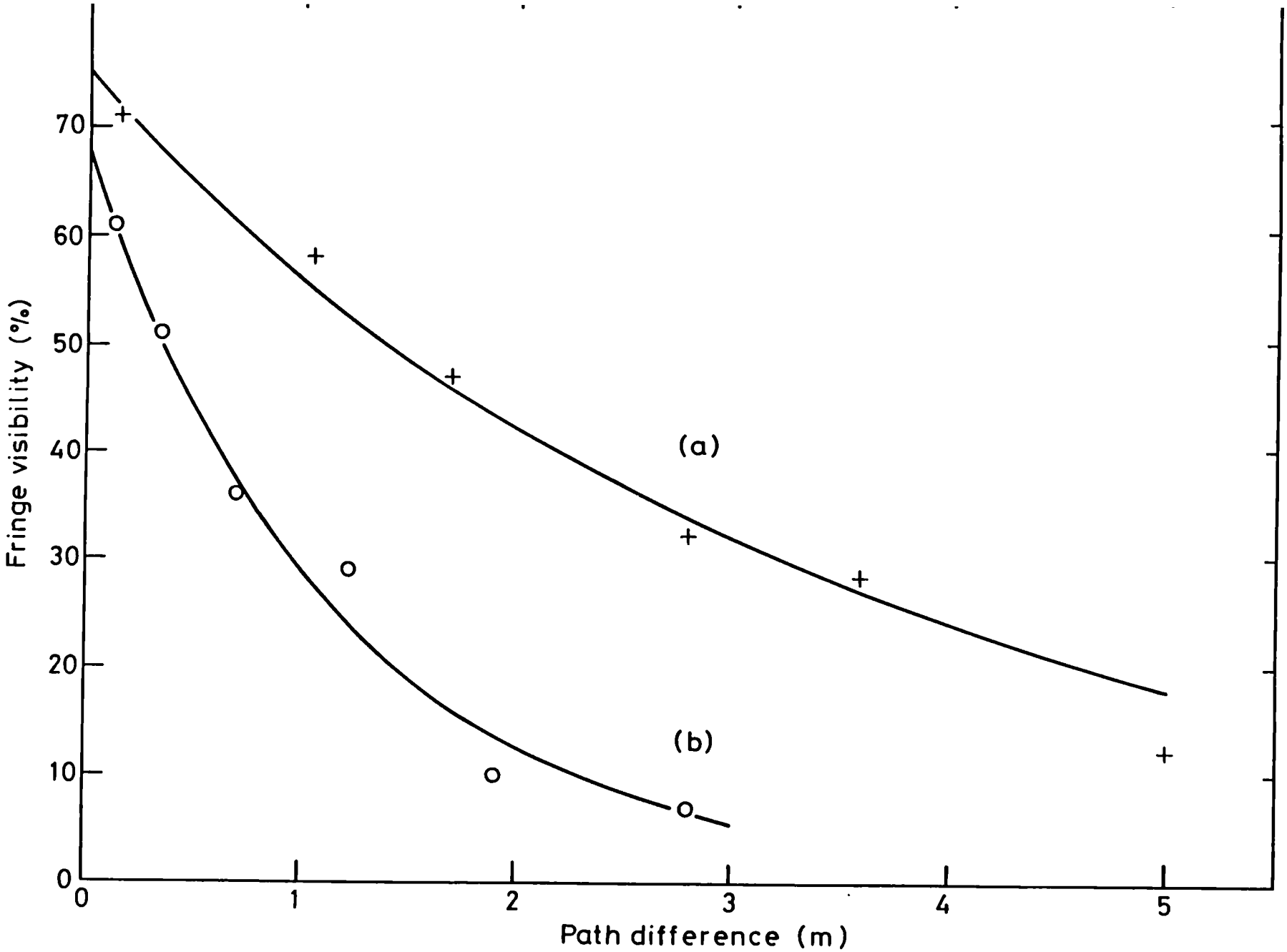

3.2.1 Laser diode fringe visibility versus optical path difference for (a) a Mitsubishi ML-4102 laser at 5 mW and (b) a Sharp LT024MD laser at 20 mW.

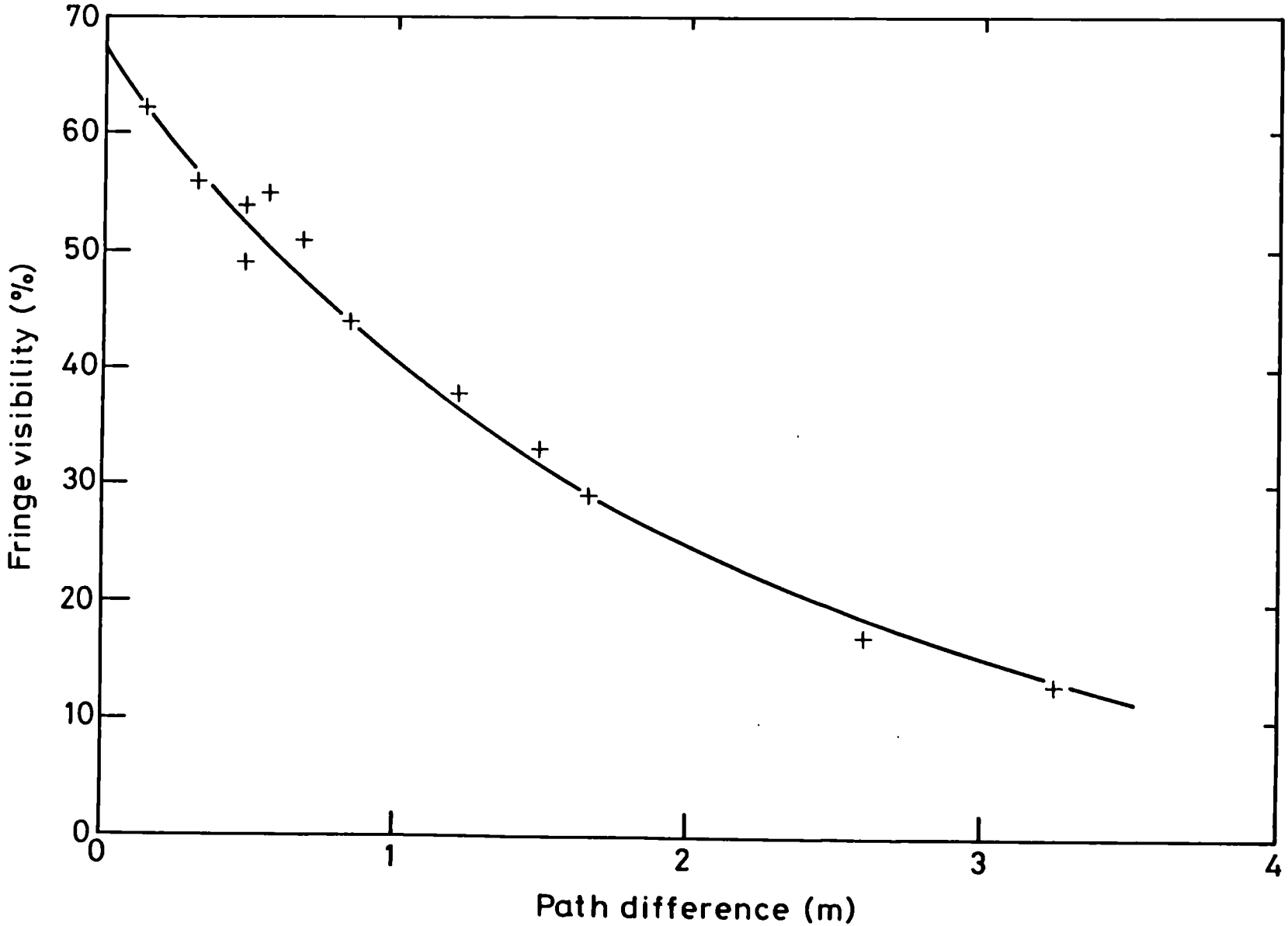

3.2.2 Laser diode fringe visibility versus optical path difference for an index-guided 670 nm laser at 3 mW (Toshiba model TOLD 9211)

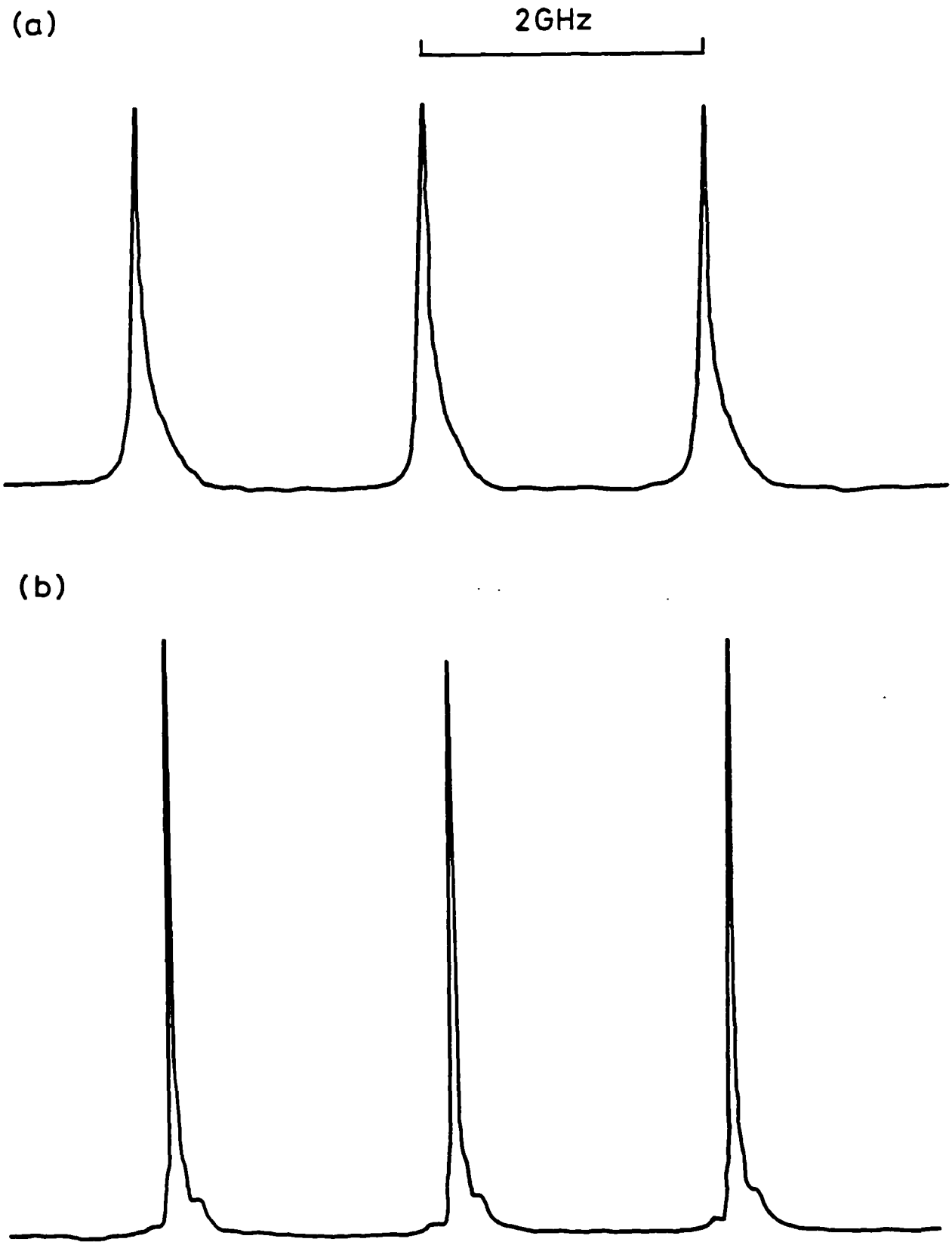

3.4.1 Effect on linewidth of weak optical feedback from a plane mirror. Note the appearance of weak external-cavity modes with feedback (lower trace). The analyser FSR is 2 GHz.

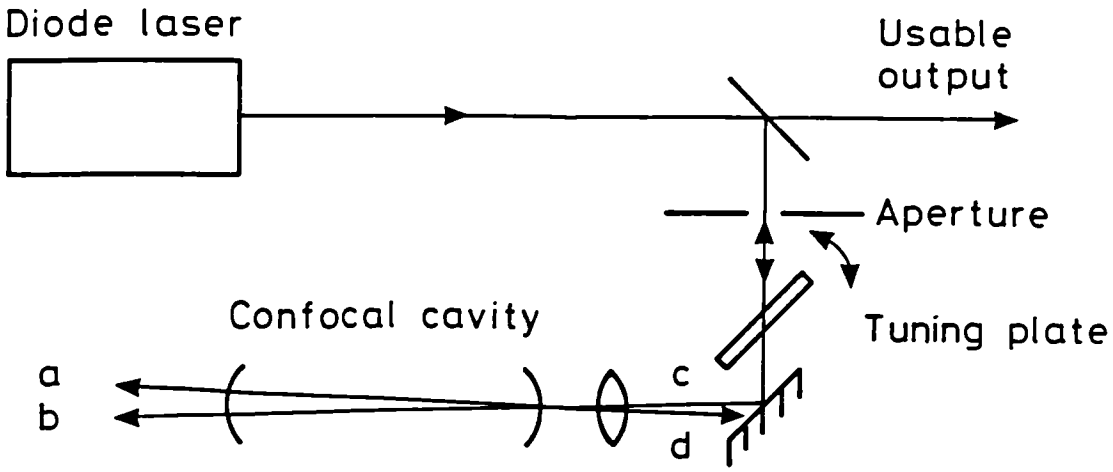

3.4.2 Basic experimental arrangement for achieving a narrow linewidth diode laser by resonant optical feedback.

a) No phase control between cavity and laser

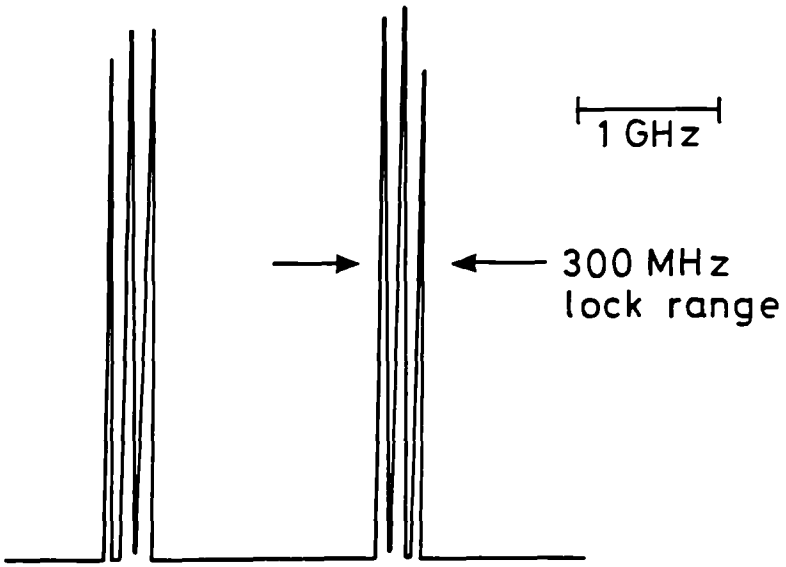

b) With phase control between cavity and laser

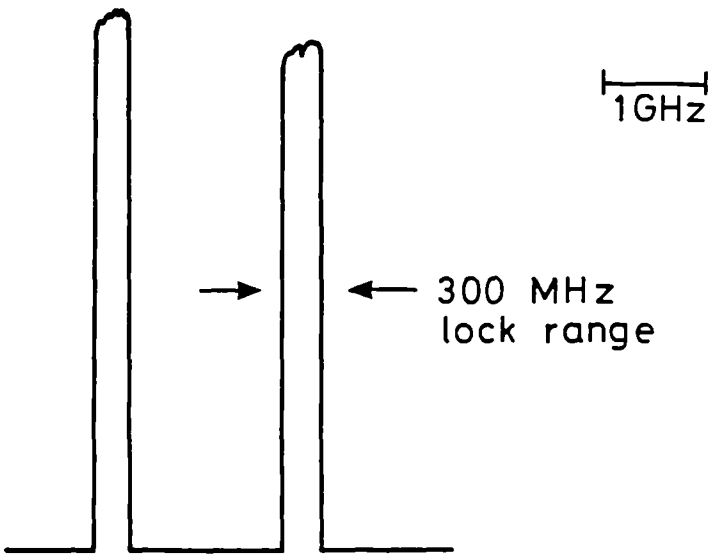

Diode laser optical lock range

3.5.1 Optical signals transmitted through the confocal cavity with resonant optical feedback.

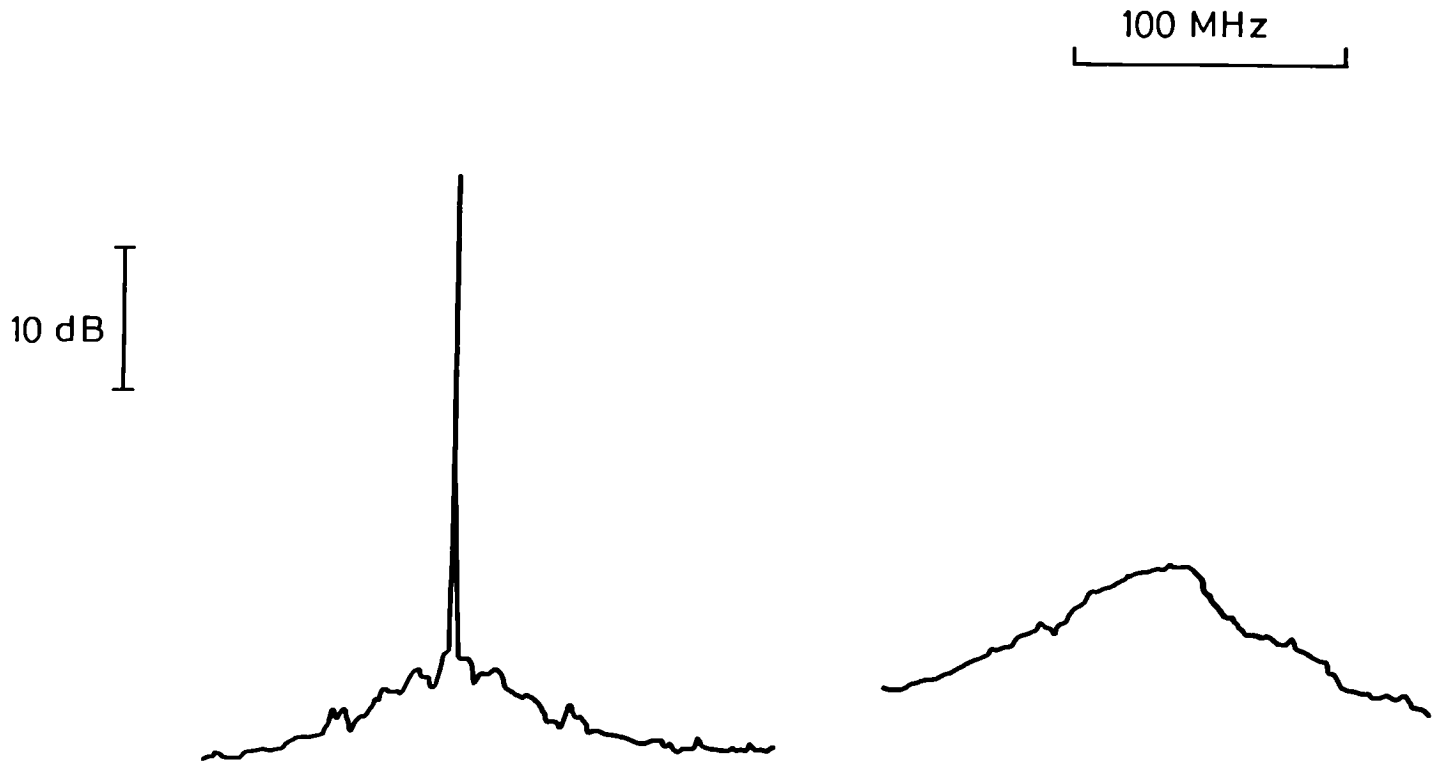

a. With optical feedback

b. No optical feedback

3.5.2 Log plot of rf beats spectrum between two linewidth-reduced lasers.

Spectral Narrowing by Optical Feedback

a. No optical feedback

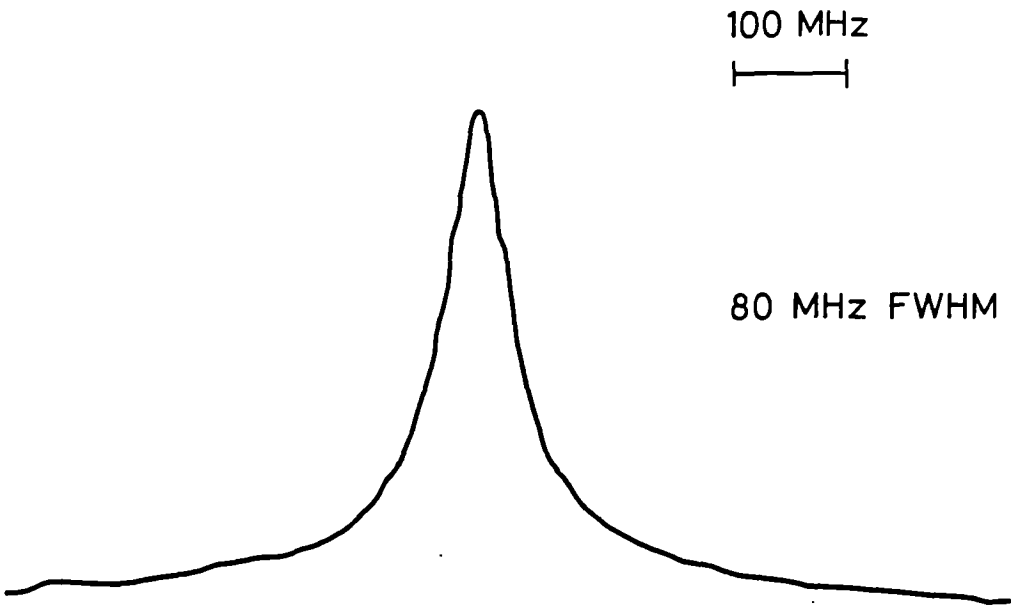

b. With optical feedback

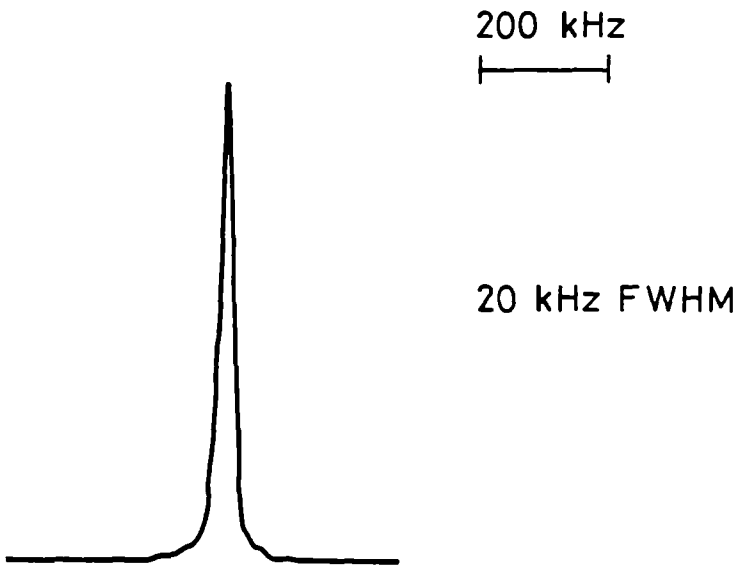

3.5.3 Plot of beat width with and without optical feedback.

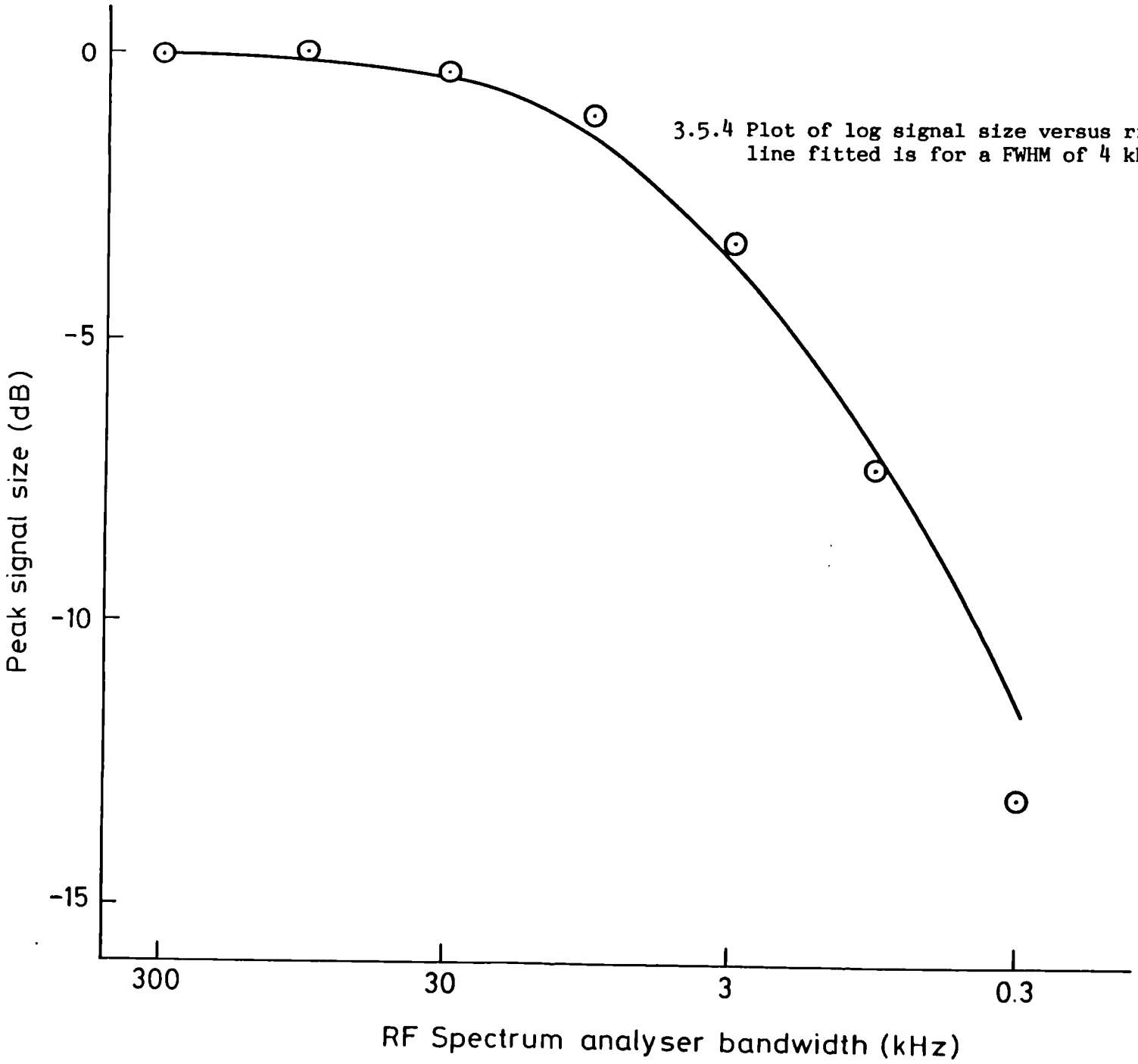

3.5.4 Plot of log signal size versus rf spectrum analyser bandwidth. The line fitted is for a FWHM of 4 kHz.

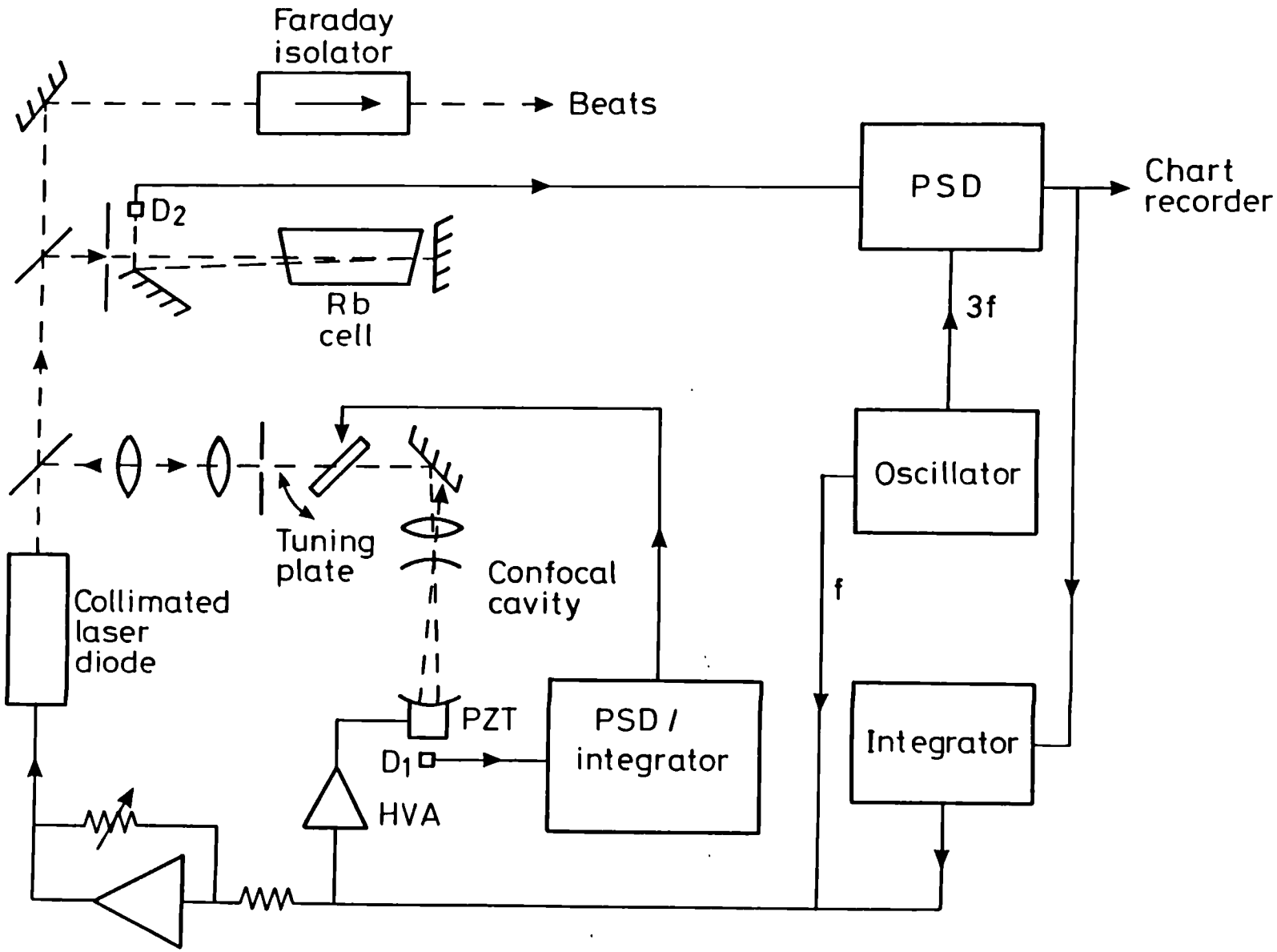

3.6.1 Scannable linewidth-reduced laser system. The laser output from this system could be combined with that from a second identical system to produce beats, as shown.

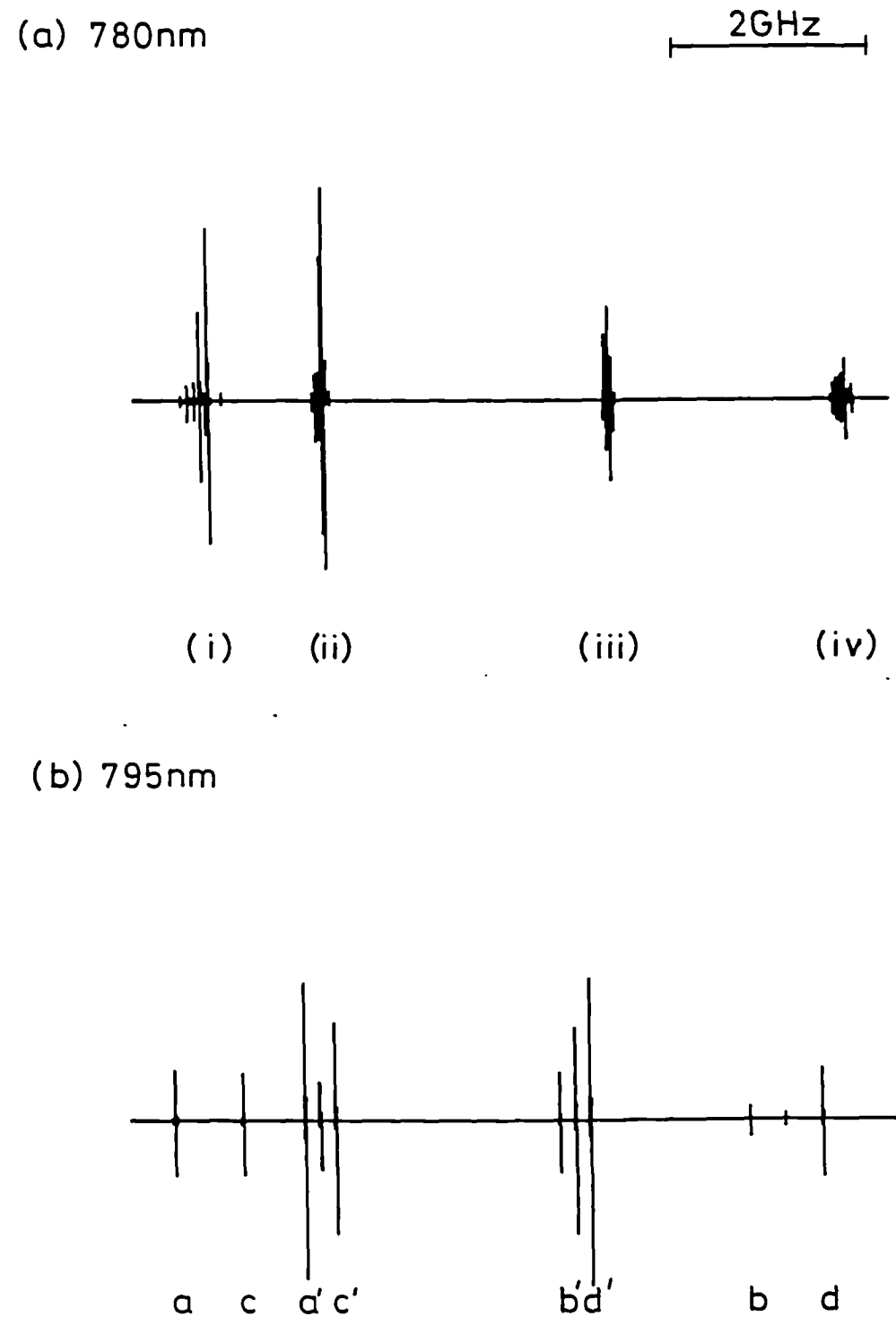

3.7.1 Scan of the complete Rb D_2 and D_1 lines at 780 nm and 795 nm

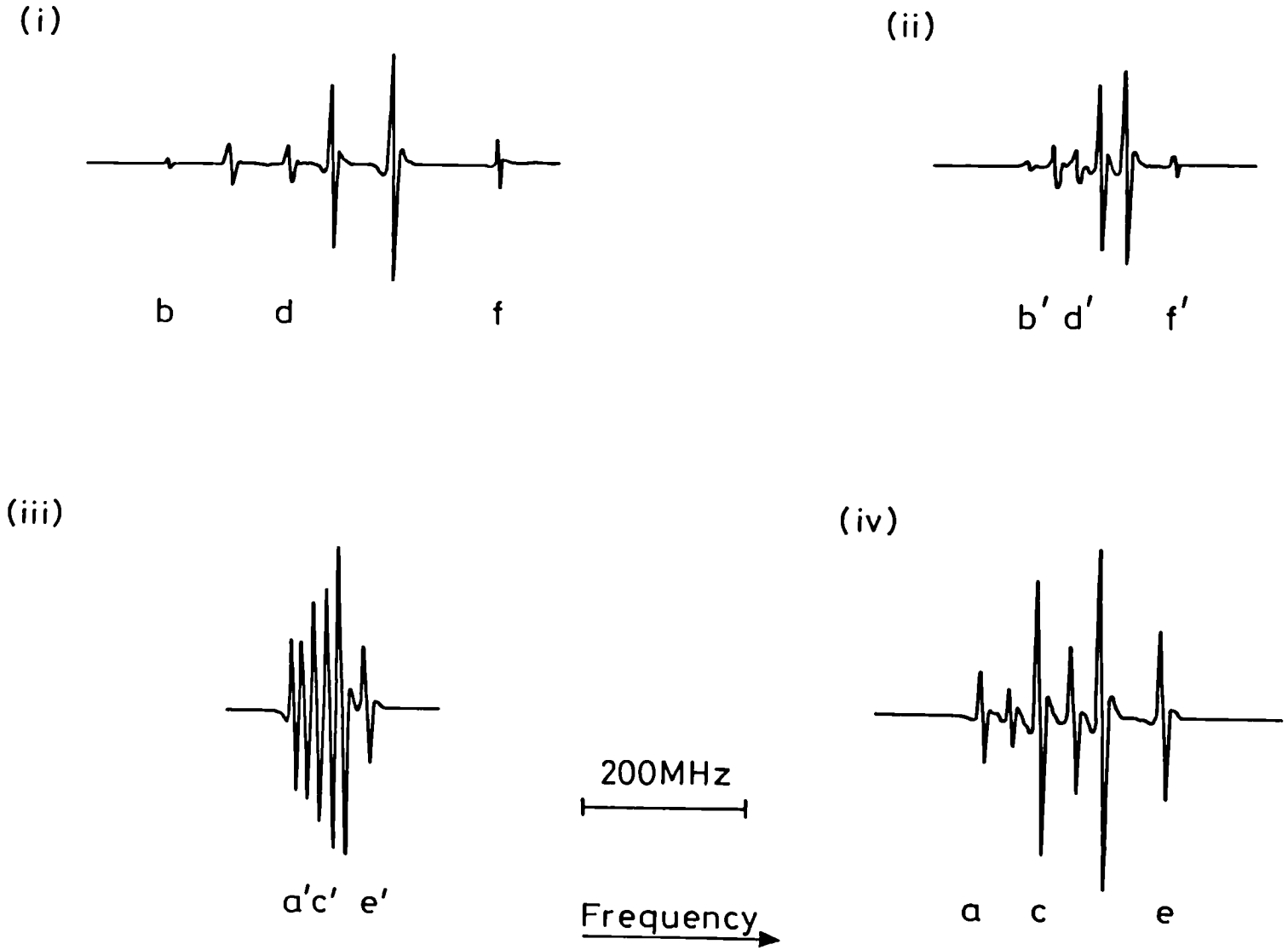

3.7.2 Individual short-range scans of each of the groups of components (i) to (iv). The electronic gains for the three groups are in the ratio 1:1:2:5.

CHAPTER 4

LASER STABILISATION AND BEAT FREQUENCY MEASUREMENTS

4.1 Introduction; Stabilisation to a Rb line or to another laser (offset locking)

This chapter describes the frequency stabilisation of laser diodes, principally to spectroscopic transitions in Rb. This draws upon data on Rb in chapter 2 where both Doppler-limited and Doppler-free spectra were presented and combines it with the linewidth reduction techniques of chapter 3. The net result of this chapter is a laser with both a frequency stable and linewidth reduced output.

Although the Rb lines might be observed in a number of ways, the techniques described in this and previous chapters are delibrately chosen to produce an electronic signal which is zero at line centre. A frequency servo-control will then reduce the electronic signal to zero, thus locking the laser to line centre. As already discussed, the third harmonic technique is a particularly convenient method for minimising the Doppler-limited background, if the laser is locked to a Doppler-free signal. Whatever feature the laser is being servo-controlled to, it is clearly imperative to ensure that the electronic zero truly reflects the line centre. Any Doppler-limited component may also be subtracted off (figure 2.5.1), if it suspected that the third harmonic technique alone will be insufficient. The servo-control methods used are very wide-ranging in their application [1], and are used to lock all types of single frequency lasers to spectral features, optical cavities and intra-cavity mode selectors, such as etalons or Fox-Smith cavities [2].

If low frequency (<100 Hz, say) servo-control is sufficient, then a suitable error signal is generally recovered through a PSD by modulating the laser frequency at a rate between a few Hz to about 10 kHz. In NPL-designed systems, frequency modulation is generally at around 500 Hz with a servo-bandwidth of ≈10 Hz. If faster servo-control is required, then it is probably necessary to use a double balanced mixer (DBM). Techniques involving the use of this are described in section 4.4

The electronic error signal, produced by the PSD for example, is fed to the laser through an NPL-designed [1] integrating control system. The integrator is required because it yields the high dc gain necessary for proper servocontrol. In the case of diode lasers, the integrator acts to control the current, since control via the heatsink temperature is too slow. The principal problem regarding this whole technique is that the laser frequency must be modulated, whether at 500 Hz for a PSD or 50 MHz for a DBM. The depth of modulation (ν_m) depends upon the application, but in spectroscopy should be comparable to the linewidth of the transition for optimum signal to noise ratio. This makes it highly undesirable to use such a laser in interferometry directly, even if the interferometric technique requires a modulated source. The problem is perceived either as a loss of visibility or as a modulation of the fringe, depending upon the bandwidth of the detector and amplifier used in the interferometer. In order to overcome this problem, two methods may be used. Firstly, one could frequency modulate externally to the laser, for example with an electro-optic phase modulator. However it is particularly easy to frequency modulate diode lasers directly, even to tens of GHz, whereas phase modulators are relatively expensive devices. The second technique, as used here, is to use two lasers and offset-lock one to the other. If this servo-bandwidth is low, it is possible to transfer the centre frequency stability from the modulated to the unmodulated laser. The

electronic technique for achieving this to high accuracy is well-established [3].

The remaining sections of this chapter discuss frequency stabilisation in various specialised applications, including linewidth reduction techniques and fast servo-control methods. The results obtained for the stabilities are all presented in section 4.5. However, first of all, it is necessary to define exactly what is meant by the term frequency stability and how results may be interpreted in terms of frequency noise.

4.2 Monitoring the beat frequency and characterisation of frequency stability

Having developed a technique to stabilise the frequency of a laser diode, the subsequent task is to measure the frequency stability. One means of achieving this, it might be thought, would be to monitor the Rb discriminant error signal when the servo loop is closed. This might also be used, with the servo loop open, to monitor the frequency instability of the free-running laser. In this case, the laser is frequency modulated and tuned close to a Rb absorption maximum. The PSD error signal can then be monitored as a function of time. This was done, and the results plotted in figure 4.2.1 for the cases of (a) free running, (b) intensity stabilised and (c) frequency stabilised lasers. Although this may seem to be a useful exercise, yielding a graphical record of frequency drift, it is fraught with problems, when interpreting the results. One such problem concerns the response time of the detection system. For modulation frequencies of ≈700 Hz, a PSD cannot be expected to show jitter at rates above a few tens of Hz. Any high frequency noise is averaged out and therefore not seen. Using a very long time-response

filter will mislead the observer still further. Such an error would seem to have already resulted in ultra-narrow linewidths being reported in error [4]. For Rb-locked lasers, or lasers locked to cavities, some early diode laser publications [5,6] used an error signal such as (c) of figure 4.2.1 to produce figures for the stability. However, this technique must result in the laser appearing anomalously stable at long times. Such measurements neglect the effect of many sources of electronic drift and noise. For very long averaging times, such a technique in general predicts ever increasing stabilty, whereas as we shall see, this is not usually the case. What we seek is an easily measurable statistical parameter, which must be a function of averaging time, to describe frequency stability.

Whilst it is not possible to count optical frequencies directly, it is possible to set up two similar laser systems and measure the difference frequency. This has already been used in this thesis to measure the linewidth of the laser, by measuring the beat width. A signal can be produced in a fast detector, in this case a Telefunken model BPW 28. This operates to 3 GHz with avalanche gain, and further gain was provided by an Avantek amplifier of suitable bandwidth. Around 30 dB to 40 dB gain is needed. To monitor higher frequency beats, a non-avalanche detector could be used (eg Plessey model CXL 082). A further 20 dB gain is then necessary to compensate for the loss of avalanche gain. Sufficient laser light is required to ensure that the detection system signal to noise ratio is optimised. This requires that there is sufficient light on the detector for the overall noise level to be limited by the photon noise. This may be verified with an rf spectrum analyser [7]. The laser power required will depend upon the noise figures of the amplifiers used. It is also possible to purchase relatively inexpensive frequency counters (eg from Racal) with a

bandwidth of up to 3 GHz. Prescalers are available to divide down the frequency, if a sufficiently fast counter is not available. For example, the Plessey SP4812 and SP8835B prescalers were used, which divide the frequency by 4 and operate at input frequencies of up to 2.3 GHz and 3.5 GHz respectively. These devices may be used to confirm whether the counter is triggering properly. A common technique [7] is to split the rf signal, feeding part of it into the normal input and part into a ratio (or external reference) input to check this. The value of the ratio confirms accurate counting. Typically, counters require at least 10 mV rms, often expressed in dB_m. To convert, we observe that 10 mV into 50 Ω produces 2×10^{-3} mW of rf power. In dB_m, this is $10\log_{10}(2 \times 10^{-3}) = -27$ dB_m. However, this requirement varies greatly with frequency and the type of counter or prescaler. As much as -5 dB_m could be required (130 mV), and the trigger levels for rf signals provided by an oscillator (ie with no rf noise) are plotted in figure 4.2.2 versus frequency for the two prescalers used. In the presence of noise, this minimum signal level will increase by a factor depending upon the noise level and bandwidth [7]. In general, a tunable bandpass rf filter is highly desirable to improve the counter performance. Use was made here of 3-sector tunable rf filters with a 5% bandpass, manufactured by Telonic Instruments. Instead of frequency prescalers, one can also reduce high beat frequencies by heterodyning against a local oscillator in a double balanced mixer. In this case, however, a bandpass filter is absolutely vital to remove the unwanted frequency components in the mixing process. The various items of equipment necessary to deal with beat frequencies up to about 3.5 GHz are therefore at present commercially available. No doubt this frequency range will increase in time. It should be added, for example, that non-avalanche detectors are already manufactured by GEC in this country and New Focus in the USA with a response up to ≈20 GHz, but such

frequencies are significantly more expensive to amplify and count at present.

The problem of laser frequency stability catagorisation therefore reduces to one of monitoring a beat frequency via a counter and processing the data obtained in a computer, to obtain a value for the stability. A similar experimental arrangement naturally may be used to obtain average values for the frequency difference between two lasers locked to adjacent Rb hyperfine components. The value for the laser beat frequency stability obtained is then assumed to reflect the stability of both lasers similarly, if the frequency noise of the two lasers is uncorrelated and they are similarly constructed. These measurements can also yield values for frequency shifts, if the operating parameters of one laser are systematically varied. A value for the day-to-day reproducibility of the frequency under nominally identical conditions can also be obtained. The parameter normally used for the frequency stability is the square root of the Allan variance, $\sigma^2(2,T,\tau)$. Here, τ is the averaging time (counter gate time) and T is the time between the start of successive readings. Ideally it is expected that $T = \tau$, but all frequency counters exhibit a "dead time" between readings, especially if it is required that data be transferred to a host computer. For this system, which comprised a BBC microcomputer and Racal 2.6 GHz counter with IEEE interface, T was of the order of a few tens of ms. The statistic σ^2 is a time-averaged variance of successive samples of the frequency averaged over time τ. If $\bar{f}_{k+1}$ and $\bar{f}_k$ are successive values of the frequency, averaged over time τ, then

$$\sigma^2(2,T,\tau) = \langle \tfrac{1}{2}(\bar{f}_{k+1} - \bar{f}_k)^2 \rangle \qquad (4.2.1)$$

and $\langle\ \rangle$ denotes a time average. If the output of the laser is

represented by

$$E = E_o \exp\{j(\Omega t + \phi(t))\} \qquad (4.2.2)$$

then the instantaneous departure from the nominal frequency is $\dot{\phi}(t)/2\pi$. Hence, at time t, we have

$$\bar{f}_k = \frac{1}{2\pi\tau}\int_t^{t+\tau} \dot{\phi}(t)dt \qquad (4.2.3)$$

It may be shown that a log-log plot of σ versus τ has various slopes, depending upon the type of frequency noise present. This is one of the most important uses of this statistic [8,9,10]. The most important σ versus τ slopes are listed in table 4.2.1, together with the characteristic noise source yielding this slope.

TABLE 4.2.1

Slope	Source
-1	White phase noise or discrete frequency modulation
$-\frac{1}{2}$	White frequency noise
0	Flicker (1/f) noise
$+\frac{1}{2}$	Random walk in frequency
+1	Steady drift in frequency

Finally, the effect of counter "dead time" should be specifically noted. This can be very significant when $\tau \leq 30$ ms. In such cases, we are usually in a region where the slope is -1, $-\frac{1}{2}$, or 0. For pure frequency modulation of the laser, σ is unaffected and this is proved here, by extending the arguments presented in [7]. In this case, $\dot{\phi} = 2\pi a_m \cos\omega_m t$, and

so from equation 4.2.1, we consider

$$\bar{f}_{k+1} - \bar{f}_k = (a_m/\omega_m\tau)(\sin\omega_m(T + \tau + t) - \sin\omega_m(T + \tau) - \sin\omega_m(t + \tau) + \sin\omega_m t) \qquad (4.2.4)$$

From the identity

$$\langle \sin\omega_m t.\sin(\omega_m t + \phi)\rangle \equiv \tfrac{1}{2}\cos\phi \qquad (4.2.5)$$

and using the definition of σ (equation 4.2.1), we have, after a little manipulation

$$\sigma^2 = (a_m/\omega_m\tau)^2(1 - \cos\omega_m T)(1 - \cos\omega_m\tau) \qquad (4.2.6)$$

This gives us

$$\sigma = (a_m/\pi\nu_m\tau)\sin(\tfrac{1}{2}\omega_m T)\sin(\tfrac{1}{2}\omega_m\tau) \qquad (4.2.7)$$

For timescales longer than $2\pi/\omega_m$, this represents a product of a rapidly varying sine function in a envelope of amplitude $a_m/\pi\nu_m\tau$. What is actually observed, for $T, \tau > 2\pi/\omega_m$, is $\sigma = a_m/\pi\nu_m\tau$, regardless of τ/T. This will hold except in the unlikely event that either $\nu_m T$ or $\nu_m\tau$ is close to an integer value.

For white frequency noise, σ is similarly unaffected because the frequency fluctuations are uncorrelated. In the case of flicker noise, σ is affected, although not very greatly. This may be proved from [8]. If $T/\tau \gg 1$, then the observed σ, becomes greater by the factor $\sqrt{(ln(T/\tau)/ln4)}$. For example, if $T/\tau = 20$, ($\tau \approx 1$ ms), then this factor becomes 1.5, and this does not appear greatly significant when plotted logarithmically.

This section has quantified statistical frequency stability. It has outlined some methods for counting the difference frequency between two similar lasers (beats), and such data are readily processed on a micro-computer. Furthermore, the interpretation of such data has also been discussed. Knowledge of the frequency noise can often help decide what improvements, if any, might be made. A good example, in this respect, is if $\sigma \propto \tau$. This could indicate steady thermal or electronic drift which might be corrected. In contrast, 1/f noise sources are far less well understood [11]. Allan variance, therefore, is a powerful diagnostic tool and considerably more useful than plots such as that of figure 4.2.1.

4.3 Frequency stabilisation with a linewidth-reduced laser

A tunable narrow linewidth laser is described in section 3.6 and is shown in schematic form in figure 3.6.1. In order to achieve most easily the optimum frequency stabilisation, various sources of laser frequency noise firstly need to be attended to. These are described in some detail in chapter 3, when a figure for the narrowest linewidth was obtained. In particular, low frequency excursions caused by draughts through the laser/cavity airspace need to be minimised. Simple screening of this airspace should be sufficient. If attention is paid to the passive short term frequency stability, then the rubidium stabilisation electronics will only need to remove the effect of long-term drift. Such drift may be caused either by thermal expansion, drift of the piezoelectric element in the cavity or atmospheric changes. This latter problem is a result of the cavity being airspaced.

The NPL servo-electronics only respond at times longer than about 0.1 s, and so faster control in this system needs to be all done through the

optical feedback. The laser is frequency modulated at about 700 Hz at 10 MHz peak to peak, when locking to rubidium. For Rb-stabilised lasers, this modulation will dominate the short-term frequency stability. Offset-locking to the Rb-stabilised system (as outlined in section 4.1) will enable the centre frequency stability and reproducibility to be transferred to a second, unmodulated, laser.

As with the free running laser, long-term narrow linewidth operation depends upon the laser drive current, operating temperature and feedback cavity all being sufficiently stable. In time, drift in one component could cause the optical lock to be lost. In the tunable narrow linewidth laser of section 3.6, a feed forward arrangement from the integrator controls the laser current sufficiently well to maintain the optical lock. When the electronic lock is closed, atmospheric changes could still cause the optical lock to be lost in time. This is because, as the atmospheric conditions change, the integrator voltage will act to keep the effective cavity length constant. This will, in turn, cause a small change to be made to the laser current. It was therefore found necessary to insert a trimpot to add a small voltage to the feed forward control to re-optimise the current if the optical lock became unstable or was lost. This correction was made manually here, but techniques for automating this adjustment are described in chapter 6.

This section, therefore, has described the first reported frequency stabilisation of a linewidth reduced laser to Rb. This provides a highly-coherent stable, reproducible frequency suitable for absolute length measurements. The task now is to measure this frequency stability for both this system and the others described in this chapter.

4.4 Effect of fast frequency modulation and servo-control to Rb

The technique of resonant optical feedback has been established chapter 3 as a successful technique for the reduction of semiconductor laser linewidths [12,13,14,15]. The best results of chapter 3 were obtained with a 300 MHz FSR cavity with a finesse of 170. Sufficient narrowing, however, is obtained with a 2 GHz FSR cavity to ensure that the laser linewidth is less than that of the Rb D lines [16]. It has been observed [17] that this technique does not affect the laser's ability to be frequency modulated at high frequencies. The only requirement, if high modulation indices are required, is that the drive frequency should be a rational fraction of the cavity free spectral range. However, it is observed here, that provided only small modulation indices ($m < 1$) are required, there are no obvious constraints on the drive frequency.

These observations suggest a novel laser source for FM spectroscopy. FM spectroscopy has been used to study transitions in Na or I_2, using an electro-optically phase modulated dye [18,19,20] or He-Ne laser [21,22]. Modulators, however, are relatively expensive devices, whereas diode lasers can be easily and directly modulated by modulating the drive current. Diode lasers are therefore well-suited for FM spectroscopy, although so far have been primarily limited in use to Doppler-limited FM spectroscopy. For example, lead-salt diodes have been used in FM Doppler-limited spectroscopy on N_2O [23] and GaAlAs lasers used on NO_2 [24], water vapour [25,26], and Rb [27]. Doppler-free spectra are also reported in [27], but are limited in resolution by the diode laser linewidth.

A signal (few MHz to 1 GHz) from a frequency generator (Philips

PM 5390S) was coupled into the current drive of the laser diode through a 400 pF capacitor and large resistor. A 1 μH inductor was used to isolate the high frequency signal from the power supply. The spectral output from the laser, initially with no optical narrowing, was examined with a 2 GHz FSR optical spectrum analyser. Modulating the laser diode current produces both amplitude and frequency modulation at the rf drive frequency, but if the modulation is not too great, the effect is predominantly frequency modulation [17]. As has been previously shown [18], the time-averaged spectrum of such a laser consists of a carrier, together with several sidebands. This is readily understood, since modulating the injection current at these frequencies phase modulates the laser. The output then becomes, neglecting the effect of amplitude modulation

$$E = E_o \sin(\Omega t + m.\sin\Omega_m t) \qquad (4.4.1)$$

where m is the modulation index. By a mathematical identity [18], this becomes

$$E = E_o[\Sigma_{n=0}^{\infty} J_n(m)\sin\{(\Omega + n\Omega_m)t\} + \Sigma_{n=+1}^{\infty}(-1)^n J_n(m)\sin\{(\Omega - n\Omega_m)t\} \qquad (4.4.2)$$

The amplitude of the n^{th} sideband is therefore $|J_n(m)|$, and the intensity $|J_n(m)|^2$. In figure 4.4.1, the spectral output is shown, as observed with the spectrum analyser, for m = 1.60 (upper trace) and 3.91 (lower trace). The drive frequency is 159 MHz. Normalising to the intensity of the carrier, the relative intensities of the modes in figure 4.4.1a are 1:1.59:0.32, compared with that predicted for m = 1.60 of 1:1.57:0.32. The value of m is estimated by a least squares fit, and the results for low and high frequency sidebands have been averaged.

The spectrum shown in figure 4.4.1b is noticeable asymmetric, however, and this may be explained by considering the effect of amplitude modulation [28]. In equation (4.4.2), E_o needs to be re-written as

$$E_o = E_1(1 + \varepsilon\cos(\Omega_m t + \phi)) \qquad (4.4.3)$$

where ϕ is the phase shift between the amplitude and instantaneous frequency excursions. By inserting (4.4.3) into (4.4.2) and using the well-known identity for a product of the form *cosA.sinB*, we obtain for the intensity of the sideband at $\Omega \pm n\Omega_m$, after some manipulation

$$I_n \propto \{(1 \pm n\varepsilon\cos\phi/m)J_n(m)\}^2 + \{\varepsilon J_n'(m)\sin\phi\}^2 \qquad (4.4.4)$$

The function $J_n'(m)$ is the derivative of the n^{th}-order Bessel function. Use has also been made of the identities

$$J_{n+1}(m) + J_{n-1}(m) \equiv 2nJ_n(m)/m \qquad (4.4.5)$$

and

$$J_{n+1}(m) - J_{n-1}(m) \equiv 2J_n'(m) \qquad (4.4.6)$$

It is expected [28] that $\phi = \pi$ in this case, and so the intensity of the n^{th} sideband becomes proportional to $|(1 \mp n\varepsilon/m)J_n(m)|^2$. In figure 4.4.1b, for $\varepsilon = 0.03$, the predicted identities are, for $m = 3.91$

0.09:0.41:1.07:0.89:0.006:1:0.006:0.95:1.17:0.47:0.10

This compares with the experimental values of

0.09:0.49:1.12:0.79:0.009:1:0.002:0.87:1.25:0.52:0.10

In order to illustrate the effect of simultaneous optical narrowing and fast frequency modulation, two optically narrowed laser diodes were constructed. Both lasers were optically narrowed using feedback from a 2 GHz FSR cavity. The beat frequency was observed with a fast avalanche photodiode and rf spectrum analyser. The current of one laser was then modulated as previously, and the effect was observed on the rf beat frequency spectrum. Such a signal is proportional to the modulus of the amplitude of both of the incident laser beams. The observed sideband amplitudes are therefore proportional to $|J_n(m)|$, rather than $|J_n(m)|^2$. This actually makes this technique particularly sensitive for detecting small modulation indices. In figure 4.4.2, the beat frequency spectrum is shown for a drive frequency of 155 MHz. The conditions in figures 4.4.2a and 4.4.2b are identical, except that in figure 4.4.2b the laser is optically narrowed. In figure 4.4.2a, the amplitudes of the modes are measured to be 1:1.3:0.4, compared with 1:1.1:0.5 as expected for m = 1.5. With optical feedback, the corresponding figures are (measured) 1:1.0:0.3:0.02, compared with 1:0.9:0.3:0.08 expected for m = 1.34, slightly less than the modulation index with no feedback. The fit is not quite so good as for the measurements with an optical spectrum analyser. The mode intensities may be slightly asymmetric owing to the associated amplitude modulation discussed earlier. Small asymmetries here could also be due to the frequency dependence of the rf beat frequency detector, amplifier and spectrum analyser. In [17], the spectrum is grossly asymmetric, perhaps owing to the associated laser amplitude modulation, although this is not specifically commented upon in [17].

In our case, there did not appear to be a need for any simple

relationship between the drive frequency and cavity FSR to achieve narrowed fm operation. Although in figure 4.4.2, the drive frequency is close to FSR/13, many other frequencies were also used. The principal constraint was that the arrangement for coupling the fm signal into the laser current supply had various electronic resonances. This was probably mainly due to the laser diode mounting. This was on a large copper block to ensure the best thermal stability, but this was not a design to ensure the best high-frequency operation. Such a design made larger modulation indices ($m > 1$) easier to achieve for some frequencies than others. The only other observed constraint was for drive frequencies less than about 2 MHz. Satisfatory optical narrowing and FM operation was not possible at such low frequencies, which correspond to $\approx$ FSR/1000 or less. At frequencies above 2 MHz, and for $m < 1$, each sideband had a short-term jitter of 200 kHz. This is identical to the jitter observed with this system with optical feedback, but no frequency modulation and arises from the 1/f frequency noise of optically narrowed lasers [14]. As a demonstration of the spectroscopic use of this laser, FM spectroscopy was performed with Rb.

FM spectroscopy has been shown to be a powerful tool for the efficient recovery of absorption signals at high frequencies. Noise levels can be reduced almost to the detector shot noise limit, and a high sensitivity is achieved, allowing detection of low levels of linear absorption [24,26]. This technique is especially useful with a dye laser which has considerable intensity noise at frequencies of less than a few MHz. Although diode lasers have low intensity noise in comparison with dye lasers, FM spectroscopy still has several advantages, especially for laser frequency servo-control. These include a fast response to laser frequency changes close to line centre and a large capture range. A large capture range enables the servo to pull in the laser frequency

towards line centre with a large initial frequency error.

For laser spectroscopy, the laser was phase modulated with a modest modulation index $m < 1$. The output spectrum then consists predominately only of the carrier and first order sidebands. The fm laser was used to observe the Rb D_1 line at 795 nm in a mixed isotope Rb cell (^{85}Rb and ^{87}Rb), using the apparatus in figure 4.4.3. The optical signal is detected, amplified and then demodulated in the double balanced mixer (DBM). The phase of the rf signal is adjusted by varying the relative length of the cables to the DBM "LO" and "RF" inputs. The rf phase is varied to allow synchronous detection of either the component in phase (dispersion) or 90° out of phase (absorption) with the rf modulation [18]. In the case of purely phase modulated light, there is no amplitude modulation, and so no photodiode current at the modulation frequency. However, as the laser is tuned near a Rb transition, an imbalance is produced in the intensity of the two sidebands. This is equivalent to an amplitude modulation and so a signal is detected by the photodiode. The signals are of characteristic shape and examples are shown in figure 4.4.4. These are scans over the b' and d' lines of the Rb D_1 line at 795 nm. The derivation of the theoretical FM lineshapes in these circumstances is somewhat complicated, but the results have been published [19]. The result may be summarised by defining $L_n \equiv L(\gamma, \nu + n\Omega_m/2\pi)$ (equation 3.2.5) and also

$$D_n \equiv (\nu_o - \nu - n\Omega_m/2\pi)(\gamma^2/4 + (\nu + n\Omega_m/2\pi - \nu_o)^2)^{-1} \qquad (4.4.7)$$

Then the photo-diode current, i, is proportional to

$$\begin{aligned} i \propto & -\cos\Omega t[(J_o(m) + J_2(m))(L_1 - L_{-1}) + J_2(m)(L_2 - L_{-2})] \\ & + \sin\Omega_m t[(J_o(m) - J_2(m))(D_1 - 2D_0 + D_{-1}) \\ & + J_2(m)(D_2 - 2D_0 + D_{-2})] \end{aligned} \qquad (4.4.8)$$

The absorption and dispersion curves are then the $\cos\Omega_m t$ and $\sin\Omega_m t$ coefficients respectively. The signal from the photodiode therefore arises from the mixing of the first sideband frequencies and the carrier.

The initial practical question to be settled in using fm spectroscopy is that of the appropriate choice of drive frequency. In spectroscopy, it can be advantageous to have a high drive frequency to obtain a high signal to noise ratio. The difference in shape between absorption and dispersion profiles is then more pronounced if high modulation frequencies are used. With this method, the central slope of the dispersion profile is still limited only by the transition linewidth, rather than the modulation frequency. Modulation frequencies of several times the transition linewidth can be used to increase the capture range without degrading the locked frequency stability. However, the drive frequency should not be so large that the adjacent transitions begin to overlap. In the case of the Rb D_1 line, a compromise drive frequency of 50 MHz was chosen, with a modulation index of 0.2. The signal is demodulated and recovered in a double balanced mixer (DBM).

The signal produced by the DBM actually consists of Doppler-free signals lying on a Doppler-limited background (figure 4.4.5). The shape of the background varies with the rf phase and this is set for absorption in figure 4.4.5. There is also an offset owing to the amplitude modulation of the diode laser. With no amplitude modulation, the background is expected to be almost flat if the rf phase is set for dispersion [18]. A derivative of the Doppler-limited absorption profile is observed if the rf phase is changed by 90° to set it for absorption. In this case, for a diode laser, the background is rather different from [18], because of the effect of amplitude modulation [23]. Furthermore, in this system,

both the probe and saturating beams are modulated, rather than just the saturating beam as in [18]. The typical power of the 8 mm saturating beam was 30 μW. The background is observed to retain the basic shape of the derivative of the Doppler profile. However, it has become grossly asymmetric owing to the amplitude modulation.

The phase sensitive detector (PSD) is then used to produce the Doppler-free components on a flat background. This is essential if it desired to use these to frequency stabilise the laser. A signal from the chopper at ≈ 1 kHz provides the PSD reference input. The PSD then only observes the difference to the DBM signal which the presence of the saturating beam causes. This only occurs at line centre, yielding the fm spectral features on a flat background. This technique also removes the offset caused by the amplitude modulation of the laser. The resulting Doppler-free components on a flat background are shown in figure 4.4.6. This is the first reported observation of the Rb line at 795 nm using an optically narrowed fm diode laser. It is, in fact, the first time that this type of laser has been used for spectroscopy. The change in feature shape with rf phase is most pronounced if the feature FWHM is much less than the drive frequency. This will not be the case in figure 4.4.6a, which was obtained with no optical narrowing. In this case, the feature FWHM is ≈ 60 MHz. In figure 4.4.6b, the D_1 line is observed with an fm optically narrowed laser, with m = 0.2. The hyperfine components are labelled using the same notation as in chapter 3, where the dash (') refers to transitions in ^{85}Rb. Unlabelled components, half-way in frequency between two labelled components, are level-crossing signals. In order to frequency stabilise the laser, the rf phase should be set for dispersion since this feature has a steep nearly linear central section suitable for frequency control to line centre. This is contrast to the absorption feature, where there is a kink in the feature at line

centre (figure 4.4.4b). The PSD output then needs to be connected to the integrator of figure 4.4.3. The signal to noise ratio of component d' is ≈ 300, limited by interference effects caused by unwanted feedback effects from various optical components. In stabilising the frequency this way, the reproducibility, as limited by this problem, will be approximately 40 kHz, or 1 x 10^{-10} of the optical frequency. This is estimated from the signal to noise ratio and the gradient of the central feature, calculated as the noise level divided by the gradient.

4.5 Frequency Stability of Various Laser Systems; free running, offset locked and locked to Rb

Techniques have been described for locking the laser to Rb and to another laser (offset locking). The laser may also be left free running, either with or without a linewidth reducing cavity, or it could be intensity stabilised. Using the statisical parameter described in section 4.2, results on frequency stability are presented in this section. Emphasis is placed on table 4.2.1 to interpret the time dependence of σ in terms of frequency noise.

The first results to be described are in figures 4.5.1 and 4.5.2 and are for a diode laser without optical feedback. Such a system clearly has the advantage of simplicity, if the best frequency stability or narrow linewidth is not required. From figures 4.5.1 and 4.5.2, the various cases are described below.

a) Free running laser

This plot represents the variation of the beat frequency between a

Rb-stabilised laser diode and a free running laser. Since a Rb-stabilised laser will be the more stable, this plot essentially represents the stability for the free running laser. These results depend strongly upon the quality of the diode laser power supply, and these particular results were obtained with an Ortel model LDPS-1. For the results in figure 4.5.1, the graph divides into three sections;

$\sigma/f \approx 1.5 \times 10^{-9}/\sqrt{\tau}$ $\quad 0.01\ s \leq \tau \leq 0.08\ s$

$\sigma/f \approx 1.9 \times 10^{-8}\sqrt{\tau}$ $\quad 0.08\ s \leq \tau \leq 6\ s$

$\sigma/f \approx 4.7 \times 10^{-8}$ $\quad 6\ s \leq \tau \leq 100\ s$

b) Intensity Stabilised laser diode

This plot of the statistical stability was obtained from the beat between a Rb-stabilised laser diode and an intensity stabilised one. As has been pointed out [29], intensity stabilisation affects frequency stability. Whether intensity stabilisation improves or degrades frequency stability depends upon the quality of the power supply. In this case there is an obvious improvement owing to a power supply instability for times greater than 0.1 s. These results are plotted in figure 4.2.1.

c) Rb-stabilised lasers

This plot shows the stability of the beat between two Rb-stabilised diode lasers. Optimum stability is achieved at a few seconds of ≈4 parts in 10^{10} of the optical frequency. However, there is drift for $\tau > 40$ s, suggesting poorer frequency reproducibility. These results relate to lasers locked to components "a" and "b" at 780 nm, using the features obtained with the lamp (figure 2.3.1). This produces a beat at 1.1 GHz,

which was reduced by 182 MHz using an acousto-optic modulator to downshift one laser frequency to provide a beat at 930 MHz. At this frequency, it proved to be rather easier to count reliably the broad beat of the unmodified lasers. The results can be summarised

$\sigma/f \approx 0.9 \times 10^{-10}/\tau$ $\quad 0.01\ s \leq \tau \leq 0.2\ s$

$\sigma/f \approx 4.2 \times 10^{-10}$ $\quad 0.2\ s \leq \tau \leq 40\ s$

$\sigma/f \approx 0.9 \times 10^{-11}\tau$ $\quad 40\ s \leq \tau \leq 100\ s$

The beat statistic measured for $\tau \leq 0.2$ s is similar to that expected for a frequency modulated laser [7]. For a single modulation of amplitude a_m and frequency ν_m, $\sigma = a_m/\pi\nu_m\tau$ (equation 4.2.7). For two modulation frequencies, as in this case, the observed statistic is a root sum of squares, yielding $0.6 \times 10^{-10}/\tau$ in this case. This is less than that observed, so there must be some other white phase noise source adding a further $1/\tau$ term, as explained below for offset-locked lasers. A rough estimate for this may made by considering the equation for the offset locked, but unmodulated lasers using similar integrators. This, as shown below, yields $\sigma/f \approx 0.5 \times 10^{-10}/\tau$. When combined with the contribution from the modulation as a root sum of squares, this gives $0.8 \times 10^{-10}/\tau$, which explains the dependence quite well.

To illustrate the problem of calculating Allan variances from electronic error signals, the results obtained from beat frequencies were compared with those calculated from the error signal. This problem was alluded to in section 4.2. Such a calculation based upon the electronic error signal neglects the many sources of electronic noise and drift, so that, at long times the laser looks anomalously stable. In this case, for example, such a calculation could not hope to predict that σ/f does not reduce below 3×10^{-10} at long times for one laser. A routine was

developed to calculate Allan variances from the PSD jitter for $\tau \leq 1$ s using a microcomputer and A/D converter reading the PSD output. As in [5], σ was then measured to vary as $1/\sqrt{\tau}$ for short averaging times and not $1/\tau$, as observed from the beats. The residual PSD jitter is therefore mainly white noise and, as observed, the servo gain can be increased so as to improve the calculated stability, whilst actually degrading the laser stability by imposing electronic noise upon it. The routine used to calculate statistical stabilities from the PSD error signal gave an estimate of the beats statistics of $\sigma/f \approx 5 \times 10^{-10}/\sqrt{\tau}$. At the PSD time constant of 30 ms, this actually agrees quite well with the direct beat measurements, even though the time dependence is not correct. Whether the beat statistics for short times will vary as $1/\tau$ or $1/\sqrt{\tau}$ will depend upon the modulation depth and frequency, the servo unit gain frequency and the amount of white noise present.

Statistical stability measurements were also made with two lasers locked to components "a" and "c" of the Doppler-free spectra at 795 nm (figure 2.5.2). These results are plotted separately in figure 4.5.2, and a minimum of 2 parts in 10^{10} (80 kHz) is obtained at $\tau = 30$ s. This observed stability figure may, unfortunately, result because, with non-narrowed diodes, counting a beat is only reliable at a level of 1 part in 10^4 (eg 80 kHz at 800 MHz). It is perhaps a little disappointing that Doppler-free spectra provide a laser which is no more than twice as stable as that stabilised to Doppler-limited spectra. Although such a laser shows better day-to-day reproducibility (by a factor of 20), we must turn to linewidth-reduced systems for the best results.

d) Offset locked lasers

This result is quite straightforward, namely

$\sigma/f \approx 5 \times 10^{-11}/\tau$ $\qquad 0.01\ s \leq \tau \leq 100\ s$

where the result applies to two unmodulated lasers. The $1/\tau$ dependence was also observed in [30]. The NPL electronics are, like [30] designed to control the phase of the beat frequency signal, although do not have such a fast response. For observation times, τ, longer than the reciprocal of the servo unit gain frequency (f_u), a $1/\tau$ dependence can be expected. The counter is, in effect, dispaying a number proportional to the signal phase divided by the gate time, τ. However, for $\tau > 1/f_u$, the phase noise is essentially white in character. If σ_ϕ is a measure of the phase jitter, then the scatter in the results is proportional to σ_ϕ/τ [8]. If a servo with a higher unit gain frequency is used, σ_ϕ would be reduced until some other limit is reached, for example noise in the phase lock loop circuit. For very long times τ, σ may not reduce as $1/\tau$, as the integrator gain approaches the open loop gain of its amplifier.

The second part of this section deals with the frequency stability of linewidth reduced lasers. In resonant optical feedback, the laser frequency is predominantly determined by the cavity and so should be more stable than the free running laser. The frequency stability of the beat was measured with optical feedback from the 300 MHz and 2 GHz FSR cavities. The stability of the laser beat using feedback from the 300 MHz cavity (and also with no feedback, for comparison purposes) is shown in figure 4.5.3. This figure shows the passive frequency stability of narrowed diodes- ie the diodes are not locked to an atomic or molecular reference. The trace without feedback was obtained with both lasers operating with a Lightwave LDX-3620 low noise power supply, and shows considerably better stability than the results in figure 4.5.1.

For $\tau < 0.1$ s, the frequency stability improves from 1.2 MHz to 8 kHz with feedback, corresponding to an improvement by a factor of 150. On a similar timescale, the improvement in stability with a 2 GHz FSR cavity, is a factor of 50. For these short averaging times, and either cavity, the curves are nearly independent of τ, indicating that 1/f noise is predominant [8,9]. For averaging times 0.1 s $< \tau <$ 10 s, σ increases as $\sqrt{\tau}$ (figure 4.5.3), indicating that the frequency is undergoing a random walk. On longer timescales, the laser beat frequency drifted at an average rate of ≈15 kHz/s for the 300 MHz cavities, even though they were manufactured from low thermal expansion Invar. Drift will also arise from atmospheric changes, since the cavity is air-spaced.

As already noted in chapter 3, there is a connection between the observed frequency noise, the relative frequency stability and the degradation of effective linewidth as a function of observation time. It is not really possible to distinguish clearly between linewidth and jitter, especially in the case of 1/f noise. A better picture is that of an oscillator where the phase does not vary at a strictly constant rate, but has some associated noise. In this case the phase noise spectrum varies as $1/f^3$ [8]. However, the results of figure 3.5.4 suggest that in any period of $1/2\pi\gamma \approx 40$ μs (γ = 4 kHz), the phase increases at a sufficiently uniform rate for one to talk of a linewidth.

The expected effect of delaying the time (T) between observations when measuring the effective linewidth has not been calculated, although the effect on the Allan variance has already been discussed (section 4.2). If $T \gg \tau$, then the observed σ is increased to $k\sigma$, where $k = (\ln(T/\tau)/\ln 4)^{1/2}$. We may attempt to calculate the linewidth of figure 3.5.3 by estimating the average rate of phase change in two periods of time $1/2\pi\gamma$ long, but 0.2 s apart. However, now we recognise that this is simply the square

root of the Allan variance, for T = 0.2 s. This argument is intended to provide a physical picture, rather than be a rigorous analysis. However, it is possible to obtain some numbers for the expected width of figure 3.5.3. Correcting for the time between observations for this measurement system, and using the formula for k above, yields 17 kHz. Although it is not clear what the precise numerical relationship should be to the FWHM of figure 3.5.3, this appears to be broadly in agreement.

Two linewidth reduced lasers have also been offset locked to a level of 70 Hz at 10 s (figure 4.5.4). This is comparable (at a level of tens of Hz) with some other recent results [14,31,32]. The upper trace in figure 4.5.4 shows the degradation in stability when one of the lasers is frequency modulated, which is neccessary if one laser is locked to a Rb component. For a laser modulated at 9 MHz peak-to-peak and at 700 Hz, the calculated relative frequency stability (section 4.2) is $5 \times 10^{-12}/\tau$, comparing well with that observed.

In figure 4.5.5, the relative frequency stability between two Rb-stabilised linewidth reduced lasers is shown. The lasers were locked to components a' and c' at 795 nm, and the beat was at about 361 MHz. The results can broadly be summarised as follows

$$\sigma/f = 6.4 \times 10^{-12}/\tau \qquad 10^{-3}\ \text{s} \le \tau \le 10^{-1}\ \text{s}$$

$$\sigma/f = 1.9 \times 10^{-11}/\sqrt{\tau} \qquad 10^{-1}\ \text{s} \le \tau \le 10\ \text{s}$$

For $\tau > 10$ s, σ/f has the unusual dependence of $\tau^{1/4}$. The minimum value for σ/f of 4×10^{-12} occurs at $\tau = 10$ s. The result for shorter averaging times agrees well with that expected for two modulated lasers modulated at 700 Hz and 10 MHz peak to peak. This is as discussed in section 4.2, $\sigma = a_m\sqrt{2}/\pi\nu_m\tau = 5.9 \times 10^{-12}/\tau$.

In conclusion, this chapter has discussed frequency stabilisation in both the simplest cases with the unmodified diode as well as in more sophisticated areas, incorporating linewidth reduction and fast frequency modulated diodes. A statistical parameter has been described to quantify the term "frequency stability" and results presented for a number of cases. This section gives the most comprehensive study to date of the stability of frequency-stabilised laser diodes. In the case of Rb-stabilisation of optically narrowed diodes, this is the first time frequency stability data have been reported. Such data, though, do not necessarily relate to frequency reproducibility. This is a vital parameter if these lasers are to be used for absolute length measurements, and this is discussed in more detail in the following chapter.

References

[1] KC Shotton, WRC Rowley, NPL Report Qu28, (revised, 1978)

[2] PW Smith, IEEE J Qu El, QE-1, 343-8, (1965)

[3] WRC Rowley, NPL Report Qu40 (1977)

[4] YC Chung, TM Shay, Electron Lett, 23, No 20, 1044-5, (1987)

[5] H Tsuchida, M Ohstu, T Tako, N Kuramochi, N Oura, Japan. J Appl Phys, 21, L561-3, (1982)

[6] S Yamaguchi, M Suzuki, IEEE J Qu El, QE-19, 1514-9, (1983)

[7] WRC Rowley, NPL Report MOM 78, (1986)

[8] JA Barnes, AR Chi, LS Cutler, DJ Healey, DB Leeson, TE McGunigal, JA Mullen Jr, WL Smith, RL Sydnor, RFC Vessot, GMR Winkler, IEEE Trans Instrum Meas., IM-20, No 2, 105-20, (1971)

[9] DW Allan, Proc IEEE, 54, No 2, 221-30, (1966)

[10] DW Allan IEEE Trans Ultrason, Ferroelectrics & Frequency Control, UFFC-34, No 6, 647-54, (1987)

[11] J-J Gagnepain, Proceedings Frequency Standards and Metrology 4th Symposium, Ancona, Italy, Sept 5-9 1988, p150-6 (Springer-Verlag)

[12] B Dahmani, L Hollberg and R Drullinger, Opt. Lett., 12, No 11, 876-8 (1987).

[13] C H Shin, M Teshima, M Ohtsu, Electron Lett., 25, No 1, 27-8 (1989).

[14] P H Laurent, A Clairon, C H Breant, IEEE J. Qu. El., 25, No 6, 1131-42 (1989).

[15] H Li and H R Telle, IEEE J. Qu. El., 25, No 3, 257-64 (1989).

[16] A Hemmerich, DH McIntyre, D Schropp Jr, D Meschede, TW Hänsch, Opt Comm, 75, No 2, 118-22 (1990)

[17] L Hollberg and M Ohtsu Appl. Phys. Lett., 53, No 11, 944-6 (1988).

[18] J L Hall, L Hollberg, T Baer, H B Robinson, Appl. Phys. Lett., 39, No 9, 680-2 (1981).

[19] GC Bjorklund, MD Levenson, W Lenth, C Ortiz, Appl Phys B32, 145-52 (1983)

[20] GC Bjorklund, Opt Lett, 5, No 1, 15-7 (1980)

[21] F Bertinetto, GB Picotto, P Cordiale, S Fontana, Frequency Standards and Metrology, Proc 4th Symposium, Ancona Italy, Sept 5-9 1988, p465-6 (Springer-Verlag 1989)

[22] U Brand, J Helmcke, Frequency Standards and Metrology, Proc 4th Symposium, Ancona, Italy, Sept 5-9 1988, p467-8 (Springer-Verlag 198)

[23] M Gehrtz, W Lenth, AT Young, HS Johnston, Opt Lett, 11, No 3, 132-4 (1986)

[24] W Lenth, M Gehrtz, Appl Phys Lett, 47, No 12, 1263-5 (1985)

[25] W Lenth, Opt Lett, 8, No 11, 575-7 (1983)

[26] L-G Wang, DA Tate, H Riris, TF Gallagher, J Opt Soc Am B, 6, No 5, 871-6, (1989)

[27] S Nakanishi, H Ariki, H Itoh, K Kondo, Opt Lett, 12, No 11, 864-6 (1987)

[28] S Kobayashi, Y Yamamoto, M Ito, T Kimura, IEEE J Qu El, QE-18, No 4, 582-95 (1982)

[29] H Tsuchida, T Tako, Japan J Appl Phys, 22, No 7, 1152-6 (1983)

[30] K Kuboki, M Ohstu, IEEE J Qu El, QE-23, No 4, 388-94 (1987)

[31] M Ohstu, K Kuboki, CH Shin, M Murato, Proceedings of the 4th Symposium on Frequency Standards and Metrology, Ancona, Italy (Springer Verlag) p242-6 (1989)

[32] J Harrison, A Mooradian, IEEE J Qu El, 25, No 6, 1152-5 (1989)

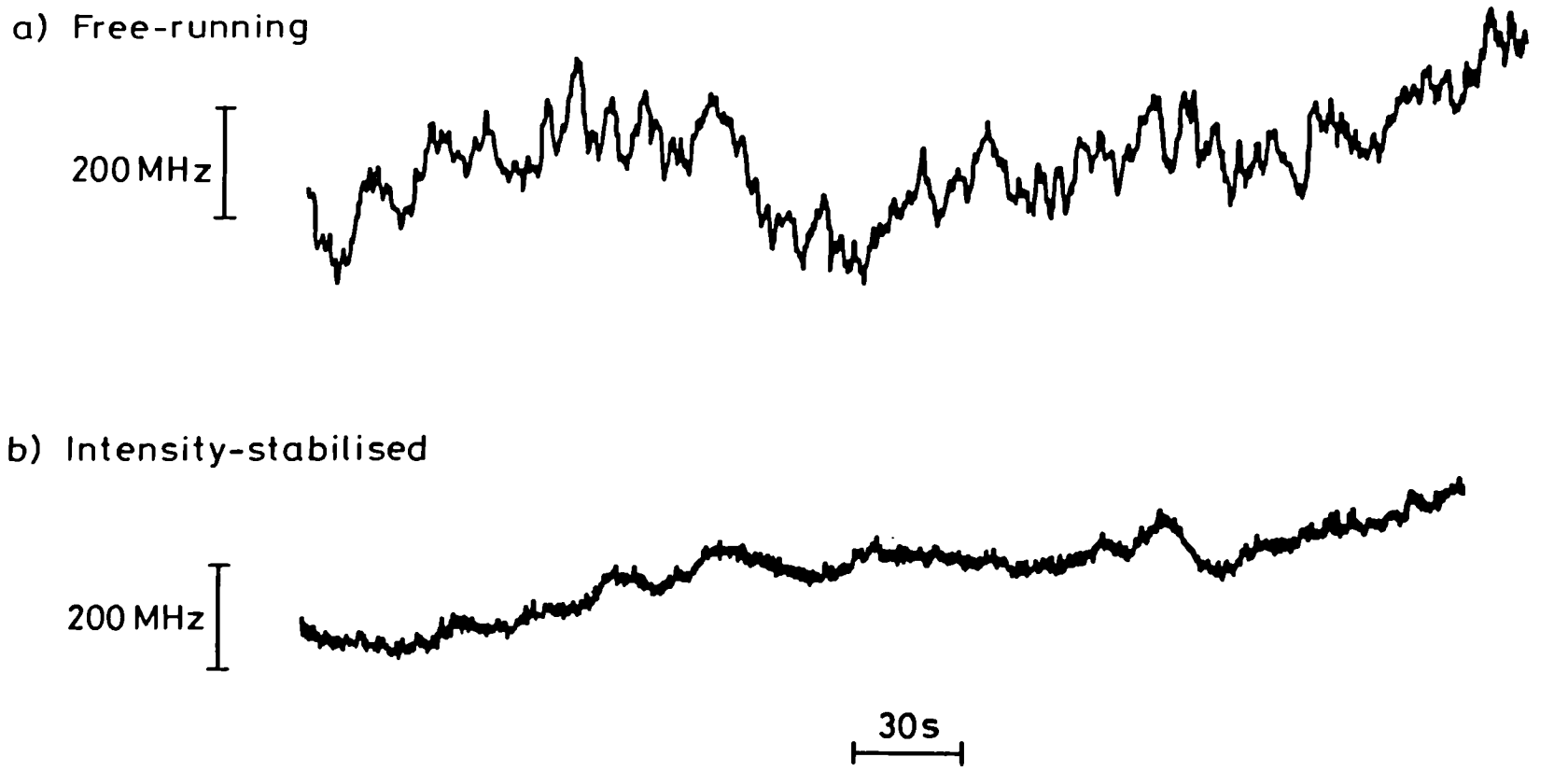

4.2.1 Plot of the frequency drift versus time obtained by monitoring the output of a PSD with the laser tuned close to a Rb absorption maximum

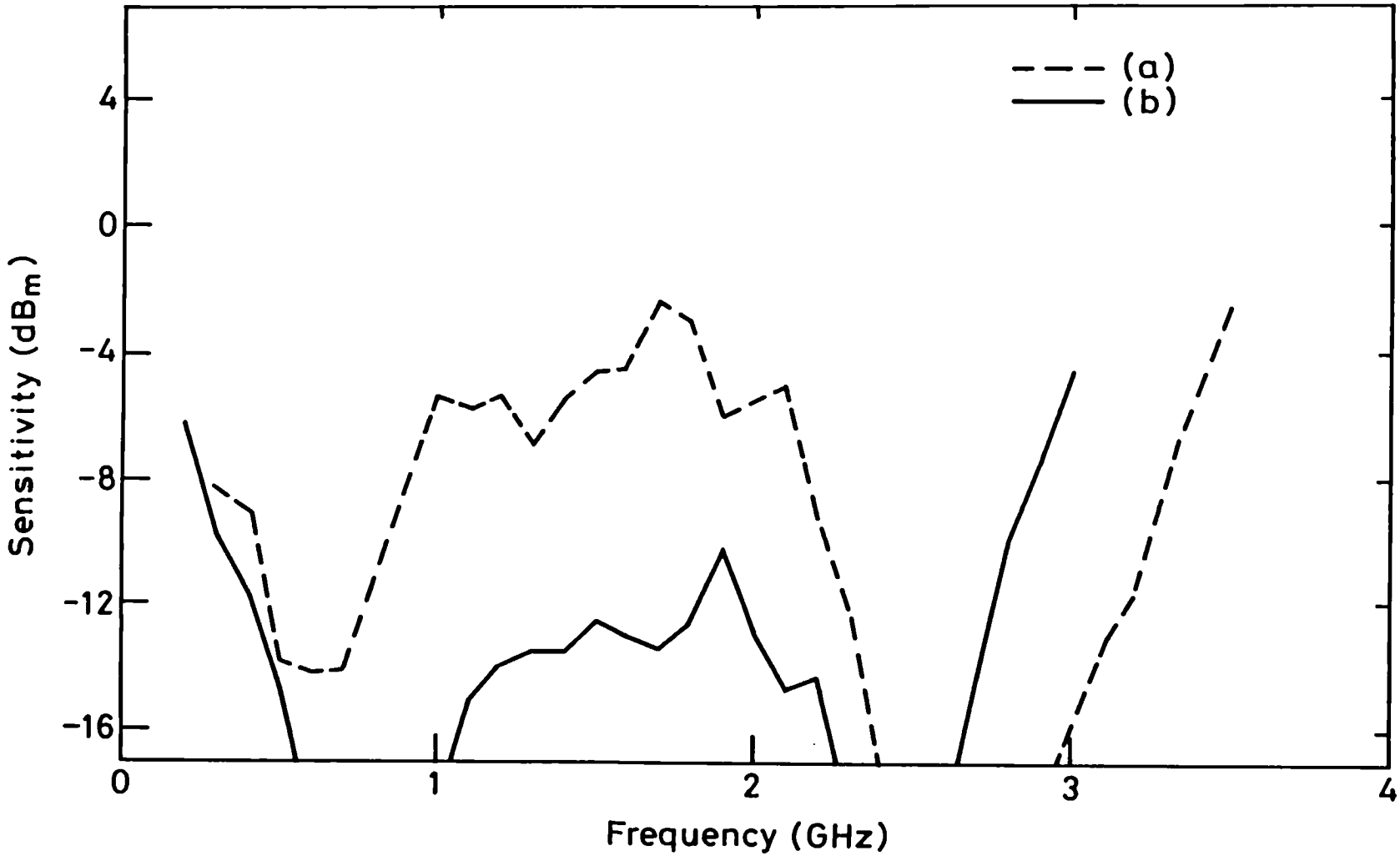

4.2.2 Plot of frequency sensitivity of 2.3 GHz and 3.5 GHz pre-scalars for clean (noise free) signals. (a) Model SP8835B (3.5 GHz, +4) and (b) SP4812 (2.3 GHz, +4) from Plessey Semiconductors. Sensitivities below -17 dB_m were not measured.

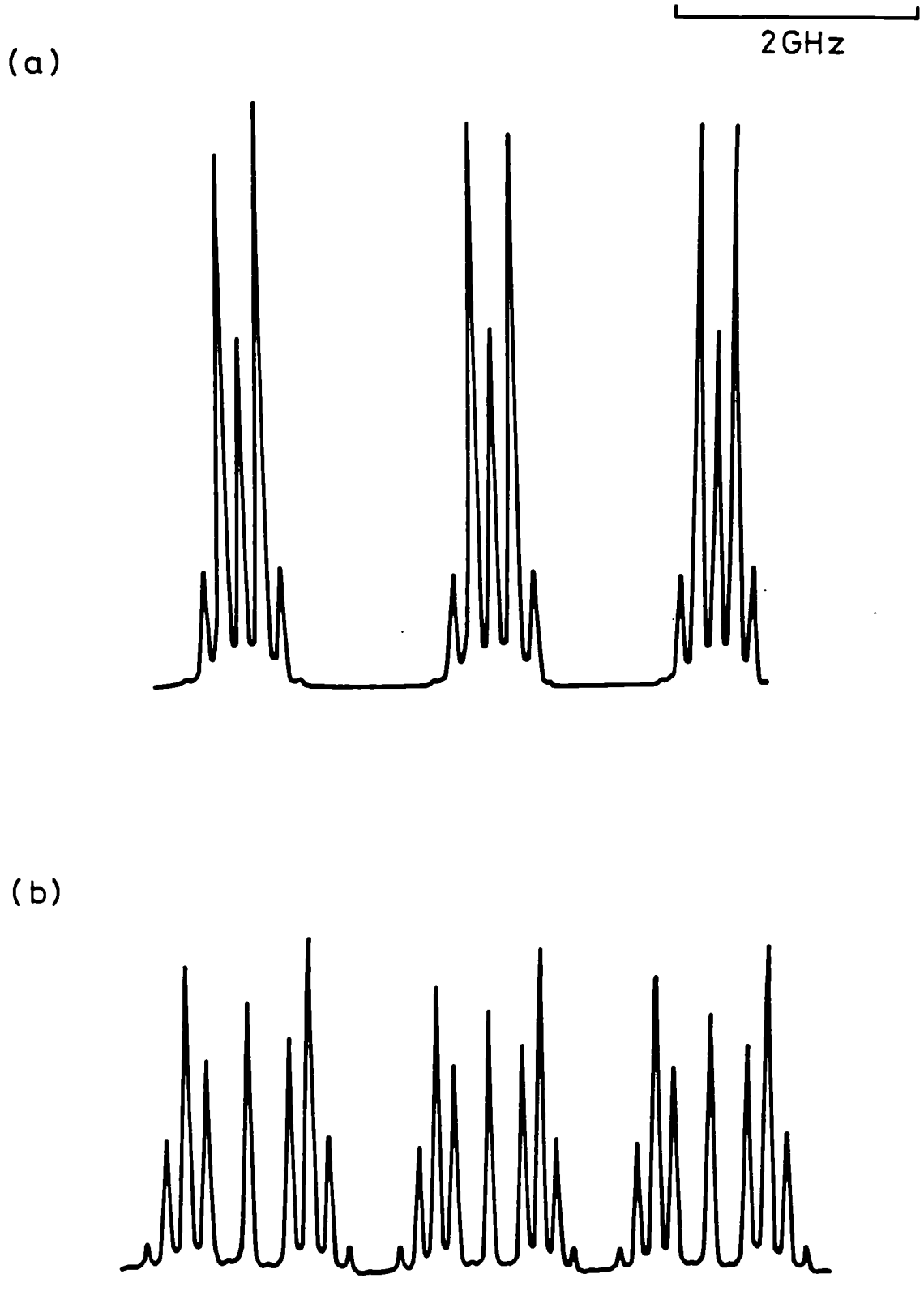

4.4.1 Sidebands of an fm diode laser as observed with a 2 GHz FSR optical spectrum analyser. Three analyser mode spacings are shown and the modulation index is 1.60 in the upper trace (a) and 3.91 in the lower trace (b).

(a) No optical feedback

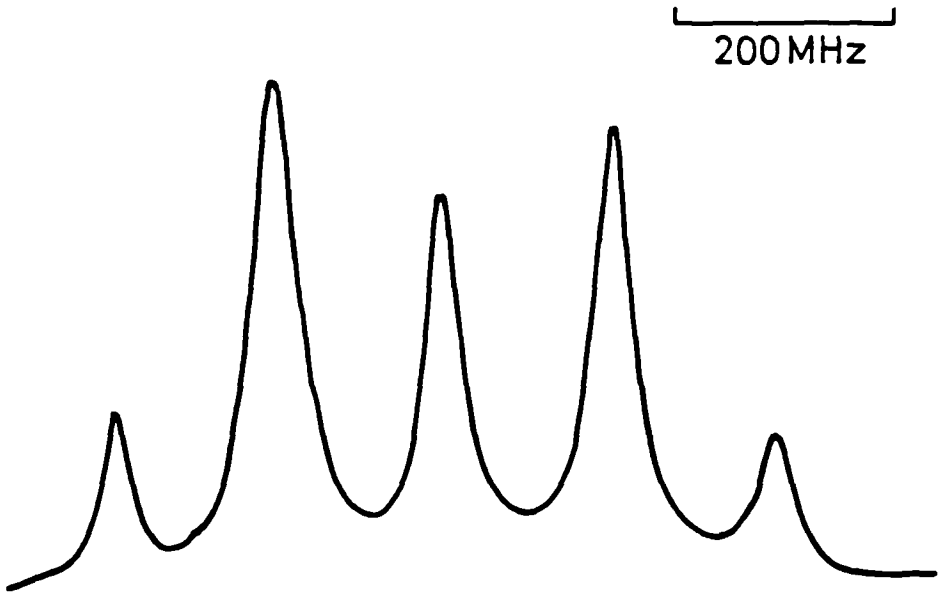

(b) With optical feedback

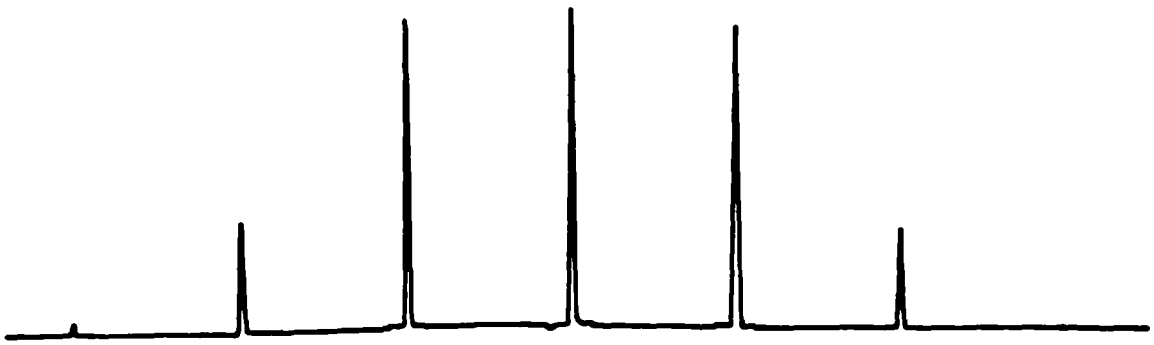

4.4.2 Sidebands of an fm diode laser as observed by a beat frequency spectrum analyser both with and without resonant optical feedback (lower and upper traces respectively). The modulation indices are 1.50 and 1.34 respectively, and the drive frequency is 155 MHz.

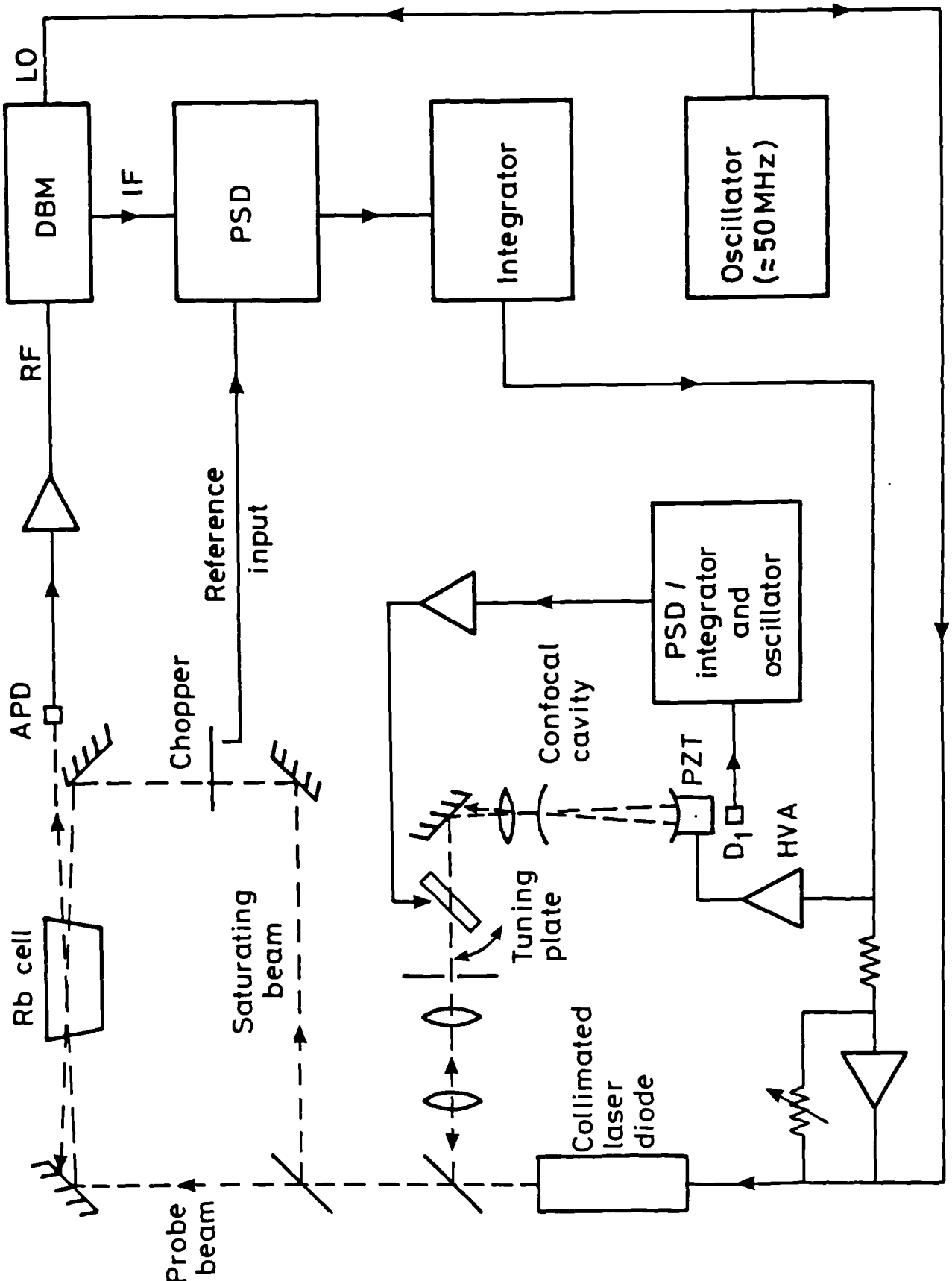

4.4.3 Schematic of apparatus for observation of Rb fm spectral features on a flat background, using an rf drive frequency of 50 MHz. The optical signal is detected, amplified and then demodulated in the double balanced mixer (see top part of the diagram).

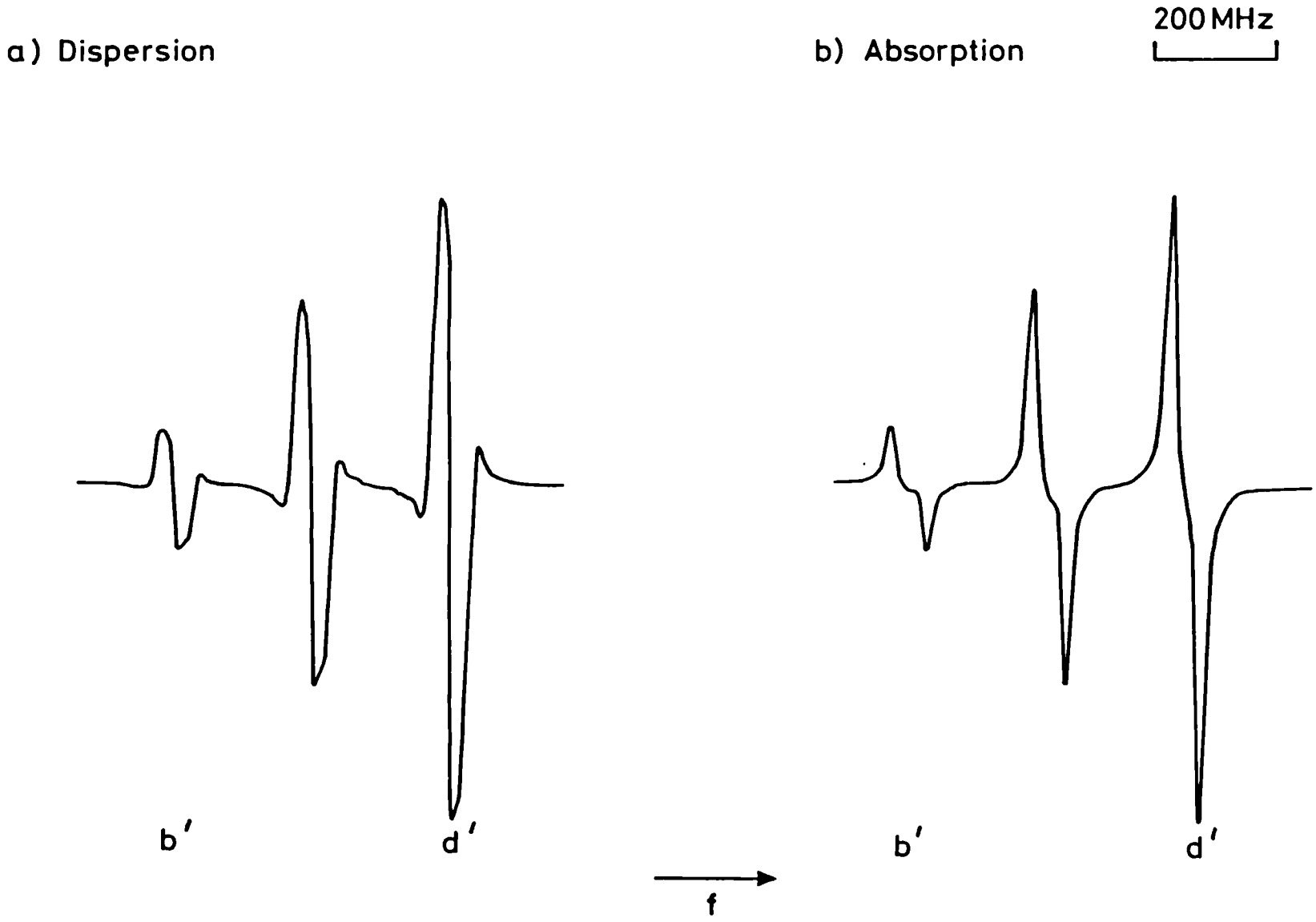

4.4.4 Saturation spectra of the Rb D_1 line, with the rf phase set for (a) dispersion and (b) absorption Doppler-free signals.

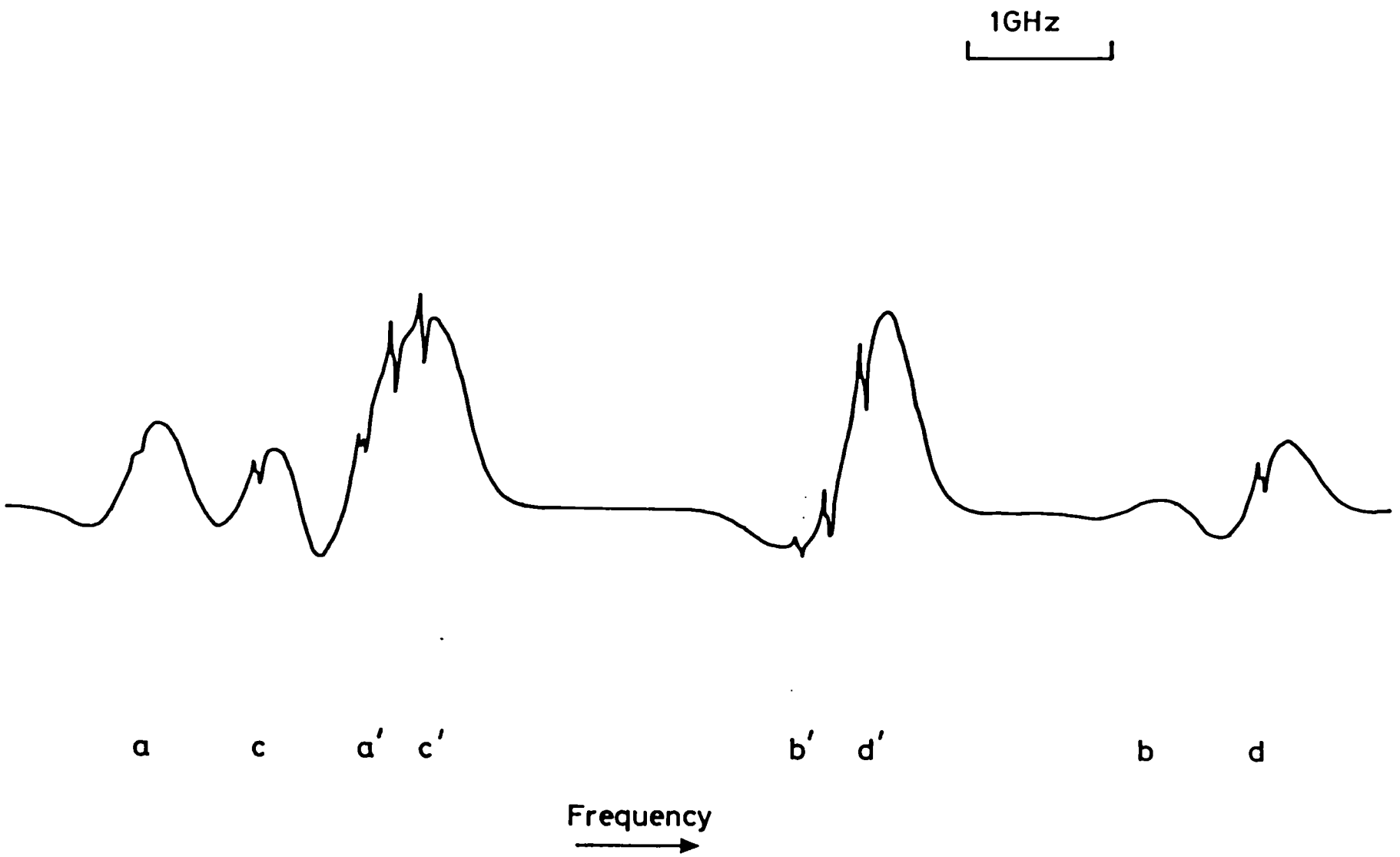

4.4.5 Doppler-free saturated signals on a Doppler-limited background of the Rb D_1 line at 795 nm. The rf phase is set for absorption.

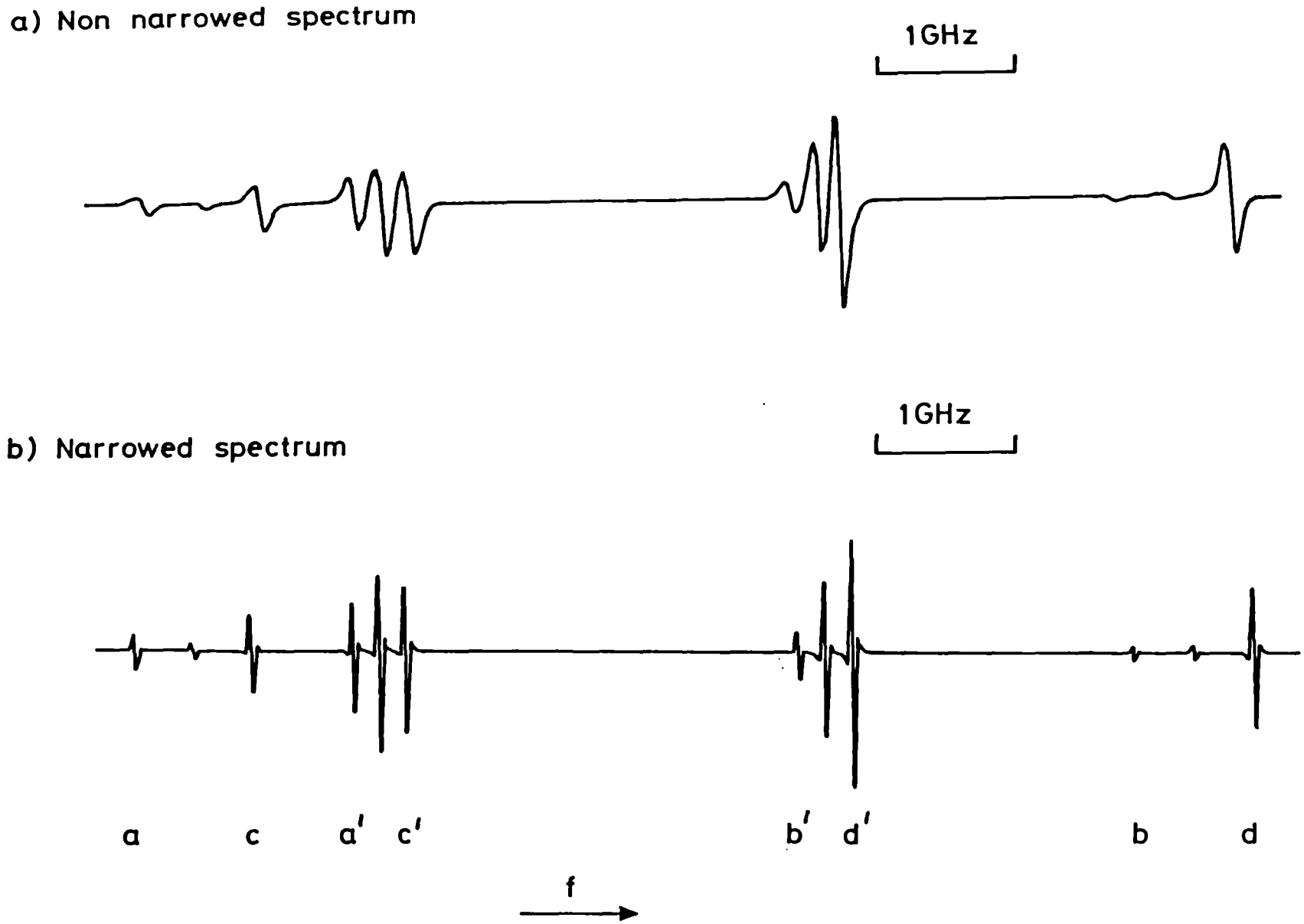

4.4.6 Saturation spectrum of the Rb D_1 line (795 nm) on a flat background, observed with (a) non-narrowed and (b) optically narrowed FM laser. The rf phase is set for dispersion.

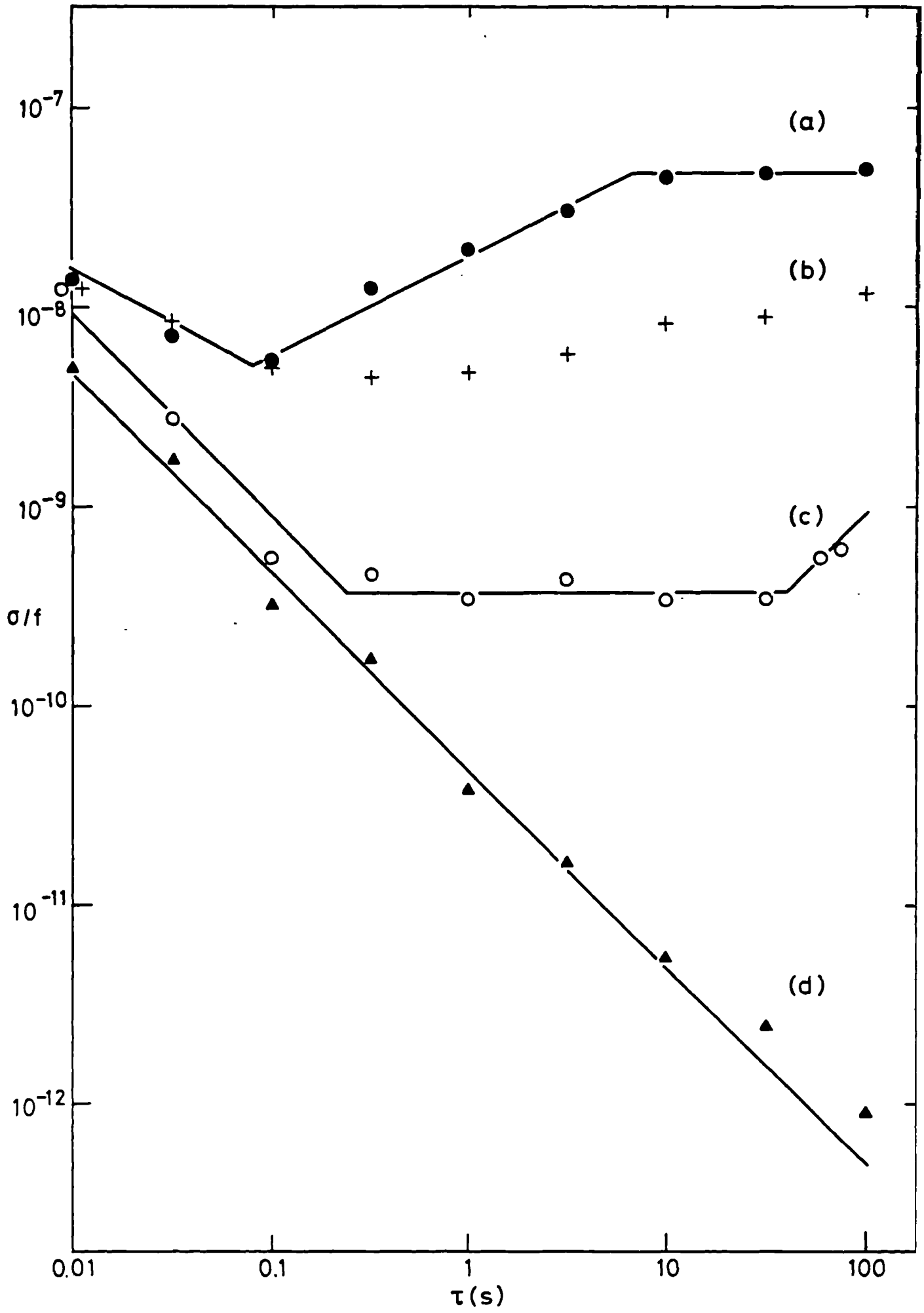

4.5.1 Relative frequency stability for non-linewidth reduced laser; a) free running, b) intensity stabilised, c) Rb stabilised and d) offset locked.

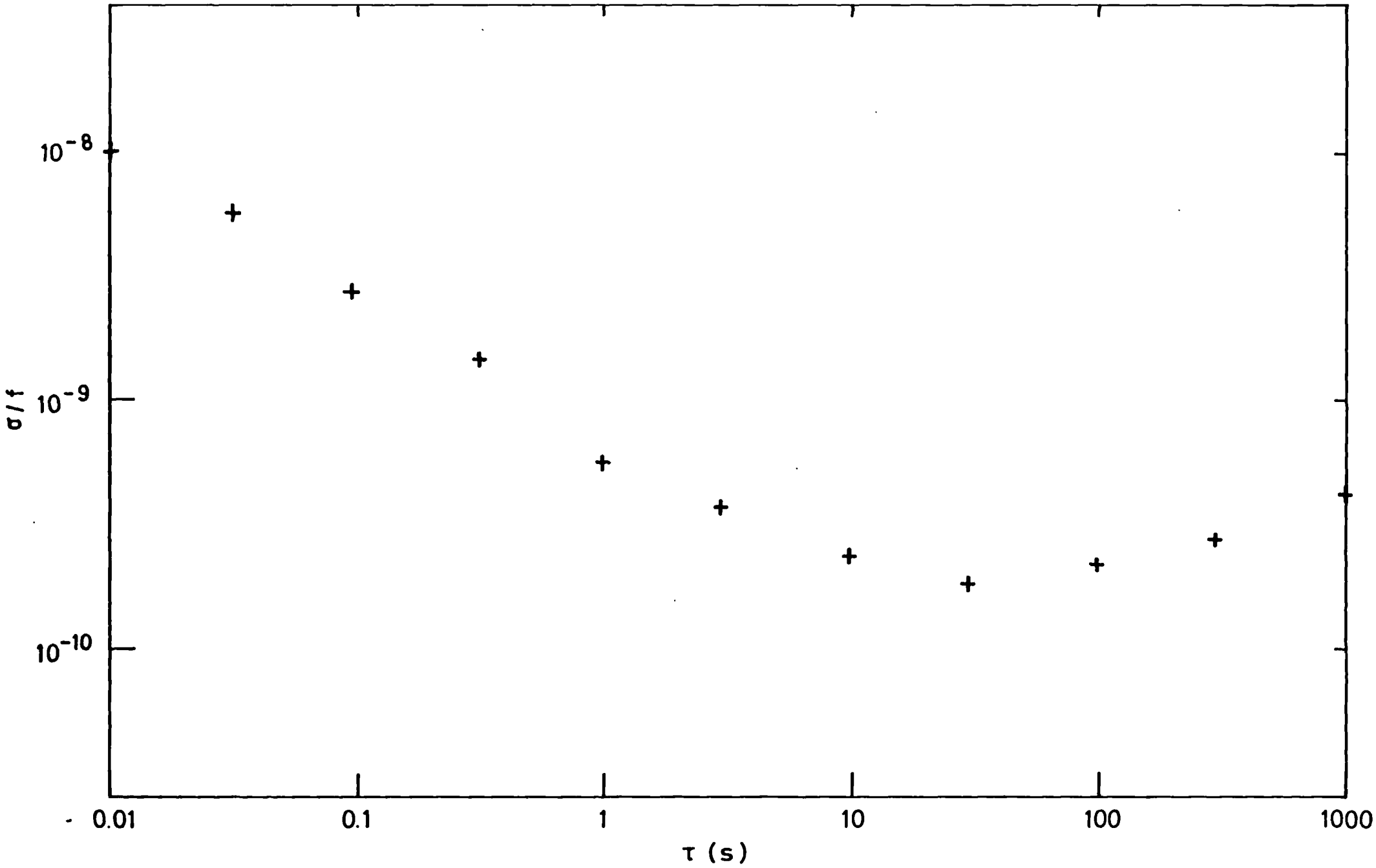

4.5.2 Relative frequency stability for non linewidth reduced laser locked to Doppler-free Rb features

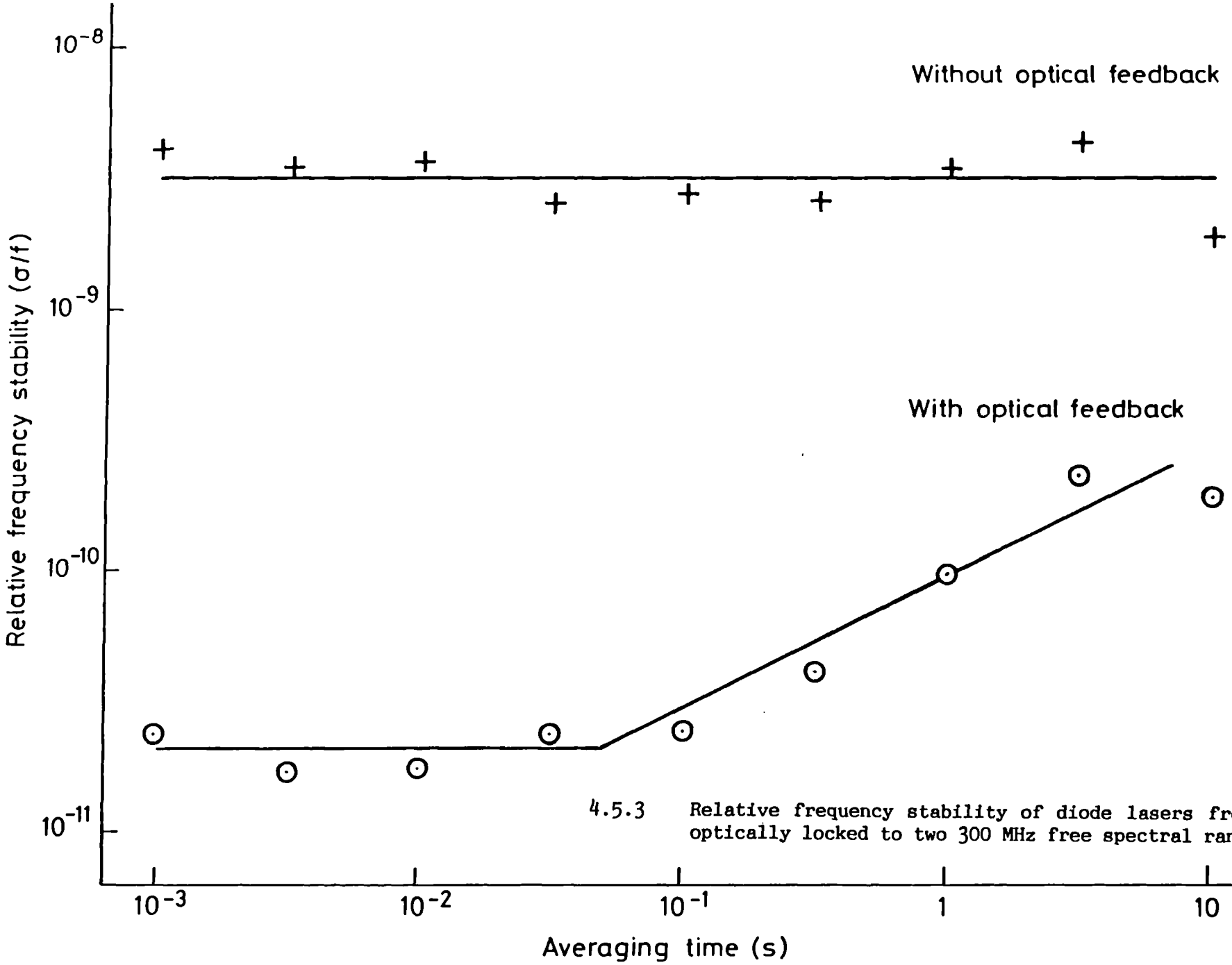

4.5.3 Relative frequency stability of diode lasers free running and optically locked to two 300 MHz free spectral range cavities.

4.5.4 Offset locked relative frequency stability for linewidth reduced lasers. The two plots are for frequency modulated (upper trace) and unmodulated (lower trace) lasers.

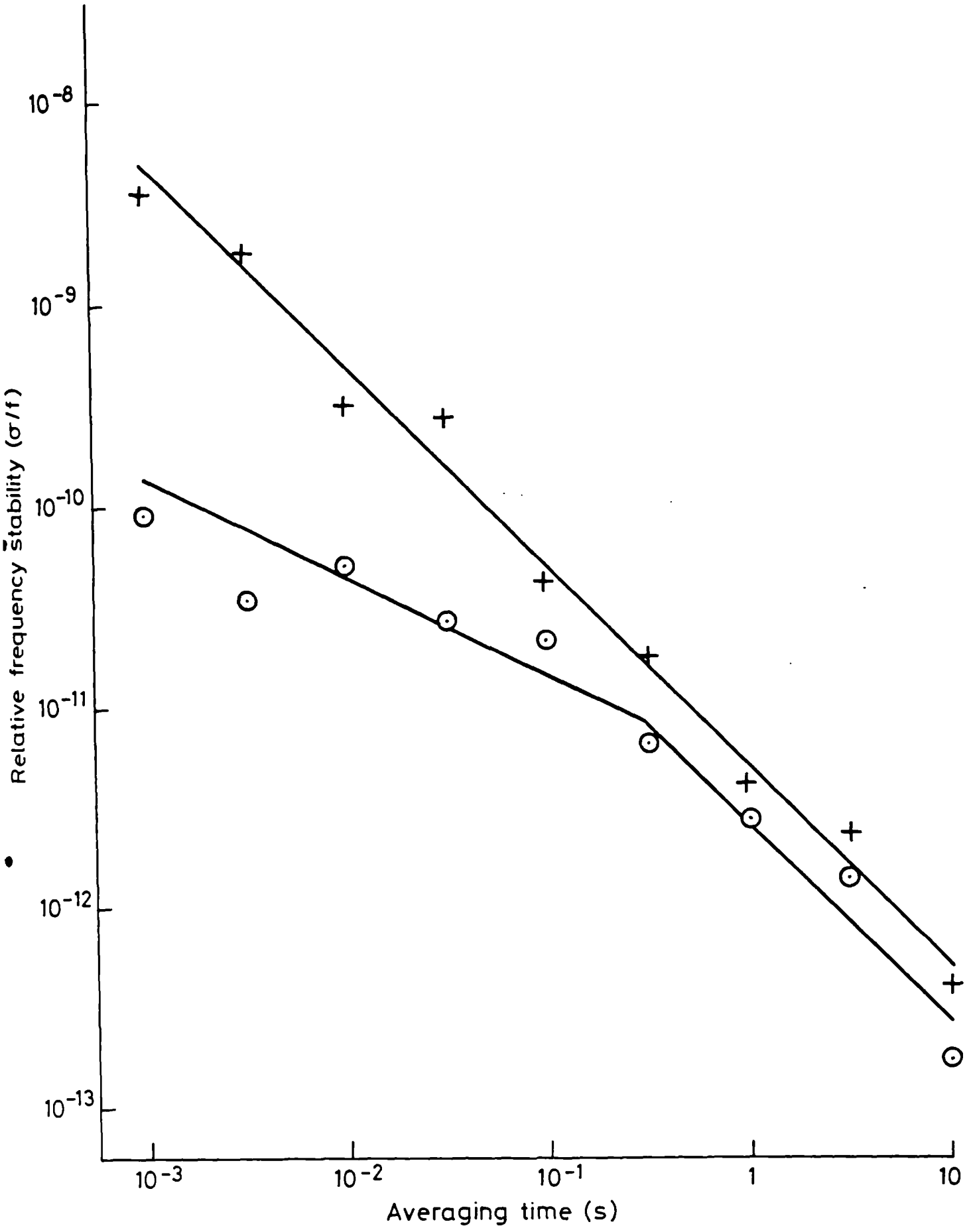

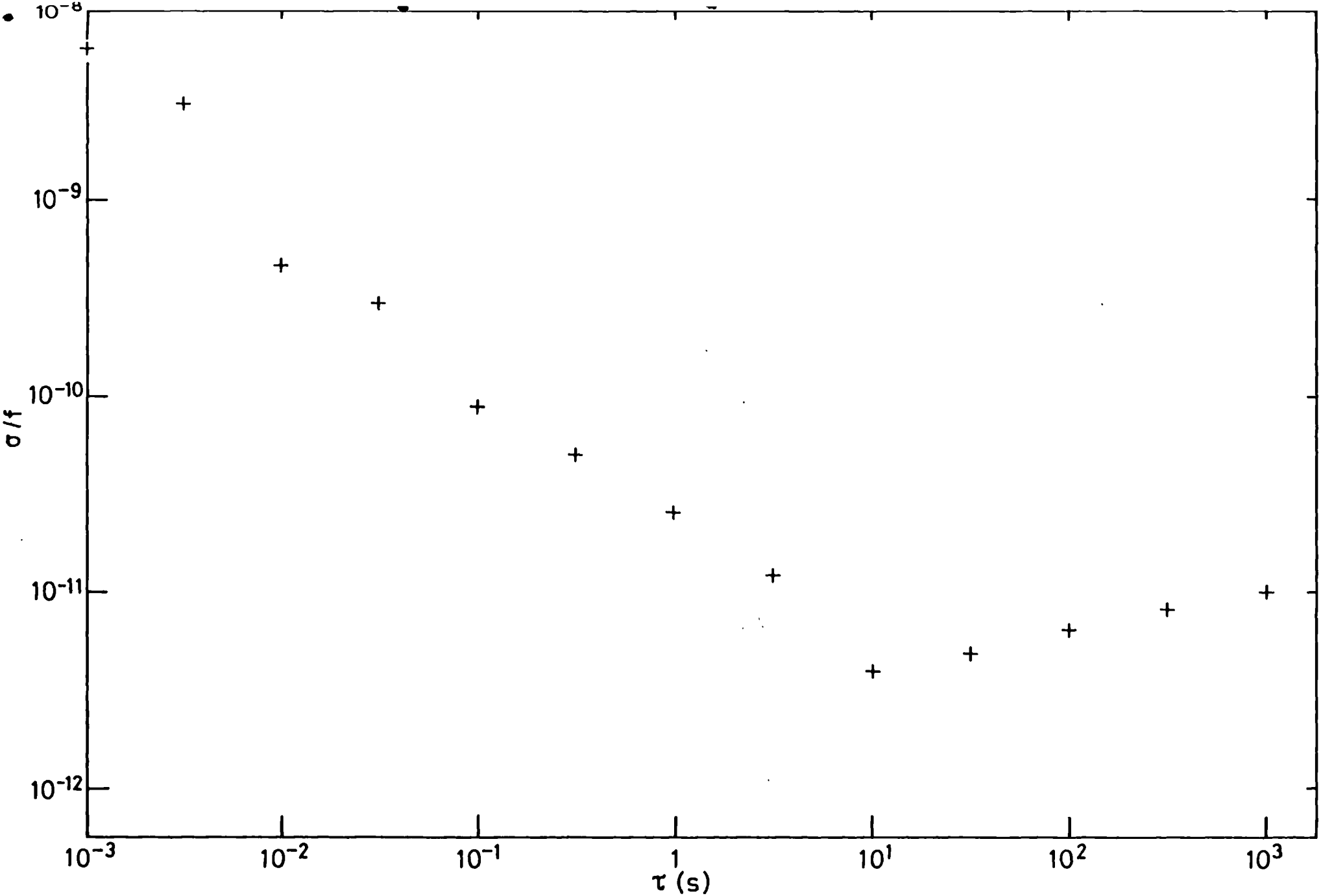

4.5.5 Rb-locked relative frequency stability between two linewidth reduced lasers.

CHAPTER 5

SPECTROSCOPIC STUDIES WITH A Rb-STABILISED LASER DIODE

5.1 Introduction; Stabilised laser frequency reproducibility and measured frequency shifts

In chapter 4, the frequency stability of a laser was defined and measured for various averaging times on different types of Rb-stabilised diodes. However, for longer averaging times, there is evidence that the frequency stability is beginning to degrade. For example, in figure 4.5.1c for stabilisation to Doppler-limited features and, $\tau \geq 40$ s, $\sigma \propto \tau$, indicating steady drift. In figure 4.5.5 for optically narrowed diodes, σ/f has a minimum value of 4×10^{-12} at $\tau = 10$ s. Although the easily-controllable parameters of the system are not changing (ie parameters such as laser power or modulation depth), there must also be unknown or uncontrollable parameters, causing frequency drift. As an example, it has already been noted that the signal to noise ratio on the strongest lines in Rb is about 300 (sections 3.7 and 4.4) with optically narrowed systems. The background appears to be limited by interference effects from unwanted optical feedback sources. In time, therefore, the dc background level at a particular frequency will change if the optical path length between the laser and feedback source were to change. Other sources of noise or drift could occur in the PSD or integrator servo-system, for example. For non-narrowed laser sources, the Rb feature width is broader, with a corresponding reduction in the expected frequency reproducibility. Doppler-limited features (section 2.3) can be obtained with a simpler optical arrangement, but provide the least reproducible frequency source. In this section, the observed

reproducibility with the various laser systems will be summarised. In addition, the laser frequency may be expected to depend upon laser modulation depth, or laser power, for example. These were investigated, and the results are given in the second half of this section.

Three main types of Rb-stabilised laser diodes have been investigated for this thesis. These are

(i) Stabilisation to Doppler-limited features with no linewidth reduction technique being used on the diode (section 2.3).

(ii) Stabilisation to Doppler-free Rb features, also using a non-narrowed diode (section 2.5)

(iii) Stabilisation to Doppler-free Rb features, using an optically narrowed diode (section 3.7).

Frequency stabilisation is also possible using optically narrowed fm diodes (section 4.4). However, from the signal to noise ratio, it is to be expected that the results would be similar to case (iii) above. This was not investigated further. In each case, the reproducibility recorded is that of the beat frequency between two nominally identical lasers locked onto two closely-spaced components.

For the case of locking to Doppler-limited components, the two zero crossings chosen were "a" and "b" at 780 nm of figure 2.3.3. The beat frequency was measured over the course of several working days, with the lasers switched off at night. The two components are chosen to have a good signal-to-noise ratio, and provide a beat frequency of ≈1 GHz which may be counted sufficiently accurately. Accurate counting is a particular problem with non-narrowed diodes, since the beat frequency spectrum is broad, as discussed previously (section 3.3). The result was a day-to-day reproducibility of the beat of ±10 MHz, under nominally

identical operating conditions. For the case of non-narrowed lasers, locked to Doppler-free features (figure 2.5.2), the corresponding figure was 400 kHz (one standard deviation, σ) or ± 1.2 MHz (3σ). A non-narrowed laser is unable to resolve the D_2 line, and so a pair of components from the D_1 line at 795 nm was chosen. Since this beat was also non-narrowed, accurate counting remained a problem, and the interval $f_c - f_a$ ($\approx$816.7 MHz) was chosen as the one which could be counted the most accurately. Accurate counting was verified using the ratio technique described on page 4.5. The most reproducible frequency is provided by the optically narrowed laser, frequency-locked to Doppler-free features (figure 3.7.1). Here, accurate counting is possible over a wide range of frequencies, and so many pairs of components could be used to provide a reproducibility figure. At 795 nm, the beat at $\approx$361 MHz between components "a'" and "c'" was chosen. The result was 44 kHz (one standard deviation), for 94 measurements extending over a period of 8 months. This is a further factor of ten improvement over the non-narrowed laser.

The next step in the characterisation of Rb-stabilised diode lasers is the determination of frequency shifts as a function of various operating parameters. In the case of a non-narrowed diode laser locked to Doppler-limited Rb spectra, as observed in either the cell or hollow-cathode lamp, the results of frequency shift measurements have already been discussed towards the end of section 2.4. These results, however, were not obtained using beat frequency techniques, and determined to an accuracy of ± 3 MHz. For Doppler-free techniques, using either narrowed or non-narrowed diodes, the much smaller offsets are best determined from the beat. For non-narrowed diodes, the saturating power was varied between 20 μW and 50 μW and modulation depth between 40 MHz and 70 MHz peak-to-peak. Within the overall reproducibility of 400 kHz, no observable shifts were found.

For optically narrowed diodes, offsets are measured from the beat, by assuming, to a first approximation, that the two lasers are offset by the same frequency on both lines under consideration. This technique is commonly used to measure offsets with I_2-stabilised He-Ne lasers [1]. To be more specific, suppose that when laser 2 is locked either to component "a" or "b", the emitted frequency is f_a or f_b respectively. However, if laser 1 is locked to these components, the emitted frequencies are $f_a + \Delta f$ and $f_b + \Delta f$ respectively. Assuming that $f_b > f_a$, and laser 1 is locked to "a" and laser 2 is locked to "b", then the beat frequency (B) will be

$$B = f_b - (f_a + \Delta f) \qquad (5.1.1)$$

If the components are exchanged, so that laser 2 is locked to "a" and laser 1 to "b", then the observed beat will become

$$B' = (f_b + \Delta f) - f_a \qquad (5.1.2)$$

The unshifted interval is therefore $\frac{1}{2}(B + B')$ and the offset Δf is given by $\frac{1}{2}(B' - B)$. If both lasers are operated under nominally identical conditions, then an evaluation of Δf yields important information about reproducibility. For example, there might be some factor, such as a difference in the two Rb cells, which cannot be varied and yet is different for the two laser systems. In the case of the non-narrowed laser locked to either the Doppler-limited or Doppler-free lines, any offset was negligible compared with the observed reproducibility. For the optically narrowed laser, the offset was 19 kHz and therefore comparable with the random statistics.

From work with the frequency stabilisation of He-Ne lasers to iodine

transitions [2,3], it might be expected that variations in parameters such as the laser power in the cell, modulation depth, and laser beam geometry might cause frequency shifts. In iodine, self-pressure broadening and shifts are a problem, but with Rb the self-pressure at 19°C is only 20 μPa (section 2.4) and so this not expected to pose a problem. However, whereas with iodine the lines are unaffected to first order by a magnetic field, all the Rb transitions at 780 nm and 795 nm split under the influence of a magnetic field (Zeeman splitting).

The most serious perturbation to the laser frequency was caused by a magnetic field. At 795 nm, the lines are expected to split up into many components - eg 15 m_F components for "c'". An inhomogeneous field of ≈1 mT broadened some lines and produced structure on others. Each component will shift by $g_F m_F eB/4\pi m$ in a field B, where $e/4\pi m$ = 14 GHz/T. Here, g_F is given by

$$g_F = g_J \frac{F(F+1) + J(J+1) - I(I+1)}{2F(F+1)} \qquad (5.1.3)$$

where g_J is the Landé factor. The main effect for low magnetic fields is expected to be a broadening of the lines, rather than a shift, if the magnetic sublevels are unresolved.

The optically narrowed system has the best reproducibility, and so this system should show up shifts masked by the lower reproducibility of the other laser arrangements. The saturating power was varied between 20 μW and 50 μW (as for the non-narrowed laser) and the modulation depth between 5 MHz and 15 MHz peak to peak. Shifts of up to 50 kHz were observed, which are comparable with the overall reproducibility. However, a 2 MHz shift was observed in an inhomogeneous magnetic field

of ≈1 mT generated by placing a bar magnet near the Rb cell. This was the strongest field which the laser could tolerate before the laser lost lock. The observed shift is significantly less than the ≈14 MHz/mT noted above because, in the low field of 1 mT, the Zeeman components are unresolved. The local magnitude of the earth's magnetic field was measured to be ≈30 μT, which would therefore cause an estimated 60 kHz shift. The offset observed between the two lasers, and the reproducibility is consistent with this estimate, based on the magnitude and variation of the earth's field. Better reproducibility might be possible by magnetic shielding of the cells from the earth's field, but this would add still further to the complexity of the system and so was not attempted.

In the arrangement shown in figure 3.6.1, the most important parameter affecting frequency, other than magnetic field, was the spatial quality of the laser beam and the angle between the counterpropagating beams in the cell. To improve spatial beam quality, it was found to be advantageous to aperture the beam, using perhaps only the central 50% of the diode laser output beam. The aperture also allowed the two counterpropagating beams to be adjusted to be nearly parallel, without optical feedback. A fairly long distance between cell and aperture (≈0.5 m) helped to achieve this. If a poor-quality, non-circular beam is used at a relatively large angle (eg ≈100 mrad), shifts of up to 1 MHz could be observed. At an angle of 20 mrad, the shift was ≈0.4 MHz. By using shallower angles (ie ≈10 mrad or less) and only selecting the central 50% of the beam, the reproducibility was improved to 44 kHz. The offset between the two lasers was then comparable with this reproducibility.

An offset due to a difference in the Rb cells might be expected, for

example, if there was a contaminant gas in one of the cells. Even if no such difference is observed, there could still be a background gas in both cells at a similar pressure, because both cells were purchased and presumably filled at the same time. This is a recognised problem in $^{127}I_2$ cells in iodine-stabilised lasers [4]. Additional evidence for contamination in these Rb cells is in the linewidth data as described in section 3.7. Furthermore, there is likely to be a frequency shift with cell wall temperature, although this was not measured. All results in this thesis relate to a cell temperature of 19 ± 2°C.

In summary, various levels of complexity may be chosen for Rb-stabilised laser diodes, depending upon the reproducibility required. Three systems have been demonstrated, with 3σ reproducibilities of ±10 MHz to ±100 kHz. Further improvement might be made by controlling or eliminating the magnetic field within the Rb cell. Improvements could be made in the cell filling procedure, to provide lower levels of contaminating gas. The unknown sources of optical feedback, which limit the signal to noise ratio to around 300, could also be traced to improve reproducibility. In the following section, the values of the unshifted intervals, and shifts observed on each interval are given, together with analysis of the results.

5.2 Rb hyperfine interval measurements

This section describes the measurement of the Rb hyperfine intervals and details the results obtained. The hyperfine features extend over a range of about 7 GHz at 780 nm and 7.6 GHz at 795 nm. These are fairly high frequencies to count directly, although there are a number of features across these two frequency ranges. This obviates the requirement to measure such high frequencies, although adjacent intervals are still as

high as 2.8 GHz at 780 nm and 2.7 GHz at 795 nm. It was therefore necessary to deal with beat frequencies up to around 3 GHz. The compromise is that between obtaining sufficient information about the intervals and that of cost.

As has already been described in section 4.2, inexpensive frequency counters are available operating up to 3 GHz, together with pre-scalers which may be used to improve the frequency response of slower counters. Small signal, low noise amplifiers with a similar frequency response are also available. Neglecting the possibility of counting errors, the only other potential source of systematic error is the counter crystal oscillator accuracy. An indication of the potential error here can be made by measuring a crystal-oscillator referenced function generator output frequency with the Racal counter. The greatest errors of up to 2 kHz in 1 GHz may be observed if one device has warmed up well before the other was switched on. This error is consistent with the manufacturer's specification.

The experimental arrangement used will naturally depend on the apparatus available. For example, 3 GHz could be counted directly, although this requires both pre-scalers and rf band-pass filters operating to this frequency. These filters generally operate over an octave; two were available for use - one from 0.5 GHz to 1 GHz and the second from 1 GHz to 2 GHz. Therefore, the arrangement of figure 5.2.1 was used to count a beat up to 3 GHz, which was downshifted to 2 GHz in a DBM, using a 1 GHz local oscillator. A tunable rf filter removed the unwanted harmonics from the DBM output. It was also verified, using an rf spectrum analyser, that these harmonics did not lie too close in frequency to the downshifted beat to cause problems when counting the frequency.

The basic limit to the accuracy of the hyperfine interval measurements is that of the laser reproducibility of 44 kHz. This figure varies somewhat from one component to another, and offsets were eliminated in the way described in section 5.1. Further checks on reproducibility of the interval measurements were made by measuring some intervals in more than one way. At 780 nm, for example, the intervals between components "a", "c" and "e" (figure 3.7.2) may be made by observing the change in beat frequency as the laser is swept between components, with the second laser locked to either components "a'", "c'" or "e'". In other words, the interval $(f_c - f_a)$ may be measured as $(f_c - f_{a'}) - (f_a - f_{a'})$ or $(f_c - f_{c'}) - (f_a - f_{c'})$ etc. Further there is the check that the level crossing signals should lie exactly half-way in frequency between the two relevant components. These techniques, described more fully in the following analysis section, yield important information on the accuracy and reproducibility of the final results. Under favourable conditions, namely where the components have good signal-to-noise ratio and are fully resolved, the overall fit should be comparable with the laser reproducibility. The fit might be expected to be better at 795 nm than 780 nm, since all the components at 795 nm are fully resolved. At 780 nm, results for lines such as "a'", "c'" and "e'" which are not fully resolved, cannot be expected to be as reproducible as those which are (eg "b", "d" or "f"). Furthermore, the two components "f" and "f'" at 780 nm were not observed to be very reproducible. Offsets of up to 0.75 MHz were observed when intervals were measured involving these two components. The frequency of the unshifted interval also did not fit the overall pattern very well. The reason for this offset is not clear, and so these components were omitted from the fit to calculate the hyperfine constants. It is also not recommended that these lines be used as precision reference frequencies.

Given that the upper limit on beat frequencies which could be accurately counted is 3 GHz, this limits the frequency intervals which may be measured. More widely spaced intervals have to be calculated from these measurements. These amount to 13 measured intervals at 795 nm and 90 at 780 nm. The results for these intervals are listed in the following tables and represent the most comprehensive study of the Rb hyperfine intervals to date. The spectra are shown in figures 3.7.1 and 3.7.2 and the notation will be referred to in the next section. There, the specific hyperfine transitions are identified, so that a global fit of the data may be obtained.

Table 5.2.1

Measured hyperfine intervals between the low frequency component groups of ^{87}Rb and ^{85}Rb (figures 3.7.1 and 3.7.2) at 780 nm. Components with a dash (') refer to ^{85}Rb. Results are in MHz.

	b	b/d	d	b/f	d/f	f
b'	1365.986	1287.467	1209.087	1154.242	1075.851	941.634
b'/f'	1397.774	1319.244	1240.867	1186.020	1107.627	973.412
d'	1429.413	1350.880	1272.507	1217.668	1139.267	1005.053
b'/f'	1458.014	1379.482	1301.107	1246.271	1167.876	1033.660
d'/f'	1489.685	1411.160	1332.783	1277.948	1199.560	1065.341
f'	1550.505	1472.472	1394.104	1339.273	1260.874	1126.645

Table 5.2.2

Measured hyperfine intervals between the two groups of components of ^{85}Rb (figures 3.7.1 and 3.7.2) at 780 nm. Results are in MHz.

	b'/f'	d'/f'	f'
a'	2914.335	2882.656	2821.356
a'/c'	2928.817	2897.143	2835.848
c'	2943.743	2912.035	2850.737
a'/e'	2960.617	2928.916	2867.614
c'/e'	2975.480	2943.789	2882.477
e'	3007.171	2975.487	2914.196

Table 5.2.3

Measured hyperfine frequency intervals between the two high frequency component groups of ^{87}Rb and ^{85}Rb (figures 3.7.1 and 3.7.2) at 780 nm. Components with a dash (') refer to ^{85}Rb. Results are in MHz.

	a'	a'/c'	c'	a'/e'	c'/e'	e'
a	2390.088	2375.608	2360.693	2343.814	2328.942	2297.231
a/c	2426.320	2411.844	2396.920	2380.046	2365.177	2333.474
c	2462.377	2447.839	2432.942	2416.062	2401.183	2369.492
a/e	2504.584	2490.110	2475.192	2458.307	2443.429	2411.729
c/e	2540 743	2526.289	2511.358	2494.489	2479.615	2447.911
e	2619.252	2604.787	2589.864	2572.980	2558.102	2526.398

Table 5.2.4

Measured hyperfine frequency intervals in ^{87}Rb and ^{85}Rb at 795 nm (figures 3.7.3 and 3.7.4). Components with a dash (') refer to ^{85}Rb. Results are in MHz.

$f_c - f_a = f_d - f_b$	= 816.656
$f_{a'} - f_a$	= 1520.048
$f_{a'/c'} - f_a$	= 1700.868
$f_{c'} - f_a$	= 1881.543
$f_{c'} - f_c$	= 1064.890
$f_{a'/c'} - f_c$	= 884.220
$f_{a'} - f_c$	= 703.404
$f_{c'} - f_{a'} = f_{d'} - f_{b'}$	= 361.496
$f_{d'} - f_b$	= 1917.387
$f_d - f_{d'}$	= 2734.063
$f_{b'} - f_{c'}$	= 2674.230

5.3 Analysis of Rb spectra at 780 nm and 795 nm

In this section, the results of the hyperfine frequency intervals are analysed and figures are calculated for the constants in the Hamilitonian for Rb. In the second part, the relative strengths of the saturated features are also calculated from the linear absorption strengths.

The analysis of the D_2 line (780 nm) is the more complicated of the two D lines. The first task is to assign the various transitions involved, and this is done with reference to figure 2.4.1. Transitions in two isotopes are involved, namely ^{85}Rb and ^{87}Rb, and the electronic

transitions involved are $5S_{1/2} \rightarrow 5P_{1/2}$, $5P_{3/2}$ for the D_1 and D_2 lines respectively. There is also hyperfine interaction present in Rb, leading to further splitting, and this results from the nuclear spin of I = 5/2 and 3/2 for ^{85}Rb and ^{87}Rb respectively. The final task, in understanding the transitions involved, is to calculate the allowed F quantum numbers. These extend from $|I - J|$ to $|I + J|$, using the usual rules for the addition of angular momentum in quantum mechanics [5]. As an example, for the $S_{1/2}$ state in ^{85}Rb, I = 5/2 and J = 1/2, so F = 2 or 3. However, for the $P_{3/2}$ state in the same isotope, F = 1,2,3 or 4. Since J is higher for the D_2 line than for the D_1 line in the upper state, there is more hyperfine structure at 780 nm than at 795 nm. We now apply the normal selection rules in this situation ($\Delta F = 0, \pm 1$) to determine the allowed transitions involved. Armed with the appropriate F, J and I quantum numbers, it is possible to use equation 2.4.4, to calculate the frequency intervals

$$H_{hfs} = \tfrac{1}{2}hAK + hB\,\frac{3K(K + 1)/2 - 2I(I + 1)J(J + 1)}{2I(2I - 1)2J(2J - 1)} \qquad (5.3.1)$$

where $K = F(F + 1) - I(I + 1) - J(J + 1)$

The constants A and B are the magnetic dipole and electric quadrupole additions to the Hamilitonian [6,7]. The electric quadrupole term is zero unless I, J $\geq$ 1. In this case, therefore, this term is present only for the $P_{3/2}$ state in both isotopes. For each transition, the constants for the excited and ground states are designated by the subscripts "e" and "g" respectively. A summary of the designations of the various transitions and the relevant Hamiltonian is given in tables 5.3.1 and 5.3.2.

Table 5.3.1

Hamiltonian and assignment of lines at 780 nm

^{87}Rb Hamiltonian	Assignment	Line
$-15A_e/4 + 5B_e/4 + 5A_g/4$	F = 1 → F = 0	a
$-11A_e/4 + B_e/4 + 5A_g/4$	1 → 1	c
$-3A_e/4 - 3B_e/4 + 5A_g/4$	1 → 2	e
$-11A_e/4 + B_e/4 - 3A_g/4$	2 → 1	b
$-3A_e/4 - 3B_e/4 - 3A_g/4$	2 → 2	d
$9A_e/4 + B_e/4 - 3A_g/4$	2 → 3	f
^{85}Rb		
$-21A_e/4 + 7B_e/10 + 7A_g/4$	2 → 1	a'
$-13A_e/4 - B_e/10 + 7A_g/4$	2 → 2	c'
$-A_e/4 - 11B_e/20 + 7A_g/4$	2 → 3	e'
$-13A_e/4 - B_e/10 - 5A_g/4$	3 → 2	b'
$-A_e/4 - 11B_e/20 - 5A_g/4$	3 → 3	d'
$15A_e/4 + B_e/4 - 5A_g/4$	3 → 4	f'

Table 5.3.2

Hamiltonian and assignment of lines at 795 nm

^{87}Rb

Hamiltonian	Assignment	Line
$-5A_e/4 + 5A_g/4$	F = 1 → F = 1	b
$3A_e/4 + 5A_g/4$	1 → 2	d
$-5A_e/4 - 3A_g/4$	2 → 1	a
$3A_e/4 - 3A_g/4$	2 → 2	c

^{85}Rb

$-7A_e/4 + 7A_g/4$	2 → 2	b'
$5A_e/4 + 7A_g/4$	2 → 3	d'
$-7A_e/4 - 5A_g/4$	3 → 2	a'
$5A_e/4 - 5A_g/4$	3 → 3	c'

In addition to the lines listed in tables 5.3.1 and 5.3.2, level crossing signals are observed between transitions with a common ground state. These are explained in section 2.5, and are often observed in saturation spectroscopy. This doubles the number of observed lines at 780 nm from 12 to 24. At 795 nm, 12 lines are observed instead of 8. In the previous section, use is made of these signals, which are designated by terms such as "a/c", for example. In this example, the signal occurs half-way between components "a" and "c" at 780 nm. The common ground state in this example is $5S_{1/2}$ (F = 1).

In order to fit the results to equation 5.3.1 at 780 nm, the first stage is to derive A_e and B_e for the two isotopes for the $5P_{3/2}$ state. These

constants determine only the separations within the four groups of the six closely-spaced lines. These separations are firstly calculated from results in tables 5.2.1 to 5.2.3. In the group comprising lines "b", "d" and "f" at 780 nm, $f_{b/d} - f_b = (f_{b'} - f_b) - (f_{b'} - f_{b/d})$, for example. This equals (1365.986 - 1287.467) = 78.519 MHz. A similar calculation for $f_{b/d} - f_b$ may be performed involving each of the six lines "b'" to "f'". In a similar way, intervals in the group "b'", "d'", and "f'" may be calculated either from results in table 5.2.1 or 5.2.2. The results for adjacent component intervals are calculated in each of these possible ways and then averaged. Some of these intervals are expected to be the same, and these are also averaged. The net result of these calculations is a set of 5 equations for both isotopes involving A_e and B_e. These are given in table 5.3.3.

Table 5.3.3

Averaged measured intervals (in MHz) for "b", "d", "f" and "a", "c", "e" in ^{87}Rb and the comparable intervals in ^{85}Rb.

(i) For ^{87}Rb;		Frequency intervals
$A_e - B_e/2$	= 78.449	$f_{b/d}-f_b$, $f_e-f_{c/e}$, $f_d-f_{b/d}$, $f_{d/f}-f_{b/f}$
$A_e/2 + B_e$	= 54.839	$f_{b/f}-f_d$
$3A_e/2 + B_e/2$	= 134.218	$f_f-f_{d/f}$
$A_e/2 - B_e/2$	= 36.141	$f_{a/c}-f_a$, $f_c-f_{a/c}$, $f_{c/e}-f_{a/e}$
$A_e/2$	= 42.249	$f_{a/e}-f_c$

(ii) For ^{85}Rb

$3A_e/2-9B_e/40 = 31.702$	$f_{b'/d'}-f_{b'}$, $f_{e'}-f_{c'/e'}$, $f_{d'}-f_{b'/d'}$, $f_{d'/f'}-f_{b'/f'}$
$A_e/2 + 5B_e/8 = 28.604$	$f_{b'/f'}-f_{d'}$
$2A_e + 2B_e/5 = 61.266$	$f_{f'}-f_{d'/f'}$
$A_e - 2B_e/5 = 14.742$	$f_{a'/c'}-f_{a'}$, $f_{c'}-f_{a'/c'}$, $f_{c'/e'}-f_{a'/e'}$
$A_e/2 + 7B_e/40= 16.876$	$f_{a'/e'}-f_{c'}$

For either isotope, therefore, this yields four equations (not involving "f" or "f'" for reasons described earlier), but only two unknowns. These equations need to be solved by a least squares method to yield "best fit" values for A_e and B_e for both isotopes. In either case we have a set of equations for which we must minimise the sum of the squares of the differences between the two sides of the equations. That is we try to minimise

$$S = \Sigma_i (a_i A_e + b_i B_e - c_i)^2 \qquad (5.3.2)$$

with respect to A_e and B_e. Therefore we have

$$\frac{\partial S}{\partial A_e} = 0 = 2\Sigma_i (a_i^2 A_e + a_i b_i B_e - a_i c_i) \qquad (5.3.3)$$

$$\frac{\partial S}{\partial B_e} = 0 = 2\Sigma_i (a_i b_i A_e + b_i^2 B_e - b_i c_i) \qquad (5.3.4)$$

Solving the above equations for A_e and B_e for the two isotopes gives, for ^{87}Rb A_e = 84.676(28) MHz and B_e = 12.475(28) MHz. For ^{85}Rb, A_e = 24.988(31) MHz and B_e = 25.693(31) MHz. The estimated errors (1σ) are given in brackets.

It is now possible to calculate the A_g values for ^{85}Rb and ^{87}Rb. For

^{85}Rb, the process is straightforward, because the ground state splitting is small enough for the resultant beat frequency to be directly counted. These results are presented in table 5.2.2. These results are processed using the formulae for the hyperfine intervals in table 5.3.1. Since A_e and B_e are known, the only remaining variable is A_g. This yields a set of 18 values for A_g, of which the average may be taken. Ignoring data involving "f" and "f'", this yields an average value of A_g of 1011.887 MHz. This compares with the well-documented value of A_g from time and frequency work of 1011.911 MHz.

The situation for ^{87}Rb is rather more complicated, because first of all a table of frequency intervals involving only transitions in ^{87}Rb and in the style of table 5.2.1 needs to be calculated from available data. Each component interval may be calculated in a number of ways from the data in tables 5.2.1 to 5.2.3. As an example, the interval $f_a - f_b$ may be calculated using any one of the six intervals involving f_a in table 5.2.3. An intervening separation in table 5.2.2 is also required. This yields a maximum 18 possible ways of calculating each similar interval. However, as already discussed, component "f'" does not fit the general pattern very well and so this was omitted from the calculations. This gives only 12 ways of calculating the various intervals between the high and low frequency lines of ^{87}Rb. The results of this calculation, using an average of the 12 results in each case, are shown in table 5.3.4.

Table 5.3.4

Calculated hyperfine intervals between the two groups of components of ^{87}Rb, using the data of tables 5.2.1 to 5.2.3. Results are in MHz. The lines are designated using the spectra of figures 3.7.1 and 3.7.2.

	b	b/d	d	b/f	d/f	f
a	6762.428	6683.899	6605.523	6550.688	6472.296	6338.079
a/c	6798.662	6720.134	6641.758	6586.922	6508.531	6374.313
c	6834.674	6756.146	6677.770	6622.934	6544.543	6410.325
a/e	6876.924	6798.396	6720.019	6665.184	6586.792	6452.575
c/e	6913.099	6834.571	6756.195	6701.359	6622.968	6488.750
e	6991.596	6913.067	6834.691	6779.856	6701.464	6567.247

It is now possible to use these data (table 5.3.4) to calculate A_g for ^{87}Rb, given that A_e and B_e are now known. Each of the 36 values in table 5.3.4 can be used to provide a value for A_g, but, as already observed, the frequency intervals involving "f" are anomalous and are ignored here. The remaining 30 points produce a mean for A_g of 3417.324 MHz with a standard error of the mean of 7 kHz. This compares with the value from time and frequency work of 3417.341 MHz.

At 795 nm, since far fewer data points and constants are involved, the analysis is very much simpler. The main task is to calculate the frequency interval $f_d - f_a$ using the data of table 5.2.4. This may be achieved in only 8 ways. The mean of the interval calculated in these ways is 7651.326 MHz. For ^{87}Rb, we have $2(A_e + A_g) = 7651.326$ MHz and $2A_e = 816.656$ MHz. Therefore $A_g = 3417.335$ MHz and $A_e = 408.328$ MHz. For ^{85}Rb, $f_{d'} - f_{a'}$ is calculated as 3397.222 MHz. Therefore $3(A_g + A_e) = 3397.222$ MHz and $3A_e = 361.496$ MHz and so $A_g = 1011.909$ MHz and $A_e =$

120.499 MHz. The values for A_g are seen to agree well with both those values obtained at 780 nm and values of a higher accuracy measured in time and frequency work. The results are summarised in table 5.3.5, and the values of A_g shown are the average of values obtained on the two D lines.

Table 5.3.5

Summary of results obtained for the atomic constants for ^{85}Rb and ^{87}Rb (in MHz). The errors (1σ) are given in brackets and previous data are given for comparison.

	New Data		Previous data [6]	
^{85}Rb	A	B	A	B
$5S_{1/2}$	1011.894(9)	-	1011.911(0)	-
$5P_{1/2}$	120.499(10)	-	120.72(25)	-
$5P_{3/2}$	24.988(31)	25.693(31)	25.009(22)	25.88(3)
^{87}Rb				
$5S_{1/2}$	3417.330(7)	-	3417.341(7)	-
$5P_{1/2}$	408.328(15)	-	406.2(8)	-
$5P_{3/2}$	84.676(28)	12.475(28)	84.845(55)	12.52(9)

The final constants to be obtained are the isotope shifts at 780 nm and 795 nm. This shift needs to be subtracted from the frequency intervals obtained from equation 5.3.1 for the isotope ^{85}Rb. At 780 nm, armed with the constants in table 5.3.5, values for the isotope shift may be obtained from each of the intervals in tables 5.2.1 and 5.2.3. This is because these two tables contain data on frequency intervals between lines in ^{85}Rb and ^{87}Rb. Once again, neglecting data involving lines "f" and "f'", this produces 25 values from table 5.2.1 and 30 values from table 5.2.3. From table 5.2.1, a mean value of 78.098 MHz is obtained,

with a standard deviation of 45 kHz and standard error of 9 kHz. The corresponding values from data in table 5.2.3 are 78.093 MHz, with a standard deviation of 115 kHz and standard error of 21 kHz. Combining gives an isotope shift of 78.095 MHz and standard error of the mean of 12 kHz. At 795 nm, an isotope shift may be calculated from eight of the eleven intervals in table 5.2.4. This yields a mean value of 77.583 MHz with a standard error of the mean of 12 kHz.

The final stage in this calculation is to use the constants in table 5.3.5, together with the isotope shifts, to calculate the expected intervals. These may be compared with the observed values and a value obtained for the rms fit. These calculations are presented in tables 5.3.6 to 5.3.9.

Table 5.3.6

Calculated hyperfine intervals between the low frequency component groups of ^{87}Rb and ^{85}Rb at 780 nm. The results may be compared with those observed in table 5.2.1.

	b	b/d	d	b/f	d/f	f
b'	1366.013	1287.565	1209.118	1154.308	1075.860	942.603
b'/d'	1397.714	1319.267	1240.819	1186.009	1107.562	974.304
d'	1429.415	1350.968	1272.520	1217.710	1139.263	1006.005
b'/f'	1457.967	1379.520	1301.072	1246.262	1167.815	1034.557
d'/f'	1489.668	1411.221	1332.773	1277.963	1199.516	1066.258
f'	1549.992	1471.474	1393.027	1338.217	1259.769	1126.512

Table 5.3.7

Calculated hyperfine intervals between the two groups of components of ^{85}Rb at 780 nm. The results may be compared with table 5.2.2.

	b'/f'	d'/f'	f'
a'	2914.306	2882.605	2822.352
a'/c'	2929.017	2897.316	2837.063
c'	2943.728	2912.027	2851.773
a'/e'	2960.718	2929.017	2868.764
c'/e'	2975.429	2943.728	2883.475
e'	3007.130	2975.429	2915.176

Table 5.3.8

Calculated hyperfine intervals between the two high frequency component groups of ^{87}Rb and ^{85}Rb. Results may be compared with table 5.2.3.

	a'	a'/c'	c'	a'/e'	c'/e'	e'
a	2390.174	2375.463	2360.752	2343.762	2329.051	2297.350
a/c	2426.280	2411.569	2396.859	2379.868	2365.157	2333.456
c	2462.387	2447.676	2432.965	2415.975	2401.264	2369.563
a/e	2504.728	2490.017	2475.306	2458.316	2443.605	2411.904
c/e	2540.834	2526.123	2511.413	2494.422	2479.711	2448.010
e	2619.282	2604.571	2589.860	2572.870	2558.159	2526.458

Table 5.3.9

Calculated hyperfine intervals in ^{87}Rb and ^{85}Rb at 795 nm. Results may be compared with table 5.2.4.

$f_c - f_a = f_d - f_b$	= 816.656
$f_{a'} - f_a$	= 1520.084
$f_{a'/c'} - f_a$	= 1700.832
$f_{c'} - f_a$	= 1881.581
$f_{c'} - f_c$	= 1064.925
$f_{a'/c'} - f_c$	= 884.176
$f_{a'} - f_c$	= 703.428
$f_{c'} - f_{a'} = f_{d'} - f_{b'}$	= 361.497
$f_{d'} - f_b$	= 1917.377
$f_d - f_{d'}$	= 2734.053
$f_{b'} - f_{c'}$	= 2674.185

In table 5.3.6, the rms fit is 45 kHz, ignoring components "f" and "f'". For some reason, which is not clear, the observed values for intervals involving component "f" is lower than that calculated by up to 970 kHz. With "f'", observed values are higher by up to 1.08 MHz. In table 5.3.7, the rms fit (excluding component "f'") is 94 kHz and in table 5.3.8 it is 112 kHz. It is highly likely that the larger error here results from components "a'" to "e'" not being properly resolved. This will almost certainly cause shifts to the lock point, making a global fit to the data less accurate. At 795 nm, where there are fewer components which are well-isolated, the rms fit is 30 kHz.

In addition to the frequency intervals, the saturated absorption relative signal sizes can also be fitted to published theory [8]. The

relative size for the saturated signals are given by

$$I_{ij} = \Sigma_{ij} |\mu_i|^2 |\mu_j|^2 (-1 + |\mu_{sp}|^2/\Gamma_F) \exp(\{(f_i - f_j)/2v_D\}^2) \qquad (5.3.5)$$

where $|\mu_i|^2$, $|\mu_j|^2$ and $|\mu_{sp}|^2$ are the probabilities of the transition induced by the pump beam, probe beam and spontaneous emission respectively. The Doppler 1/e half-width is given by v_D, and the values of the transition probabilities are given in table 2.4.1. Further, Γ_F is the total transition probability of each hyperfine interval F. Equation 5.3.5 is valid in the limit of a saturating beam intensity which is small compared with the saturation parameter. The equation only considers optical pumping effects, and so, for some transitions, this leads to unexpected results. For example, this equation predicts that $I = 0$ if $|\mu_{sp}|^2 = \Gamma_F$, and this is the case for components "a", "f", "a'" and "f'" at 780 nm. However, these transitions are observed in figure 3.7.2. The equation predicts $I = 0$ because, for these components, the spontaneous emission can only occur from the excited state to one hyperfine ground state. For example, for line "a", ($F = 1 \rightarrow F = 0$), the upper state ($F = 0$) can only decay back to the $F = 1$ ground state. However, this theory is fairly straightforward, and goes some way towards providing an understanding of the relative feature sizes. To understand how to use this equation, consider transition "a" at 795 nm, assigned as $F = 2 \rightarrow F = 1$ (table 5.3.2). From the $F = 1$ upper state, the $\Delta F = 0, \pm 1$ selection rule means that decay is allowed back to the $F = 2$ or $F = 1$ ground states (figure 2.4.1). The probe and saturating beams both induce the same transition, and $|\mu_i|^2 = |\mu_j|^2 = 0.374$. The value of $|\mu_{sp}|^2/\Gamma_F$ is the branching ratio for the $F = 1$ upper state. The probability for the $F = 1$ to $F = 1$ transition is 0.075 and so $|\mu_{sp}|^2/\Gamma_F = 0.374/(0.374 + 0.075)$. Hence $I = 0.374^2(0.374/0.449 - 1) = -0.0234$. Level crossing signal strengths may similarly be evaluated as in the

following example, for the "a/c" level crossing signal at 795 nm. In this case, the common lower ground state giving rise to the signal is F = 2, since component "a" is due to F = 2 → F = 1 and "c" due to F = 2 → F = 2. The corresponding line strengths are both 0.374. The saturating and probe beams interact with transitions "a" and "c". For transition "a", which leaves the Rb atom in the F = 1 upper state, the decay branching ratio is 0.374/(0.374 + 0.075). For transition "c", the decay branching ratio is 0.374/(0.374 + 0.374). From equation 5.3.5, we therefore evaluate $0.374^2\{(-1 + \frac{1}{2}) + (-1 + 0.374/0.449)\} = -0.093$. Finally, this number must be multiplied by the Doppler factor $exp(-\{(f_c - f_a)/2\nu_D\}^2)$. Now ν_D = 300 MHz, and $f_c - f_a$ = 812 MHz, and so this factor is 0.160 and the actual level crossing signal is -0.093 x 0.160 = -0.0149. Similar calculations may be made for each of the 24 signals at 780 nm and 12 signals at 795 nm.

At 795 nm, comparison may be made between observed relative line strengths and calculated values for three cases. These are using the non-narrowed laser (figure 2.5.2), a narrowed laser (figure 3.7.1) and narrowed fm laser (figure 4.4.6). The results of the calculations and observed values for each of the three cases st 795 nm is shown in table 5.3.10. In order to fit the observed to the calculated line strengths, a fit is made for the two isotopes. The fit is made by a least-squares method, along the lines of equations 5.3.2 to 5.3.5. If e_i and t_i represent the experimental and theoretical values, then the ratio r which minimises $\Sigma_i (e_i - rt_i)^2$ relates the experimental to the theoretical values. This gives $r = \Sigma_i e_i t_i / \Sigma_i t_i^2$.

Table 5.3.10

Comparison between experimental and theoretical line strengths at 795 nm

Line	Theoretical	Experimental Results			Theoretical fit		
	Value	Non-Narrowed	3f Narrowed	fm Narrowed	Non-Narrowed	3f Narrowed	fm Narrowed
a	0.0234	12	15	6	8	6	6
a/c	0.0149	4	0.5	2	5	4	4
c	0.0699	21	15	14	24	17	19
a'	0.222	38	43	19	30	19	19
a'/c'	0.433	51	13	31	59	37	37
c'	0.356	45	31	25	49	31	30
b'	0.0636	14	15	8	9	5	5
b'/d'	0.243	43	30	27	33	21	21
d'	0.444	64	45	43	61	38	37
b	4.69×10^{-3}	3	5	2	2	1	1
b/d	5.98×10^{-3}	2	2	2	2	2	2
d	0.0699	25	16	24	24	17	19

Unfortunately, the relative line strengths are not very reproducible, thus making experimental verification difficult. However, there is broad agreement - for example component "b" and level crossing "b/d" are consistently weak, as predicted. To give an alternative visual means of comparison, one of the above experimental results (with the non-narrowed laser) has been reproduced along with the theoretical spectrum in figure 5.3.1.

A similar comparison to the above may be made for the D_2 line at 780 nm. In this case, only data using third harmonic spectra and a narrowed

diode may be used for a rigorous comparison (figure 3.7.2). The comparison of line strengths is made in table 5.3.11, although unfortunately the fit does not appear as satisfactory as at 795 nm. One problem is that, since saturation effects are not taken into account by equation 5.3.5, some line strengths are predicted to be zero, although all the components in figure 3.7.2 are easily observed. This indicates that saturation effects should be taken into account for the chosen operating conditions on all lines. An additional problem is the non-reproducibility of the observed line-strengths, as noted on the 795 nm line.

Table 5.3.11

Comparison between experimental and theoretical line strengths for the 780 nm D_2 line (figure 3.7.2)

Line	Theoretical Strength	Experimental Value	Theoretical Fit
Group (i)			
b	5.65×10^{-4}	2	1
b/d	4.32×10^{-3}	6	11
d	8.84×10^{-3}	4	22
b/f	4.94×10^{-3}	25	12
d/f	0.0204	33	50
f	0	6	0

Group (ii)			
b'	0.0118	1	3
b'/d'	0.0643	6	16
d'	0.0830	3	21
b'/f'	0.0872	25	22
d'/f'	0.185	29	46
f'	0	3	0
Group (iii)			
a'	0	23	0
a'/c'	0.0318	23	8
c'	0.0414	33	10
a'/e'	0.0625	39	16
c'/e'	0.115	47	29
e'	0.0665	17	17
Group (iv)			
a	0	13	0
a/c	1.14×10^{-3}	8	3
c	2.89×10^{-3}	42	7
a/e	3.05×10^{-3}	21	7
c/e	0.0110	53	27
e	8.84×10^{-3}	25	22

Having measured the frequency intervals between closely spaced hyperfine intervals, the final two sections of this chapter are concerned with measurement of the absolute frequency of one line at 780 nm and one at 795 nm. Measurements are made of the absolute frequencies of the lasers tuned both to linear absorption maxima and also to Doppler-free saturated features. These interferomeric measurements are made using optically narrowed diode lasers. Before the measurements are described, possible causes of systematic error in the interferometric measurements

are discussed.

5.4 Discussion of systematic errors of interferometric laser frequency measurements

At NPL, two types of interferometer are necessary for precision wavelength measurements. An accuracy of around $\pm 1 \times 10^{-10}$ of the optical frequency is possible, if the laser diode is sufficiently reproducible. The first of these two NPL interferometers, a Michelson system, can provide a result of sufficient accuracy to be used as a "start" value for the second high-precision Fabry-Perot device.

The Michelson wavemeter consists of a scanning cube corner, counter electronics, computer and reference laser. Details of this system have previously been published [9]. The reference laser is an NPL-designed Zeeman-beat stabilised He-Ne laser [10]. The electronics provide a count of the number of fringes of the diode laser for a pre-set number of He-Ne fringes, typically between 1×10^5 and 1×10^6. A measurement of the fringe fraction of the diode laser fringes at the beginning and end of the count improves the resolution. An overall accuracy (3σ value) of around ±5 parts in 10^8 (±25 MHz at visible frequencies) is achieved and the various component errors are described with a summary in table 5.4.1. Potential sources of error are in the reference laser frequency, estimation of the refractive index of air and laser beam alignment. Of these, laser frequency uncertainty of the Zeeman reference laser [10] is the smallest. These lasers exhibit a very linear but low frequency drift with use. Once this rate and initial frequency are determined, ±2 MHz or better in accuracy is readily assured. A small contribution to the overall uncertainty is also provided by the dispersion in air between the diode and reference laser

wavelengths [11]. Although the refractive index of air cannot be determined absolutely to much better than $\pm 1 \times 10^{-7}$ from Edlen's equations without a refractometer, it is only the ratio n_{diode}/n_{HeNe} which is relevant here. A lot of the errors cancel, and the estimated error in the ratio is around $\pm 1 \times 10^{-8}$ [11]. An example of such an error is the effect of contaminating gases (eg SO_2 or CO_2) in the air. Sensor errors (in measuring air temperature, pressure and humidity) are also a potential but small source of error. Measurement of air temperature, pressure and humidity to better than ±0.1°C, ±0.1 mbar, and ±5 % are readily made and all contribute less than ±1 part in 10^8 to the overall error.

Laser alignment errors are, by far, the greatest problem and limit the overall accuracy. Such "cosine errors" are well-known to users of displacement measuring interferometers. In this case, the problem is that either the He-Ne laser or diode beams may not be properly overlapped, or that one or other beam may not be quite parallel to the travel of the corner cube. In practice, the 633-nm He-Ne beam is a good circular Gaussian beam and easily visible, so that it is easy to align, especially using a position sensitive detector. However, a diode beam is barely visible to the eye and is not necessarily circular or Gaussian (figure 1.3.2). It was found, therefore, that it was generally the diode beam which tended to be mis-aligned. In such a case, the answer could become biassed, since the wavemeter produces a result $f.\cos\theta$, where θ is the angular misalignment of the diode beam. The answer produced by the wavemeter then has a relative error ($\Delta f/f$) of $\approx \frac{1}{2}\theta^2$, where θ is in radians. The results therefore exclude any which appear anomalously low, outside the general level of statistics. In general, around half a dozen different optical alignments were made for each measurement. Estimates of the error sources are summarised in table 5.4.1.

Table 5.4.1

Summary of estimated errors for the NPL Michelson wavemeter for measurement of diode laser frequencies.

Error source	MHz (standard deviation)
Zeeman laser reference	1
Edlen formula	3
Air sensor errors	1
Alignment errors	7
Overall error (root sum of squares)	8

The second NPL wavelength comparator is an evacuated Fabry-Perot interferometer, described fully in a number of publications [12,13,14]. The Michelson system only has a ≈0.5 m path difference and has modest coherence requirements on the source to be measured. In contrast, the Fabry-Perot system requires a linewidth of ≈2 MHz or less, so that the observed fringes are not significantly broadened. This restricts its use to optically narrowed diodes. If the laser source is not sufficiently coherent or is frequency modulated, the broadening of the fringes in the Fabry-Perot system is accompanied by an associated shift in the observed frequency.

The length of the Fabry-Perot is initially determined with frequency stabilised He-Ne lasers at 543 nm, 594 nm and 612 nm of known frequency [15]. The length is also known to within an accuracy of a few fringes from the previous history extending over more than ten years.

Major changes in length take place only when the cavity is removed from its evacuated chamber. It is also necessary to know the diode laser frequency sufficiently well to determine the diode laser light order number of the 1-m etalon.

The ±24 MHz (3σ) accuracy of the Michelson system is just sufficient to determine the 1-m etalon diode light order number, which has a 150 MHz FSR. If the diode laser is sufficiently stable, the 1-m etalon measurement is limited in accuracy to around $\pm 1 \times 10^{-10}$ of the optical frequency. For these measurements, the error budget is given in table 5.4.2. Most of the entries are self-explanatory although one or two points require explanation. The etalon plates are coated with silver, and there is a phase shift on reflection which is wavelength dependent. Measurements have previously been made at 10 wavelengths between 486 nm and 670 nm [16,17]. These data were fitted to a cubic curve with an rms error of 5×10^{-11} of the optical frequency. This curve was extrapolated to 780 nm and 795 nm to obtain an estimated phase shift at these wavelengths. The entry under "prismatic imbalance" refers to a potential problem associated with a wedge in the input window of the etalon evacuated chamber and also a wedge in the plates. These wedges are aligned to give no net relative displacement between the two wavelengths of the image of the entrance pinhole. This entry in table 5.4.2 is an estimate of this error based upon the maximum likely misaligment of these wedges.

Table 5.4.2

Frequency ratio measurement uncertainties for the 1-m etalon

Source of uncertainty	Standard deviation (x 10^{-11})
Observation statistics	3
Phase shift extrapolation	5
Flatness and illumination	3
Prismatic imbalance	6
Diffraction effects	2
Servo errors	2
Diode laser reproducibility	12
633 nm laser reproducibility	2
Total (root sum of squares)	15 (58 kHz)

To the error budget must be added the uncertainty of international agreement on the 633 nm reference frequency [18]. The NPL reference lasers were operated under their preferred reference conditions. They are within 4 parts in 10^{11} of other lasers with which they have been compared [19]. Unfortunately, the uncertainty in the reference frequency of ±1 part in 10^{9} (3σ uncertainty) is very significantly larger than any error of table 5.4.2. The two error budgets for the frequency ratio and absolute frequency therefore need to treated separately.

The following section details results for the frequencies of non-narrowed diodes locked to Doppler-limited Rb absorptions and also optically narrowed diodes locked to Doppler-free Rb features. The former measurements could only be made on the Michelson interferometer, because

of the coherence problems outlined earlier. The latter measurements to Doppler-free features were also made on the 1-m etalon.

5.5 Interferometric Laser Frequency measurements

5.5.1 Measurements with the laser locked to Doppler free features

The simplest Rb frequency-stabilised diode laser system is that locked to linear absorption maxima, using non-narrowed diodes. This system is described in sections 2.3 and 2.4. For measurements of the frequency, the power density in the Rb cell was kept below the saturation intensity. In the cell, this corresponds to $\leq$ 10 μW in an 8 mm diameter beam ($\leq$ 0.4 Wm^{-2}). For the Rb cell, a modulation depth of 100 MHz peak-to-peak was used. Measurements were made on the NPL-designed wavemeter, the systematic errors of which were discussed in the previous section. The laser frequency reproducibility was estimated to be ±10 MHz in section 2.4. For the cell, measurements were made on components "c" and "b" on the D_2 line and "c" and "b" on the D_1 line (figures 2.3.1 and 2.3.3).

For the cell, the measured frequencies are, for the D_2 line

f_c = 384 232 061 ± 28 MHz

f_b = 384 229 173 ± 29 MHz

and for the D_1 line

f_c = 377 109 264 ± 26 MHz

f_b = 377 106 004 ± 31 MHz

where the frequencies quoted are the means of 15 results and the

uncertainties are three times the standard error of the mean. In each case, the wavemeter was re-aligned a number of times, and, in addition at 795 nm, some of the results were taken with a second diode. It is possible to use the calculations of section 2.4 used to produce figure 2.4.3 to provide a useful check on these results by calculating, for both D lines, the separation $f_c - f_b$. For the D_2 line, this is calculated to be 2908 MHz, which compares very well with the difference in the wavemeter readings of 2888 MHz. For the D_1 line, this separation is predicted to be 3252 MHz compared with a difference in wavemeter readings of 3260 MHz.

From the measurements between f_{cell} and f_{lamp} detailed in section 2.4, the above results may be used to calculate values for the lamp. It is also instructive to compare these results with previously published values. Again, developing the calculations in section 2.4, the D_1 line centre of gravity can be estimated to be $(f_c - 1.9)$ GHz or 377 107.3 GHz. This compares with the value in [20] of 377 107.7 GHz. A similar calculation for the D_2 line yields $(f_c - 1.7)$ GHz or 384 230.4 MHz for the centre of gravity. This compares with the value of 384 230.8 GHz in [20]. These results may also be related to those of the hyperfine components, as described in the following sub-section.

5.5.2 Measurements with a linewidth reduced laser locked to Doppler-free features

As described in section 5.4, the first stage in the measurement of the frequency of linewidth reduced frequency stabilised diodes uses the Michelson interferometer. Diode lasers were locked to the "d/f" level crossing at 780 nm and component "c'" at 795 nm. Both lines were chosen because they were strong well-isolated components. Checks were made, by

beat frequency techniques already described, to look for frequency offsets. This was done before, during and after the interferometric measurements to ensure that there was no anomalous behaviour at that time. The results of the frequency determinations on the Michelson system, to an estimated accuracy of ±24 MHz (3σ value, table 5.4.1), are

$f_{d/f}$ = 384 227 977 MHz

$f_{c'}$ = 377 106 265 MHz

These results may be compared directly with the results of laser frequency measurements involving the Doppler-limited features. The hyperfine intervals (section 5.2) and linear absorption line-strengths (table 2.4.1) can be used to construct a Doppler-limited profile. The frequencies corresponding to absorption maxima (where the derivative profile is zero) can then be compared with the frequencies of individual hyperfine components. This was done and the frequencies of "d/f" at 780 nm and "c'" at 795 nm were calculated to be $f_{d/f}$ = 384 227 939 MHz and $f_{c'}$ = 377 106 256 MHz from the results in the previous sub-section. The excellent agreement between these estimated values and those directly measured gives added confidence in all these results.

With the preliminary values for the hyperfine component frequencies, it is possible to employ the Fabry-Perot system for the final result. Since the reference laser frequency (a 633-nm He-Ne laser stabilised to component "i" of the 11-5 R(127) line of $^{127}I_2$) is only known to ±1 x 10^{-9} (3σ uncertainty) by international agreement, both frequency ratio and absolute frequency results are quoted. The uncertainty in the frequency ratio is given in table 5.4.2 and that of the frequency is dominated by the reference frequency uncertainty. The results are

$f_{d/f}/f_i$ = 0.811 271 267 797

$f_{c'}/f_i$ = 0.796 234 260 392

Combining these ratios with the internationally agreed value for the reference frequency of 473 612 214.8 MHz, gives

$f_{d/f}$ = 384 227 981.9 MHz

$f_{c'}$ = 377 106 271.6 MHz

The final exercise involves the determination of the offset to be added to the above frequencies for each component. These offsets may be determined from the results in section 5.3. For offsets of over 3 GHz, which were not determined directly, these were determined by adding intervals involving intermediate components. As an example, at 795 nm, the interval $f_d - f_{c'}$ was determined as $(f_{b'} - f_{c'}) + (f_{d'} - f_{b'}) + (f_d - f_{d'})$ or $(f_{b'} - f_{c'}) + (f_{d'} - f_{b'}) + (f_b - f_{d'}) + (f_d - f_b)$. The results of all such equivalent sums have been averaged and these averages presented in tables 5.5.2.1 and 5.5.2.2. Also, in these tables, the results of calculating these intervals from the constants in table 5.3.4 are presented for comparison.

Table 5.5.2.1

Values for the offsets between the "d/f" level crossing at 780 nm and each component. The results are those directly observed (LHS column) and those calculated from table 5.3.4 (RHS column).

Component	Measured	Calculated
	$f - f_{d/f}$	
b	-290.138	-290.129
d	-133.234	-133.252
f	+134.216	+133.252
b'	+1075.851	+1075.866
d'	+1139.267	+1139.269
f'	+1260.874	+1259.776
a'	+4082.219	+4082.128
c'	+4111.608	+4111.549
e'	+4175.055	+4174.951
a	+6472.296	+6472.331
c	+6544.543	+6544.532
e	+6701.464	+6701.409

Table 5.5.2.2

Values for the offsets between the "c'" line at 795 nm and each component. The results are those observed (LHS column) and those calculated from table 5.3.4 (RHS column).

Component	Measured	Calculated
	$f - f_{c'}$	
a	-1881.547	-1881.581
c	-1064.895	-1064.925
a'	-361.496	-361.497
c'	-	-
b'	+2674.230	+2674.185
d'	+3035.726	+3035.682
b	+4953.113	+4953.080
d	+5769.779	+5769.736

This chapter presents the most comprehensive set of results to date of the absolute frequencies and frequency intervals of the two Rb D lines. The hyperfine intervals have been used to produce values for the hyperfine constants and isotope shifts on both D lines. Further, interferometric frequency measurements have been made of laser diodes locked to Doppler limited and Doppler free features of both D lines. This also represents the first optical frequency standard in the far red, and the first to use laser diodes. It is, therefore, a significant step in the development of GaAlAs lasers for length or displacement measurement. As a further step towards this goal, a swept wavelength system is developed and this is described in the following chapter.

References

[1] See, for example, HP Layer, WRC Rowley, BR Marx, Opt Lett, 6 188-90, (1981)

[2] WRC Rowley, NPL Report, MOM 54 (1981)

[3] WRC Rowley, NPL Report, MOM 56 (1981)

[4] WRC Rowley, BR Marx, Metrologia, 17, 65-6 (1981)

[5] E Merzbacher, "Quantum Mechanics", 2nd edition, John Wiley & Sons (1970)

[6] E Arimondo, M Inguscio, P Violino, Rev Mod Phys, 49, No 1, 31-75, (1977)

[7] JR Beacham, KL Andrew, J Opt Soc Am, 61, No 2, 231-5 (1977)

[8] S Nakayama, Jap J Appl Phys, 23, No 7, 879-83 (1984)

[9] SJ Bennett, P Gill, J Phys E; Sci Instrum 13, 174-7 (1980)

[10] WRC Rowley, Meas Sci Technol, 1, 348-51 (1990)

[11] B Edlen, Metrologia, 2, 71-80, (1966)

[12] PT Woods, KC Shotton, WRC Rowley, Appl Opt, 17, 1048-54, (1978)

[13] GP Barwood, WRC Rowley, Metrologia, 20, 19-23, (1984)

[14] GP Barwood, WRC Rowley, PT Woods, Metrologia, 20, 157-61 (1984)

[15] WRC Rowley, P Gill, Appl Phys B51, No 6, 421-6 (1990)

[16] JRM Barr, JM Girkin, AI Ferguson, GP Barwood, P Gill, WRC Rowley, RC Thompson, Opt Comm, 54, No 4, 217-21 (1985)

[17] GP Barwood, P Gill, WRC Rowley, JL Flowers, BW Petley, Rev Phys A 43, No 9, 4783-90 (1991)

[18] Metrologia, 19, 163-77 (1984)

[19] RB Hurst, N Brown, VD Dandawate, GR Hanes, J Helmcke, HP Layer, L Zhongyou, WRC Rowley, T Sakurai, MS Chung, Metrologia 24, 39-44 (1987)

[20] CE Moore, "Atomic energy levels", National Bureau of Standards, (1952)

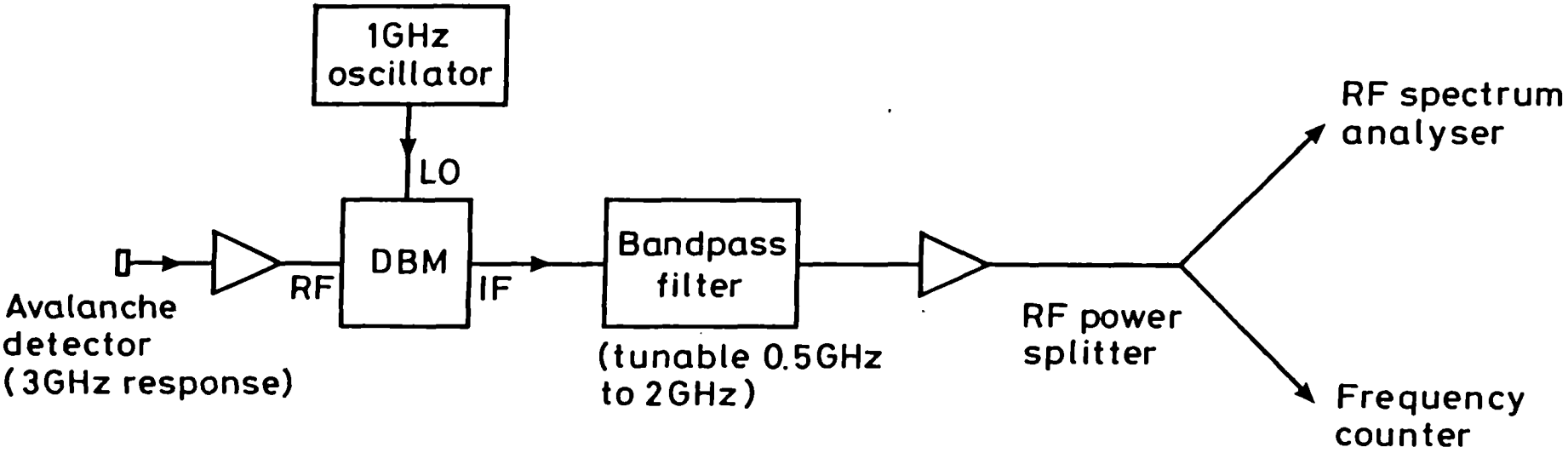

5.2.1 Schematic arrangement of the apparatus used to measure beat frequencies up to 3 GHz

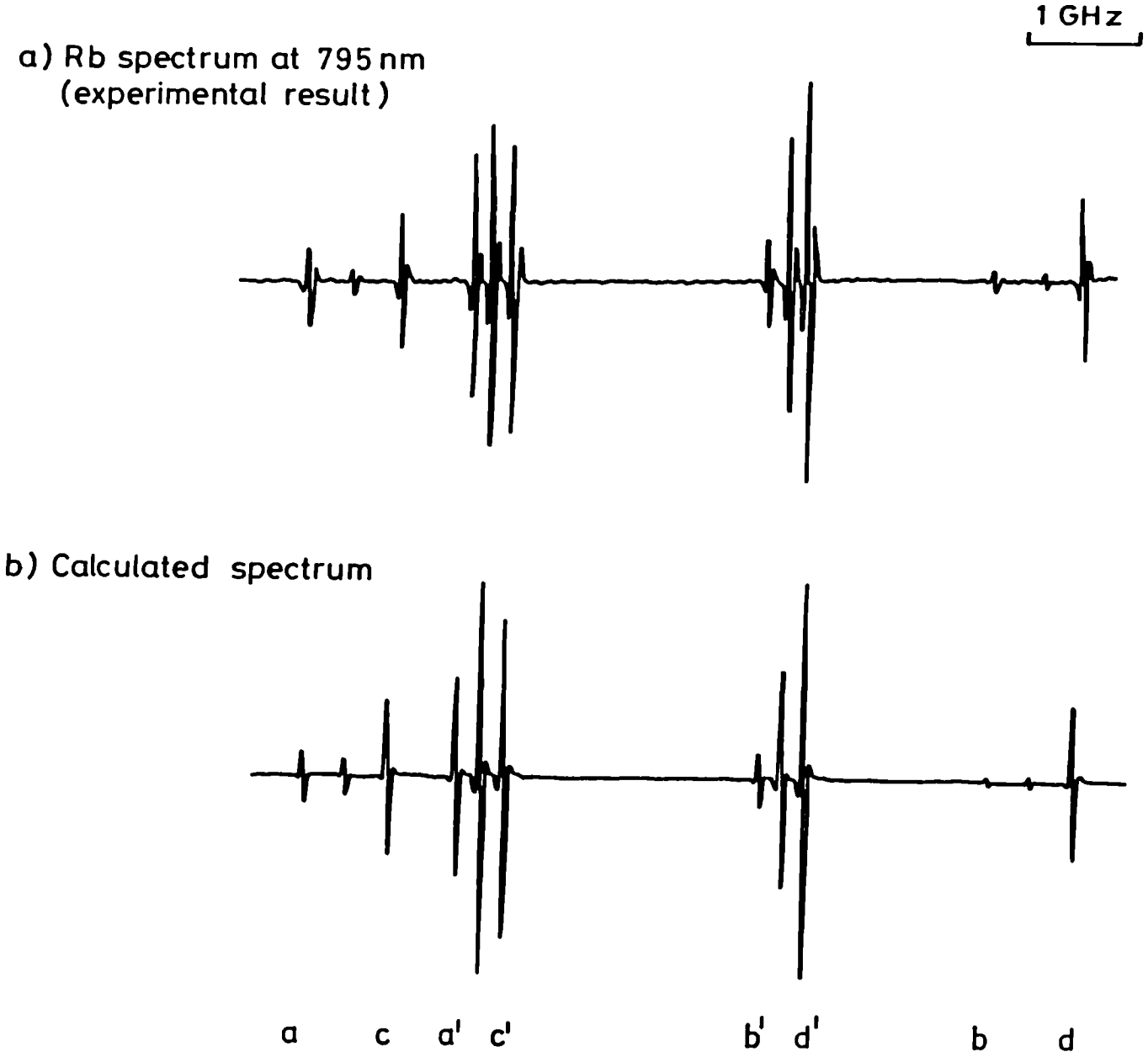

5.3.1 Comparison between experimental and theoretically calculated spectrum of the Rb D_1 line at 795 nm with a non-narrowed diode laser.

CHAPTER 6

APPLICATIONS IN LENGTH METROLOGY

6.1 Introduction; Measurement of distance and displacement

Interferometry is a commonly used technique for the measurement of length, but the particular form of the technique needs to be carefully chosen to match the application. We may need to measure tens of metres to an accuracy of 1 part per million (ppm), or only ≈1 μm to an accuracy of 1%. In the former case, we need a laser with the necessary spectral and spatial coherence for use over tens of metres. This precludes the use of a laser diode which does not have sufficient spatial coherence (figure 1.3.2), even if the spectral coherence (figure 3.2.1) can be improved by optical feedback. The laser frequency also needs to be stabilised to a level of better than 1 part per million. These considerations make the HeNe laser an ideal choice for this application. In contrast, to measure distances ≈1 μm to 1%, frequency stabilisation to an atomic reference is probably unnecessary and a laser diode is a more compact and suitable source than the HeNe laser. For such distances, the principal problem will be to sub-divide the optical fringe to $\lambda/100$, as the distance involved is only of the order of one wavelength.

An important distinction to be made is between the measurement of distance and displacement. Michelson interferometers, when used with a single laser (figure 1.1.1) only measure displacement of the moving corner cube. This can, of course, be used to measure the length of a

scale or tape with suitable scale markings which can be viewed with a microscope if this is attached to the corner cube. The electronic fringe counter is zeroed at one line on a scale and read at the second line. However, this system cannot cope with distance measurement - ie situations where neither corner cube can be moved or accessed, and only the static interferometric fringe can be observed. Alternative methods must be devised, for example by using more than one laser wavelength [1,2,3]. One method, swept wavelength interferometry [4], is the subject of this chapter. This technique exploits the frequency tunability of diodes, which is one of a number of advantages that diodes have over HeNe lasers.

There have been a number of publications to date which exploit the property of diode tunability to explore new ideas for the measurement of distance [5,6,7,8,9], displacement [10,11] or both [12]. A common theme of published schemes is that of high resolution, for example from a few microns [8] to a few nanometres [3,11]. Sometimes, the interferometers are designed to operate over only a few microns [11], although more commonly the maximum operating range is around 1 m. It is important to note that, in general, high resolution rather than high accuracy is claimed. The problem is that although modulating the current frequency modulates the laser, the conversion between the two is difficult to determine reproducibly to high accuracy. In one article [4], this problem is overcome by using an etalon of known length, so that a frequency sweep allows a length ratio (known etalon: unknown interferometer) to be determined. In [9], a frequency change of a diode is also used to determine distance, although here the change comprises a discontinuous mode hop. In contrast, the results of the Rb frequency intervals (chapter 5) allow us to provide a known and controllable frequency sweep. The hyperfine components extend over a range of ≈7 GHz

at 780 nm and 7.6 GHz at 795 nm. In addition, the absolute frequencies of each component are known to a relative accuracy of $\pm 1 \times 10^{-9}$. This provides a unique opportunity to devise methods which have both high resolution and accuracy. The values for the absolute frequencies of the hyperfine components allow the diode laser of chapter 5 to be used in displacement measuring interferometers. The same source can also be swept to provide a dual displacement or distance measuring system.

To discuss the principle of swept wavelength interferometry [4], we consider a Michelson system (figure 1.1.1) where neither cube corner can be scanned. In this case, the path difference is fixed at L and the laser can be scanned between ν_2 and ν_1. Following equation 1.1.4, we write $\nu_1 = N_1 c/2Ln$ and $\nu_2 = N_2 c/2Ln$. Neither N_1 nor N_2 need be known, but only $N_2 - N_1$. Writing the frequency sweep as $\Delta\nu = \nu_2 - \nu_1$, we have

$$L = (N_2 - N_1)c/2n\Delta\nu \qquad (6.1.1)$$

since the refractive index (n) is virtually identical at both frequencies for scan ranges of only a few GHz. Equation 6.1.1 involves only parameters which we can measure or know. The number $(N_2 - N_1)$ need not necessarily be integral, but is the number of observed fringes as we sweep the laser frequency. Alternatively, we could choose to make $(N_2 - N_1)$ integral and measure $\Delta\nu$ as a change in beat frequency between the swept laser and a stable reference laser. This latter method is the one chosen for the demonstration system (section 6.2.2) because this obviates the need to measure fringe fractions to high accuracy.

Swept-wavelength interferometry is somewhat difficult to implement accurately over short distances. In practice, the longest frequency sweep possible with the system described here is <10 GHz. This is

limited by the frequency spread of the Rb hyperfine components and the maximum beat frequency (≈3 GHz) which may be counted with the system shown in figure 5.2.1. Even if a wider sweep could be used, there would be a limit to the sweep possible before a mode hop occured (figure 1.3.3). To understand how a small frequency sweep limits the accuracy over short distances, we introduce the "synthetic wavelength", λ_s. Working with vacuum wavelengths, we can re-write equation 6.1.1 as $L = \frac{1}{2}(N_2 - N_1)\lambda_s/n$, where $\lambda_s = c/\Delta\nu = \lambda_1\lambda_2/(\lambda_1 - \lambda_2)$. As L is decreased, a point is reached where $N_2 - N_1 = 1$ and if $\Delta\nu$ = 10 GHz, then $\lambda_s \approx 3$ cm. For such short distances, the accuracy is soley that achievable by fringe subdivision or an equivalent process.

Two optically narrowed diode lasers, as illustrated in figure 3.6.1, are available. One is locked to Rb or a fixed mode of the cavity to provide a long-term frequency stabilised reference. The second diode laser, also optically narrowed, is swept between convenient modes of the cavity, so that there is no need to measure fringe fractions. The change in beat as the second laser is unlocked, scanned and re-locked can then be measured. We might think that the larger laser frequency scan available, if the laser locked to Rb were also scanned, would improve the accuracy of the measurement. However, this is not the case, and this is because of the laser reproducibility. In un-locking and re-locking the Rb system, the scan accuracy is likely to be comparable with the reproducibility of the laser of 44 kHz, rather than just the stability. Regardless of the reproducibility of this scan, the Rb hyperfine intervals have not been measured here to better than the laser reproducibility. The greater scan range available does not compensate for the loss in accuracy owing to the Rb laser reproducibility. A simpler and more accurate system therefore results if the Rb reference laser is not unlocked during the measurement. The software necessary for

this measurement is described in the following section.

6.2 Swept Wavelength Interferometry - A Tool for determining distance

6.2.1 Computer-controlled frequency sweep and lock monitor

As with the frequency stabilisation of diodes, there is the possibility of experimental arrangements with varying degrees of complexity depending on the accuracy required. However, we are required here to provide either fixed or swept wavelength standards. To achieve this, we need to use optically narrowed diodes referenced to Rb saturated features. A brief discussion of lower accuracy systems which might be developed is given in section 7.2.

The hardware used to provide a precision computer controlled frequency sweep comprises a BBC microcomputer with IEEE interface, frequency counter, and a CED model 1401 intelligent interface. Although this latter device can perform a wide variety of tasks, it is primarily used here as a general purpose analogue input/output device. The digital output feature is also used. The overall schematic is shown in figure 6.2.1.1. The analogue input feature is used to read integrator voltages (proportional to the diode frequency tuning), the PSD outputs and the signals from the optical feedback cavity detectors. The analogue outputs are used to tune the optical feedback cavities and hence the laser frequency and also adjust the laser current to maintain optical lock. The digital output signals are used to unlock and re-lock the NPL-designed PSD/integrator lock boxes [13]. A full list of the input and output control features possible is shown in table 6.2.1.1. This table also contains a list of BBC Basic commands needed to perform the listed functions.

Table 6.2.1.1

List of commands and functions controllable by the BBC microcomputer for the optically locked wavelength swept diodes. The CED 1401 interface is IEEE device 8.

Function	Basic command
PSD/integrator system for locking to Rb	
Read integrator output voltage	PRINT#8,"ADC,4":INPUT#8,A$(*1)
Set integrator volts	PRINT#8,"DAC,2,"+B$(*2)
Unlock/re-lock (to unlock, (*3))	PRINT#8,"DIG,0,1,15"
Read PSD output	PRINT#8,"ADC,5":INPUT#8,A$
Set laser current	PRINT#8,"DAC,0,"+B$
Brewster lock for above	
Read integrator output voltage	PRINT#8,"ADC,2":INPUT#8,A$
Set integrator volts	PRINT#8,"DIG,0,1,10"(*4)
Unlock/re-lock	PRINT#8,"DIG,0,1,14"
Read PSD input (*5)	PRINT#8,"ADC,3":INPUT#8,A$
Swept laser	
Read integrator output voltage	PRINT#8,"ADC,1":INPUT#8,A$
Set integrator volts	PRINT#8,"DAC,3,"+B$
Unlock/re-lock	PRINT#8,"DIG,0,1,13"
Read PSD output	PRINT#8,"ADC,6":INPUT#8,A$
Set laser current	PRINT#8,"DAC,1,"+B$

Swept laser Brewster lock

Read integrator output voltage	PRINT#8,"ADC,0":INPUT#8,A$
Set integrator volts	PRINT#8,"DIG,0,1,9"
Unlock/re-lock	PRINT#8,"DIG,0,1,12"
Read PSD input	PRINT#8,"ADC,7":INPUT#8,A$

Notes

(*1) The voltage is read into A$. The CED 1401 can read up to ±5 V, and similar statements above also use A$.

(*2) The voltage is set by the value of B$, which is a value between ±32767 corresponding to ±5 V output

(*3) The comparable re-lock statement is PRINT#8,"DIG,0,0,15". Similar statements for unlocking have a comparable re-lock command.

(*4) Since the CED 1401 did not have sufficient analogue outputs, and the Brewster integrator lock did not need fine tuning, the digital output was used. This could scan between two integrator voltages, and a capacitor was used to reduce the scan rate to a few seconds as the CED 1401 output undergoes a step voltage change.

(*5) Note that this is also the output from the detector situated behind the optical locking cavity (detector D_1 in figure 3.6.1).

For most of the commands in table 6.2.1.1, the electrical connections are straightforward. An example of this is the reading of an integrator or PSD voltage. For the commands to set the laser current, the voltage is added to that provided by the integrator in the "feed-forward" arrangement shown in figure 3.6.1. More elaborate modifications are necessary to unlock or re-lock the various integrator lock boxes [13]. Having described the input and output facilities of the micro-computer, the remaining part of this sub-section describes how it is programmed to

operate.

Firstly, the part of the program is described which checks the optical lock of the diode lasers to the resonant feedback cavity. The program also needs to re-acquire both the optical lock and the Rb or lock to a ULE cavity mode, as appropriate. A flow diagram for this program is shown in figure 6.2.1.2. It was found that there were two indications of optical lock failure. The more obvious of the two was that there was no transmitted signal through the optical cavity. The program firstly checks the initial transmitted signal in both cavities and flags an error if either falls below (say) 80% of this initial transmitted signal. However, just before the lock is lost completely, it was also observed that there was a situation where the lock was lost very briefly but then recovered. The transmitted signal through the cavity began to suffer "drop-outs" before the signal was completely lost. These were too fast for the CED 1401 to observe, but they did cause the counter monitoring the beat frequency to miscount. The frequency read by the counter suddenly changes by tens of kHz or more as the optical lock begins to fail. This fact was used by the computer program to indicate that the optical lock was lost or about to be lost. Therefore the program checked the signal transmitted through the two cavities, read the beat frequency via the Racal counter and also read the ULE cavity lock and Rb locked laser integrator voltages. If the optical lock was lost or about to be lost, then the computer firstly has to ascertain which laser has lost lock. If the signal transmitted through the cavity is permanently lost, then this is a trivial matter. If not, then the computer has to adjust each laser current slightly to see which laser is almost at the end of its optical lock range. Once this is established, a small step change can be made to the laser current to bring it back nearer the middle of the lock range. The computer unlocks the

appropriate Brewster plate lock, scans the Brewster plate for a short range, and re-locks this if the optical lock is re-acquired. The computer then waits to see that the optical lock looks stable. The Rb locked laser (or ULE cavity locked laser, as appropriate) is unlocked and the integrator voltage adjusted to that measured just before the lock was lost. After the optical lock is re-acquired, the Rb or ULE cavity locked laser is scanned to find the feature and re-locked. The computer finally checks that the beat frequency is the "correct value", namely the frequency just before the optical lock was lost.

Secondly, the program described above needs to be modified to produce, on demand, a frequency scan between a known number of ULE cavity modes. In this section, therefore, a program to scan a pre-determined integral number of modes of a demonstration interferometer cavity is described. A flow diagram showing the operation of this program is given in figure 6.2.1.3. This mode of operation raises an immediate problem, namely that the beat frequency will be different at the end of the scan, and so the tunable rf filter will not be set for the correct frequency. Remotely controllable rf filters are available, but an alternative method is to employ an IEEE controllable high frequency oscillator. This may then be used to up- or down-shift the beat frequency by mixing the frequencies in a double balanced mixer (DBM) to produce the frequency for which the rf filter is set. In addition to requesting a measurement through the BBC computer, it is necessary to request the number of modes that the offset laser should be swept through. The computer is told the approximate interferometer free spectral range. Using the conversion between integrator output voltage change and frequency sweep, the computer sweeps the laser by approximately the correct frequency. It also calculates the oscillator frequency necessary to mix with the beat frequency to make it the same magnitude (but opposite sign) as before

the scan. If it cannot do this, because the oscillator frequency necessary is more than the maximum 1 GHz, the program requests the operator to change the scan range. The program then changes the oscillator frequency and searches for an inteferometer fringe near the expected frequency. As with the routine described in the previous paragraph, the computer checks the optical lock after each frequency scan, and before a beat measurement is made. If this is lost, then the computer attempts to re-acquire the lock. Once the laser is re-locked after the scan, the beat frequency is measured. The laser is then scanned back to the original interferometer fringe and the beat is measured for a third time. These three measurements of the beat are used to remove the effects of linear drift of the interferometer being measured. To see how this is achieved, suppose the three beat measurements are taken at times t_1, t_2 and t_3 and the results are B_1, B_2 and B_3. Beat frequencies B_1 and B_3 are for the same cavity mode and taken before and after the scan. If the cavity length is drifting linearly with time, we may write this beat (B) at time t as

$$B = B_1 + (B_3 - B_1)(t - t_1)/(t_3 - t_1) \qquad (6.2.1.1)$$

At the time t_2 that the beat B_2 is measured, we can infer the beat which would have resulted with the laser locked to the original cavity mode. Hence we can remove the effect of linear drift by calculating the cavity FSR for a sweep of N modes as

$$FSR = \{B_2 + B_1 + (B_3 - B_1)(t_2 - t_1)/(t_3 - t_1)\}/N \qquad (6.2.1.2)$$

This equation assumes that we record all the beats as positive numbers, although the beat will pass through zero as the sweep is made.

The potential accuracy of the method described in this section is discussed in the next sub-section. This is then followed by a discussion of an application to two demonstration interferometers.

6.2.2 Estimated accuracy of spectrometer for distance determination

This section describes the accuracy to be expected in various experimental arrangements using swept wavelength interferometry. This accuracy will depend on the frequency sweep range and reproducibility, knowledge of the range of the frequency sweep and the stability of the interferometer system being measured.

In the demonstration system described in this chapter, the frequency sweep is fairly small, typically around 4 GHz. The first task is to estimate the accuracy of the frequency sweep. Figure 4.5.5 shows the stability of the beat between two Rb-stabilised diode lasers at 795 nm. Similar stability results are presumably possible at 780 nm on the stronger well-resolved lines. For a measurement lasting typically of the order of 100 s, the beat stability will be ≈2 kHz from figure 4.5.5. For one laser, it may be satisfactory to divide this by a factor of $\sqrt{2}$, giving ≈1.5 kHz at τ = 100 s. The actual value of this factor will depend upon the frequency noise characteristics. This factor is particularly difficult to estimate for this system since, in figure 4.5.4 for 10 s > τ > 100 s, σ varies roughly as $\tau^{1/4}$. No simple noise source can give rise to this (see table 4.2.1). On this basis alone, therefore, for a 4 GHz scan, the estimated 1σ accuracy is ≈1.5 kHz in 4 GHz or ≈4 parts in 10^7. To this error, we should add any errors resulting from miscounting of the beat or the accuracy of the Racal counter crystal oscillator and 1 GHz oscillator. The accuracy of crystal oscillators was briefly discussed near the beginning of section 5.2, where it was concluded that

a typical error was ±1 part in 10^6. In terms of the accuracy we expect therefore, we are limited to a similar degree by both laser and crystal oscillator stability. Scans of much greater than 4 GHz would achieve a proportionally better accuracy, but we should then need to use a better frequency counter to measure the scan sweep. We would otherwise only obtain better *resolution*, rather than *accuracy* with a wider range sweep system. The combined errors yield an estimated 1σ error of ≈0.7 ppm.

We now need to specify the requirements of the interferometer necessary to demonstrate the limit to measurement reproducibility and accuracy derived in the previous paragraph. A scan of 4 GHz is, in fact, rather a small scan range for this application, as we shall see. As previously discussed in section 6.1, heavy emphasis needs to be placed on fringe fractioning when using small scan ranges to achieve a 1 ppm accuracy. The two slight variations in measurement method used here involve the reference laser locked either to Rb or to a fixed cavity mode. The disadvantage of using Rb as a reference frequency is that the etalon to be measured must be highly stable. To estimate the cavity stability required, consider an etalon of length ≈1 m with a free spectral range of 150 MHz. This will produce only 27 fringes as the laser is scanned, and so we need to subdivide to 2.7×10^{-5} of a fringe (one fringe ≈ 400 nm) to achieve 1 ppm accuracy. Regardless of whether we can develop the electronics to achieve this, this puts a very stringent requirement on the stability of the device to be measured. It needs to be stable to ≈10 pm over a period of a minute or two (the time taken for the measurement). For a cavity length ≈1 m and a scan range of 4 GHz, we therefore require a cavity stable to $\approx 10^{-11}$ of its length, in order to demonstrate a measurement to $\approx 10^{-6}$. Finally, for the electronic servocontrol to provide a stability comparable with the Rb stabilised lasers, the interferometer linewidth should be similar or better than

the Rb linewidth measured as 12 MHz for our cells (section 3.7). In the following section, a suitable Fabry-Perot cavity is described which fulfils these requirements and we can then compare the reproducibility of the results estimated here with those obtained.

The high stability required of the interferometer is, in part, due to the low frequency scan available. However, it is possible to reduce the stability requirement by locking the reference laser to a convenient mode of the etalon to be measured, rather than to Rb. If this is done, and the etalon drifts in length, then the measured length will only drift in the same proportion as the length change. This second method was therefore performed on a silica etalon (≈ 150 MHz FSR) which had a slightly higher drift rate than the ULE cavity, but whose length could be independently measured. The beams from the lasers were combined and both fed down a multi-mode optical fibre to another laboratory. The two lasers were frequency modulated at two different frequencies and detected by a single detector. The signals were then fed into two separate PSD/lock-in systems to lock both lasers to two different cavity modes, using first derivative locks. The disadvantage of this technique is that the noise from one laser is transferred to the second laser lock, degrading frequency stability. It was observed that the noise level (predominantly 1/f noise) was higher than for the ULE cavity or Rb lock as measured from the beat frequency between the two lasers. This extended out to long times ($\tau > 100$ s) making measurements less reproducible.

6.2.3 Application to a demonstration Interferometer system

At the end of the previous section, cavity stability requirements of the etalon were derived for a swept wavelength measurement. Fortunately,

optical cavities with this stability have already been developed at NPL and elsewhere for use in laser frequency stabilisation and measurement. The lengths of two etalons were measured using the techniques described in the previous section. The first measurement to be described is on a stable cavity of 750 MHz FSR, and the reference laser is locked to Rb. The cavity is non-scannable because any tuning element, such as a piezoelectrically mounted mirror, would have a large drift rate by comparison with the rest of the cavity. The cavity is made from an ultra-low-expansion (ULE) material. The material is made into the shape of a hollow tube, with the cavity mirrors wrung onto the polished end faces. The cavity nominal free spectral range is 750 MHz. The cavity is mounted in an evacuated chamber, and kept pumped down at a pressure of $\approx 10^{-8}$ torr using an ion pump. The cavity is optically isolated from the diode laser using a Faraday isolator, to prevent optical locking to the ULE cavity.

We need to show that the ULE cavity described here is, indeed, sufficiently stable and has the necessary linewidth. Firstly, the finesse was measured as ≈100, giving a 7.5 MHz FWHM, therefore satisfying the requirement on linewidth. Since two optically narrowed diodes are available, the simplest and most accurate way of measuring cavity stability is to lock one laser to Rb and the other to a suitable cavity fringe. The cavity fringe chosen should produce a convenient beat frequency between the two diodes. If the cavity were truly confocal, then all off-axis modes should be degenerate. This should mean that different re-alignments of the diode beam into the cavity should produce the same optical beat, when the laser is locked. However, it was observed that different re-alignments produced changes in the beat of up to ±20 MHz. A much more stable day-to-day value of the beat was observed if the diode laser beam was not re-aligned, although there was still

observed steady drift. The length of the ULE cavity was observed in this way over a period of 3 months and the results are shown in figure 6.2.3.1. Both the steady drift of ≈18 MHz/month and the scatter due to re-alignment are shown in this figure. Since the free spectral range of 750 MHz corresponds to a $\lambda/4$ (≈200 nm) change in length, 18 MHz corresponds to ≈5 nm. This actually demonstrates the extreme sensitivity of this method in detecting small changes in length. For these measurements, the laser locked to the ULE cavity was lower in frequency than the Rb reference laser and so the cavity must be slowly expanding. However, 18 MHz/month corresponds to only ≈0.4 kHz/min or a relative length change of 1×10^{-12}/min. This cavity therefore fulfils the requirements listed in the previous section for stability.

A number of computer-controlled scans were made and the free spectral range measured. A total of 48 measurements were taken over a frequency sweep corresponding to 5 ULE cavity modes. The spread of the 48 results had a standard deviation of 4.6 kHz. The standard error of the mean was therefore 0.7 kHz or 1×10^{-6} of the free spectral range. In terms of the overall cavity length, an error of 1×10^{-6} corresponds to a standard error of the mean of 0.5 of a fringe. As expected, it was confirmed that the spread of results using a shorter scan of two ULE cavity modes was approximately double that of the five mode scan. The mean of all the measurements taken gave a free spectral range of 749.569 5 MHz. This corresponds to a length of 99988.2 μm, using equation 6.1.1. Note that the factor 2 in the denominator must be replaced by a 4 for a confocal system. Furthermore, the frequency of the laser locked to the cavity mode monitored in figure 6.2.3.1 corresponded to an order number of 512 597.3. However, it is important to note that this calculation neglects the effect of the phase change on reflection at the dielectrically coated mirror. This correction is likely to be

significant in view of the nature of dielectric coatings.

In the measurement on the second etalon (≈150 MHz FSR), laser light from both diodes was fed to the etalon via a multi-mode fibre, as described at the end of the previous section. A measured reproducibility on 42 results over a scan of 34 modes was 0.94 kHz or 6×10^{-6} (one standard error of the mean). Although the linewidths of the cavities were comparable, these results are clearly not so reproducible as with the first etalon. This is, in part, due to the worse stability on the etalon lock as discussed at the end of the previous section. Using swept wavelength interferometry, the FSR of the cavity is measured as 146.709 8 MHz corresponding to a length of 1.021 719 m. This compares very satisfactorily with the length determined from a long history of wavelength measurements (eg those described on Rb in chapter 5) of 1.021 714 m. This difference corresponds to a relative error of only 5 parts in 10^6.

The results in this section are very encouraging in that a reproducibility in the answer of a few ppm (one standard deviation) can be achieved. Furthermore, there is agreement to this same level between the results of this method and that of multi-wavelength interferometry for the length of an etalon. However, the sweep is clearly not large enough for us to obtain a measurement accuracy to significantly better than a fringe. Were this the case, we would be able to use the results from the swept-wavelength technique to determine the order number unambiguously of the Rb-stabilised diode. We would then have been able to put an absolute length scale on figure 6.2.3.1, for example. An important result of this chapter is that it enables us to make an estimate of the necessary sweep range to make an order number determination for the etalons measured here. Future developments in this

area are discussed further towards the end of section 7.2.

6.3 Discussion of other length/distance measuring techniques

With the advent of the 633-nm He-Ne laser in 1963, interferometry rapidly grew as a method of displacement measurement. This is because the 633 nm HeNe laser could be stabilised by easy-to-use methods [14,15] as well as the more reproducible method stabilising to iodine [16]. These latter lasers are readily used with beat frequency techniques to calibrate the less stable but easy-to-use lasers. These measurements provide direct traceability to the definition of the metre via the internationally agreed value for the frequency of the iodine stabilised He-Ne laser. A number of commercial displacement measuring interferometers are available using frequency stabilised HeNe lasers comparable with those described in [14,15]. They have a wide range of applications, since, with fringe subdivision, displacements from a few nanometres to tens of metres may be measured.

Several distance measurement techniques are available and an early review article is [2]. The first of these methods used, for example, for the measurement of gauge blocks, is the method of exact fractions. In this method, two or more stabilised laser sources are required, but the interferometer is non-scannable. Therefore, only the fraction by which the interferometer length exceeds an integral number of half-wavelengths may be measured. The number of wavelengths required depends on how accurately this fraction may be measured and how well the length is known in the first place. For example, if two wavelengths (λ_1, λ_2) are available, and $\lambda_2 = 11\lambda_1/10$, then the length can be determined unambiguously if it already known to 10λ and the fraction can be determined to better than $\pm 0.1\lambda$. The wavelengths of available lasers can

also be a limitation, and at present these are [15,17] He-Ne lines at 543 nm, 594 nm, 612 nm and 633 nm.

A second class of distance measurement (EDM or electromagnetic distance measurement) uses some form of modulated laser beam. An example of this is the NPL-designed mekometer, where the polarisation of the output beam is modulated [2,18]. The light is passed through a Pockels cell with a ≈500 MHz drive frequency. The emitted light, which is then circularly polarised, is returned from a reflector through the same Pockels cell. If the distance measured is an integral number of half-wavelengths of the modulation frequency (30 cm), then the returned light is linearly polarised after being double passed through the Pockels cell. A suitably orientated polariser will then transmit no light on this condition. Varying the modulation frequency to achieve the extinction condition and using different frequencies can then be used to determine the absolute distance. Systems have also been developed using either intensity or frequency modulation of the carrier, rather than polarisation modulation [2].

Finally, for very long distances, time of flight of pulsed laser light may be used, as implied in the definition of the metre. This technique is particularly appropriate for lunar or satellite ranging. A typical accuracy is a few cms in the total distance of $\approx 8 \times 10^6$ m (a relative accuracy of a few parts in 10^9). This is limited by variations in the optical thickness in the earth's atmosphere (see, for example, [19]).

This chapter has, therefore, explained the development of diode laser swept wavelength interferometry, using some of the techniques developed in chapters 1 to 5. Swept wavelength interferometry has proved to be a promising alternative to the methods given in this section for the

determination of distance. The method shows considerable potential and possible future developments are discussed in the final chapter of this thesis.

References

[1] C Polhemus, Appl Opt 12, No 9, 2071-8 (1973)

[2] KM Baird, Metrologia 4, No 3, 135-44 (1968)

[3] P De Groot, S Kishner, Appl Opt 30, No 28, 4026-33 (1991)

[4] R Ohba, I Uehira, S Kakuma, Meas Sci Tech, 1, 500-4 (1990)

[5] H Kikuta, K Iwata, R Nagata, Appl Opt, 25, No 17, 2976-80 (1986)

[6] G Beheim, K Fritsch, Appl Opt, 25, No 9, 1439-42 (1986)

[7] CC Williams, HK Wickramasinghe, Opt Lett, 14, No 11, 542-4, (1989)

[8] CC Williams, HK Wickramasinghe, J Appl Phys, 60, No 6, 1900-3 (1986)

[9] K Seta, BK Ward, Opt Comm, 77, No 4, 275-8 (1990)

[10] G Beheim, K Fritsch, Electron Lett, 21, No 3, 93-4 (1985)

[11] M Imai, K Kawakita, Opt Comm, 78, No 2, 113-7 (1990)

[12] T Kubota, M Nara, T Yoshino, Opt Lett, 12, No 5, 310-2 (1987)

[13] KC Shotton, WRC Rowley, NPL Report Qu28 (revised 1978)

[14] SJ Bennett, RE Ward, DC Wilson, Appl Opt, 12, No 7, 1406 (1973)

[15] WRC Rowley, Meas Sci Technol 1, 348-51 (1990)

[16] AJ Wallard, J Phys E 5, 926-30 (1972)

[17] WRC Rowley, P Gill, Appl Phys B51, No 6, 421-6 (1990)

[18] KD Froome, RH Bradsell, J Sci Instrum 43, No 3, 129-33 (1966)

[19] Yu L Kokurin, VV Kurbasov, VF Lobanov, AN Sukhanovskii, Sov J Qu El 13, No 6, 766-71 (1983)

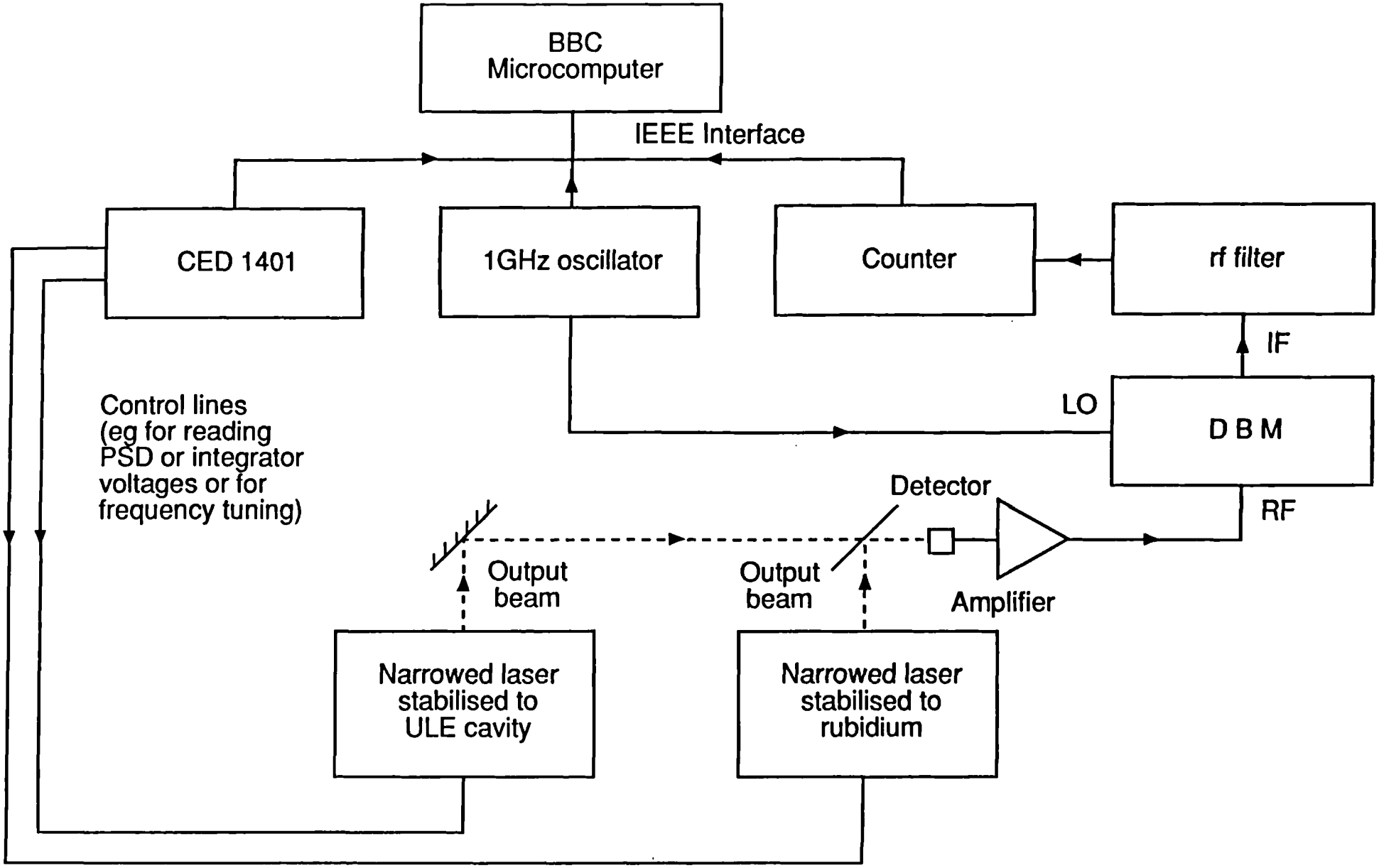

6.2.1.1 Overall schematic of the hardware used to produce a known and controllable frequency sweep.

A00197-1

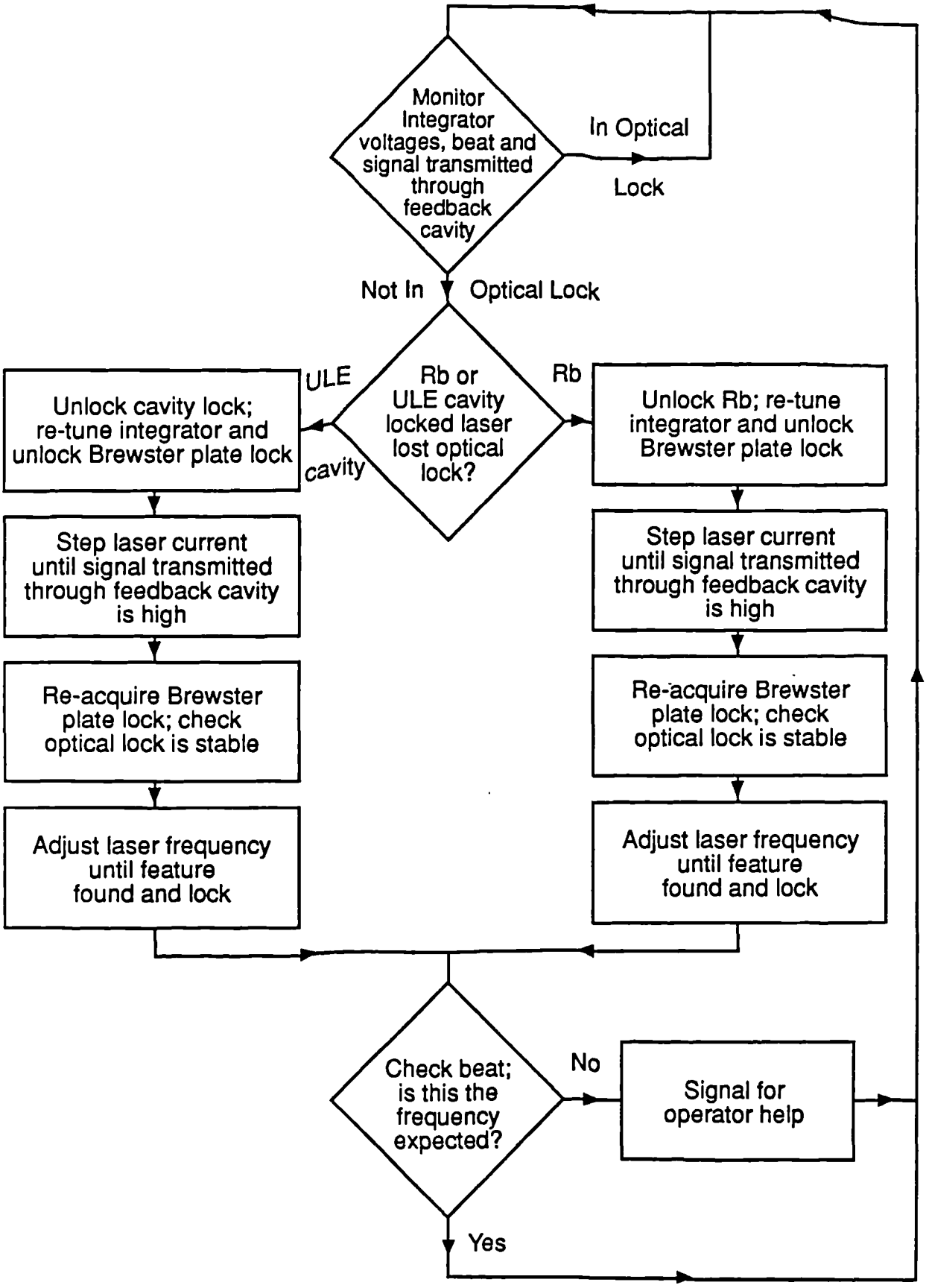

6.2.1.2 Flow diagram for the BBC Basic program used to check the optical lock of the two narrowed laser diodes and re-acquire it if it is lost.

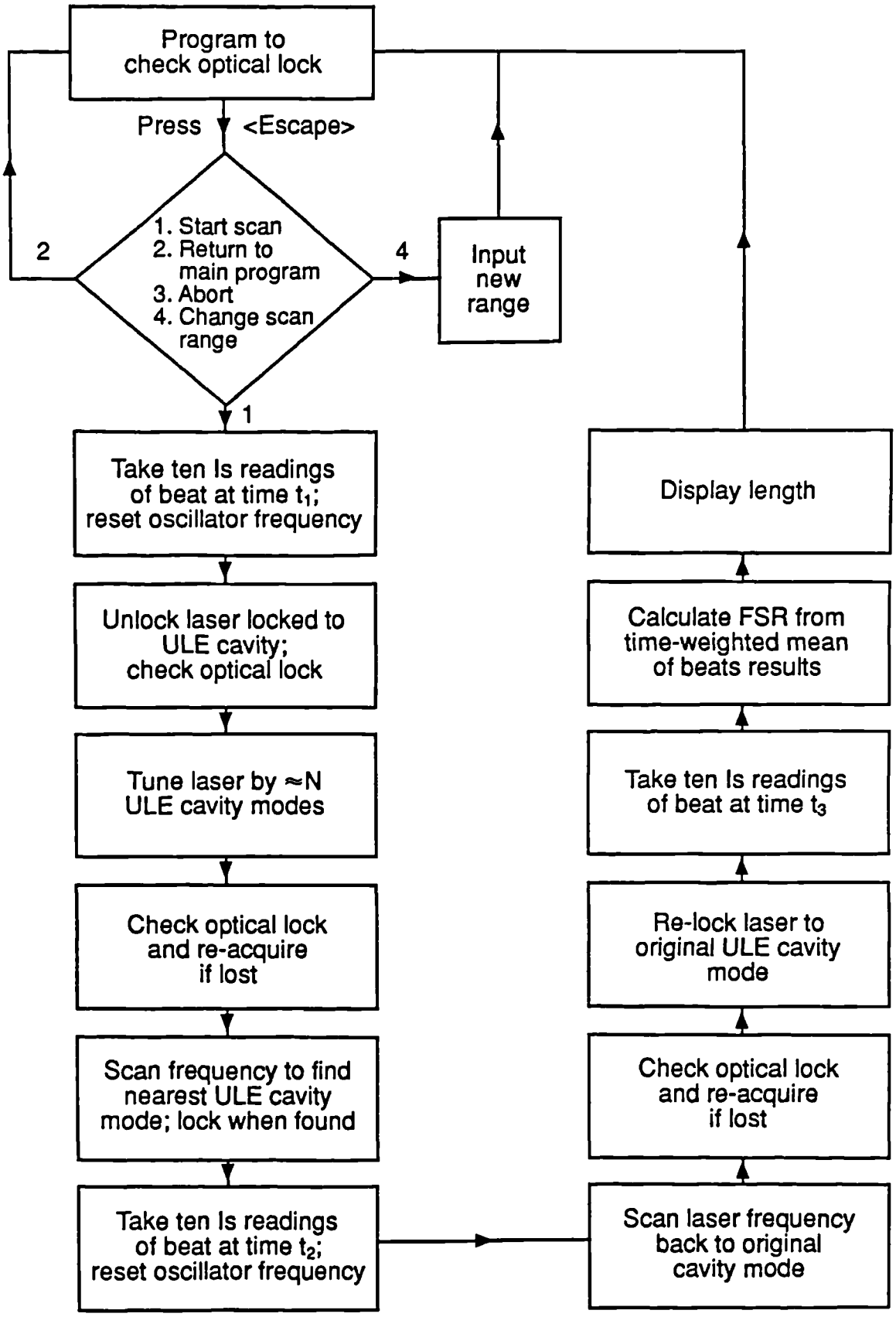

6.2.1.3 Flow diagram of the BBC Basic program to sweep the offset laser a pre-determined number of modes of a demonstration interferometer.

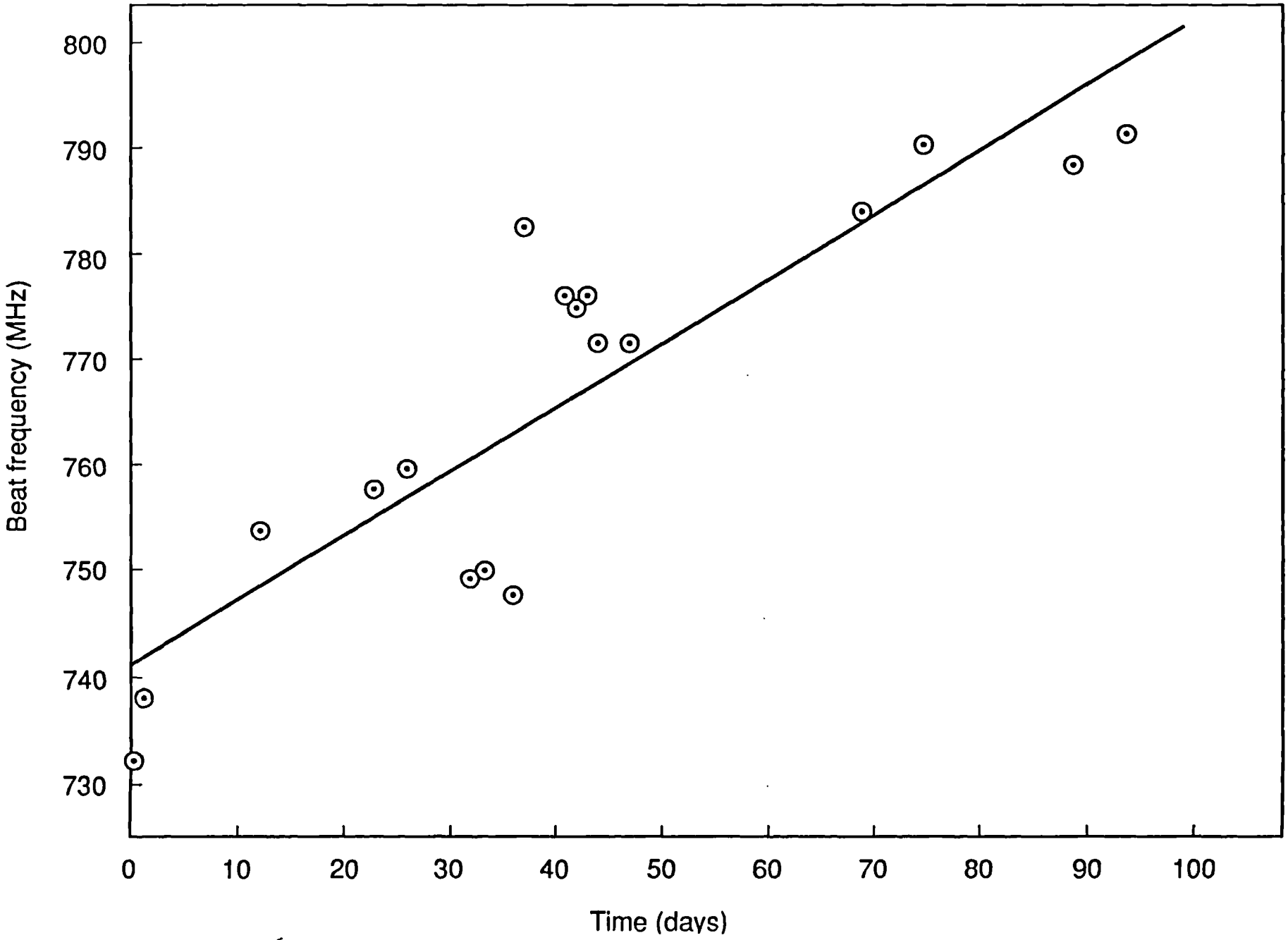

A00197-2

6.2.3.1 Frequency drift of a laser locked to an evacuated ULE cavity with respect to a Rb stabilised laser.

CHAPTER 7

SUMMARY

7.1 Summary of main achievements of thesis

This thesis has described experimental investigations necessary to transform the inexpensive diodes marketed for use in compact disc (CD) players into a tool for high-resolution spectroscopy and length metrology. Chapter 1 deals predominately with the various operational problems of laser diodes and also describes their advantages. Problems such as beam divergence or beam quality need to be overcome for any work involving diodes in spectroscopy or interferometry. Results obtained by the author and presented in chapter 1 are comparable with those published elsewhere. The results have enabled us to exploit the advantages of laser diodes in this thesis, namely their long-range tunability, ease of operation and very low electrical power consumption.

Having produced a usable diode system, chapter 2 describes results using a diode in various spectroscopic applications, chiefly with Rb. These results in chapter 2 all use a diode with no linewidth reduction. These were the first published [1] saturated absorption spectra at 780 nm and 795 nm on a flat background, suitable for frequency servocontrol, although there was work published on Rb prior to this. The optical frequency measurements in [1] and chapter 5 represent the most accurate results to date on linear absorption profiles. The third derivative Doppler free signals were also used, for the first time, for frequency stabilisation purposes [2], as described in section 2.5.

In chapter 3, optical narrowing using resonant optical feedback was demonstrated. The results for the narrowed linewidth [3] are among the best reported. This was also the first time that an optically narrowed laser was used in high resolution Rb spectroscopy. This enabled a laser diode to be used to resolve all the hyperfine components and level crossing signals of the 780 nm D_2 line, for the first time. Chapter 4 contains results on frequency stabilisation in a number of situations, most of which have been published [1-3]. This chapter also contains, in section 4.4, results on the effect of high frequency modulation (FM) of laser diodes and its use in spectroscopy. These results are the first published [4] of the use of an optically narrowed FM diode laser to obtain Rb spectra.

In chapter 5, the most accurate and complete determination to date of the Rb hyperfine constants and ^{87}Rb:^{85}Rb isotope shift is presented [5]. In addition, the absolute optical frequencies of components of the two Rb D lines are presented with an accuracy limited only by a knowledge of the reference I_2-stabilised HeNe laser frequency. Together with information on the laser frequency reproducibility of Rb-stabilised diodes, chapter 5 gives important information enabling diodes to provide either a fixed or swept frequency reference. In chapter 6, an important metrological application of a frequency-stabilised diode is demonstrated, namely swept wavelength interferometry [6]. The result for the cavity length determinations demonstrate the most reproducible length measurements to date using this method. It has considerable potential as an alternative means to measure distance and chapter 6 helps set the scan ranges necessary to determine the interferometer order numbers unambiguously. Ways of extending and improving the method are briefly discussed in this chapter. Finally, in this concluding chapter, a wider view is taken of potential future developments, in

particular the possibility of diodes replacing dye lasers in the NPL program on ion trap frequency standards. The techniques developed in chapter 3 for linewidth reduction may be used on a variety of diodes at different wavelengths. As resonant optical feedback is such a successful method in reducing diode laser linewidths, this suggests that the narrow linewidths obtained may be used in ion trap spectroscopy. In ion traps, the narrow linewidths of forbidden transitions in ions may be observed and, potentially, used as an optical frequency standard, but they require an ultra-narrow frequency stable laser to interrogate them. The lasers developed in chapter 3 could be ideal for this application, if a suitable transition can be found at a wavelength accessible with a diode. However, the lasers necessary generally cost considerably more than the 780 nm 5 mW diodes used for most of this thesis. This extra cost may arise either because the wavelengths required are not as commercially popular as 780 nm, or a higher power than 5 mW is required. High powers allow the use of non-linear crystals to generate modest powers in the blue by an all solid-state system. Powers of several milliwatts have already been reported [7,8]. It may also be necessary to request that the diode is wavelength selected to, say, ±3 nm, further adding to the cost. Commercial suppliers are able to supply wavelength selected diodes, either GaAlAs devices (740 nm to 870 nm) or InGaAs quantum well lasers (930 nm to 990 nm) sold to pump erbium fibre amplifiers [9]. Cost, therefore, prohibits the buying of half a dozen diodes to overcome the problem that any one diode may mode-hop over the ion transition frequency, as was done for Rb in chapter 2. An alternative method is necessary to force laser oscillation at any frequency within the band gap tuning of the diode. As part of the aim to widen the spectroscopic potential of laser diodes, a technique must be developed to achieve longitudinal mode selection. The results to be presented in this chapter have been submitted for publication [10]. This

is the most detailed presentation of experimental results to date on this method of mode selection. This is discussed in the concluding section to this thesis, which also outlines resulting future possibilities of the development and use of laser diodes in frequency metrology.

7.2 Discussion of future possibilities

The achievements summarised in section 7.1 have produced, amongst other things, a diode laser narrowed in linewidth and usable in high-resolution spectroscopy. Chapter 3, in particular, has described a method for producing a laser with a linewidth of only ≈10 kHz. The passive frequency stability of this laser is limited only by that of the cavity used for the resonant optical feedback. This is a laser which has very strong potential in optical frequency metrology. The NPL already has a program investigating ion traps as potential optical frequency standards [11,12] using dye lasers. However, with a suitable choice of ion, in particular strontium [13], solid-state lasers could replace dye lasers for most, if not all, of the necessary wavelengths. This greatly simplifies the laser technology required. For the reasons outlined at the end of section 7.1 it is firstly necessary to demonstrate a method of longitudinal mode selection for laser diodes. Initial results of a suitable technique are discussed. This is followed by a brief discussion of various spectroscopic applications and further possible developments in swept wavelength interferometry.

The technique of mode selection needs to enable diodes to tune to any wavelength within the bandgap tuning, overcoming the problem of "forbidden frequencies" created by the "staircase tuning" of figures 1.3.3 and 1.3.4. Some workers, therefore, strongly favour the

use of external cavity diode lasers, where strong feedback is provided by a grating and which do not have such tuning problems. However, these devices have their own set of operational problems; for example the diodes firstly need to be AR coated. This process is reported to cause a significant number of diodes to fail, although this appears to depend upon the coating process [14]. A technique of longitudinal mode control which may be combined with the resonant optical feedback method of chapter 3 has therefore been investigated. Preliminary results with some diodes are described here. Further experience needs to be gained with this method, but it promises to be highly useful in atomic and molecular spectroscopy.

In order to overcome the problem of longitudinal mode control, some workers [15,16,17] have used a thin plate only ≈150 μm thick, and in some cases mounted only ≈50 μm from the front diode facet. Other workers have used a graded-index (GRIN) lens rod near the front facet, with the rod surface nearer the diode coated to give a 30% reflectivity [18]. All these optical elements are piezoelectrically (PZT) mounted, and the different modes are selected by varying the PZT voltage. These are similar to methods previously reported for forcing multi-mode InGaAsP (≈1.3 μm) [19,20,21] and GaAlAs [22] diodes into single mode operation. To achieve single mode operation in these diodes, feedback was provided either by a GRIN rod reflection-coated on the surface nearer the laser, or by use of a small mirror near the rear facet.

For this thesis a thin plate and GRIN rod (Melles Griot part 06LGS216, which has a numerical aperture of 0.6) have both been tried with three different diodes, and varying effects. Detailed results are presented of the mode controlling properties of the GRIN rod. The surface nearer the diode was re-polished to remove the AR coating. To consider the effect

of the GRIN rod or thin plate, we examine the properties of a three-mirror cavity (figure 7.2.1) [23]. The diode laser cavity is of length L and both facets have reflectivity (amplitude coefficient) R. The third surface has reflectivity r ($r \ll R$ and $r \ll 1$) distance l from the front main cavity mirror. Since r is small, we consider only terms first order in r, or equivalently terms only involving one reflection from this surface. The main cavity mirrors have transmission T and the weak reflector transmission t. For lossless surfaces, $T^2 = 1 - R^2$ and $t^2 = 1 - r^2$. Following the usual analysis for Fabry-Perot cavities, but taking into account the presence of the third surface yields a transmitted amplitude coefficient of the compound cavity as

$$A_T \propto \frac{T^2 t}{1 - R(R + T^2 r e^{2ikl}) e^{2ikL}} \qquad (7.2.1)$$

The term $(R + T^2 r e^{2ikl})$ in the denominator may be re-cast in the form $R' e^{i\phi}$. The effect of this is to show that the multiple mirror cavity behaves as a simple cavity, but with mirror reflectivities R' and R. One mirror also introduces a phase shift ϕ. To first order in r, we have

$$R'^2 = R^2 + (2RT^2 r)\cos(2kl) \qquad (7.2.2)$$

and

$$\phi = (T^2 r/R)\sin(2kl) \qquad (7.2.3)$$

Cavity resonances occur when

$$L = \tfrac{1}{2}\lambda\{N - \frac{T^2 r}{2\pi R}\sin(2kl)\} \qquad (7.2.4)$$

negelecting any constant phase change on relection at the diode facets. As the GRIN rod PZT voltage is varied, the order number of the main cavity may be varied by up to $T^2r/\pi R$, if mode hops do not occur. For a diode with uncoated facets, $R^2 = 0.32$ [24]. We also assume that $r^2 = 0.04$, based on the on-axis design refractive index for the GRIN rods used [25]. The effective value for r will probably be rather less, owing to the large angular divergence of diode laser beams. Additionally, equations 7.2.1 to 7.2.4 are only strictly valid for collimated light. Using these values of R and r gives $T^2r/\pi R = 0.077$ of a free spectral range (FSR). For a Mitsubishi diode ML-4102, with an FSR of 120 GHz, this is ≈9 GHz. This compares with the 2 GHz frequency pulling observed. The discrepancy is probably due either to the effective value of r^2 being lower than the expected value of 0.04 owing to beam divergence, or because the laser mode hops before the full 9 GHz pulling is observed. Equation 7.2.2 gives the frequency dependence of the output coupling as the PZT voltage ($\propto 1$) is varied. This can vary significantly by up to $R^2 \pm 2RT^2r$ or from 0.2 to 0.5, providing the mode selection. Different diode laser types do not show the same mode selecting properties. This is presumably because the facet reflectivities are not the same for different diodes since manufacturers often coat one facet to enhance the power, changing the mode selecting properties.

The modes allowed by the main cavity are given by $kL = N\pi$ or $L = \frac{1}{2}N\lambda$, neglecting the small phase change effect of equation 7.2.3. According to equation 7.2.2, we then need to adjust l by changing the PZT voltage, so that $2kl = 2\pi n$ or $l = \frac{1}{2}n\lambda$. The mode-selecting pattern is expected to repeat on every displacement of $\frac{1}{2}\lambda$ of the GRIN rod, consistent with that observed. The GRIN rod, in providing a periodic loss in the cavity, is behaving rather like an etalon of length l in a conventional laser

cavity length L. We might therefore expect that, for effective mode selection, we require l < L. The GRIN rod to diode separation is also required to be short because the GRIN rod is reflecting a rapidly diverging laser beam, and the feedback provided will decrease rapidly for increasing l.

Mode control was achieved using a thin plate or GRIN rod with diodes at 820 nm (Hitachi HLP 1400), 780 nm (Mitsubishi ML-4102) and 670 nm (Toshiba model TOLD 9211). The thin plate was 150 μm thick and uncoated, and the diode light was then collimated with a commercially available lens. The GRIN rod used was a 0.25 pitch lens, re-polished at the end nearer the diode to remove the anti-reflection coating. The re-polishing made the lens slightly shorter than the nominal 0.25 pitch and increased the level of optical feedback. This lens rod therefore collimated the diode light with the re-polished end approximately 50 μm from the diode facet. In order to use either a thin plate or GRIN rod with some diodes such as the ML 4102, the window must firstly be removed. Other diodes, like the Hitachi HLP-1400 are of an "open package" design with no window. In general, it was found that the GRIN rods provided better mode selection and were much easier to handle than the thin plate. Furthermore, the GRIN rods served the dual purpose of both mode selection and collimation. Whereas the thin plate could force the HLP 1400 diode to lase on one of around 8 modes, the GRIN rod could force laser operation in one of up to 13 modes. It was observed that different lasers of the same type behaved similarly, although it appears that different laser model types will require individual characterisation.

The simplest behaviour observed is with a GRIN rod and a 5 mW diode, the Mitsubishi ML-4102. Here, operation on one of around four modes at any

operating temperature was possible, and the tuning behaviour over a limited temperature range is shown in figure 7.2.2. The GRIN rod can be used to select any frequency within those allowed by the band gap tuning. Between mode hops, the laser frequency is pulled a little (by ≈2 GHz) as the PZT voltage is tuned. The pattern of frequencies obtained is a cyclic function of PZT voltage, repeating every ≈0.5 μm, using the nominal value of the PZT constant supplied by the manufacturer, which has a stated accuracy of only ±20%. The variation of frequency with PZT voltage is shown in figure 7.2.3, for a fixed diode operating current and heatsink temperature. Not surprisingly, in view of the complex tuning behaviour of the unmodified diode, the tuning behaviour of the mode selector was not as straightforward as hoped. It might be expected, for example, that if four modes are selected, then a mode hop should occur for each $\lambda/8$ change of the GRIN rod to diode separation. Moreover, we might expect each lasing mode to be selected when the output coupler reflectivity (R' of equation 7.2.2), modified by the presence of the GRIN rod, was at a maximum. However, some modes are clearly "preferred" by the diode, and lase for unexpectedly large changes in the GRIN rod PZT voltage. Other modes can be harder to select.

The linewidth was observed by observing the beat between a mode-selected ML-4102 and a second diode which was linewidth reduced using the technique of resonant optical feedback (chapter 3). Since the GRIN rod is so close to the laser, it cannot be expected to reduce the laser linewidth, by reducing the Schawlow-Townes linewidth (equation 3.1.8). This is observed to be the case. Indeed, any vibration or instability of mounting between the laser and the GRIN rod can cause a slight broadening of the linewidth. This can occur as the laser frequency is pulled by changes in the diode to GRIN rod separation. However, the mode-selected laser could be linewidth-reduced by resonant optical

feedback. The extra feedback from the resonant cavity does not interfere with the mode selecting property of the GRIN rod. The linewidth of this laser is identical to that measured in chapter 3 for lasers with no mode selection.

Using a GRIN rod, mode selection was also successfully tried with a Hitachi 820 nm HLP 1400 diode and the results are shown in figure 7.2.4. For this diode, the GRIN rod could select up to 13 modes, which were not necessarily adjacent. In cases where up to 13 modes were selected, there was ≤ 200 MHz frequency pulling between mode hops. Although tuning to any frequency could be achieved in these diodes, some modes refused to lase (figure 7.2.4). Some modes could also not be selected at all temperatures, and apparent gaps in the tuning at 368.75 THz or 369.35 THz could be accessed by changing the operating temperature outside the range shown. Figure 7.2.4 also shows that, with no optical feedback, this diode has considerable tuning hysteresis.

The results for the 670 nm diode are shown in figure 7.2.5 for two levels of feedback. Firstly an 0.23 pitch lens rod was used, AR coated on both surfaces, with a design working distance of 200 μm. This provided a lower level of feedback than an 0.25 pitch rod owing to the larger working distance and rapidly diverging diode laser beam. The 0.23 pitch lens was used and selected 3 to 4 adjacent modes, giving few gaps in frequency. Secondly an 0.25 pitch lens was used with no AR coating on the surface nearer the diode, and this completed the coverage in frequency. Selecting fewer modes can make the laser system easier to operate, although it does not necessarily allow us to select all possible laser frequencies.

With the development of a narrow linewidth mode selectable diode laser,

consideration can be given to their wider potential. As already mentioned, an immediate application may be to replace dye lasers with diodes in the NPL ion trap programme. It is beyond the scope of this thesis to give a detailed description of ion trapping, but with this technique, the ions are confined and then cooled in an electromagnetic trap. The cooling process is achieved on a strong allowed transition, which is generally in the blue or ultra-violet part of the spectrum. A second laser source is also sometimes required to pump the ions out of a third quantum level. The frequency standard is then expected to be based on a long-lived state in the ion and typically the linewidths expected are less then a few Hz. Present NPL work centres on the ytterbium ion, where wavelengths of 369 nm and either 935 nm or 2.44 μm are needed for cooling [12]. Other ions, in particular strontium or calcium, require wavelengths more amenable to solid state lasers. In strontium [13], the wavelengths required to cool are 422 nm and 1.1 μm. The former wavelength can be provided by a 100 mW 844 nm frequency doubled laser diode [7,8]. The infra-red wavelength can be provided by a fibre laser [26], pumped by a high-power diode laser. The optical reference frequency is at 674 nm, which is directly accessible by the range of 670 nm band of laser diodes. The lasers necessary for this ion are currently under development.

The overlap of the emission wavelength of 780 nm diodes with the Rb D resonance transition could be used in work directed towards microwave frequency metrology using laser cooled beams of Rb atoms. There have already been several papers published where a beam of Rb has been cooled using a laser diode [27]. As with the ion trap work, it is not possible to give a detailed description of atom cooling and trapping. There are several important advantages and disadvantages in using atoms rather than ions for frequency metrology. For example, ions generally have the

strong resonance transitions suitable for cooling in the ultra-violet, rather than the visible part of the spectrum, which is generally the case for atoms. Visible radiation is much easier to generate directly with dye or diode lasers. However, atom traps are generally very shallow and trapping times are very short (eg ~200 ms [28]). However, whether future microwave or optical frequency standards are based on ion or atom traps, diode lasers will be vital to make the standards compact and practicable.

The work described in chapter 6 suggests that various improvements to the swept wavelength system could be made. In particular, a wider frequency sweep is required to achieve a proportionally higher accuracy. From the results in chapter 6, we need to work towards a sweep of ten to a hundred times the 4 GHz scan obtained here. If the length is already known sufficiently well (or can be approximately measured using a lower sweep) then the ~400 GHz sweep need not be continuous. A wide sweep could be obtained by using a GRIN rod to prevent mode hopping (as described in this chapter) or by using an external cavity [14]. Suitable spectral references might be available in iodine, accessed by using a diode at 660 nm.

It should also be possible to develop less complex and less accurate systems, which would be easier to implement and operate. The reference could, for example, be the linear absorption profile of Rb, or the resonances of a stable cavity such as that used in chapter 6 to test out the swept wavelength system. There is also the option that the lasers need not be linewidth reduced by resonant optical feedback, if the spectral coherence of the basic diode is sufficient.

A further alternative may be to lock both diodes to different modes of

the ULE cavity to produce a convenient beat at, say, ≈ 2 GHz, but not to scan the laser. The measured beat would then directly relate to a multiple of the cavity FSR. This would provide a faster measurement than that in chapter 6 and drift of the cavity would provide far less of a measurement problem. However, this was attempted but was not successful. Significant changes in the beat were observed if, for example, the two beams were not perfectly co-linear. This is observed to cause several MHz change in the beat (figure 6.2.3.1) on different alignments into the ULE cavity. Electronic offsets in the sevocontrol electronics will also cause shifts and the net result is that this does not prove to be an accurate means of measurement.

A future approach to swept wavelength interferometry might be possible using iodine stabilised laser diodes, particularly as commercially available laser diode wavelengths become shorter. In an effort to investigate the possibility of this with diodes now available, a 670 nm diode (Toshiba TOLD 9211) was used to investigate linear absorption in iodine. However, at such a long wavelength, the absorption is expected to be fairly weak, since the ground states involved have a high vibrational quantum number. These states are not well populated at room temperature. The strongest I_2 lines measured only had a linear absorption of (1.5 ± 0.5)% in a 0.5 m long cell at room temperature (19°C). With the 3 mW diode used, it proved impossible to saturate the transitions. Even using linear absorption, I_2 did not provide a satisfactory feature for servocontrol purposes. As with the optogalvanic features investigated in section 2.2, a modulation depth of ≈300 MHz peak-to-peak was required to provide a feature with a reasonable signal to noise. With diodes, frequency modulation also gives amplitude modulation. Therefore the derivative feature obtained not only had a poor signal to noise ratio, but lay on a DC offset larger than the

signal size. However, with the vast comb of transitions available in I_2 [29], it should ultimately be possible to generate either fixed or swept wavelength standards in shorter wavelength laser diodes. When a 630 nm single frequency diode becomes available (manufacturers expect this to be from 1993) it may be possible to stabilise this to iodine to, say, 50 kHz. A sweep of > 50 GHz between iodine components would then provide a measurement to $< 1 \times 10^{-6}$. The sweep frequency range could then be measured by separate interferometric frequency measurements of the two iodine components at the ends of the scan.

By 1990, laboratory produced laser diodes had been demonstrated at 576 nm [30] with a GaInP/AlInP multiple quantum well device, although this was operated well below room temperature. Only one year later, pulsed operation at 490 nm [31] was demonstrated, in a ZnSe based single quantum well device operating at 77 K. In conclusion then, diode lasers are set for a promising future in interferometry and spectroscopy. Shorter wavelengths and higher powers will enhance their usefulness. If the recently reported lasers diodes at 490 nm can eventually operate cw and single mode, then a very wide spectral coverage will be possible with all solid-state lasers. These could ultimately replace dye and even Ti:sapphire lasers, which both require an argon ion pump laser. This is a clear future trend towards all solid-state lasers.

References

[1] GP Barwood, P Gill, WRC Rowley, J Phys E; Sci Instrum 21, 966-71 (1988)

[2] GP Barwood, P Gill, WRC Rowley, Electron Lett 24, No 13, 769-70 (1988)

[3] GP Barwood, P Gill, WRC Rowley, J Mod Optics 37, No 4, 749-58 (1990)

[4] GP Barwood, P Gill, WRC Rowley, Opt Comm 80, No 5,6, 359-64 (1991)

[5] GP Barwood, P Gill, WRC Rowley, Appl Phys B53, 142-7 (1991)

[6] GP Barwood, P Gill, WRC Rowley, to be published 1992

[7] A Hemmerich, DH McIntyre, C Zimmerman, TW Hänsch, Opt Lett 15, No 7, 372-4 (1990)

[8] EJ Lim, MM Fejer, RL Byer, WJ Kozlovsky, Electron Lett 25, No 11, 731-2 (1989)

[9] JS Major Jun., WE Plano, DF Welch, D Scifres, Electron Lett 27, No 6, 539-40 (1991)

[10] GP Barwood, P Gill, WRC Rowley, Meas Sci Tech, 3, No 4, 406-10, (1992)

[11] HA Klein, AS Bell, GP Barwood, P Gill, Appl Phys B, 50, 13-17 (1990)

[12] HA Klein, AS Bell, GP Barwood, P Gill, WRC Rowley, IEEE Trans. Instrum. Meas., 40, No 2, 129-31 (1991)

[13] AA Madej, JD Sankey, Opt Lett, 15, No 11, 634-6 (1990)

[14] MG Boshier, D Berkland, EA Hinds, V Sandoghdar, Opt Comm 85, No 4, 355-9 (1991)

[15] A Hemmerich, DH McIntyre, D Schropp Jr, D Meschede, TW Hänsch, Opt Comm 75, No 2, 118-22 (1990)

[16] A Hemmerich, DH McIntyre, C Zimmermann, TW Hänsch, Opt Lett, 15,

No 7, 372-4 (1990)

[17] F Wittgrefe, MD Hoogerland, JP Woerdman, Meas. Sci Technol 2, 304-11 (1991)

[18] P Laurent, A Clairon, C Breant, IEEE J Qu El, 25, No 6, 1131-42 (1989)

[19] C Lin, CA Burrus, RA Linke, IP Kaminow, JS Ko, AG Dentai, RA Logan, BI Miller, Electron Lett, 19, No 15, 561-2 (1983)

[20] K-Y Liou, Electon Lett, 19, No 19, 750-1 (1983)

[21] JP Van der Ziel, RM Mikulyak, IEEE J Qu El, QE-20, No 3, 223-9 (1984)

[22] D Renner, JE Carroll, Electron Lett, 15, No 3, 73-4 (1979)

[23] L Goldberg, HF Taylor, A Dandridge, JF Weller, RO Miles, IEEE J Qu El, QE-18, No 4, 555-64 (1982)

[24] JC Camparo, Contemp Phys 26, No 5, 443-77 (1985)

[25] Melles Griot Optics Guide 4, p 18-52

[26] AA Madej, WE Berger, GR Hanes, MS O'Sullivan, Opt Comm, 73, No 2, 147-52 (1989)

[27] RN Watts, CE Wieman, Opt Lett, 11, No 5, 291-3 (1986)

[28] D Sesko, CG Fan, CE Wieman, J Opt Soc Am B, 5, No 6, 1225-7 (1988)

[29] P Luc, J Mol Spect, 80, 41-55 (1980)

[30] Y Kaneko, A Kikuchi, I Nomura, K Kishino, Electron Lett, 26, No 10, 657-8 (1990)

[31] MA Haase, J Qiu, JM DePuydt, H Cheng, Appl Phys Lett, 59, No 11, 1272-4 (1991)

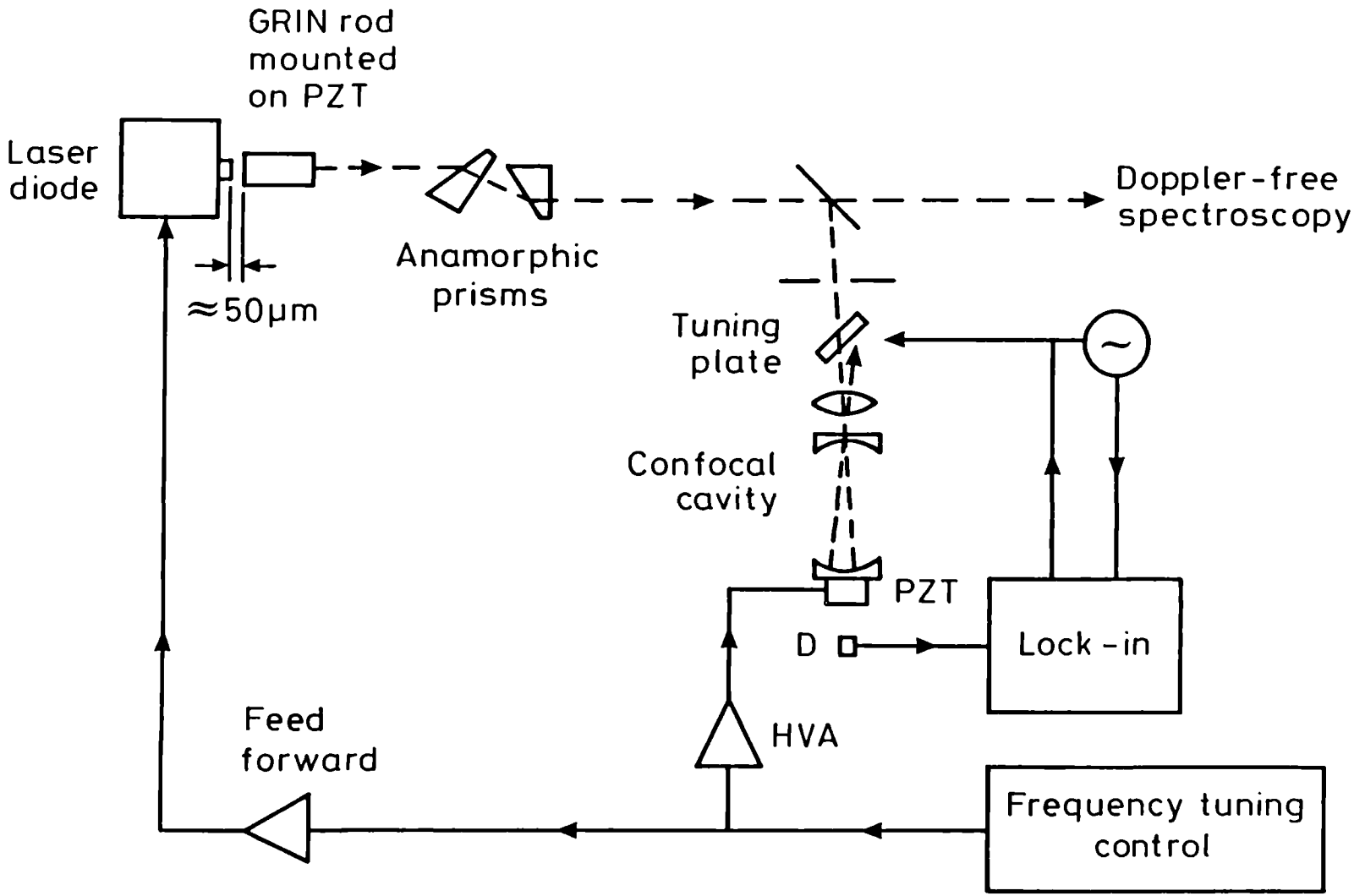

7.2.1 Schematic of multiple cavity created by the diode and GRIN rod.

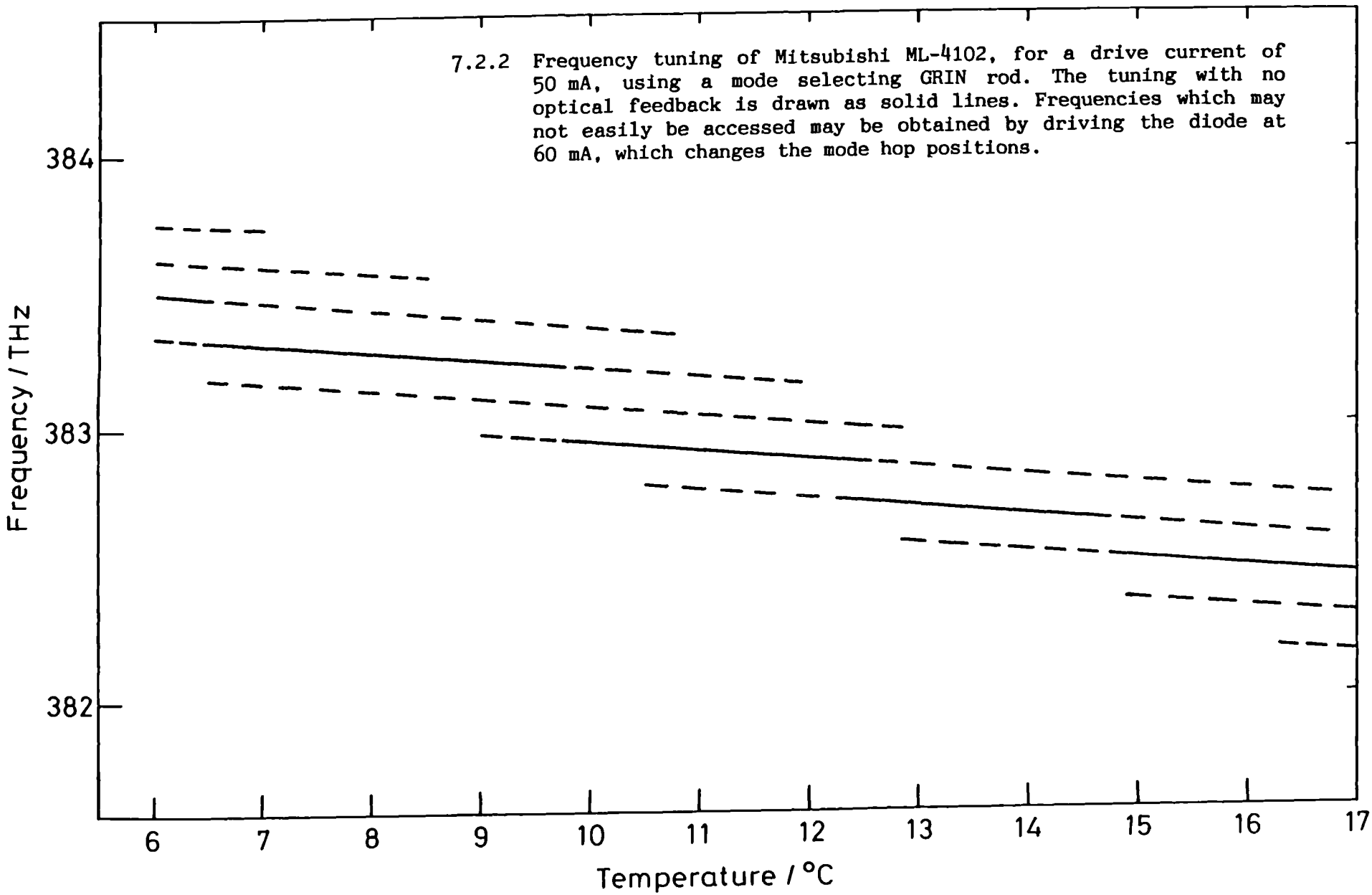

7.2.2 Frequency tuning of Mitsubishi ML-4102, for a drive current of 50 mA, using a mode selecting GRIN rod. The tuning with no optical feedback is drawn as solid lines. Frequencies which may not easily be accessed may be obtained by driving the diode at 60 mA, which changes the mode hop positions.

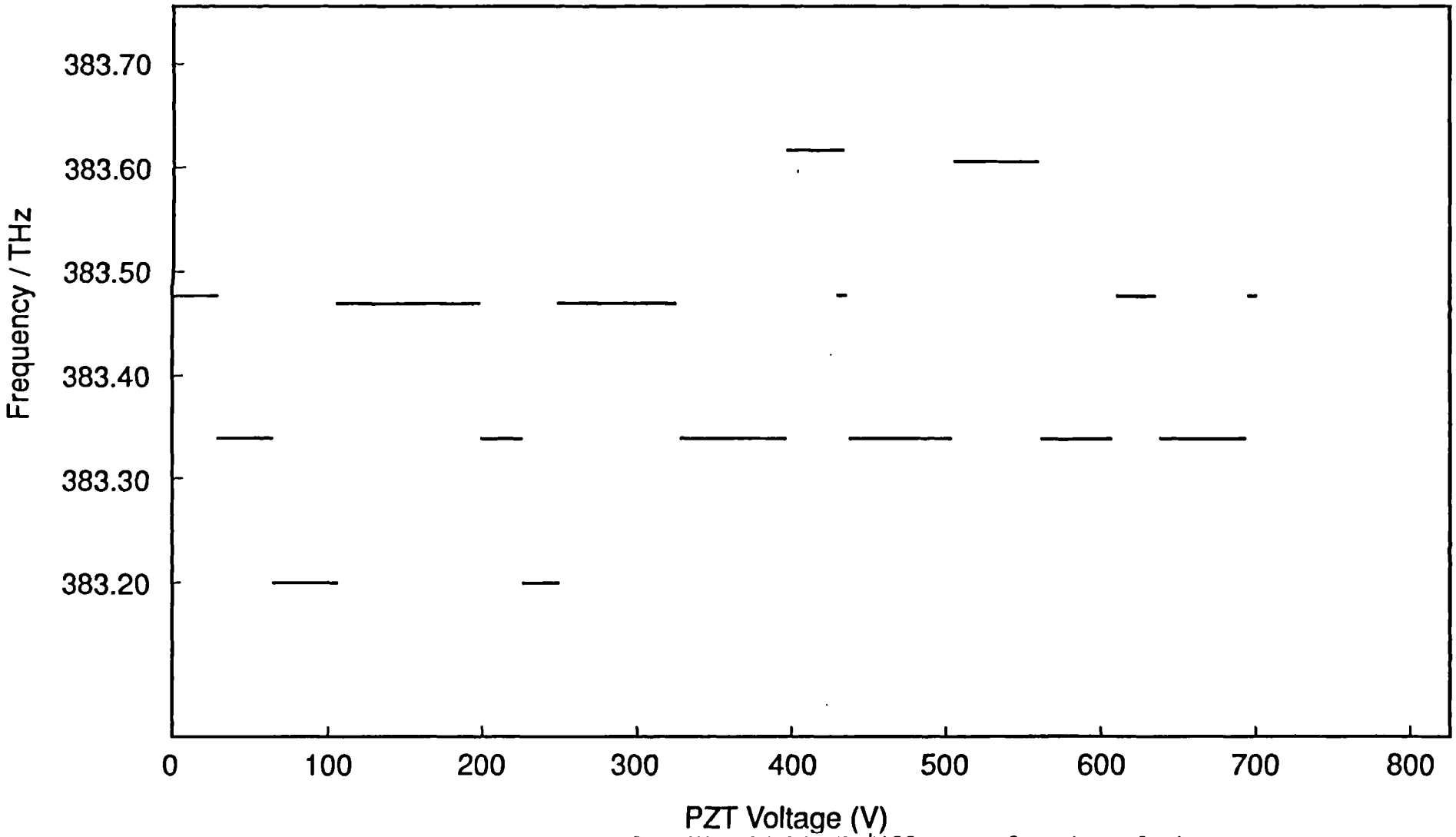

7.2.3 Frequency tuning of a Mitsubishi ML-4102 as a function of the voltage on the PZT controlling the GRIN rod to diode distance. The results are for a fixed diode drive current and heatsink temperature. The PZT is a tube 12.7 mm long, 6.35 mm outer diameter and 0.51 mm wall thickness. The material is "PZT5H" from Vernitron (Morgan Matroc).

A00197-3

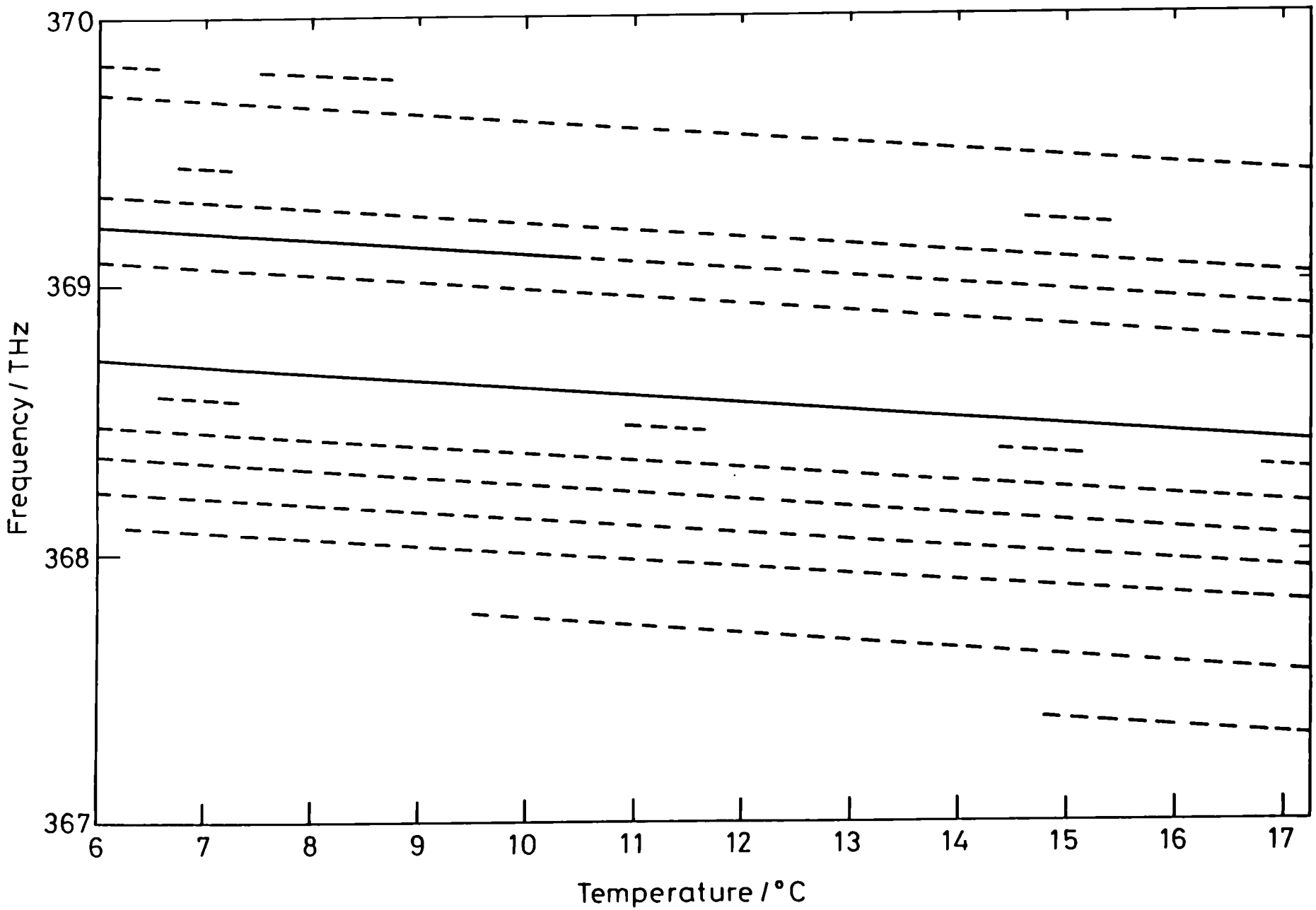

7.2.4 Frequency tuning of Hitachi HLP 1400, for a drive current of 75 mA, using a mode selecting GRIN rod. The tuning with no mode selection is indicated as solid lines.

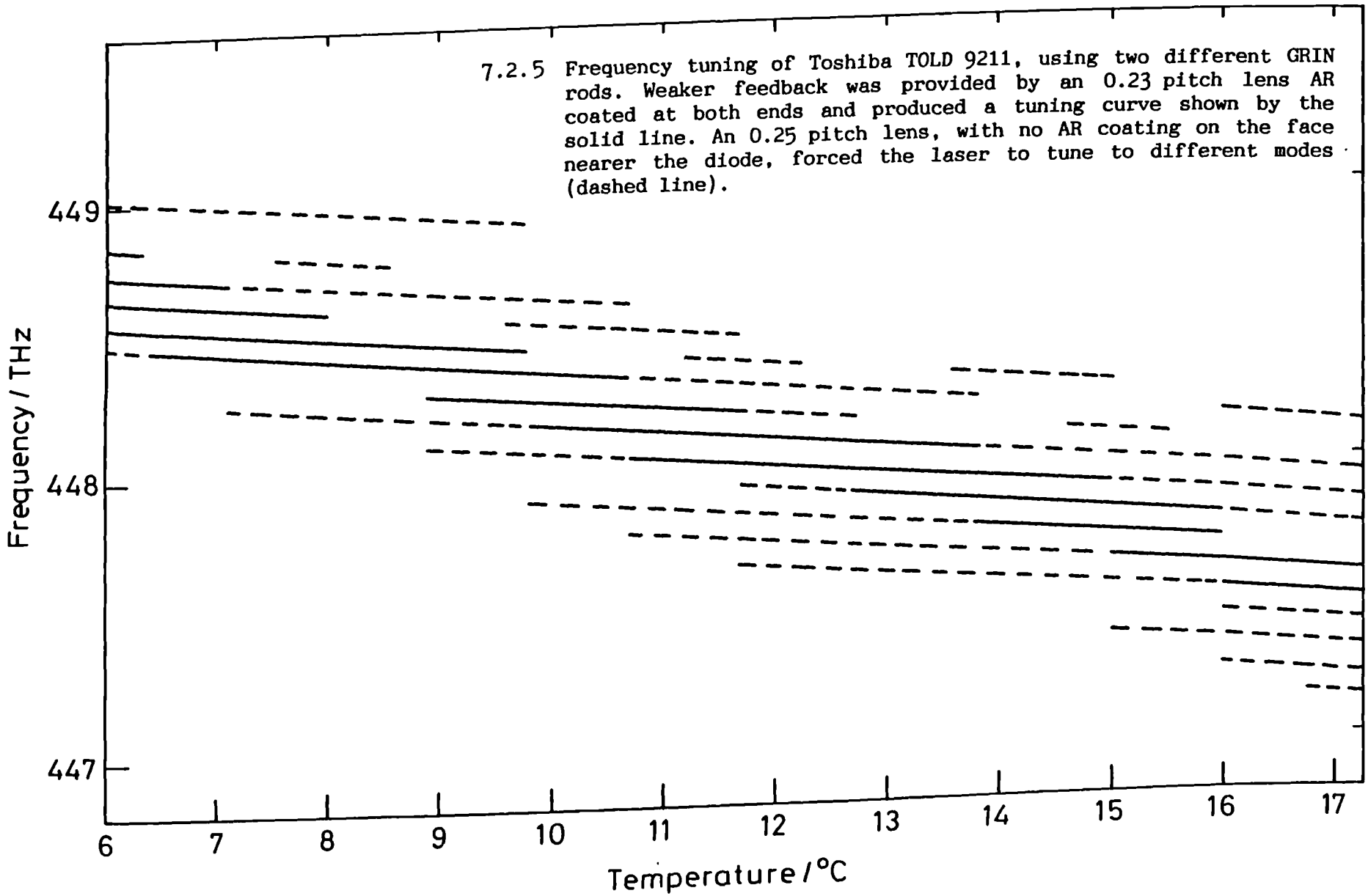

7.2.5 Frequency tuning of Toshiba TOLD 9211, using two different GRIN rods. Weaker feedback was provided by an 0.23 pitch lens AR coated at both ends and produced a tuning curve shown by the solid line. An 0.25 pitch lens, with no AR coating on the face nearer the diode, forced the laser to tune to different modes (dashed line).